The University of Liverpool

Study of Uropathogenic *Escherichia coli* Host-Pathogen Interactions Using Novel Infection Models

Thesis submitted in accordance with the requirements of the University of Liverpool for the degree of Doctor in Philosophy by:

Milena Marianna Lewańczyk, B.Sc. (Hons), M.Sc.

29th September, 2017

Abstract

Urinary tract infections (UTIs) are the second most common infectious disease in humans resulting in widespread morbidity worldwide. The vast majority of UTIs are of bacterial origin and ~80% of those is caused by uropathogenic *Escherichia coli* (UPEC) upon bladder colonisation (cystitis). It predominantly affects women of reproductive age. About 60% of them will experience at least one UTI in their lifetime, and ~44% of theseUTI patients suffers from recurrent infections within a year. Treatment of this condition, which typically involves antibiotic therapy, accounts for 1-3% of all general practice visits in the UK alone, and results in considerable financial burden (~£172 million each year). Facing the antibiotic resistance crisis, development of new antimicrobial strategies is important, for which a comprehensive understanding of host-pathogen interactions is indispensible. One step identified during establishment of UTI is the binding of UPEC to bladder epithelial cells, which leads to their subsequent invasion into the host cell. Mouse animal and cell line models have given us insights into the invasion process of UPEC. However, our knowledge about the host pathways that are important for infection is less developed.

To identify potential new targets for developing UTI treatments, the work presented in this thesis aimed to further understand the invasion process by the following means: single cell proteomic analysis of mouse urothelium upon invasion by UPEC; development of a novel primary culture system for human urothelial cells; and establishment of a screenable invasion assay to enable a genome-wide siRNA screen for host factors important for UPEC invasion.

The proof of concept study of single cell proteomics led to proving not only the feasibility of the endeavour with the use of untagged mass spectrometry, but also discovery of a potential intercellular heterogeneity among mouse bladder urothelial cells. The normal human urothelial (NHU) *in vitro* model was found to represent a useful tool in studying UTIs. It could have a particular value in the evaluation of anti-adhesive drugs, as a potential improvement on previous studies, which used classical immortalized cell lines. While further studies are still necessary, overall these data highlight the complexity of the host-pathogen interaction during UTIs, bringing us closer to finding innovative methods for infection management and discovery of

biomarkers that might be applied to human urine analysis and identification of an intracellular infection.

Declaration of institutions involved in this work

This thesis is the result of work performed within two institutions: University of Liverpool (U.K.), under the supervision of Prof. Craig Winstanley, Dr Rachel Floyd, and Prof. Susan Wray; and Genome Institute of Singapore (Singapore), under the supervision of Dr Swaine Chen. While the UoL is the degree awarding body, the course of this four year long PhD was split into equal time courses between the two places in a following manner: 1 year in U.K., 2 years in Singapore, 1 year in U.K..

The work presented in this thesis' chapters 4 and 5 was almost entirely performed in Singapore, with exception for the immunohistochemical analysis, and some computational data analysis that were completed upon return to the U.K.. Work described in Chapter 3, and thesis write up were both carried out across the two 1 year-long stays in U.K..

Some of the results are the outcome of collaborations, as specifically indicated in the text. In brief, all the LC-Ms/Ms related work was done by Dr Xuezhi Bi at BTI, A*STAR. Dr Jaran Jainhuknan performed MALDI-TOF testing. Dr Debarka Sengupta designed and performed the initial t-SNE and k-means clustering and analysis. The IHC validation experiments were performed by Sarah Northey, a research technitian at University of Liverpool.

Acknowledgements

Writing this thesis wouldn't be possible without some people, to whom I would like to express my most sincere thank you.

First and foremost I'd like to thank all my PhD supervisors **Craig Winstanley, Swaine Chen, Rachel Floyd, and Susan Wray** for accepting me as their PhD student. I'm forever indebted to them for their active support, input, expert knowledge and impressive responsiveness despite having very busy schedules. They have been routinely fire fighting my worries and concerns and fostered my scientific and personal progression at the highest levels of scientific integrity. I feel very fortunate for being able to work under their supervision.

I'd like to thank further **Craig** for all the help and guidance offered when needed during this four year period, especially the thesis write-up time, his trust in my independence, and for sprinkling our meetings with the finest English humour I have ever come across. **Rachel** for being such a great, strong woman in science model, embodying how commitment to science should look like. Her cheerful enthusiasm and encouragement that helped me in all the time of research, and for teaching me the truest life wisdoms *"Popili phalli sunt".* Thanks to her my useful English vocabulary has never been so flamboyant. **Susan** for her inexhaustible optimism, trust, and being an example that one can always aspire to.

I am deeply grateful to **Swaine** for all the unprecedented theoretical advice, infinite optimism and inexhaustible support. Working with him was an unforgettable and invaluable experience. He is such a vibrant and compelling mentor of unbelievable perceptiveness, who gave my vision of doing science a new shape. His ever-friendly nature was critical towards completion of my placement in Singapore which has been an exercise in sustained suffering. I hope someday I could be as enthusiastic and energetic and be able to command an audience as well as he can.

Next, some people of outstanding importance for my research:

Balamurugan Periaswamy who has been a constant source of stimulating suggestions, many long discussions (especially those on strandedness), encouragement and belief in my programming skills. He was my primary resource for getting my statistics questions answered and his dedication for pursuing daunting computational analysis was truly inspiring. **Majid Eshaghi,** for teaching me a number of experimental techniques. Seeing his professional discipline together with straightforward criticism have been very empowering. I feel like I haven't benefitted enough from his lab-competence.

Kristin Lees has been very helpful in providing me with advice and support on countless occasions and on pretty much everything during my stay in Singapore and beyond. Thank you for living with me through some mice and other frustrations, and all the mutual lunches, but not for introducing me to *Edinburgh Rocks* candy. **Zhu Yuan** for sharing her feminine passions, introducing me to xiao long bao, and her sisterly love. "You will be a permanent scar on my life". **Gökçe Oğuz** and **Asmaa Almohanna** for boosting work happiness

(and colour in my life). Their smiles are contagious and I will miss their sense of humour. They are a couple of people you will just love instantly. I hope PhDs won't turn them into bitter old shrews like me. **Pauline Yoong** for being a nice and helpful person, a friendly office mate and partner in crime, with much alike life perception.

I am deeply grateful to my collaborators **Xuezhi Bi** for performing the single cell LC-Ms/Ms, **Debarka Sengupta** for his help and valuable feedback on the analysis of our single cell omics data, and **Ajay Sharma** for providing us with ureter samples.

A good support system is important to surviving and staying sane during a PhD. I'd like to thank my friends **Ewa Klein**, **Ozanna Burnicka-Turek**, and **Michał Filus** for their friendship, help and support at all times. All of them have always been close to me through the good and bad times. **Ewa**'s heart-warming support has given me unremitting encouragement. I have never met such a good and selfless person. I know I can always count on her when times are rough. Thank you for bringing out the best in me. **Ozanna** is a true and non-judgmental supporter and also another inspiring scientist, with an impressive work rigour. Our work and life discussions were always lively and, although generally longer than planned, always ended too soon. I wish I could be as lively and energetic as her. **Michał** for his kindness, great conversations, common travels and all the fun activities we've done together. He's one of a very few people I can trust, and reminds me of how I used to be before this PhD. I'd like to also express appreciation to **Mikołaj Mikicki** for his support and extenuating my agonies associated with writing this thesis and other English issues.

I wouldn't be the same person if not for my friends in Liverpool who managed to stay in touch during my exile in Singapore. **Kayode Owojori** a wonderful and generous friend whom I value a lot. He has always been there for me to turn to. His listening skills and patience are impressive and I admire his positive outlook. I thank **Alain Kamden** for his perseverance to stick by my side at all times of my stay in Singapore in spite of my consistently low spirits. I couldn't have made it without you. **Kenechi Okoli**, who was instrumental in instilling confidence back in me. **Daniel Bloembergen** and **Amer Nubgan** who always appreciated my taste in fashion, had time for my late-announced visits, good selection of teas and zeal for cooking. And other **Salseros** y **Salseras** enriching my life and making me feel welcome during my stay in Liverpool. Their peculiarity and drive resulted in the most extraordinary stories and moments.

I also would like to thank my parents and family, for the support in all forms that they've provided me with, with a special mark to my beloved godfather **Adam Karaszewski** (1975-2014), who never got to see me complete this PhD, but who has always been an incredibly empowering and inspirational figure. I feel like I haven't learned enough from his vast life experiences. You will always be in my mind, in my heart, and in your grave.

There are many more people I could thank, but time, space, and modesty compel me to stop here.

Contents

List of abbreviations

aa	Amino acids
Ab.	Antibody
Amp	Ampicillin
ANOVA	Analysis of variances
APES	3-Aminopropyltriethoxysilane
APS	Ammonium persulfate
AUM	Asymmetric unit membrane
BSA	Bovine serum albumin
^{o}C	Degrees celsius
CFU	Colony forming units
Chlor.	Chloramphenicol
DAPI	4',6-diamidino-2-phenylindole
dATP	Deoxyadenosine triphosphate
DE	Differential expression
dH_2O	Distilled water
ddH_2O	Ultrapure water
DNA	Deoxyribonucleic acid
dNTP	Deoxyribonucleotide triphosphate
DPBS	Dulbecco's phosphate-buffered saline
E. coli	*Escherichia coli*
EDTA	Ethylenediaminetetraacetic acid
EM	Electron microscopy
Et al.	*Et alii* or "and others"
EtBr	Ethidium bromide
EtOH	Ethanol
ExPEC	Extraintestinal pathogenic *E. coli*
FACS	Fluorescence-activated cell sorting
FBS	Foetal bovine serum

g	Gram
GFP	Green fluorescent protein
h	Hour(s)
HA	Haemagglutination
hpi	Hours post infection
IL	Interleukin
Kan	Kanamycin
KSFM	Keratinocyte serum free medium
KSFMc	Keratinocyte serum free medium complete
LB	Lysogeny broth
LC-Ms/Ms	Liquid chromatography tandem mass spectrometry
LN_2	Liquid nitrogen
LPS	Lipopolysaccharides
MαDM	Methyl α-D-mannopyrannoside
mg	Milligram(s)
min	Minute(s)
ml	Milliliter(s)
mM	Millimolar
MOI	Multiplicity of infection
mRNA	Messenger RNA
Ms	Mass spectrometry
NBF	Neutral buffered formalin
NHU	Normal human urothelium
PBS	Phosphate-buffered saline
PBST	Phosphate buffer saline with Tween 20
PC	Principle component
PCA	Principle component analysis
PCR	Polymerase chain reaction
PFA	Paraformaldehyde
Q-Q	Quantile- quantile

RBCs	Red blood cells
RNA	Ribonucleic acid
RPM	Revolutions per minute
RT	Room temperature
SDS-PAGE	Sodium dodecyl sulfate polyacrylamide gel electrophoresis
siEC	Single infected epithelial cell
STs	Multilocus sequence types
siRNA	Small interfering RNA
TAE	Tris-acetate-EDTA
TBS	Tris-buffered saline
TBST	Tris-buffered saline/1% (v/v) Tween-20
Tet	Tetracycline
TLR	Toll-like receptor
TRIF	TIR-domain-containing adaptor protein inducing IFN-β
t-SNE	T-distributed stochastic neighbour embedding
UP	Uroplakin protein
µg	Microgram
µl	Microliter
µM	Micromolar
UPEC	Uropathogenic *Escherichia coli*
UTI	Urinary tract infection
UV	Ultraviolet
V	Volts
vs	Versus
WGA	Wheat germ agglutinin
WHO	World Health Organisation
xg	Times gravity
α	Alpha
β	Beta
Δ	Delta

θ	Theta
λ	Lambda
σ	Sigma
∞	Infinity

1 Introduction

1.1 Urinary bladder – function and anatomy

The urinary bladder together with the kidneys, ureters, and urethra form the urinary tract. While kidneys produce urine continuously, the main function of the bladder is to store urine and maintain its composition similar to that generated by kidneys [1]. The musculature within the bladder wall which is comprised of three layers of smooth (involuntary) muscles (Figure 1.1) facilitates the voluntary voiding of urine [2]. The outer and inner layers have a longitudinal arrangement, while the middle muscle fibres are arranged circularly. The entire structure is covered by a peritoneum- derived serosa [2]. Being a hollow structure, the bladder is lined with an epithelium (uroepithelium) that forms the main protective interface between urine, potential pathogens, and the underlying musculature. The uroepithelium is separated from the muscular layer of the bladder by the lamina propria, which contains blood vessels, nerve fibres and loose, fibrous connective tissue. Apart from its role in maintaining barrier function, the urothelium is also known to play a sensory role, by which it can detect physiological (e.g. temperature, osmolarity) and chemical (e.g. ATP, or chemical irritants such as capsaicin, the spicy component found in chili peppers) stimuli and respond accordingly by regulating voiding frequency and urgency [3].

1.1.1 Uroepithelium

The uroepithelium, also referred to as urothelium, lines the inside of the bladder, as well as the renal pelvis, ureters, upper urethra and in men it is also found in the glandular ducts of the prostate [1, 4]. This ~60µm thick layer consists of stratified, tightly connected epithelial cells [5] that exhibit a gradient of size and differentiation state. The basal urothelial cells are small (~5-10µm in diameter), and relatively un-differentiated, as compared to the larger (~10-15µm) intermediate cells (Figure 1.1). By comparison and depending on the degree of bladder stretch, terminally differentiated superficial cells lining the distal part of the bladder can be ~25-250µm in length [4, 5]. The urothelium typically contains just a single layer of both basal and superficial cells. However, the number of intermediate strata can vary depending on the species, and so

among rodents it is 1-2 layers thick, whereas in humans there can be up to five intermediate cell layers [6]. The thickness of the intermediate cell layer is also dependent on the state of bladder filling, where thinner intermediate cell layers are found in a full bladder, compared to that of a voided bladder [4].

Simultaneous differentiation and migration of basal cells to the upper cell layer provides the basis for the self-renewing properties of urothelial tissue [7]. Basal cells have the slowest turnover rate of all mammalian epithelial cells [3]. Most literature estimates urothelial cell turnover to be about 3-6 months in a normal undamaged bladder [2, 8]. However, an exact half-life is difficult to pinpoint due to the very low labelling indices obtained by incubating normal human urothelium (NHU) biopsies with tritiated thymidine. This radioactively labelled nucleoside incorporates into dividing cells and can be measured by radioautography and used as a marker of cell turnover. Upon physical or chemical injury, or bacterial infection that causes loss of the superficial cell layer, the regeneration of urothelium is much faster and has been reported to take place within days to weeks [2, 4].

Basal and intermediate cells show classical epithelial morphology characterised by a regular 'cobblestone' phenotype, whereas superficial cells, also referred to as facet or umbrella cells, are distinctive due to a number of unique features. Superficial cells are typically binucleate and may have up to 11 nuclei [9]. Their apical membrane is a highly dynamic structure, due to high vesicular traffic that controls changes in its surface area, and associated bladder filling or urine voiding. Constant trafficking of specialized sub-apical fusiform vesicles can increase the surface area of umbrella cells, allowing for greater urine storage capacity [10, 11]. Uroepithelial vesicles are comprised of asymmetric unit membrane (AUM) regions, and their exocytosis contributes to formation of plaques that give the apical surface of umbrella cells their distinct scalloped shape. The plaques consist of ~1000-3000 AUMs. They are mostly composed of several types of transmembrane proteins called uroplakins (UPs). The uroplakin family of proteins include UP1a, UP1b, UP2 and UP3. In urothelial cells these are also markers of terminal cytodifferentiation. Though it needs to be noted that while UP1b can be found across both intermediate and superficial cell layers, conjunctiva and cornea, expression of UP1a, UP2 and UP3 is restricted to facet cells only [4, 12, 13]. AUM luminal plaques confer urothelium one of its

unique characteristics, namely maintaining its low, but finite transcellular permeability to water, urea and ions [4, 14, 15]. No other epithelium has been found to provide a satisfactory substitute for regeneration of the bladder that successfully mimics its impermeability between tissue fluids and urine ("blood-urine barrier") [2]. Other specialized features of the urothelium include the presence of tight junctions between superficial cells (a few desmosomes stabilizing lower strata can be also found) as determined by high transepithelial resistance (20,000–30,000 $\Omega \cdot cm^2$) [1, 2, 15] which maintains low permeability and high resilience against infection. Urothelial cells have also been shown to regulate fluid balance via the action of amiloride-sensitive sodium channels with a short circuit current typically ~2µA/cm^2 [1, 14, 16].

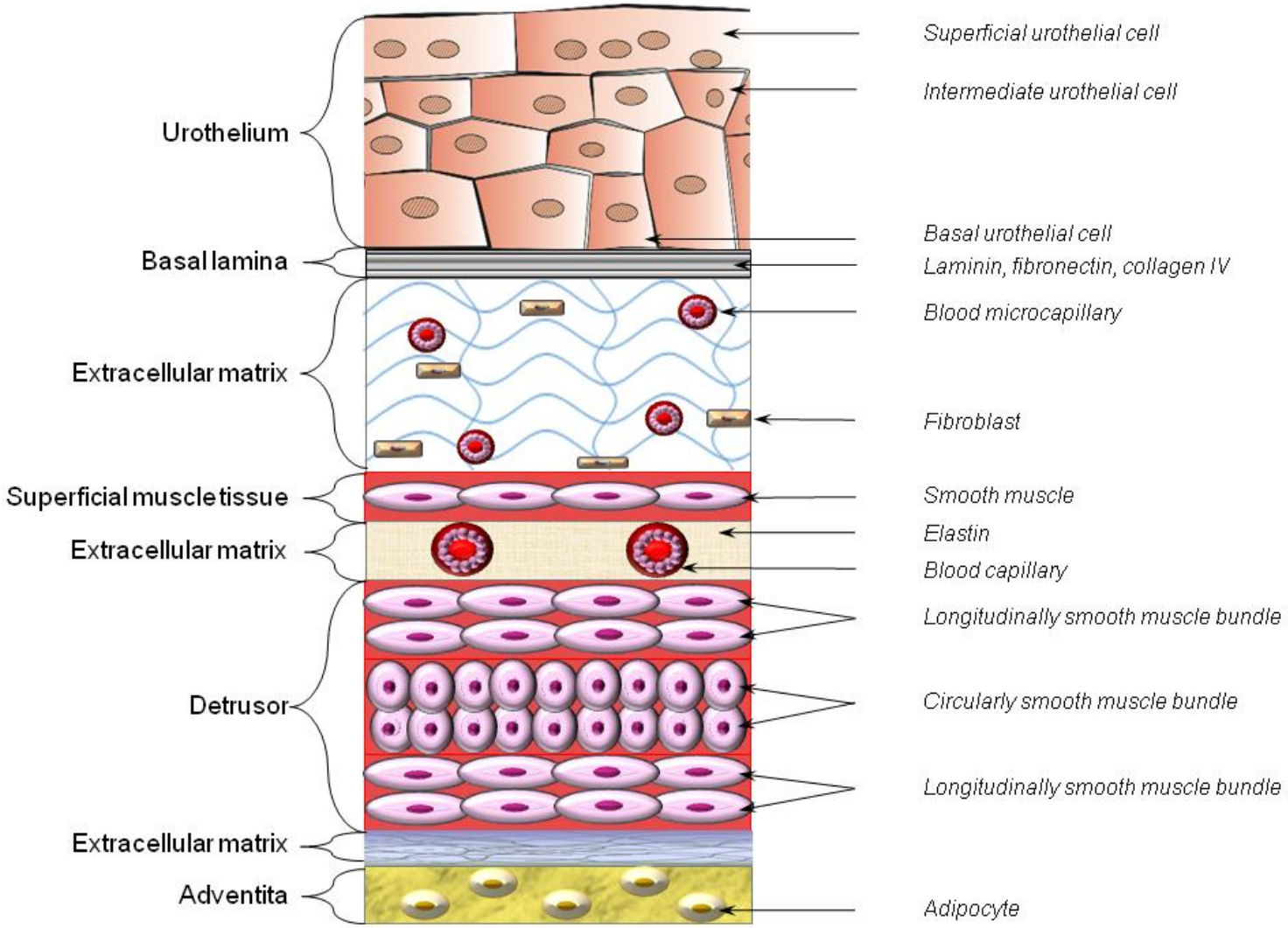

Figure 1.1 – Schematic representation of structure of the urinary bladder wall and urothelium. Based on [17].

1.2 Urinary tract infections

1.2.1 Classification and symptoms

Urinary tract infections (UTIs) are defined by the presence of a pathogen in any site of the urinary tract (Table 1.1). While the vast majority of UTIs are symptomatic, UTIs can also be asymptomatic, whereby the presence of bacteria in urine (bacteriuria) is not associated with any other clinical manifestations. Unlike symptomatic UTI's, bacteriuria is usually self-resolving and doesn't require further treatment. Depending on the site of infection shown in Table 1.1, UTIs can be associated with a variety of symptoms. Infections of the lower urinary tract include urethritis (infection of the urethra) and cystitis (bladder infection), which is the most frequent UTI. Cystitis is usually characterised by an acute onset of frequent and painful urination. As the infection is usually confined within the bladder, it is believed to be a benign condition with no long-term impact on patient's health. When pathogenic bacteria ascend the urinary tract, or in rare instances where bacteria reach the kidneys from the bloodstream and travel downwards, they give rise to infections of the upper urinary tract [18, 19]. These can be categorised into: ureteritis (a rare infection of the ureter) and pyelonephritis (acute kidney infection) [20]. Symptoms in addition to those caused by cystitis, include flank pain, blood in the urine (haematuria) and a fever. Although only 1 in 200 UTIs progress to the kidney, these infections are associated with a greater risk of kidney failure, renal scarring or, in a small number of cases, fatalities [21]. UTIs can be further classified as either complicated or uncomplicated. The former refer to cases where metabolic, functional, or structural abnormalities of the urinary tracts, such as diabetes, reflux or ureteral stones, have augmented the infection [22]. Uncomplicated UTIs can be found in otherwise healthy patients. For the purpose of this work, the main focus will be put on acute, recurrent uncomplicated cystitis.

Table 1.1 – Categorisation of urinary tract infections depending on their site, frequency, symptoms caused or association with predisposing factors. Based on [23].

Classification of UTIs		
Anatomy	Upper	Pyelonephritis Ureteritis
	Lower	Cystitis Urethritis Bacteriuria
Complicating factors	Uncomplicated	Structurally and functionally normal
	Complicated	Structural/ functional abnormality
Time of persistence	Acute	Lasts less than 3 months
	Chronic	Lasts longer than 3 months
Frequency of occurrence	First time	One time UTI
	Sporadic	1 UTI ≤ 6 months
	Recurrent	1 UTI > 6 months
Type of recurrence	Re-infection	UTI caused by a different species than the one causing a previous episode
	Relapse	UTI caused due to the same pathogen, as the last infection
Symptoms	Asymptomatic	Bacteriuria
	Symptomatic	Cystitis Pyelonephritis

1.2.2 Prevalence and recurrence

UTIs are the second most common human infectious disease that can be acquired both nosocomially or within the community. Hospital acquired UTIs account for ~40% of all healthcare associated infections in the UK. The vast majority of these (~80%) arise due to catheterisation [24-27]. Community acquired UTIs account for ~1-3% of all general practice visits in the UK, and cost healthcare ~£172 million each year [28-30]. The estimated general prevalence of asymptomatic bacteriuria is 3.5% and increases linearly with age [20, 31]. Conversely, the

frequency of symptomatic acute infections is highest in women of reproductive age (15-29 years old) with a 20% risk of infection, as compared to other groups between 0 and 80 years old. It is estimated that ~40% of women will experience at least one UTI in their lifetime. Recurrence is frequent, with 44% of patients experiencing at least one further episode within a year and 27% of recurrence occurring within 6 months of the initial infection [20, 31-34]. What's more, untreated UTIs can lead to sepsis, 25% of which result in morbidity [35]. However, since UTIs can be asymptomatic and self-resolving, often they are not reported. The true incidence, therefore, is expected to be greater.

UTIs among males aged 20-60 are uncommon (less than 1% prevalence) and mostly due to underlying urological pathologies, such as benign prostatic hyperplasia, bladder stone or tumour [36, 37]. Other potential risk factors among young men are lack of circumcision, or having a partner who has vaginal colonisation with P-fimbriated bacteria [19]. The divergence in the incidence of UTIs among men and women is mainly due to differences in anatomy. The close proximity of the urethra to the vaginal cavity and anus, both being rich sources of bacteria, increases the chance of pathogen transfer during sexual intercourse putting women at greater risk of infection [31]. Bacteria are usually washed away during micturition, but as the female urethra is 4 to 5 times shorter than in males, there is a shorter distance to cover by a pathogen to reach the bladder. Infections are also more likely to happen in people with impaired renal function and end-stage renal disease as a result of decreased output of urine, which helps to clear bacteria from the system, and the inability to concentrate urine among this group of patients, resulting in hypo tonic urine that may be inhibitory on some uropathogens [38-40]. Other risk factors include genetic predisposition, vaginal infection, and sexual activity [25].

1.2.3 Etiology and therapy

UTIs can be caused by Gram negative or Gram positive bacteria and certain types of fungi, such as *Candida* spp. However, the main causative agent of both community- and hospital-acquired infections is *Escherichia coli* (*E. coli*), which can cause up ~77% of all UTIs. A small percentage of UTIs are caused by *Klebsiella pneumoniae*, *Staphylococcus aureus, Staphylococcus saprophyticus*, *Enterococcus faecalis*, *Proteus mirabilis*, group B *Streptococcus*, and *Pseudomonas*

aeruginosa (Figure 1.2) [25]. Since infection with these pathogens is less likely, typically the treatment approach is an empirical antibiotic therapy. These are often supplied without supporting information from urine culture or dipstick tests to verify the microbiological cause of patient's symptoms [29]. Trimethoprim and ciprofloxacin are the first choice antibiotics to use in treatments of uncomplicated community-acquired UTIs in U.K. For many years small doses of trimethoprim (100mg) were found useful also in continuous (a six-month trial), or post-coital (within two hours of intercourse) prophylaxis of recurrent infections [41]. But following the steady increase in the spread of microbial resistance to the drug, poorer treatment outcomes slowly emerge with their use. Consequently, alternative antimicrobial agents need to be considered, though the choice is not necessarily clear-cut due to costs and an uneven spread of resistance to these drugs [42-45].

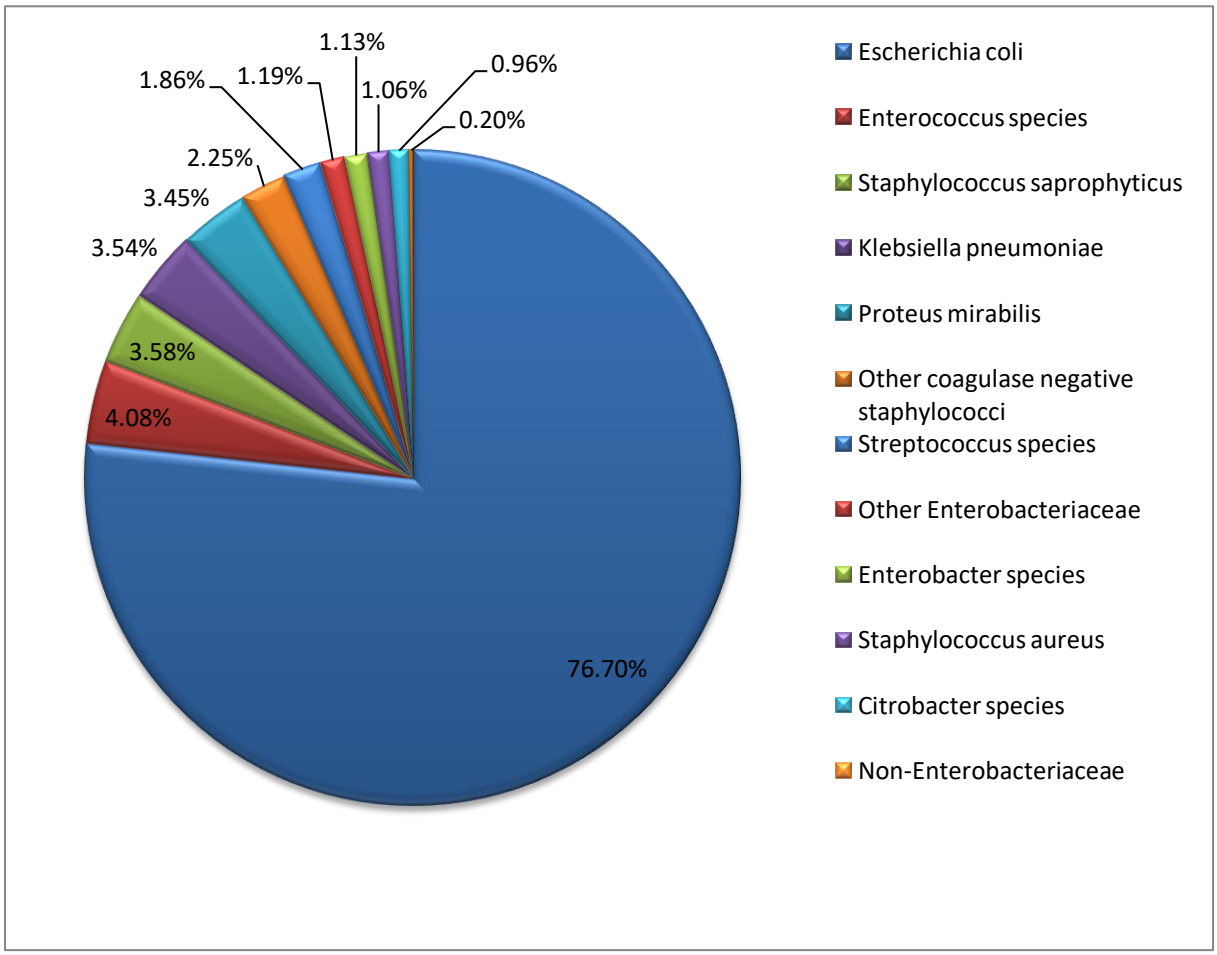

Figure 1.2 – Aetiology of community acquired UTIs in nine European countries and Brazil. The proportions of infections caused by particular organisms or groups of organisms is presented in percentages. Based on: [46].

1.3 Uropathogenic *Escherichia coli*

E. coli are rod-shaped, Gram negative facultative anaerobic bacteria commonly found in the environment and in animal hosts, where they form part of the commensal flora of the intestines. Pathogenic *E. coli* can be divided into diarrheagenic strains that are mostly associated with gastroenteritis and generally lack the ability to cause disease outside of the gut, or extraintestinal pathogenic *E. coli* (ExPEC), predominantly associated with infections in other niches, such as the blood or central nervous system [47]. Uropathogenic *E. coli* (UPEC) which cause infections of the urinary tract are classified as ExPEC.

Bacterial strains can be further discriminated by using various typing methods, such as phenotyping, serotyping or genotyping. Many epidemiological studies, to track the spread of infections, use a method called multilocus sequence typing [48]. Genomes of bacterial isolates are sequenced, and each variant of multiple housekeeping genes is designated as a different allele. The set of variants describing the isolate's profile is referred to as sequence type (ST). Out of 300 UPEC isolates obtained from the North West England, over 50% were represented by 6 STs: ST73, ST131, ST69, ST95, ST10 and ST127. These isolates exhibit high antibiotic resistance, carry a high number of virulence genes and are still evolving, signifying a major health threat [35, 49, 50].

1.3.1 Virulence factors

Virulence factors facilitate the effectiveness in causing diseases or adapting to new niches by bacteria. It's the ability to accumulate and express such virulence-associated genes that distinguishes pathogenic from the commensal bacteria. When encoded on mobile elements, like plasmids, transposons, bacteriophages, or pathogenicity islands, virulence genes can be acquired by bacteria via horizontal gene transfer and inserted into the core genome or plasmid [47, 51]. There is a broad spectrum of virulence traits reported to be associated with UPEC's pathogenic nature. In 1986, it was first discovered that these virulence genes tend to group together into large (10-200kb) clusters that were later called pathogenicity islands [52-54]. Variation in the number of pathogenic islands and the virulence genes they encode is the major source of genetic

and phenotypic divergence between UPEC strains in terms of their virulence [52, 54]. The major virulence traits found in UPEC strains have been described in this section.

1.3.1.1 Toxins

Haemolysin and cytotoxic necrotising factor-1 (CNF-1) are the most widespread UPEC-associated toxins. At least one copy of the *hlyCABD* (haemolysin) operon can be found in ~30-50% of UPEC strains with a higher prevalence among those associated with pyelonephritis. The expression of haemolysin is associated with increased invasiveness in UTI patients. While the gene is found in ~40% of bacteraemia and miscellaneous extraintestinal isolates, it is encoded by only ~15% of faecal isolates [47, 55-57]. The haemolysin operon consists of the *hlyA,* precursor of the extracellular cytolytic toxin, *hlyC,* an acetylase required for *hlyA* maturation, and *hlyBD* encoding proteins which form a secretion system [58]. HlyA can cause lysis of erythrocytes and epithelial cells, leading to a release of nutrients from the cytosol [51, 59]. Sublytic concentrations of HlyA were found to result in changes in the host signalling pathways, including induction of oscillations of calcium ions and inhibition of the activation of Protein Kinase B (Akt) [51, 58]. While calcium oscillations have been shown to induce release of chemokine and cytokine, such as interleukin (IL)-8 and IL-6 from renal epithelium, Akt is a key regulator of epithelial cells survival, proliferation, metabolism and inflammatory responses [58, 60, 61].

The toxicity of CNF-1 exotoxin is associated with its ability to constitutively activate Rho and Rac GTPases and/or Cdc42. This induces a profound reorganisation of the actin cytoskeleton and modulates inflammatory signalling pathways [47]. Prolonged activation of Rho leads to its degradation. That, together with its temporal hyperactivity stimulate apoptosis of bladder epithelial cells and their exfoliation, leading to exposure of the underlying layers of cells to invading pathogens for further rounds of infection. Just like the *hly* genes, the presence of *cnf1* is more prevalent among UPEC (~30% of UPEC strains, including a cystitis strain UTI89), than faecal isolates (~1%) [47, 55, 57]. The co-occurrence of specific virulence genes was found to predestine *E. coli* to reside in a particular niche (rectal, periurethral, urinary), or undergo a specific pathogenesis process. The genes encoding *hly* and *cnf1* virulence factors frequently co-occur due to their integration in the same pathogenicity island, but they were also found to be an integral part of several signature patterns associated with uropathogenicity of *E. coli* [57].

1.3.1.2 Immune evasion

UPEC operate several strategies to subvert, resist or suppress host defences [51]. One such subversion mechanism involves bacterial invasion of urothelial cells. Residing inside host cells shields the bacteria from the phagocytic activity of neutrophils [59, 62, 63]. During this process, a portion of bacteria undergo a non-septated growth leading to their filamentation up to 70μm in length. Macrophages and neutrophils preferentially engulf bacillary (1-2μm long) forms of bacteria. Thus filamentous UPEC which are 30 times longer, are more successful at evading detection by macrophages upon escape from host cells [63-65].

Unlike laboratory *E. coli* strains, UPEC were found to be able to attenuate early production of cytokines by urothelial cells, and inhibit neutrophil recruitment [66]. UPEC does so in response to for example neutralisation of the effect of toxins (such as α-haemolysin, or CNF-1) on neutrophilic activity and NF-κB [67-70]; UPEC also induce production of anti-inflammatory molecules, such as indoleamine 2,3-dioxygenase that suppresses neutrophil migration [71, 72], and inhibits NF-κB activity (and therefore cytokine production) by stabilising NF-κB inhibitor [66, 73-75].

1.3.1.3 Adherence

Attachment to host epithelium by UPEC is believed to be a necessary step preceding bacterial invasion and colonisation [27]. Type 1 and type P fimbriae, encoded by *fim* and *pap* operons respectively, are the most commonly utilised adhesive organelles () [50, 55]. P type fimbriae are mostly associated with pyelonephritis-causing UPEC strains, and consist of six types of protein subunits: PapC, PapA, PapK, PapE, PapF, and PapG (Figure 1.3) [76, 77]. The most distal protein subunit PapG, is a capping protein that recognises kidney-specific glycosphingolipids containing the Gal-α(1-4)β-Gal moiety. Around 90% of pyelonephritis-causing strains contain genes for this type of pili, and 70-80% of them expresses its adhesive properties [78]. The expression of P fimbriae has been shown to be environmentally regulated and subject to phase variation [79-81].

Unlike the *pap* operon, the *fim* operon can be found in almost all (91%) UPEC strains [82]. It encodes four proteins (FimA, FimF, FimG, and FimH) that give rise to a type 1 pilus [76, 77]. FimH is a mannose-binding protein found at the tip of the fimbrial fibre (Figure 1.3a). FimH

targets a vast range of mannosylated proteins, such as uroplakin 1a, which is an abundant, differentiation dependent glycoprotein specific to urothelium, and serves as a major receptor for the FimH attachment. *In vitro* assays showed that strains with knocked out *fimH* gene were found non-invasive, while *in vivo* experiments demonstrated deficient colonisation of mice bladders by these strains [83, 84].

Table 1.2 – Adherence traits found in three *E. coli* strains: uropathogenic cystitis strains UTI89, pyelonephritis strain CFT073 and non-pathogenic laboratory strain K12 MG1655. The + or – signs indicate the presence or absence of a particular gene respectively. Double + indicates two copies of the gene. nf signifies the presence of a non-functional gene. Adapted from: [47, 85, 86].

Adherence genes	**UTI89**	**CFT073**	**K12 MG1655**
fim (type 1)	+	+	+
pap (P)	++	+	-
sfa (S)	+	-	-
foc (F1C)	-	+	-
yad	+	+	+
auf	nf	+	-
yfc	+	+	+
yqi	+	+	+
yeh	+	+	+
fml	nf	+	nf
ycb	+	-	-
sfm	-	-	+
EHEC-pilus	-	-	-
yra	-	-	+

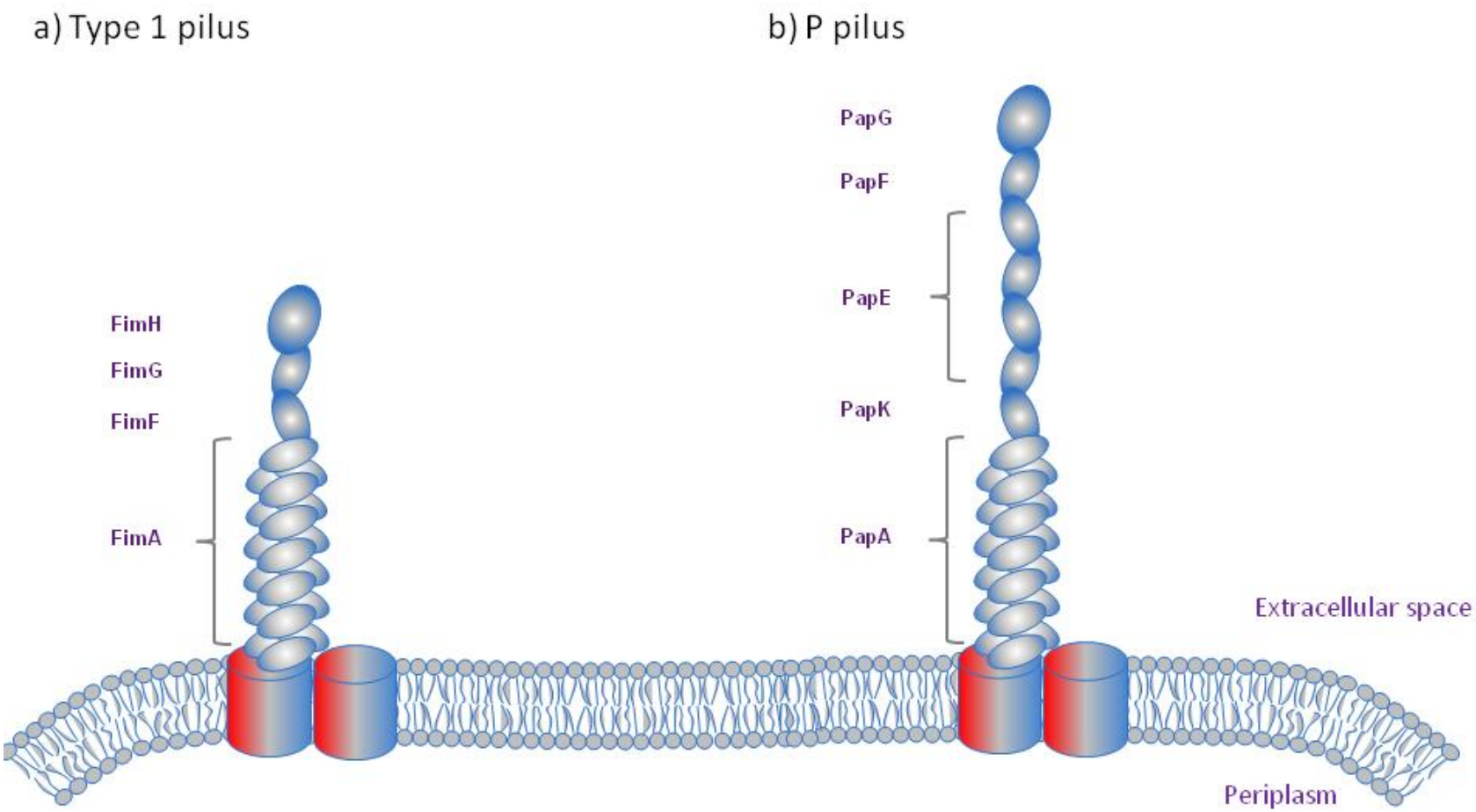

Figure 1.3 – A simplified schematic representations of (a) Type 1, and (b) P pili. Pilus' rod assembled by a Fim system consist of ~1000 subunits of FimA proteins. Its tip consists of singe units of FimF, FimG and a mannose binding cupping protein FimH. Similarly, rod of P pili consists of more than 1000 PapA subunits. The tip of P pili is longer than that of type 1. Between single units of PapK and PapF, 5 to 10 PapE proteins can be found. The tip is cupped with PapG. The usher assembly platforms embedded in outer membrane (FimD and PapC) are red tinted. Based on [76, 77].

1.3.1.4 Iron acquisition

Iron is an integral part of many proteins, enzymes and cofactors essential for normal functioning of prokaryotic and eukaryotic organisms. Nevertheless, while its concentration within body fluids averages around 10^{-25}M, the cytoplasmic concentration required by bacteria is equivalent to 10^{-6}M. This difference results in a competition over limited iron availability in urine between a pathogen and host. As a result, UPEC utilises a range of iron scavenging proteins, such as enterobactins to enhance iron acquisition. These secretory proteins show a high affinity for insoluble ferric iron, Fe^{3+}, which is then retrieved and concentrated by bacteria [47]. To counteract these actions, the enterobactin-binding proteins, lipocalin 2, and other siderophores called transferrins are produced across urinary tracts. Studies have shown that knocking out lipocalin 2 in mice severely impairs their ability to clear the bacterial urinary tract infection [87, 88]. Genomic analysis of UPEC isolates, including UTI89, and pyelonephritis strains CFT073 and J96, showed that the prevalence of genes associated with iron scavenging, toxins and the production of type 1 and P fimbriae (Table 1.2), associated with host cell colonisation, is variable between strains [47, 85, 89, 90].

1.3.2 Pathogenesis of uropathogenic *Escherichia coli*

Due to the difficulties associated with infection-inducing human challenge experiments using human subjects [91], the pathogenic cycle was inferred using a combination of cell line and animal experimental models. The urinary tract infection is initiated upon transfer of pathogens from the periurethral area to the urethra, which is subsequently colonized. Bacteria ascend towards the bladder, where they can cause cystitis. Bacterial entry into urothelial cells can then take place in a type-1 pilus dependent manner. Type-1 pili bind mannosylated uroplakins, which are abundant on the luminal surface of urothelial cells (Figure 1.4) [83]. The interaction specifically between the FimH adhesion and UP1a or UP1b induces localised reorganisation of host's actin cytoskeleton and cell membrane facilitating bacterial entry into urothelial cell [78, 83]. Once inside, *E. coli* can break out of the phagocytic vacuoles, entering the host cell cytosol. Animal models suggest that this happens within 4h of bladder cell internalisation [92]. UPEC rapidly replicate to form clonal biofilm-like structures, referred to as intracellular bacterial communities (IBCs). Early IBCs are amorphous in structure [93], but over the course of time as

bacteria continue to divide IBCs undertake a more defined, compact and organised 3D architecture (mid-IBC). In the final stage, IBCs occupy a large portion of the cytoplasmic space, causing a visible bulging of the host cell membrane into the lumen of the bladder (late-IBC) (Figure 1.4). Bacteria eventually flux out of the epithelial cell, where they can bind to and invade neighbouring epithelial cells, and start the whole cycle all over again [63] (Figure 1.4). Some studies have indicated that a portion of fluxing cells adopt a filamentous form, a phenomenon likely to take place in response to host factors. Filamentous bacteria have been shown to be more resistant to neutrophil attacks than rod-shaped bacteria, hence having a survival advantage during the pathogenic cycle [63, 92]. In spite of robust host responses, some intracellular bacteria can become dormant, forming an alternative pathway to the pathogenic cycle (Figure 1.4). Idle bacteria, referred to as quiescent intracellular reservoirs (QIRs), are believed to act as seeds for future recurrent infections, when the conditions become favourable [26, 63, 84, 94, 95].

1.4 Host responses to UTIs

Normally, constitutive host defences, such as low pH, osmolarity, composition (presence of salts, urea, and organic acids) and shear flow of urine provide adequate defence against bacterial colonisation [51, 96, 97]. However, because the adaptive immune responses within the urinary bladder are limited, any failure in the constitutive defence can leave the innate immune system as the primary defensive mechanism against bacterial colonisation [98, 99]. Cellular components of innate immunity comprise of uroepithelial and immune cells. The latter include neutrophils, that migrate to the bladder from blood, mast cells that reside in the lamina propria, and macrophages found in submucosa [100, 101]. Recent reports suggest that there is additional involvement of dendritic (antigen presenting) cells and natural killer cells, which play a major role in viral clearance [100]. But it is still unclear to what extent do these contribute during bacterial clearance [100, 102, 103]. Most bacterial elimination is achieved by neutrophil phagocytosis [63]. The process is accompanied by release of reactive oxygen species that, when an excessive neutrophil response is elicited, can damage bladder tissue due to their cytotoxicity [104]. For the purpose of this work only responses elicited by epithelial cells will be described.

1.4.1 Signalling in response to UPEC recognition

Upon UPEC making contact with urothelial cells, pattern recognition receptors such as toll-like receptors (TLRs) are triggered. These include TLR2, TLR5, TLR11 and TLR4, and their triggering induces a rapid pro-inflammatory response [100, 105]. TLR4 plays an essential role in superficial bladder cells where it is abundantly expressed on their apical surface and in intracellular compartments, such as $Rab27b^{+}$ membranes [106]. Lipopolysaccharides (LPS), or direct interaction with bacterial fimbriae can trigger TLR4. Activation of TLR4 induces a cascade of events leading to production of chemokines, the main one being IL-8, which is involved in the recruitment of polymorphonuclear leukocytes [107, 108].

Others include members of CXC- [109, 110] and CC-chemokine families. Especially CXCL1 and CCL5 ligands of the chemokine receptor CXCR2 and CCR5 play important roles in attracting neutrophils [100, 111-113]. TLR4 also results in the release of the pro-inflammatory cytokines interleukin (IL)-6 [114], IL-1β and tumor necrosis factor-α. While many of these pathways are activated via a classical MyD88-dependent NF-κB pathway [115, 116], TLR4 was found in human bladder epithelial cells to induce IL-6 via a more rapid, non-canonical response involving calcium, cAMP, and cAMP-dependent response element- binding protein [114]. Employment of multiple signalling pathways for immune cells recruitment that operate at different speeds is advantageous in case bacteria were able to suppress one of the responses.

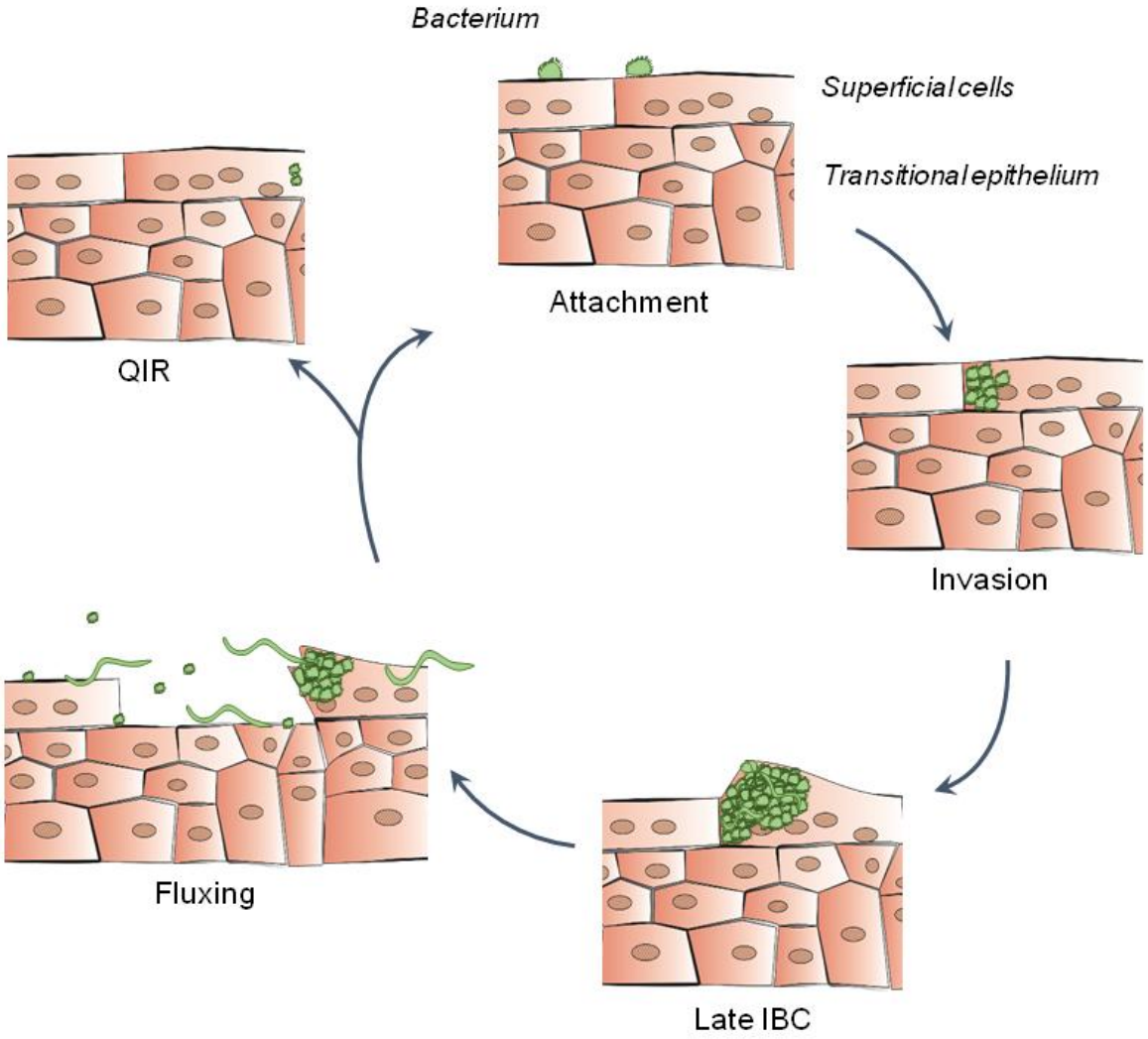

Figure 1.4 – Pathogenic cycle of UPEC. Each stage of UPEC infection starting with bacterial attachment was depicted, and consecutive steps are indicated by grey arrows. Loss of the superficial cells sets the stage to two potential bacterial fates: expulsion or stay in epithelial cell's cytoplasm. Source: [117].

1.4.2 Intracellular UPEC expulsion

Bladder epithelial cells have a number of mechanisms in place to efficiently expel bacteria when facing their invasion. To accommodate changes in stretch that determine whether the bladder fills up with urine or undergoes voiding, superficial bladder cells change their surface area by use of exo- and endocytosis. Bacteria hijack Rab27b$^+$ endocytic vesicles to gain access to the inside of epithelial cells. During the interaction with the host-cell membrane, TLR4 triggers a cascade of events that leads to an immediate increase in cytoplasmic cAMP levels and activation of MyRIP-mediated exocytosis of Rab27b$^+$ vesicles, preventing bacteria entering the host cell [114, 118, 119]. Despite these mechanisms, some bacteria are still internalised. This prompts TLR4 localised on the Rab27b$^+$ membrane to mediate a second wave of bacterial expulsion via TIR-domain-containing adaptor protein inducing IFN-β (TRIF) and TRIF-related adaptor molecule that normally are responsible for hormones transportation [100, 106, 115, 120].

Pathogens that successfully evade expulsion have been shown to break out of Rab27b$^+$ vesicles activating an autophagosomal system to capture bacteria and transport them to lysosomes for degradation. UPEC, unlike laboratory *E. coli* strains, are able to circumvent being killed by neutralising lysosomal activity. TRPML3 senses the change in lysosomal pH and recognising it as dysfunctional, removes it together with its bacterial load from the cell to maintain homeostasis [121]. Once bacteria have been expelled from the cells, they can be either removed together with urine, or phagocytosed.

1.4.3 Bladder exfoliation

Another effective way of reducing bacterial load within the bladder is via activation of cell death. This mechanism is induced shortly after invasion by type-1 piliated UPEC and results in the interaction of FimH with UP3a that induces a spike in intracellular calcium influx in the host cell, which leads to activation of the intrinsic (mitochondrial) apoptotic pathway. Following translocation of a Bid protein from mitochondria to cytosol results in a cross talk between the intrinsic and extrinsic apoptotic pathways and leads to activation of a caspase-dependent death receptor. Both mechanisms lead to cell apoptosis and detachment from urothelium [94, 101, 122,

123]. Bacteria-containing superficial cells are shed into urine and removed from the system when urine is voided [94, 96, 97].

1.5 Study models and strains

UTIs have been studied using a vast array of *in vitro* and *in vivo* models utilising cultured bladder and kidney cells, zebra fish, swine, and birds, though mouse and cell line models are most abundantly used. Humans are usually studied primarily using population-based studies because biopsies from healthy donors or whole bladders are difficult to obtain. Consequently, urine samples are the main human specimen used [124-127]. Many of these models have been applied to study a number of uropathogens, such as *Klebsiella pneumonia, Enterococcus faecalis* and *Proteus mirabilis* [128-134]. Nevertheless, due to UPEC being the predominant causative agent of UTIs, and its propensity to cause longer lasting infections among women with rUTIs (a result of IBC and QIR formation), it has become the most frequently used model organism for studying rUTIs [135]. The most common UPEC strains used to study pyelonephritis are J96 [89], CFT073 [136], and 536 [137], whereas the most commonly studied cystitis strains are UTI89 [85], and NU14 [82, 138]. Due to the focus of this work on cystitis, UTI89 was chosen as a model organism in this study to allow comparison with the most current literature.

1.5.1 Studies of rUTIs

The fact that *E. coli* can be internalised by bladder epithelial cells has been known for almost 40 years [139, 140]. Within a decade, studies identified that intracellular multiplication of bacteria occurred both *in vivo* and *in vitro* [94]. However, the discovery of IBCs, which are believed to contribute to recurrent urinary tract infections didn't happen until almost a decade later using mouse models [141, 142] that mostly involve C3H and C57BL/6 mouse genetic backgrounds. A combination of trans- and intra-urethral inoculation techniques, catheter assemblies and bacterial loads and inoculant volumes were tested across the years. All in an attempt to optimise the most efficient way of introducing bacteria into the bladder for the purpose of studying ascending UTIs. The results varied in the induction of vesicoureteral reflux and the amount of time the bladder or kidney infections took to resolve [92, 143-151].

In such models peak IBCs are formed by UTI89 at 6hpi [62, 93, 94, 141, 142, 152], a timepoint coinciding with peak neutrophil recruitment to urine [153]. Formation of IBCs in humans was later verified using retrospective studies on human urine samples [95].

In cultured cells, UPEC's adherence to non-phagocytic urothelial cells, colonisation and persistence in both mouse and cell line models have been documented in a number of studies. *In vitro* studies primarily use a 5637 cell line [83, 141, 152, 154]. Binding and intracellularisation rates are approximately 40% and 1% respectively. In spite of bacteria multiplying within cells, and being able to persist for days, IBCs are generally not observed [155]. Instead, the UPEC typically form small clusters that rarely attain the dimensions of IBCs found *in vivo* [141, 156]. Membrane permeabilisation of host cells, or treatment with the cholesterol-sequestering agent, filipin, proved successful in achieving IBC-like structures within cell lines [26, 156], but due to this and other discrepancies there appears to be no good intermediate model that would enhance our abilities to translate *in vitro* studies of rUTIs to animal model and vice versa.

1.6 Conclusions and aims of the study

UTIs are one of the most common infectious diseases in humans, affecting mostly women of reproductive age. Since there is no currently available vaccination to prevent UTI, treatment usually involves an *ad hoc* antibiotic therapy. Nevertheless, antibiotic resistance is on the rise. Despite a growing understanding of the pathogenesis of UTI caused by UPEC, our ability to treat these infections effectively is hindered by clear gaps in our knowledge that deters drug discovery. Therefore, new approaches towards understanding host-pathogen interactions that occur during UTI with a focus on the host response remain an ongoing target. These could help advance translational studies to improve our therapeutic approach to tackling rUTIs.

The objective of the work described in this thesis was to use both mouse models and human cell-lines to study host responses to bacterial pathogens. None of these models have been previously utilised for high-resolution analysis such as genome-wide siRNA screens, or single-cell proteomics to characterise host responses to UTI. Therefore, the aims of this thesis were to characterise novel urothelial cell responses to intracellular UPEC infections. More specifically:

- To characterise responses of the urothelial cells to UPEC infection from whole-genome siRNA screen data *in vitro*.
- To characterise responses in the urothelial cell to intracellular UPEC infection from single mouse urothelial cell data *in vivo*.
- To establish a novel *in vitro* model to analyse infections in normal, human urothelium.

2 Materials and Methods

All reagents were purchased from Sigma-Aldrich (UK) unless otherwise specified.

2.1 Sterilisation of solutions and equipment

For bacterial and mammalian cell culture, all glassware was autoclaved at 121°C for 15min. Media were sterilised at 121°C for 15min. Heat sensitive solutions, such as collagenase, were filter sterilised using 0.2µl pore size syringe filters (Millipore, UK).

2.2 Bacterial strains

The *E. coli* UTI89 strains used for the work presented in this thesis were taken from the frozen stocks found in the S.L.C. Chen Laboratory. The remaining strains were obtained from frozen glycerol stocks in the R. Floyd Laboratory. The list of all the *E. coli* strains and their relevant characteristics can be found in Table 2.1.

2.3 Bacterial culture

Bacterial strains were firstly streaked on to lysogeny broth (LB) (Oxoid, UK) agar plates and grown overnight at 37°C. Single colonies were used to inoculate 5ml of LB in a 50ml Erlenmeyer flask and grown statically for 24h at 37°C. 10µl of the culture was used to inoculate 10ml LB in a 100ml Erlenmeyer flask and allowed to grow for a further 24h. Where appropriate LB agar plates and LB broth were supplemented with antibiotics at appropriate concentrations (Table 2.2). Static incubation induces Type 1 pili production, which was then evaluated using a haemagglutination assay and, where appropriate, phase assay (See sections 2.6) [154, 157].

Following growth for two periods of 24h, bacterial cultures were centrifuged in Eppendorf 5804 benchtop centrifuge at 5000RPM for 7min. The supernatant was discarded, and the pellet was resuspended in cold, sterile Phosphate-buffered saline (PBS). For all *in vitro* and *in vivo* assays, the OD_{600nm} was adjusted to 0.5 with PBS unless otherwise stated.

Table 2.1 – List of bacterial strains and their relevant characteristics

Strain	Relevant characteristics	References
CFT073	Clinical pyelonephritis isolate; No chromosomal resistance	[89]
J96	Clinical pyelonephritis isolate; No chromosomal resistance.	[158]
SLC-6	Clinical cystitis isolate UTI89; No chromosomal resistance.	[85]
SLC-7	K12 substrain MG1655- gut derived, non-pathogenic laboratory strain.	[159-161]
SLC-67	UTI89-*fimH*-Q133K; Contains a point mutation in the FimH mannose-binding pocket that abrogates mannose binding; Kanamycin resistant.	[155]
SLC-154	UTI89 with full *fim* operon knockout (UTI89Δ*fim*); Chloramphenicol resistant.	[84]
SLC-273	TOP10/pSC101; Plasmid carries P2 GFP and tetracycline resistance genes.	S.L. Chen Lab
SLC-282	UTI89 with full *fim* operon knockout (UTI89Δ*fim*); No antibiotic resistance; Derived from SLC-154, generated using a negative selection system; after excision of chloramphenicol; pANT4 with GFPmut3 replaced by sfGFP.	[162]
SLC-295	UTI89/pANT4; Ampicillin and kanamycin resistant, both on plasmid; pANT4 from formerly called pComGFP. Has *LacIq* interrupted by kanamycin gene and *Ptac* driving GFPmut3 expression.	[163]
SLC-478	UTI89-FimH-Q133K; Indigenous from SLC-67, generated by replacing *kan-Prha-relE* cassette with *fimH*-Q133K using a negative selection system; Construction Details CSY1-47-3/pKM208 (UTI89 *fimH:kan-PrhaB-relE*); No chromosomal resistance.	[162]
SLC-719	UTI89 carrying a chromosomal vsfGFP-9, hereafter referred to as the vsGFP.	[164]
SLC-911	Complement for SLC-154, with *fim* operon, P2 GFP and tetracycline resistance found on a plasmid.	S.L. Chen Lab
SLC-67 + pSC101 P2 GFP	SLC-67 strain transformed with pSC101 plasmid containing P2 GFP and conferring tetracycline resistance.	This study
SLC-154 + pSC101 P2 GFP	SLC-154 strain transformed with pSC101 plasmid containing P2 GFP and conferring tetracycline resistance.	This study

Table 2.2 – List of antibiotics used in this work, with corresponding concentrations. Stocks of antibiotics were diluted with water to a final stock concentrations, filter sterilised and stored at -20°C. With the exception for gentamicin, a ready solution bought from Sigma Aldrich (G1397, UK). Antibiotics were added to the appropriate media after its temperature was below 55°C.

Antibiotic	Stock solution concentration (mg/ml)	Solvent	Final concentration (µg/ml)
Ampicillin	50	H_2O	50
Chloramphenicol	20	ethanol	20
Kanamycin	50	H_2O	50
Tetracycline	10	H_2O	10
Gentamicin	50	deionised H_2O	If not otherwise stated 100

2.4 Determination of microbial numbers by colony forming units at OD_{600nm}

To allow later adjustment of bacteria-to-cell ratio, the number of bacteria found in 1ml of PBS at OD_{600nm} when equal to 0.5 had to be defined. To do this, seven 1 in 10 serial dilutions in PBS were carried out for two UPEC strains (UTI89 and UTI89-FimH-Q133K). In total 50µl of each dilution was spotted on LB agar plates, by placing 5×10µl aliquots in separate spots on an agar plate (Figure 2.1b and c). To limit spreading of the spots, the plates were dried at 37°C for 1h just prior to spotting the bacterial suspensions. Once the LB plates dried, they were incubated at 37°C overnight. Colony forming units (CFUs) at the lowest countable dilution were counted then used to calculate CFU/ml in the original sample.

2.5 Plasmid transformation into UPEC strains

For the purpose of multiplicity of infection (MOI) optimisation by using fluorescence-activated cell sorting (FACS), bacterial strains that were not GFP-tagged (UTI89-FimH-Q133K and UTI89Δ*fim*) were transformed with a plasmid carrying a P2-GFP (also known as P2-IRES-tauGFP) construct cloned into a pSC101 backbone (referred to as pSLC-346) to generate a measurable fluorescent signal. The pSC101 plasmid was purified from a 10ml overnight culture of SLC-273 (plasmid donor) in LB using the Exprep Plasmid SV Kit (GeneAll Biotechnology,

South Korea) according to the manufacturer's instructions, except an additional 2min drying step at 37°C was added after the ethanol precipitation to fully remove residual ethanol. Plasmid was then eluted using a 20µl volume of RNAse-free water.

3ml of each of the two strains were grown overnight in LB, at 37°C shaking at 180RPM. The receiver strains were subsequently sub-cultured at 1:100 ratio in 40ml of fresh LB, and further grown for another 3h at 37°C shaking. After the specified time, cells were harvested in a microcentrifuge at maximum speed (5000RPM) for 6-7min. Supernatant was discarded, and bacterial pellet resuspended in 1ml of ice-cold sterile water. Upon completion, cell suspension was topped up to 40ml total volume, and once again centrifuged using the same parameters. The process was repeated twice more. After the 3rd centrifugation cell pellet was resuspended in 100µl of ice-cold sterile water.

10µl of plasmid extract was added to the 100µl of competent cell suspension, gently mixed by pipetting, and cells were electroporated using 1mm gap MicroPulser Electroporation Cuvettes (Bio-Rad, UK) and the following settings: 1800V, 200Ω, 25µF on a Gene Pulser Xcell™ Electroporation System (Bio-Rad, UK). Electroporated cells were plated on LB agar plates supplemented with tetracycline and incubated overnight at 37°C. Transformation was confirmed by checking for GFP production by the bacterial colonies using a fluorescent microscope.

2.6 Assessment of Type-1 piliation

2.6.1 Haemagglutination assay

HA assays were used to assess the level of type 1 pili expression by bacterial strains. FimH is a lectin terminally expressed on the type 1 pili of UPEC. Its mannose binding properties allow bacterial attachment to urothelial cells, and have also been shown to agglutinate guinea pig red blood cells [154, 165-167].

HA titres were measured as described in Hultgren *et al.* [138]. Briefly, 2ml of bacterial cells at OD_{600nm}=1, prepared as described in section 2.3, were harvested in a benchtop centrifuge (Eppendorf, UK) at 6400RPM for 2min. The supernatant was discarded and the pellet was

resuspended in 200µl of PBS forming a bacterial suspension of OD_{600nm}=10. This suspension was used to perform 12 two-fold serial dilutions using 25µl volumes in 96-v-welled plates. Dilutions were performed in triplicate using sterile PBS, and in triplicate using freshly prepared 4% (w/v) methyl α-D-mannopyrannoside (MαDM) solution in PBS, which was used as a negative control.

Simultaneously, 0.5ml of guinea pig blood was resuspended in 9.5ml of sterile PBS, and centrifuged at 3000RPM for 3min. The supernatant was discarded and red blood cells (RBCs) were resuspended in PBS. If the supernatant was not clear (i.e. red), additional PBS washes were done until the supernatant had no visible red colour. Washed RBCs were resuspended in 12ml total volume of PBS and 25µl aliquots were added to wells of a 96-v-welled plate that already contained bacterial solutions. Plates mixed by gentle tapping them were covered and incubated overnight at 4ºC to allow clumping of erythrocytes. The HA titre was defined as the last bacterial dilution that showed any visible agglutination. The higher the number the greater the extent of agglutination observed.

2.6.2 Phase On/Off PCR test

Expression of type 1 pili is phase-variable, and mediated by inversion of a DNA switch termed *fimS*, which contains the *fimA* promoter. Transcription of the *fim* operon only occurs when *fimS* is in the ON orientation. The opposite (inverted) orientation is therefore referred to as the OFF orientation. A phase assay quantifies the proportions of bacteria within a culture that have *fimS* in the ON and OFF orientations. The *fimS* phase assay was performed as described previously [157]. In brief, 0.5µl of bacterial culture grown as described in section 2.3 was used as a template for phase PCR**.** Forward (5′-GAGAAGAGGTTTGATTTAACTTATTG-3′) and reverse (5′-AGAGCCGCTGTAGAACTGAGG-3′) PCR primers [157] were used to amplify a 559 base pair DNA element covering the *fim* switch region. All reagents used in this section are from New England Biolabs (UK). The reaction mixture was as follows:

Component	**50µl reaction**
DNA template (bacterial culture)	0.5µl
Reaction buffer 10x	5µl
dNTPs 10mM	1µl
Forward primer (10pmol/µl)	1µl
Reverse primer (10pmol/µl)	1µl
T4 DNA Taq polymerase (5U/µl)	0.25µl
ddH_2O	41.25µl

The reaction mixture was placed in a 0.2ml PCR reaction tube (Qiagen, Germany) in an automatic thermocycler (Bio-Rad, UK). The PCR programme established for the purpose of this reaction was as follows:

Step	**Temperature**	**Time**	**Cycle**
Initial denaturation	95°C	5min	1
Denaturation	95°C	30s	35
Primer annealing	55°C	30s	
Primer extension	72°C	1min	
Final extension	72°C	10min	1
Hold	12°C	∞	

The PCR product was digested with the *Hinf*1 restriction enzyme. The asymmetric location of the restriction site within the invertible switch results in different product sizes and allows comparing the proportions of genes in an ON and OFF orientation. A 20µl reaction was incubated at 37°C for 1h, and analyzed on a 1% (w/v) agarose gel, using the following mixture:

Reagent	**20µl reaction**
Buffer 4 20x	1µl
*Hinf*1	1µl
Template	10µl
ddH_2O	8µl

2.6.3 Agarose gel electrophoresis of DNA

Agarose gel electrophoresis was used to separate nucleic acid molecules resulting from PCR amplification. For this purpose a 1% (w/v) agarose gel (0.6g of agarose + 50ml Tris-acetate-EDTA (TAE) (40mM Tris base (pH 7.6), 20mM acetic acid, 1mM EDTA) buffer) was made by boiling an agarose slurry in TAE until all agarose was visibly dissolved. This agarose solution was allowed to cool to ~60°C, 3µl of ethidium bromide (10mg/ml) was added, and a gel was cast by pouring this into a horizontal gel chamber to cool to room temperature. TAE buffer was used as an electrophoresis buffer. 10µl of samples were mixed with 2µl of a loading buffer, and loaded onto the wells of the gel. Samples, as well as 5µl of a 100bp DNA ladder (NEB, UK) were electrophoresed at 120V for 25-30min. DNA fragments were visualised under UV light.

2.7 Cell lines culture methods

The cell lines used in this work are listed and described in Table 2.3.

Table 2.3 – A list of cell lines used in this work and their corresponding culture media.

Cell line	Description	Culture media
5637 (ATCC HTB-9)	Human urinary bladder grade II carcinoma cell line	RPMI-1640 (Gibco®, UK) cell culture media supplemented with 10% (v/v) Fetal Bovine Serum (Gibco®, UK)
T24 (ATCC HTB-4)	Human urinary bladder transitional cell carcinoma	ATCC-formulated McCoy's 5A with L-Glutamine (Catalog No. 30-2007) cell culture media supplemented with 10% (v/v) Fetal Bovine Serum (Gibco®, UK)
RT4 (ATCC HTB-2)	Human urinary bladder transitional cell papilloma	ATCC-formulated McCoy's 5A with L-Glutamine (Catalog No. 30-2007) cell culture media supplemented with 10% (v/v) Fetal Bovine Serum (Gibco®, UK)

2.7.1 Thawing and seeding cryopreserved cells

Cryovials containing frozen cells were placed in a water bath at 37°C for 1min. Cells were resuspended in 18ml of warm cell culture medium (supplemented with 10% (v/v) FBS) and transferred to a T75 culture flask (Corning, USA). Cells were incubated at 37°C in humidified atmosphere with 5% (v/v) CO_2. After 24h cell culture medium was changed, and then refreshed every 3 days until confluence.

2.7.2 Cell culture and expansion

Cells were harvested prior to reaching 95% confluency to ensure optimum health and good recovery. The culture medium was removed, after which the cells were first rinsed with PBS to remove any traces of Fetal Bovine Serum (FBS), then subsequently incubated with 5ml of warm Trypsin/EDTA for 2min (for T24 cells), or 10min (for 5637 or RT4 cells) at 37°C in a cell

culture incubator. Following three sharp taps, cells were detached, and tryptic activity was neutralized by adding 20ml of an appropriate cell culture medium supplemented with FBS.

Cells were serially subcultured by splitting in a 1:8 ratio for 5637 and T24 cell lines, or a 1:4 ratio for RT4 cells. Cells were grown at 37°C with 5% (v/v) CO_2. The medium was exchanged after 24h and then refreshed every 3 days by aseptic removal of all but 5ml and replacing it with warm, fresh culture medium supplemented with 10% FBS.

2.7.3 Cryopreservation

Cells were harvested from T75 flasks as described in section 2.7.2 and collected by centrifugation in 50ml Falcon® conical tube at 300 times gravity (xg), for 4min at 4°C. The supernatant was discarded and residual medium was used to loosen the cell pellet by lightly flicking the tube. Harvested cells were resuspended in 8ml (for 5637, T24), or 4ml (for RT4) of freezing medium, that consisted of the appropriate (FBS supplemented) cell line culture medium (90% v/v) and DMSO (10% v/v). Cells were then dispensed in 1ml volumes into plastic Corning® cryogenic vials, cooled at a rate of -1°C/min using a Mr. Frosty™ freezing container (Nalgene, UK) and transferred to -196°C liquid nitrogen for storage.

2.8 Culture of normal human urothelial cells

Manipulation of normal human urothelial cells was performed as described in [14]. In total, NHU cells were collected from 49 healthy kidney donors (20 males, 27 females, 2 of unknown sex). Patients ranged between 19-74 (average 46) years old. The samples were obtained with informed consent from the Royal Liverpool University Hospital, UK. For the studies presented in this thesis, proliferating cultures of NHU cells were generated from 45 patients of known sex.

2.8.1 NHU isolation

Normal human primary urothelial cells were isolated from surgical specimens of healthy kidney donors with no history of urothelial cell carcinoma. Directly after extraction, each specimen was placed in a transport medium (HBSS $Ca^{2+}Mg^{2+}$, HEPES 10mM, Aprotinin 20

KIU/ml) and returned on ice to the laboratory within 1h. Under a dissecting microscope the ureter was cleaned of extraneous connective tissue, serosa and fat. The cleaned ureter was bisected, cut into 1cm^2 pieces and transferred into a 15ml Falcon® tube containing 15ml of stripping solution (HBSS $^-$Ca $^-$Mg, HEPES 10mM, Aprotinin 20 KIU/ml, EDTA disodium salt 0.1% (w/v), Penicillin-streptomycin-fungizone 1X) for a maximum of 16 hours (h) at 4°C (or 4h at 37°C). After incubation in stripping solution, tissue segments were transferred into a 6-well plate. Using tweezers and a cell scraper, urothelial sheets were teased away into the medium. The stroma was discarded, while the cell suspension was centrifuged at 250xg for 4min. The supernatant was carefully poured out and the cell pellet was resuspended in the residual medium by gently flicking the tube. Urothelial sheets were further dissociated into single cells using 2ml of Type IV collagenase (HBSS $Ca^{2+}Mg^{2+}$, Collagenase Type IV 100U/ml, HEPES 10mM) at 37°C for 20min. Collagenase activity was neutralised by adding 3ml of Keratinocyte Serum Free Medium (KSFM) completed by supplementation with proliferation factors (KSFMc): human recombinant epidermal growth factor (5ng/ml), bovine pituitary extract (50ng/ml), and cholera toxin (30ng/ml; an attachment promoter). Cells were gently pipetted up and down to disaggregate the remaining clumps, and centrifuged at 250xg for 4min. The medium was gently poured off, the cell pellet was resuspended in the residual medium, followed by addition of 5ml of KSFMc. Cell counts were determined using a haemocytometer, and cells were seeded in T25 culture flasks at 4x10^4 cells/cm^2 and maintained at 37°C humidified incubator with 5% (v/v) CO_2 in air. Medium was replaced after 24h and then refreshed on alternate days.

2.8.2 NHU cell culture and expansion

Cell harvest and subculture was performed when cells were 90% confluent to ensure cells did not become senescent. KSFMc was removed and cell monolayers were briefly washed with calcium and magnesium-free PBS/0.1% (w/v) EDTA and then incubated in 10ml of fresh PBS/0.1% (w/v) EDTA per T75 (4ml per T25) flask for 5min at 37°C. When cells began to round-up, the PBS/0.1% (v/v) EDTA was discarded and 1ml of trypsin 0.25%/EDTA 0.02% per flask was added at 37°C for 1.5min. Cells were detached by tapping the flask sharply and tryptic activity was neutralised with 2ml of 1X soybean trypsin inhibitor (T6414 Sigma-Aldrich, USA)

and 3ml of KSFMc. Cells were transferred into 15ml Falcon® tubes and centrifuged at 300xg for 4min. The supernatant was discarded and the cell pellet was resuspended in the residual medium by gently flicking the tube. Cells were resuspended in 1-5ml of KSFMc and counted using a haemocytometer. At this stage, cells were either further subcultured by splitting 1 in 3 or cryopreserved (See section 2.8.3). The expected yield from T25 is $2x10^6$ cells. For experimental consistency cells were only used up to the third passage.

2.8.3 NHU cryopreservation

Cells harvested as described above (See section 2.8.2) were collected by centrifugation at 300xg for 4min. The medium was discarded, and the pellet was flicked to resuspend in the residual medium, diluted to $2x10^6$ cells/ml using ice-cold freezing medium (KSFMc, FBS, DMSO at 8:1:1 proportions) and dispensed into 1ml volumes in 2ml plastic cryotubes. Confluent T75 flasks yielded an average of 3ml of cell suspension. Cells were cooled at a rate of -1°C/min and transferred to -196°C liquid nitrogen storage using a Mr. Frosty™ freezing container (Nalgene, UK).

2.8.4 Thawing and seeding cryopreserved cells

Cryopreserved cells were transferred to the laboratory on dry ice and thawed rapidly by placing in a 37°C water bath with the lid on. Thawed cells were transferred to a 15ml Falcon® tube containing 9ml of warm KSFMc and centrifuged at 250xg for 4min. The supernatant was discarded and the cell pellet gently flicked to resuspend in the residual medium, then diluted further in 3ml of KSFMc. The cell suspension was seeded into a single T75 flask or divided among three T25 flasks. Cells were maintained as described previously.

2.8.5 Differentiation of normal human urothelial cells

Prior to cell differentiation, cells were preconditioned by growth in stratification-inducing differentiation medium A (KSFMc containing 5% (v/v) FBS) for 4 days. Cell subculture was performed as described in section 2.8.2 with the exception that after the centrifugation step the cell pellet was resuspended in 1-5ml of differentiation medium A instead of KSFMc. Media were

exchanged after 24h and on alternate days. After 4 days of preconditioning in differentiation medium A, cells were detached from the flask, pelleted by centrifugation at 300xg for 4min and resuspended in 2ml of differentiation medium A. Cells were counted and resuspended further in differentiation medium A to allow seeding at 20,000cells/cm^2. After 24h, the media were replaced with differentiation medium B (KSFMc, 5% (v/v) FBS, Calcium chloride 2mM), which induces terminal differentiation, as reflected by high transepithelial resistance [168]. The medium was replenished on alternate days and cells were maintained in differentiation medium B for 7 days, after which time they were ready to use.

2.9 Gentamicin protection assay

A gentamicin protection assay was used to quantify bacterial invasion into epithelial cells. Two variations of this method were used. Method #1, was adapted from Song *et al.,* [118] and gives an insight into bacterial invasion potential, their ability to multiply intracellularly and intracellular persistence. Method #2, however, was based on [83], and allows assessment and comparison of rates at which bacteria can associate with urothelial cells, a step necessary for invasion, as well as rates at which bacteria can invade them. The key differences between the two methods are the time allowed for bacteria to invade urothelial cells (1h in Method #1 and 2h in Method #2) and timepoints. All mammalian cells incubations were done in a humidified tissue culture incubator at 37°C, 5% v/v CO_2.

The number of CFUs found in UTI89 cultures at OD_{600nm}=0.5, and number of CFU recovered from wells at any stage of gentamicin protection assay were determined by performing seven 1 in 10 serial dilutions in PBS (Figure 2.1b), and subsequent plating five 10µl of each dilution on LB agar plates (Figure 2.1c). Plates were incubated overnight at 37°C. CFUs at the lowest countable dilution were counted.

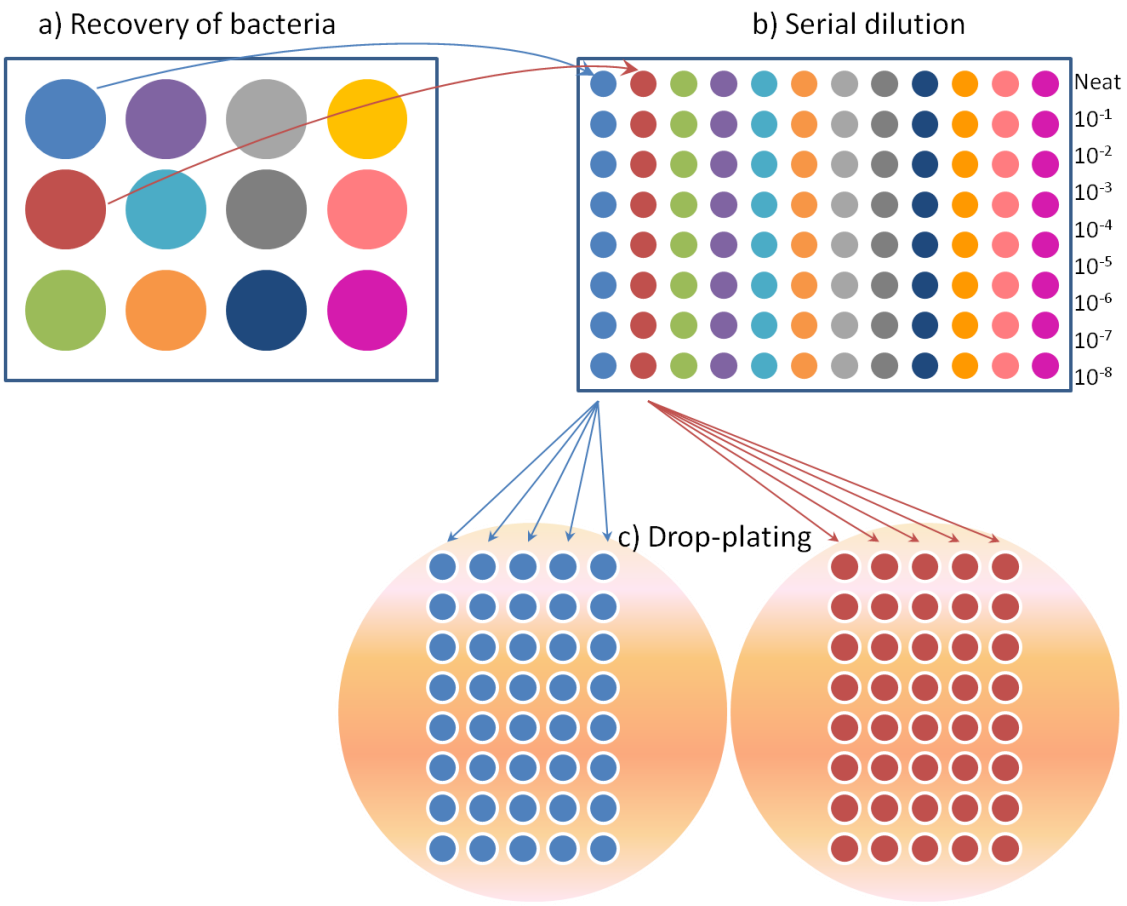

Figure 2.1 – Enumeration of bacterial CFUs. To isolate intracellular bacteria, epithelial cells lining bottoms of wells in multi-welled plates were scrapped to enhance eukaryotic cell lysis (a). A portion of each well's content was transferred to individual wells in a top row of a 96-welled U-bottom plate. It was then used for a series of 1 in 10 dilutions (b), followed by drop-plating on LB agar plates (c). 50µl in total (five 10µl spots) was plated for each dilution.

2.9.1 Method #1

12-well cell culture plates (Corning, USA) were seeded with $7x10^4$ NHU cells/well and differentiated over the period of 7 days as described in section 2.8.5. Cells were washed with Dulbecco's PBS (DPBS) (pH 7.4) (Gibco®, UK) [169] and covered with 1ml of fresh KSFMc medium per well. PBS suspensions of bacterial strains at OD_{600nm}=0.5 were added to each well at MOI of 10. Plates were centrifuged at 600xg for 5min to synchronise bacterial contact with urothelial cells. Cells were then incubated for 1h, after which time the culture medium was removed, cells were washed three times with DPBS and 1ml of KSFMc medium containing 100µg/ml gentamicin was added to each well, and incubated for 1h (Figure 2.2). Gentamicin is a

membrane impermeable antibiotic able to kill all bacteria attached to urothelial cells, as well as the extracellular bacteria, but not those already found intracellularly. Media were then discarded, and cells were washed once with DPBS, and incubated with KSFMc containing 30µg/ml gentamicin for another 1h, 4h, 10h or 22h depending on the chosen timepoint. After the specified time, cells were washed three times with DPBS. All the residual media were removed using a 1ml pipette, and 1ml of 0.1% (v/v) Triton™ X-100 was added per well.

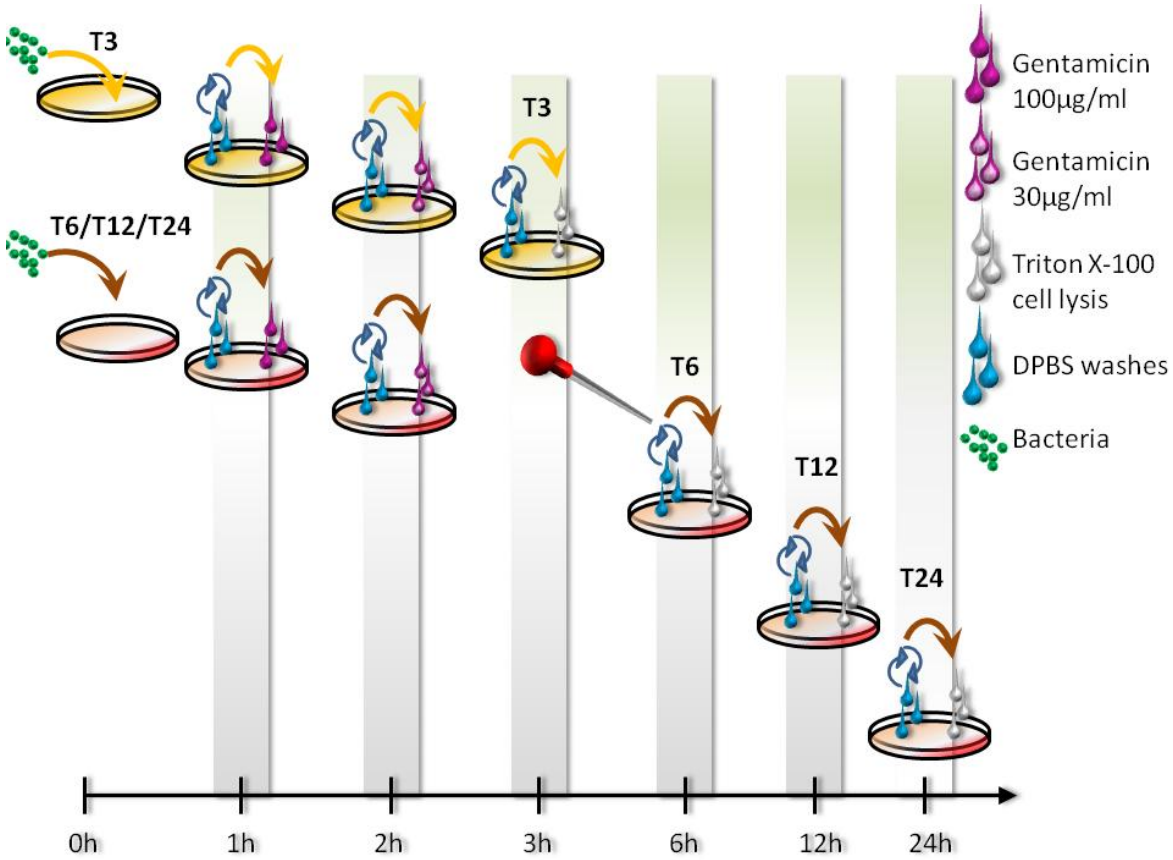

Figure 2.2 – Schematic representation of experimental design of method #1 gentamicin protection assay. Confluent monolayers of urothelial cells grown in multi-welled plates were inoculated with bacteria. Sets of these were designated depending on the time since infection that cell lysis was intended "T3", "T6", "T12" and "T24". An hour after inoculation all cells were washed with DPBS and treated with 100µg/ml gentamicin for one hour. Subsequently, to avoid antibiotic leakage into epithelial cells upon a prolonged exposure, gentamicin concentration was lowered to 30µg/ml, and maintained until the time of intended cell lysis. DPBS washes of cells were performed just prior to removing any residual gentamicin that could potentially kill bacteria upon their release from cells. Triton™ X-100 was used to perform cell lysis to determine the number of bacteria residing intracellularly for different amounts of time.

Plates were then incubated on ice for 10min, following scraping of the wells and vigorous pipetting up and down. Each well's suspension was then serially diluted 7 times 1:10 in a round-bottom 96-well plate in PBS. Each dilution from each well was spotted as described in section 2.4 and Figure 2.1.

2.9.2 Method #2

Three replicate 12-well cell culture plates were prepared with either cell lines or NHU cells as described in sections 2.7.2 and 2.8.5. Cell culture media were removed, and cells were washed with PBS containing calcium and magnesium. Fresh culture media specific for the cell type were introduced, and bacteria at OD_{600nm}=0.5 were added to each well so that the total volume was equal to 0.98ml, and to reach an MOI of 10. Bacteria at OD_{600nm}=0.5 are equivalent to 1-1.5x10^8 CFU/ml (See results section 3.3.3). To synchronise bacterial contact with cells, plates were centrifuged at 600xg for 5min and then incubated in a tissue culture incubator for 2h.

Total bacterial counts were determined as follows (Figure 2.3). After the 2h incubation period, 20µl of 5% (v/v) Triton™ X-100/PBS was added to each well of one plate to lyse cells and release live bacteria into the media. The plate was incubated on ice for 10min. The total number of bacteria was determined by performing a serial 1:10 dilution on media coming from each well and subsequent plating as described in section 2.4 and Figure 2.1.

At this timepoint, bacteria-containing media were removed from the wells in the remaining two plates. One plate was used to quantify cell-associated bacteria (Figure 2.3) by gently washing NHU cells three to five times with DPBS and adding 1ml of 0.1% (v/v) Triton™ X-100/PBS per well. Bacteria recovered from these wells (Figure 2.1) represent a portion of cell-associated bacteria, i.e. intracellular and extracellular attached to the surface of the cells.

Intracellular bacterial quantification was performed by washing NHU cells with DPBS and incubating cells for a further 2h in 1ml of warm cell culture media containing 100µg/ml gentamicin (Figure 2.3). The media was then removed, cells were washed three times using PBS (lack of $Ca^{2+}$and Mg^{2+} speeds up cell detachment), and incubated for 10min on ice with 0.1%

(v/v) Triton™ X-100. Numbers of intracellular bacteria only were assessed as described in section 2.9.1, using 1 in 10 serial dilution and plating (Figure 2.1).

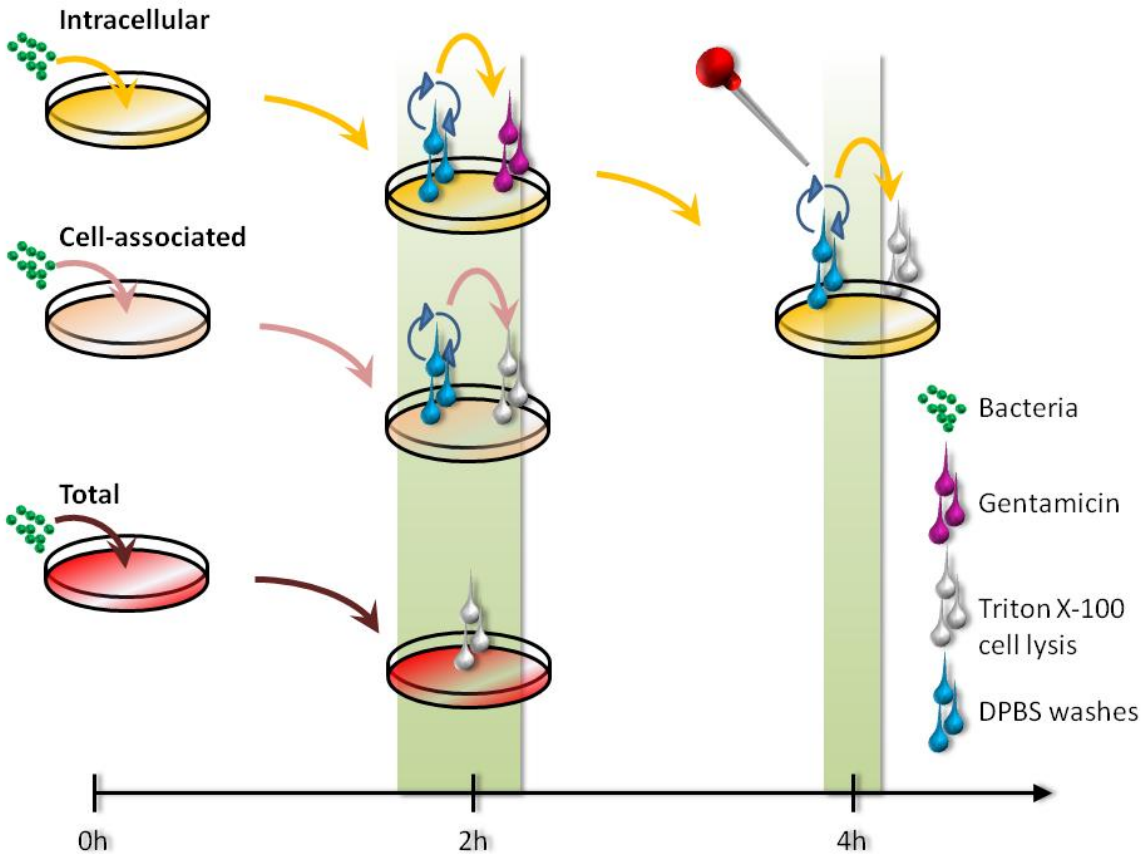

Figure 2.3 – Schematic representation of experimental design of method #2 gentamicin protection assay. Three sets of confluent monolayers of urothelial cells grown in multi-welled plates were inoculated with bacteria. Sets were designated "Total", "Cell-associated" and "Intracellular". "Total" represents the absolute number of bacteria found in a well (cytoplasmic, bound and extracellular bacteria) two hours after the inoculation; "Cell-associated" and "Intracellular" sets were washed with DPBS two hours post inoculation and either lysed to determine the number of bacteria found in cell cytoplasm and attached to their outer surface; or treated with gentamicin for another two hours. Gentamicin-treated "Intracellular" set was used to determine bacterial invasion into the cells.

2.10 Murine UTI model

2.10.1 Ethics statement

All animal experimental protocols were reviewed and accepted by the A*STAR Biological Resource Centre Institutional Animal Care and Use Committee under protocol no. 130853 and performed in accordance with the Singapore National Advisory Committee for Laboratory Animal Research (NACLAR) guidelines.

2.10.2 Preparation of hand-pulled glass capillary pipettes

Glass capillary pipettes were custom-made to facilitate isolation of single infected bladder epithelial cells. Briefly, the middle of an 8cm long glass capillary tube (0.8mm diameter) (Hilgenberg, Germany) was placed over a Bunsen flame to heat up the glass to enable it to be manipulated. The ends of the tube were gently pulled apart to create a fine capillary strand that was shortened as required. The capillary was held using an aspirator tube assembly for microcapillary pipettes (Sigma-Aldrich, USA).

2.10.3 Preparation of mouse catheters

Mouse catheters were prepared as described previously [92]. In brief, a sterile 30 gauge 13mm hypodermic needle (BD Biosciences) was sheathed with Intramedic™ non-radiopaque polyethylene tubing (PE 10) 100' (BD Biosciences), on a 1ml tuberculin Slip-Tip syringe. Catheters were sterilised by irradiation with UV for 5min.

2.10.4 Transurethral

Seven to eight week old female C57BL/6J mice (InVivos, Singapore) were infected as detailed in [92]. In brief, following anaesthesia with isoflurane, mice were transurotherally infected with SLC-719 bacteria using mouse catheters. Bacteria at OD_{600nm}=0.5 are equivalent to 1-1.5*10^8 CFU/ml (See results section 3.3.3). 50µl of bacteria at OD_{600nm}=0.5 was instilled into the urinary bladder, which corresponds to 5-7.5*10^6 CFU. After 6 hours of infection (6hpi) mice were sacrificed, and urinary bladders were aseptically removed and gently washed three times

with sterile PBS in preparation for further processing towards single cell isolation (See section 2.10.5), whole bladder fixation (Section 2.10.6) for immunohistochemical analysis (Section 2.14) or splaying for whole-mount immunofluorescence imaging (Section 2.13.2).

2.10.5 Isolation of single mouse bladder epithelial cells

A diagram summarising the steps used to isolate single mouse bladder urothelial cells is depicted in Figure 2.4. All cells were collected within 30min of mouse sacrifice.

2.10.6 Mouse bladder fixation

Excised mouse bladders were fixed with a view to validate differential expression of proteins of interest by means of immunofluorescencent or immunohistochemical analysis, in either sections of whole organs, or whole mount on stretched bladders. Infected bladders were infected as described in section 2.10.4. Both infected and uninfected mouse bladders were harvested aseptically as described previously [92].

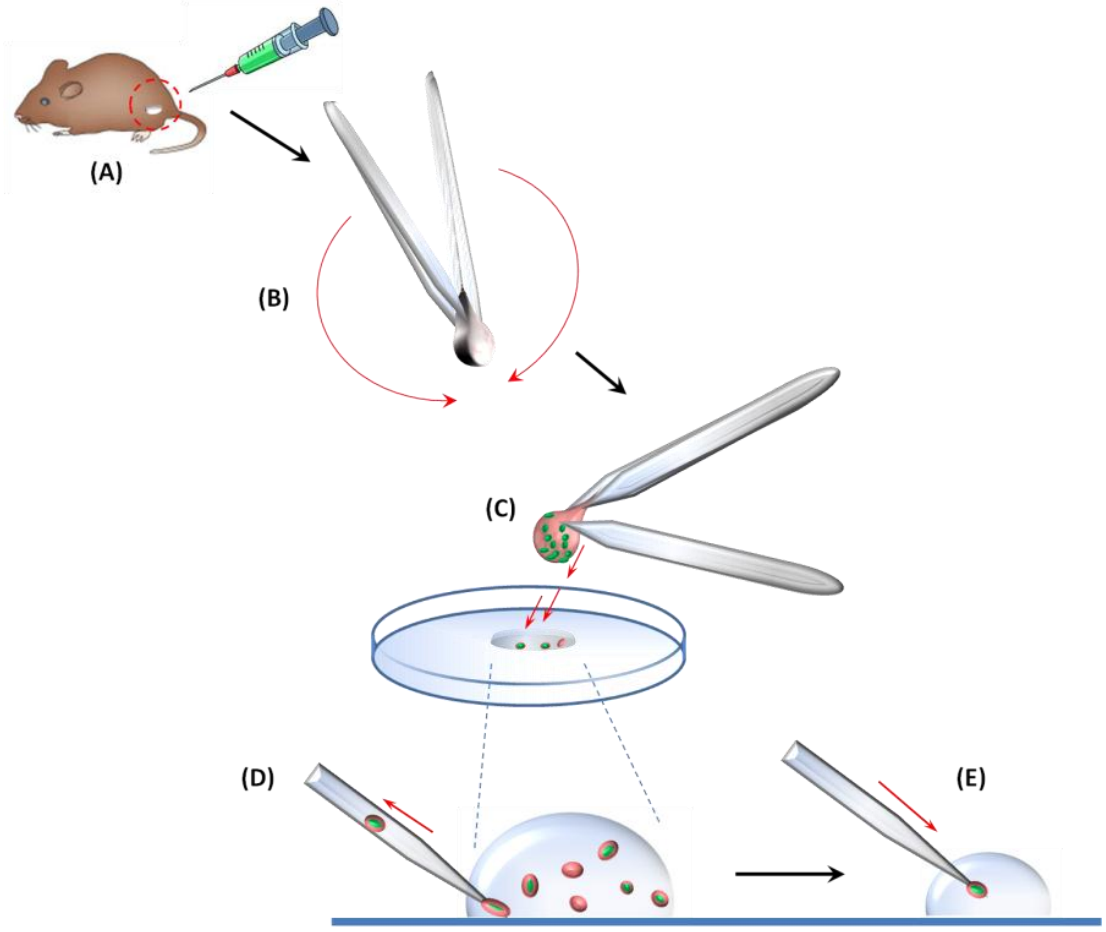

Figure 2.4 – Overview of single urothelial cell isolation from murine urinary bladders.

(A) Where appropriate, mice were transurethrally infected with GFP-producing bacteria, and 6hpi bladders were aseptically removed as described previously [92].

(B) Following PBS (unless otherwise stated) washes, the bladder was inverted inside out using two pairs of forceps and placed in a petri dish in a 1ml PBS droplet.

(C) Suspension of cells were obtained by gently scraping the surface of the bladder using curved, iris forceps (World Precision Instruments).

(D) Infected cells were easily distinguished from uninfected cells by the presence of GFP, which was clearly visible in low-light conditions. Using a dissecting microscope and a hand pulled glass capillary pipette, individual cells were selected and transferred into a droplet of PBS for an additional wash.

(E) Finally, each cell was transferred individually into 0.2ml PCR tubes that were flash frozen in liquid nitrogen and stored at -80°C.

2.10.6.1 Whole bladders

Whole bladders were fixed after PBS washes by incubating them in 4% (w/v) paraformaldehyde (PFA) (pH 6.9) for 20h at 4°C. After the required incubation, bladders were washed with PBS several times, and stored at 4°C in PBS.

2.10.6.2 Stretched bladders

Bladders were stretched as described previously [92]. 6-well tissue culture plates half-filled with silicone elastomer were used for this purpose (Sylgard® 184, Dow Corning, USA). In brief, bladders were bisected across their urethral opening. Tweezers and Minutien pins (0.2 mm base diameter (Fine Science Tools) were used to stretch each half of the bladder to its maximal potential. These steps were done in PBS, to prevent the tissue from drying out before bladders were incubated in 4% (w/v) PFA for 1.5h at 4°C. After this, tissues were gently washed three times with PBS and stored in fresh PBS in 4°C prior to being used for whole mount immunofluorescence (See section 2.13.2).

2.11 Liquid chromatography tandem mass spectrometry

This section presents the strategies used to prepare and process mammalian cell samples for mass spectrometric analysis by liquid chromatography tandem mass spectrometry (LC-Ms/Ms) towards proteomic analysis of single mouse urothelial cells.

2.11.1 Sample digestion

Following extraction and flash freezing of single mouse urothelial cells (Section 2.10.5), individual cells were lysed for 30min at 36°C with 10µl of 9.5M urea/25mM triethylammonium bicarbonate buffer/20mM dithiothreitol. The samples were then alkylated with 40mM iodoacetamide for 30min at RT, and topped up to a volume of 100µL with 50mM ammonium bicarbonate buffer. The proteins were chemically digested overnight at 37°C with 1µg trypsin. The reaction was stopped by acidification of the resulting peptides with 0.3% (v/v) Trifluoroacetic acid.

2.11.2 Sample desalting and cleanup

To maximise the sensitivity of the mass spectrometric analysis, peptide mixtures resulting from protein digest were cleaned up using C_{18} ZipTip® spin (Millipore, USA) according to manufacturer's instructions. Peptides were eluted in 50% (v/v) acetonitrile/0.1% (v/v) trifluoroacetic acid solution. After elution samples were dried in SpeedVac Concentrator (Labconco, USA), and resuspended in 1% (v/v) formic acid/2% (v/v) acetonitrile solution for analysis by LC-Ms/Ms. The entire digested material was further cleaned up using a trap column. This was accomplished using Symmetry C_{18} column (180µm x 20mm; 5 µm particle size, Waters, USA), 2% eluent B (0.1% (v/v) formic acid in acetonitrile) at 8µl/min for 5min.

2.11.3 Separation of proteins

The eluted peptides were separated online in nanoACQUITY UPLC BEH130 C_{18} column (75µm × 200mm; 1.7µm particle size; Waters, USA). The separation flow rate was 0.3µl/min, and the column temperature was maintained at 35°C. The column was equilibrated with eluent A (0.1% (v/v) formic acid in water), and developed with eluent B. The analytical gradient started at 5%, and increased to 40% (v/v) acetonitrile over a 50min period.

2.11.4 Protein identification

To identify and characterise the separated proteins, mass spectrometric analysis was performed on LTQ velos pro-Orbitrap Elite ETD Mass Spectrometer (ThermoFisher, USA). Nanoelectrospray in positive ionization mode (collision-induced dissociation) at 1.8kV was used. The mass spectrometry (Ms) was operated in a top 15 peak data dependent survey scans from 350 to 1600 m/z at a resolution of 120,000. Collision-induced dissociation ion trap tandem Ms scans were acquired with normalized collision energy of 35. Ms spectral data files were subjected to database search using PEAK Studio software version 8.0 (Bioinformatics Solutions Inc., USA). The peptide and fragment ion mass tolerances used were ±10ppm and ±0.5Da respectively. The specified search parameters were carbamidomethylation of cysteine fixed modification, oxidation of methionine, deamidation of asparagine and glutamine as dynamic modification, and tryptic digestion with maximum of 2 missed cleavages. The databases were

combined with Uniprot mouse database with 16718 entries and in-house created *E. coli* UTI89 database with 5211 entries. Protein identity results were filtered by 0.1% FDR and at least 1 unique peptide.

2.12 Analysis of single cell mass spectrometry data

Raw peptide counts used in this analysis were identified as described in section 2.16. Data for individual cells were concatenated using R programming language ver. 3.3.2. R environment was used for all statistical, computational and graphical analysis using default settings unless otherwise stated.

Raw peptide counts were normalised using a pseudo-counted-quantile normalisation available in NOn-parametric Differential Expression for Single cells (NODES) R package [175]. Any residual batch effect was overcome by performing batch-mean-centering. Next, the data underwent t-Distributed Stochastic Neighbour Embedding (t-SNE) reduction of feature using Rtsne package (perplexity=2, check_duplicates= FALSE, pca= FALSE), followed by *k*-means clustering. Differential expression (DE) analysis was performed by between-groups comparison of the average expression of each gene in every group of cells. Cut-off for DE proteins was set to q-values ≤ 0.05 and $\log_2$ fold change ≥ 1. Clustering simulation was done by measuring the consistency of clustering using 1000 iterations of t-SNE embedding followed by *k*-means clustering (using k=3, 4, and 5).

2.13 Immunofluorescent staining

2.13.1 NHU cells containing intracellular E. coli

NHU cells differentiated as described in section 2.8.5 were fixed with 10% (v/v) neutral buffered formalin (NBF) for 1h, washed three times for 5min with PBS, and then stored in fresh PBS. Prior to immunofluorescent (IF) staining, cells were rehydrated by three washes 5min each. All washes in this protocol were done using PBS 0.05% (w/v) Tween 20 (PBST) and shaking in a Belly Dancer® orbital shaker at RT, three times for 5min. Cells were then incubated for 15min with 10µg/ml wheat germ agglutinin (WGA), Alexa Fluor® 555 Conjugate (Invitrogen) in PBST at RT. These conditions were found to give best results out of a range of staining variations tested (Table 2.4). Next, cells were washed, followed by blocking and permeabilisation done overnight in a humidified chamber. A series of optimisation protocols were performed to optimise blocking and permeabilisation steps (Table 2.4 and Table 2.5), these determined that incubating cells overnight with 0.2% (w/v) saponin/3% (w/v) bovine serum albumin (BSA)/0.5% (w/v) milk in PBST at 4°C produced optimum staining (Table 2.6). Same was done for primary antibodies against *E. coli* (Table 2.6). Cells were washed and anti-*E. coli* primary antibodies (B650001R) (Table 2.7) were applied at 1:200 dilution in 0.02% (w/v) saponin/1% (w/v) BSA in PBST 2h at RT. Cells were washed again before applying a secondary antibody (goat α rabbit Alexa Fluor® 488 Conjugate) 1:1000 in PBST for 1h at RT. Following another three washes, cells were incubated in 100ng/ml DAPI/PBST for 30min at RT. Cells were washed and mounted in ProLong® Gold or ProLong® Diamond antifade (ThermoFisher, USA). Samples were left overnight to cure, then put in the fridge at 4°C for prolonged storage.

Table 2.4 – A range of conditions used in finding optimal WGA, Alexa Fluor 555 Conjugate staining conditions towards IF staining of NHU cells. RT- room temperature; WGA- wheat germ agglutinin; BSA- bovine serum albumin; PBST- Phosphate buffer saline with Tween 20.

		1°Ab 1:200 in 0.02% saponin/1% BSA in PBST 2h, RT	Wheat germ agglutinin					
			1µg/ml	5µg/ml	10µg/ml	15µg/ml	10min, RT	20min, RT
WGA, Alexa Fluor 555 Conjugate	Applied prior to permeabilisation	x	x				x	
		x		x			x	
		x			x		x	
		x				x	x	
		x	x					X
		x		x				X
		x			x			X
		x				x		X
	Applied after permeabilisation	x	x				x	
		x		x			x	
		x			x		x	
		x				x	x	
		x	x					X
		x		x				X
		x			x			X
		x				x		X

Table 2.5 – A range of conditions used in finding optimal permeabilisation conditions towards IF staining of NHU cells. RT- room temperature; PBST- Phosphate buffer saline with Tween 20.

Permeabilisation	Triton 0.1% in PBST			Triton 0.1% in 3% goat serum	1°Ab 1:200 in 3% goat serum
	10min, RT	20min, RT	30min, RT	1h, RT	Overnight, 4°C
	x				X
		x			X
			x		X
				x	X

Table 2.6 – A range of conditions used in finding an optimal concentration and condition of primary anti-*E. coli* antibodies towards IF staining of NHU cells. RT- room temperature; BSA- bovine serum albumin; PBST- Phosphate buffer saline with Tween 20.

1°Ab	0.2% saponin/3% BSA/0.5% milk in PBST overnight	1°Ab in 0.02% saponin/1% BSA in PBST 2h, RT			
		1 in 50	1 in 100	1 in 200	1 in 400
	x	x			
	x		x		
	x			x	
	x				x

Table 2.7 – List of primary and secondary antibodies used in this work and optimised dilutions for immunofluorescence experiments

Antibody	Antigen	Host species	Clonality	Dilutions tested	Supplier (Catalogue No.)
Primary antibodies					
Kallikrein 1	Full length protein corresponding to Mouse Kallikrein 1 aa 25-261	Rabbit	Monoclonal	1:500-1000	Abcam (Ab191014)
Proteasome subunit α type 6	Synthetic peptide corresponding to Human Proteasome 20S alpha 6 aa 200-300 (C terminal)	Rabbit	Monoclonal	1:250-500	Abcam (Ab109377)
ACOT1	Synthetic peptide conjugated to KLH derived from within residues 300 - 400 of Human ACOT1	Rabbit	Polyclonal	1:20-40	Abcam (Ab133948)
E. coli 404	A pool of *E. coli* serotypes, associated with urinary tract infections: O18:B21, O44:K74, O112:B11, O125:B15	Mouse	Monoclonal	1:300	Santa Cruz Biotech (SC-66037)
E. coli	All "O" and "K" antigenic serotypes of *Escherichia coli*	Rabbit	Polyclonal	1:200	Meridian Life Sciences (B650001R)
Secondary antibodies					
Alexa Fluor® 488 Conjugate (green) anti rabbit	Pooled human and mouse serum, purified human paraproteins and plasmacytoma/ hybridoma proteins	Goat	Polyclonal	1:1000	Cell Signaling Technology™ (#4412)

2.13.2 Whole mount mouse bladders

Mouse urinary bladders were stretched and fixed as described in section 2.10.6. The bladders were firstly washed. All the washes were done with PBS three times 5min each on a Belly Dancer® orbital shaker. The PBS washes were followed by three washes in PBS/0.5% (v/v) Triton™ X-100 for 30min each time. Tissues were blocked with 1% (w/v) BSA/0.3% (v/v) Triton™ X-100 in PBS for 1 h at RT and subsequently incubated overnight at 4°C with two types of primary antibodies, one being a mouse anti-*E. coli* 404, and another being one of the 3 proteins identified as differentially expressed (Table 2.7), all in blocking solution. Samples were then washed with PBS, followed by three washes 10min each with PBS/0.5% (v/v) Triton™ X-100, before applying two types of secondary antibodies (Goat anti-Mouse and anti-Rabbit) diluted in a blocking solution for 2h at RT. All unbound antibodies were removed during three consecutive washes. Cell nuclei were stained with 100ng/ml of DAPI (30min at RT). Bladders went through a final washing stage before being mounted with Vectashield® mounting medium.

2.14 Flow cytometry

5637 cells were sorted based on a GFP signal coming from GFP-producing UPEC used to infect the mammalian cells. Uninfected cells were used as a negative control. 5637 cells had undergone gentamicin protection assay, as described in Materials and Methods 2.9.2. But only procedures corresponding to intracellular bacterial quantification were followed. Where appropriate, varied MOIs were used. At 4hpi, after cell washes, instead of applying Triton™ X-100, cells were detached by trypsinisation, as described in Materials and Methods 2.7.2. Cell clumps were removed by gravity filtration with sterile 30µm pre-separation filters (Miltenyl Biotec, Germany). Cells were pelleted by centrifugation at 400xg for 6min, and resuspended in 1ml of DPBS. 100µl of this suspension was further diluted in 4ml of DPBS and subjected to FACS sorting and analysis using an S3 Cell Sorter (Bio-Rad, UK) in accordance with the manufacturer's instructions. GFP-negative cells that were exposed to bacteria were assumed to be uninfected, while GFP-positive cells were considered infected. For MOI optimisation studies, 3000 cells per condition were analysed. Desired numbers of cells from each population were

collected to be processed towards Western blot analysis. The strategy applied to FACS gating is described in Figure 2.4. To avoid analysis of cells of a transient physiological state, the focus of this study was only on distinct GFP-positive (region gate R5) and GFP-negative (region gate R6) populations of epithelial cells. For this reason, rigorous gating with a distinct gap separating regions R5 and R6 was used to allow an adequate analysis.

2.14.1 Trypan blue cell viability test

Trypan blue vital staining was performed on FACS-sorted 5637 cells, in order to test their viability at the point of protein denaturation. For this purpose, 5µl of 5637 cell suspension prepared as described in section 2.10 (~3h post tripsinisation), was placed on 24x60mm glass slide (Menzel-Glaser, UK) and mixed with equal part of 0.4% trypan blue solution (ThermoFisher, USA). An 18x18mm cover slip was placed over the cells that were then incubated at RT for 1min. Cells were then immediately imaged using a dissecting microscope. This process was carried out for both GFP-positive and GFP-negative populations of FACS-sorted 5637 cells. Unlike dead cell,s trypan blue does not colour live cells that have intact membranes. Hence, dark blue coloured cells were scored as dead, and cells with bright centers were assumed to be live.

2.15 SDS-PAGE

Extracted proteins were separated by sodium dodecyl sulfate polyacrylamide gel electrophoresis (SDS-PAGE) on 12% polyacrylamide gels for analysis of identified target proteins in the range of ~15-250kDa.

2.15.1 Sample preparation

For each target protein, the number of 5637 cells that were uninfected, or infected with SLC-719 bacterial strain, was optimised to ensure optimal signal resolution. Cell numbers obtained via FACS sorting (See section 2.10) were between $1x10^4$-$1x10^5$. Upon collection cells were centrifuged for 1min at 13200RPM in a bench-top centrifuge (Eppendorf, UK), resuspended in 18-25µl of a 2x Laemmli Sample Buffer (Bio-Rad, UK) supplemented with 335mM 2-

mercaptoethanol (Bio-Rad, UK), and boiled for 5min at 100°C in a heating block. Insoluble material in samples was centrifuged at maximum speed (13200RPM) for 5min. Samples were frozen at -20°C prior to being used for Western blotting.

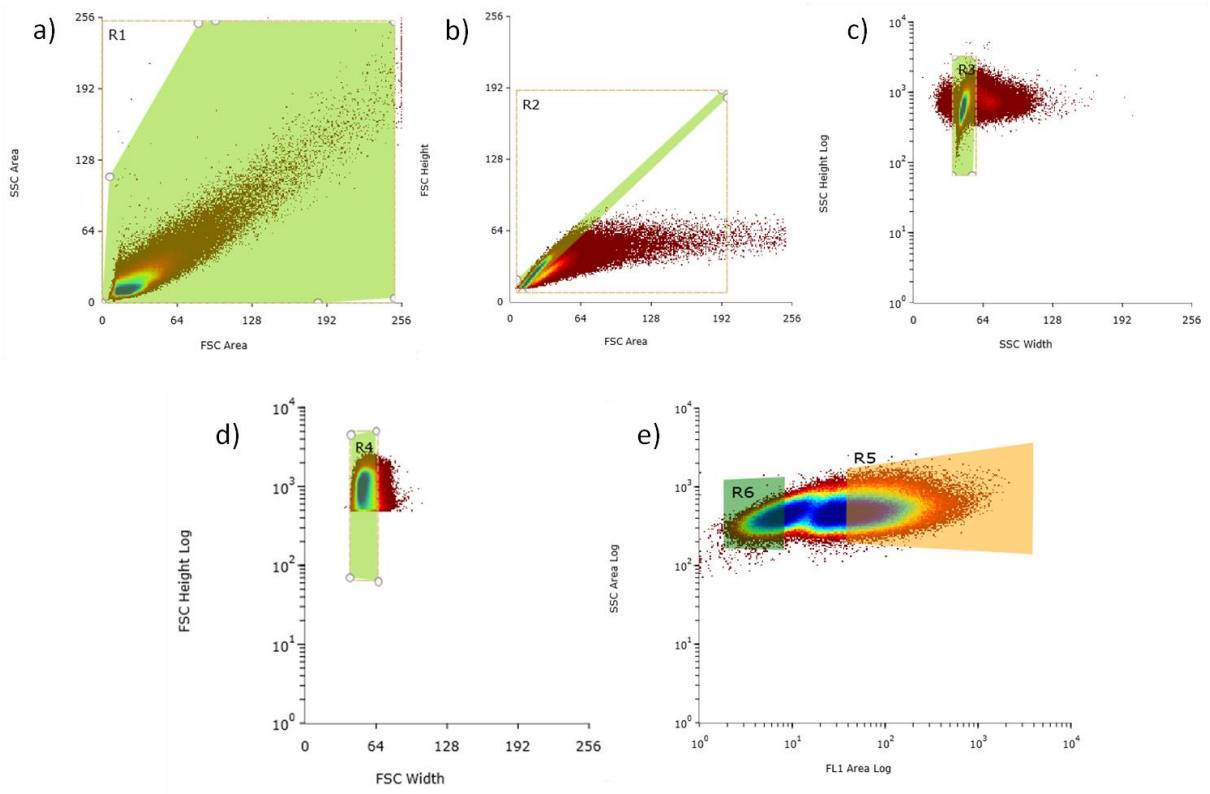

Figure 2.5 – FACS gating strategy. The main cell population was resolved from debris by region gate R1, created on a side scatter area (SSC-A) logarithmic scale versus (vs) forward scatter area (FSC-A) logarithmic scale; (b) Doublets were eliminated using forward scatter height (FSC-H) vs FSC-A by region gate R2; (c) Gating within SSC-Height (log scale) vs log scale SSC-Width (just like FSC-H vs FSC-W plot) was used to exclude doublets and debris; (d) Single cells were isolated by region gate R4 on FSC-H log scale versus FSC-Width (FSC-W); (e) GFP-positive mammalian cells are defined by region gate R5. On the same plot GFP negative cells are defined by region gate R6 on the SSC-A vs GFP fluorescence-Area (FL1-A) plot.

2.15.2 PAGE gel preparation

1mm-thick SDS-PAGE gels were prepared using 12% resolving and 4% stacking gels (Table 2.4) as first described in [170-172]. Resolving gels were prepared and poured to a depth of 5cm between 10x8cm plates with integrated 1mm spacers and a casting module (Bio-Rad, UK), and covered with 1ml of isopropanol to create a flat interface to prevent air interference with the crosslinking reaction. Once the gels had polymerised, the isopropanol was washed away with dH_2O. Stacking gels were poured onto the resolving gels and 1mm thick combs were inserted. Following gel polymerisation, protein samples, along with 7µl of protein ladder (Prestained ExactPro Broad Range (10-245kDa), 1st Base) were loaded into the wells and one-dimensionally electrophoresed for ~1.5h, using a running buffer (Table 2.4). The following settings were used to run 2 gels simultaneously: 3.0Å, 300W and 80-100V.

Table 2.8 – SDS-PAGE reagents

Running Buffer	**1L**
Tris base (pH 8.3)	25mM
Glycine	190mM
SDS	0.1%
dH_2O	Top up to 1L

Stacking Gel	**4ml**
dH_2O	2.70ml
1M Tris (pH 6.8)	0.50ml
30% (w/v) Acrylamide	0.67ml
10% (w/v) SDS	0.04ml
TEMED	0.004ml
10% (w/v) APS	0.04ml

12% Resolving Gel	**15ml**
dH_2O	4.9ml
1M Tris (pH 8.8)	6.0ml
30% (w/v) Acrylamide	3.8ml
10% (w/v) SDS	0.15ml
TEMED	0.006ml
10% (w/v) APS	0.15ml

2.16 Western blotting

Western blot analysis was used to validate differential expression of proteins of interest in pools of infected and uninfected 5637 cells. Following electrophoretic separation (See section 2.11), gels were removed from the cast and washed for 10min in transfer buffer (Table 2.5) to remove excess of SDS. Proteins were transferred onto a nitrocellulose membrane (Bio-Rad, UK) [173] using a wet transfer apparatus set at 100V, 3.00Å, 300W for 1h. The membrane was then blocked with 5% (w/v) milk/Tris-buffered saline (TBS)/1% (v/v) Tween-20 (TBST) (Table 2.5) for 1h at room temperature (RT). Incubations with primary antibodies were performed overnight at 4°C in a Labquake® tube shaker and rotator (Thermo Scientific®). A panel of dilutions was tested for each antibody to optimise incubation parameters. Optimal concentrations are shown in Table 2.6 and Table 2.7. After incubation with primary antibodies, blots were washed three times for 10min each in TBST, followed by a 1.5h incubation at RT with horseradish perodixdase (HRP) conjugated secondary antibodies from an appropriate host (Table 2.7), diluted in blocking solution (Table 2.5). All antibody incubations were performed on a Belly Dancer® orbital shaker. Blots were washed three times for 10min each with TBST and proteins of interest were visualised using Amersham™ enhanced chemiluminescent™ Western Blotting Detection Reagents (GE Healthcare) according to manufacturer's instructions, and imaged using a ChemiDoc (Bio-Rad, UK). Blots were stripped with Western Blot Stripping Buffer (ThermoFisher, USA) for 2h, followed by multiple washes with water, and a final wash with TBST for 10-30min, before reprobing with primary antibodies against the loading control (β-actin). Protein concentrations relative to their loading controls were determined by densitometric analysis using the measure function of ImageJ 1.48v. (NIH, USA).

Table 2.9 – Buffers used for Western blotting:

Tris-buffered saline (TBS) (10x) 1L	
Tris base	24.23g
NaCl	80.06g
dH_20	800ml
HCl	Adjust pH to 7.6
dH_2O	Top up to 1L

TBST	**1L**
TBS 10x	100ml
Tween 20 (10% w/v)	10ml
dH_2O	890ml

Transfer Buffer (10x)	**4L**
Tris base	121.1g
Glycine	576g
dH_2O	Top up to 4L

Transfer Buffer (1x)	**1L**
10x Transfer buffer	700ml
Methanol	200ml
dH_20	100ml

Blocking Buffer 100ml	
Dry milk	
(Sigma- Aldrich, USA)	5g
TBST	Adjust to 100ml

Table 2.10 – List of primary antibodies used in this work and optimised dilutions for Western blot experiments

Antibody	Antigen	Host species	Clonality	Dilution	Supplier (Catalogue No.)
Calpain 1	The large subunit of Human Calpain	Rabbit	Monoclonal	1:500	Abcam (Ab108400)
TCP1 alpha	Synthetic peptide corresponding to residues in Human TCP1 alpha	Rabbit	Monoclonal	1:2000	Abcam (Ab109126)
TCP1 theta	Synthetic peptide within Human TCP1 theta amino acids (aa) 498-548	Rabbit	Polyclonal	1:2000	Abcam (Ab176691)
ENO3	Synthetic peptide corresponding to Human ENO3 aa 400-500.	Rabbit	Monoclonal	1:400	Abcam (Ab157474)
Kallikrein1	Full length protein corresponding to Mouse Kallikrein 1 aa 25-261	Rabbit	Monoclonal	1:2000	Abcam (Ab191014)
Proteasome subunit alpha type 6	Synthetic peptide corresponding to Human Proteasome 20S alpha 6 aa 200-300 (C terminal)	Rabbit	Monoclonal	1:2000	Abcam (Ab109377)
ACOT1	Synthetic peptide conjugated to KLH derived from within residues 300 - 400 of Human ACOT1	Rabbit	Polyclonal	1:500	Abcam (Ab133948)
beta-actin	Epitope located on the N-terminal end of the β-isoform of actin	Mouse	Monoclonal	1:60000	Sigma (A2228)
GFP B-2	Aa 1-238 representing full length GFP (green fluorescent protein) of Aequorea victoria origin	Mouse	Monoclonal	1:4000	Santa Cruz Biotech (sc-9996)

Table 2.11 – List of secondary antibodies used in this work and optimized dilutions for Western blot experiments

Antibody	Antigen	Host species	Clonality	Dilution	Supplier (Catalogue No.)
Anti-rabbit HRP-conjugated IgG	Rabbit IgG	Donkey	Polyclonal	1:2000	ECL (NA934)
Anti-mouse HRP-conjugated IgG	Purified immunoglobulin fractions from normal mouse serum	Sheep	Polyclonal	1:15000	ECL (NA931)

2.17 Immunohistochemistry

Validation of protein targets in mouse bladders were performed using immunohistochemical analysis. Immunohistochemistry (IHC) was performed in accordance to standard operating procedures established at Liverpool Women's Hospital (UK).

2.17.1 Tissue processing, embedding, and sectioning

Whole bladders infected with SLC-719 (extracted 6hpi) and uninfected mouse urinary bladders were aseptically removed and fixed as described in section 2.10.6. Fixed tissue was incubated at 4% NBF for 45min and dehydrated by an increasing series of one hour long ethanol alcohol baths (60%, 70%, 90%, 100%) and two extra washes in 100% ethanol for 1.5 and 2h respectively. Samples were then cleared by three consecutive xylene incubations (for 1, 1.5, and 2h respectively), and impregnated with paraffin wax (Histoplast PE REF8330, Thermo Scientific) during 2.5 and 3.5h wax runs. Each wax block had five bladders embedded. All the processes were performed using the automated Shandon Citadel 1000 and The Shandon Histocentre (Thermo Electron Corporation, UK) machine. A Microm HM335 rotary microtome (Microm) was used to section the paraffin wax blocks at 6µm thickness onto poly-L lysine coated slides (VWR, UK). Rat and human liver tissue samples were a generous contribution from the collection of Dr R. Floyd and used as internal controls.

2.17.2 Slide coating for improved sample adhesion

A 3-Aminopropyltriethoxysilane (APES) (Sigma-Aldrich, USA) coating procedure was used to improve tissue adhesion by producing a positive charge on the surface of the slide. The protocol described below was modified from the original method described by Maddox and Jenkins [174], and was performed using staining racks and glass jars supplied by Raymond A. Lamb Ltd (UK). Slides were dipped several times in absolute ethanol to dislodge dust. Excess solvent was drained using absorbent paper towels, followed by incubation in APES working solution (2% (v/v) APES in absolute ethanol) for 5min. Slides were then rinsed three times with dH_2O (2min each time) and dried overnight.

2.17.3 Antigen retrieval

Prior to IHC staining, samples were dewaxed by heating at 60°C for 1h prior to 2x10min incubations in a clearing agent (xylene). Subsequent rehydration was performed in a decreasing series of alcohol baths (100% (2x5min), 90% (1min), and 70% (1min)) followed by transfer of the samples to dH_2O for 5min. Antigen retrieval was performed to break any protein cross-links by boiling slides for 1min in a pressure cooker (Tefal Clipso Easy 6L) in 10mM sodium citrate buffer (3.15g of citric acid, 1.5 litre of dH_2O) (pH=6), and subsequent cooling under cold running tap water.

2.17.4 Haematoxylin and eosin stain

TBS was used to equilibrate the samples prior to staining nuclei with Gills haematoxylin (6g haematoxylin, 0.6g sodium iodate, 52.8g aluminium sulphate, 690ml dH_2O, 250ml ethylene glycol, 60ml glacial acetic acid) for 1.5min. Staining was followed by sample clearing with a 10min tap water rinse, dip in acid alcohol (1ml of concentrated HCl/100ml 70% ethanol), 5min tap water rinse, and 1min washes with 70% and 95% ethanol. Cell cytoplasm and smooth muscle layers were counterstained by a 4min incubation with eosin stain (0.5g eosin Y, 100ml 96% ethanol, 2 drops glacial acetic acid). Eosin staining could be substituted with probing with protein-specific antibody. Counterstained samples were then rinsed with tap water twice, and then incubated in water for 2min, prior to a 30s wash with 95% ethanol, and two 3min washes with 100% ethanol. Further 5 and 10min washes with xylene were done before mounting sections

with Shandon Consul-Mount (Thermo Scientific, USA). Finally, specimens were photographed and examined at 20x and 40x magnification using a Nikon Fluorescent CSY digital camera.

2.17.5 Detecting specific antigens in tissues

Unlabelled test samples were prepared as described in sections 2.17.1, 2.17.2, and 2.17.3, incubated at RT for 5min in TBS buffer, followed by 10min incubation in 0.3% H_2O_2/TBS. After the appropriate time, and upon removal of excess liquid, two more 5min incubations in TBS were performed. Borders of the tissue sections were marked with DAKO hydrophobic marker pen (Agilent, USA) to prevent excessive spread of antibodies and sample drying. Samples were then probed with a rabbit, A1AT-specific, polyclonal primary antibody (Proteintech Group Inc, 16382-1-AP) at an appropriate dilution in TBS/0.5% BSA diluent. 50µl volume of the primary antibody solution per section was used. Samples were incubated overnight in a humidified chamber at 4°C to allow antibody-antigen binding. A series of dilutions in the range of 1:25 to 1:200 was tested to optimise incubation parameters. Optimal antibody concentration was found to be at 1:200 dilution. The unbound antibodies were removed during two consecutive 5min washes in TBS at RT. Sections were subsequently incubated with ready-to-use ImmPRESS™ reagent containing HRP-conjugated secondary anti-rabbit antibodies raised in goat (ImmPRESS™ HRP Anti-Rabbit IgG (Peroxidase) Polymer Detection Kit, made in Goat) in accordance with manufacturer's instructions. Sections were counterstained with Gills haematoxylin, cleared and mounted as described in section 2.17.4. Specimens were photographed and examined at 20x and 40x magnification using a Nikon Fluorescent CSY digital camera and examined for apparent changes in A1AT expression.

3 Normal human urothelium cell model for studying UPEC infection

3.1 Introduction

3.1.1 The first bladder cell line

In 1917 Burrows *et al.,* were the very first to cultivate bladder epithelial cells from primary biopsies of malignant tumours [176]. Even though they managed to establish only a 'temporary' culture, the idea was built upon by others [177, 178]. All of the following attempts yielded just short-term cultures of human epithelial tumours of bladder origin, until 1967 when Jones managed to maintain epideromoid bladder cancer cells for a period of over 20 months, and 25 passages [179]. The limitation for all of these cultures was primarily due to fibroblast contamination from connective tissue or body fluids, or bacterial contamination. In the former case, the growth rate of epithelial cells progressively slows down, allowing fibroblasts to eventually outgrow them [180]. None of these issues were resolved until specially formulated media that inhibits fibroblasts growth was developed, and sterile techniques were improved [181].

3.1.2 Long-term bladder cancer cell lines

The first long-term bladder-like cell line, RT4, was isolated from a low-grade papilloma from a 63 year old male. RT4 cells expressed some characteristics of native urothelium and had a consistent morphology and growth pattern [182]. Further cultures of primary or metastatic bladder cancers followed in subsequent years: KU-1, T24, J82, SW-780, SW-733, SW-800, 5637, 235J, SCaBER, TCCSUP, HT-1197, HT-1376, UCRU-BL-17CL JMSU1 [183-196]. Despite continuous efforts to establish a uroepithelial cell culture model that would give the best reflection of *in vivo* conditions, bladder cancer cell lines retain abnormal tumour-specific characteristics, such as aberrant karyotypes and multiple genetic mutations, and can potentially display the genetic and phenotypic diversity of the tumour it was derived from [197]. Furthermore, most of these cell lines grow in monolayers, retaining little of the original stratified structure. As a result they lack the molecular and chemical gradients consistent with *in vivo* urothelial cells and generally do not express any characteristics of differentiation [198, 199].

3.1.3 Immortalised bladder cell lines

In later years, new cell lines were established by immortalisation of normal urothelial cells with oncogenic viruses that inactivate tumour suppressor genes [200-202] or disrupt telomerase activity [203]. Unlike many cancer cell lines, these cells failed to grow in soft agar or upon transplantation to nude mice, indicating lack of the neoplastic nature [201]. The BL-1 cell line established by Perrrone *et al.* is one of the more recognised models of this type [16]. This cell line was generated by immortalisation of cells derived from an uroepithelial biopsy from a patient with interstitial cystitis using simian virus 40 large T antigen. When grown on permeable supports, cells underwent stratification and showed amiloride-sensitive sodium absorption and elevated transepithelial resistance. Nevertheless, some of the morphological hallmarks of urothelial cells were either not present or not determined [1]. It should also be noted that due to immortalisation, cells cannot be considered "normal", and as such are prone to accumulating genetic mutations that can potentially lead to an unstable karyotype. Furthermore, viral inactivation of p53 or p16 proteins leads to inactivation of pathways associated with cell cycle progression, proliferation and/or apoptosis, and thus additional pathways can also be affected. Therefore, caution should be exercised when assuming its phenotype to be normal [197, 204].

3.1.4 Other approaches to establishing in vitro cultures of urothelial cells

Culturing cells isolated from urine was another approach to establishing a urothelial *in vitro* model [205-209]. However, this approach has faced a lot of criticism, as exfoliated cells can originate from any part of urogenital tract, including tissues of non-urothelial origin, such as the renal pelvis or genital tracts [210], and unless further confirmation of their type is obtained, the cell type is speculative. A few successful reports on culturing urine-derived stem cells have been published [211, 212]. The subsequent differentiation of the cells has been found to be a superior alternative to the previous reports. Nevertheless, transepithelial resistance, which is an indicator of *in vitro* differentiation, has not been determined in these cell types [208].

3.1.5 Primary cell cultures

In view of these shortcomings, the use of normal primary cells holds significant potential in terms of establishing the most physiologically relevant representation of urothelial

characteristics *in vivo,* despite demanding cell maintenance, finite lifespan and inter-individual variation due to multiple tissue donors [197]. In 1975 Elliot *et al.* [213] were the first to propagate a pure urothelial culture of mammalian origin by peeling the urothelium off the bladder muscle layer. Subsequent reports highlighted the use of human and animal cells from bladder/ureter with an array of isolation and growing techniques [136, 214-221]. One of the more accepted techniques established by Truschel *et al.* [198], demonstrated that cultured primary rabbit urothelium displayed most of the characteristics found *in vivo,* apart from the scalloped appearance of the apical membrane [1, 14]. Collectively these works led to our current understanding of urothelial cell culture and the factors that are important in generating cell models retaining the characteristics of an *in vivo* bladder urothelium, namely that the process primarily relies on propagation of normal undifferentiated cells in monolayers, followed by induction of their stratification and differentiation by modifying culture media composition. Cells generated in this way have a slow turnover rate and express the vast majority of differentiation markers (cytokeratins, uroplakins) and morphological characteristics (stratification and desquamation) [222, 223].

3.1.6 In vitro UTI study models

The emergence of modern tissue culture techniques has provided an invaluable tool for an in-depth analysis of specific pathways, target validation, and host-pathogen interactions. Their ease of use, clonality, immortalised nature and the relative ease of manipulation of their genetics pose an inexpensive alternative to animal models and allow high reproducibility of experiments, particularly in high-throughput screens [124, 224]. For these reasons they have been a precious tool in advancing our understanding of UPEC pathogenesis [224-226]. The papilloma line RT4, the highly malignant and muscle invasive T24, and a non-muscle-invasive 5637 are some of the most commonly used cell lines in the UTI field. These cell lines are generally well characterised from both the genetic and phenotypic standpoints [195, 196, 227-230]. Most *in vitro* models used to investigate interactions between UPEC and urothelium have failed to recreate the differentiated tissue components and structure seen in NHU [231]. Instead, efforts were focused on recreating the host-pathogen phenotype found in mice [94]. The 5637 cell line was found to be particularly useful in this respect, due to its characteristic uroplakin expression. Using this cell

type to mimic the FimH-UPIIIa-mediated internalisation of UPEC [123], allowed further dissection of mechanistic and molecular cascades driving bacterial invasion and persistence within urothelial cells [83, 96, 123, 141, 230, 232, 233]. Analysis of 5637 cytokine expression has been well defined in terms of response to bacterial exposure, which shows a good overlap with the expression profile found *in vivo* [230, 234-239]. This cell line has also been successfully used to establish a model incorporating neutrophil migration [240]. Unlike T24, 5637 cells were fit to grow under microgravity conditions to establish a 3D organotypic model, where the cell line was found to express an even higher level of E-cadherins, cingulins, CK20 and UP1a, increasing its resemblance to a human tissue phenotype [231].

3.1.7 Normal human urothelial cell model

In 1994 Professor Jennifer Southgate's research group in York established a finite NHU cell model, which utilises primary cells from the ureters of living patients with no previous history of urothelial dysplasia or neoplasia [14, 223, 241]. These normally slow-growing cells can be propagated relatively quickly in monolayers in a low-calcium and serum-free medium thanks to the "wound healing response" [242, 243]. They can be then induced to stratify by the addition of bovine serum, and further differentiation can be acquired by raising calcium concentration to the near physiological concentrations (2mM) [14, 221, 244]. NHU cells display other features of cell differentiation such as the presence, and localisation of tight junctions between superficial cells [168], retaining a permeability barrier, as reflected by a transepithelial resistance of $>3000\Omega cm^2$ and amiloride-sensitive transport system. The differentiated cells in culture also show a very similar cytokeratin profile to that found *in vivo.* However, *in vivo* superficial cells express CK20, but this is absent in cultured superficial cells. Furthermore CK14, which is not typically found in native cells, is found at low levels in the cultured cells [14]. While cultured cells retain the pattern of intercellular adhesion molecules, such as E-cadherins, CD44 core and v3, v4/5, v5, and v6 splice variants, as well as integrins α3β1, localisation of α2β1 and α6β4 integrins was found to be different *in vitro.* Integrin α2β1 is usually found uniformly across all layers, and is primarily involved in homotypic cell-cell interaction. Conversely, α6β4, which is normally basally expressed, was found to be diffusely distributed across all layers. Furthermore NHU cells were found to express an additional type of integrin α5β1 [210, 245, 246]. Ultimately, urothelial cell

differentiation was confirmed by a specific localisation of AUM to the apical membrane of superficial cells [168, 247-250]. This is currently the best characterised *in vitro* model of human urothelium and it has proven benefits in enabling research into the physiology, biochemistry and cancer biology of the bladder. The NHU cell model also provides a physiologically relevant human model for studying host-pathogen interactions during UTIs.

3.2 Aims of this chapter

- To optimise plating and growth conditions for NHU cells for the purpose of gentamicin protection assays to study bacterial invasion.
- To optimise fixation, permeabilisation and immunostaining for the purpose of imaging intracellular bacteria.
- To determine the binding and invasion characteristics of the cystitis strain *E. coli* UTI89 in NHU cells and their dependence on FimH.

3.3 Results

3.3.1 Optimisation of the NHU cell model in relation to UTI89 UPEC infection

Previously published work by Cross *et al.,* [14] reported successful propagation and differentiation of urothelial cells isolated from the NHU. To evaluate the feasibility of using the NHU model as a study model for UPEC infections, the ability to reproduce cell differentiation was assessed based on cell morphology. Cell morphology displayed at each stage of cell culture was in agreement with published data, suggesting that the cells retained their capacity to undergo cytodifferentiation. When grown in KSFMc media (Figure 3.1a-c), cells grew in monolayers with a morphology typical for epithelial cells, (as they don't express genes or proteins associated with differentiation). At a preconditioning stage, where calcium is at a near to physiological level, cells interacted with each other to stratify. This process was assisted by a morphological change and more squamous appearance, but no characteristics of differentiation (Figure 3.1d-e). At the differentiation stage, where media has calcium level increased to 2mM, cells not only stratified, but there was also an increase in morphological complexity of the uppermost layer, such as the increase in cell size and multinucleation (Figure 3.1f). This was further confirmed by immunofluorescence, delineating cell outline with WGA, a lectin binding a monosaccharide N-acetyl-D-glucosamine, and cell nuclei using DAPI (See section 2.13.1). The fluoromicrographs showed a well stratified morphology of NHU cells (Figure 3.2a), with a layer of distinctly larger, pentagonal and often binucleated superficial cells (Figure 3.2a and upper panel of Figure 3.2d). Underlying cells were found much smaller in size, and where confluent, were cuboidal (Figure 3.2a and lower panel of Figure 3.2d).

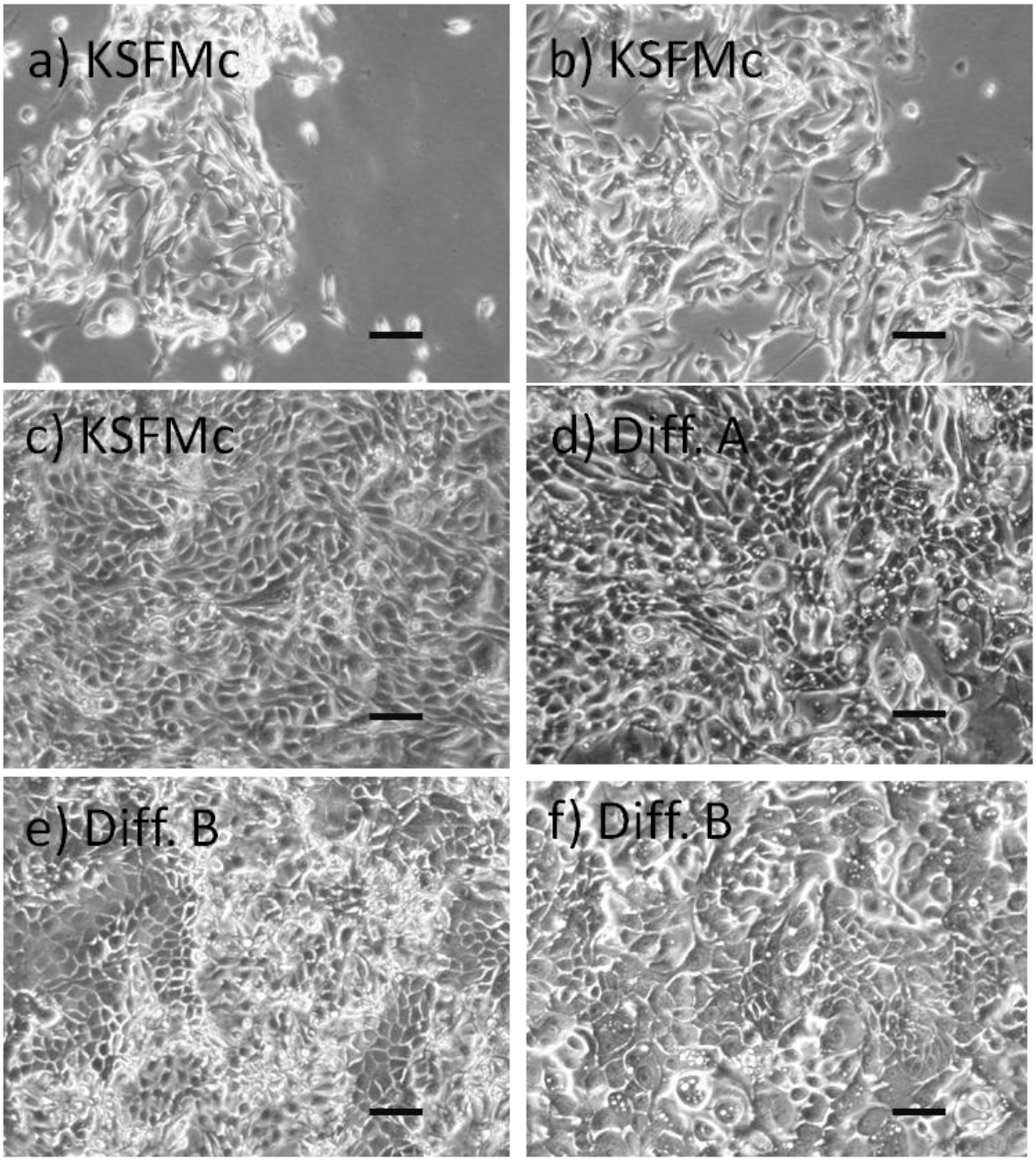

Figure 3.1 – Light micrographs of live normal human urothelial cells at different developmental stages. (A) Cells in keratinocyte media 1 day post seeding; (B) Cells in keratinocyte media at early passage number, 3 days post seeding; (C) Cells in keratinocyte media at early passage number, propagated as a monolayer nearing confluence 6 days post seeding; (D) Cells during a preconditioning stage, 2 days post seeding; (E) Cells at a differentiating stage, 5 days post seeding; (F) Differentiated cells, 7^{th} day of conditioning. Scale bars = 0.1mm. All images were taken at 6.4x magnification

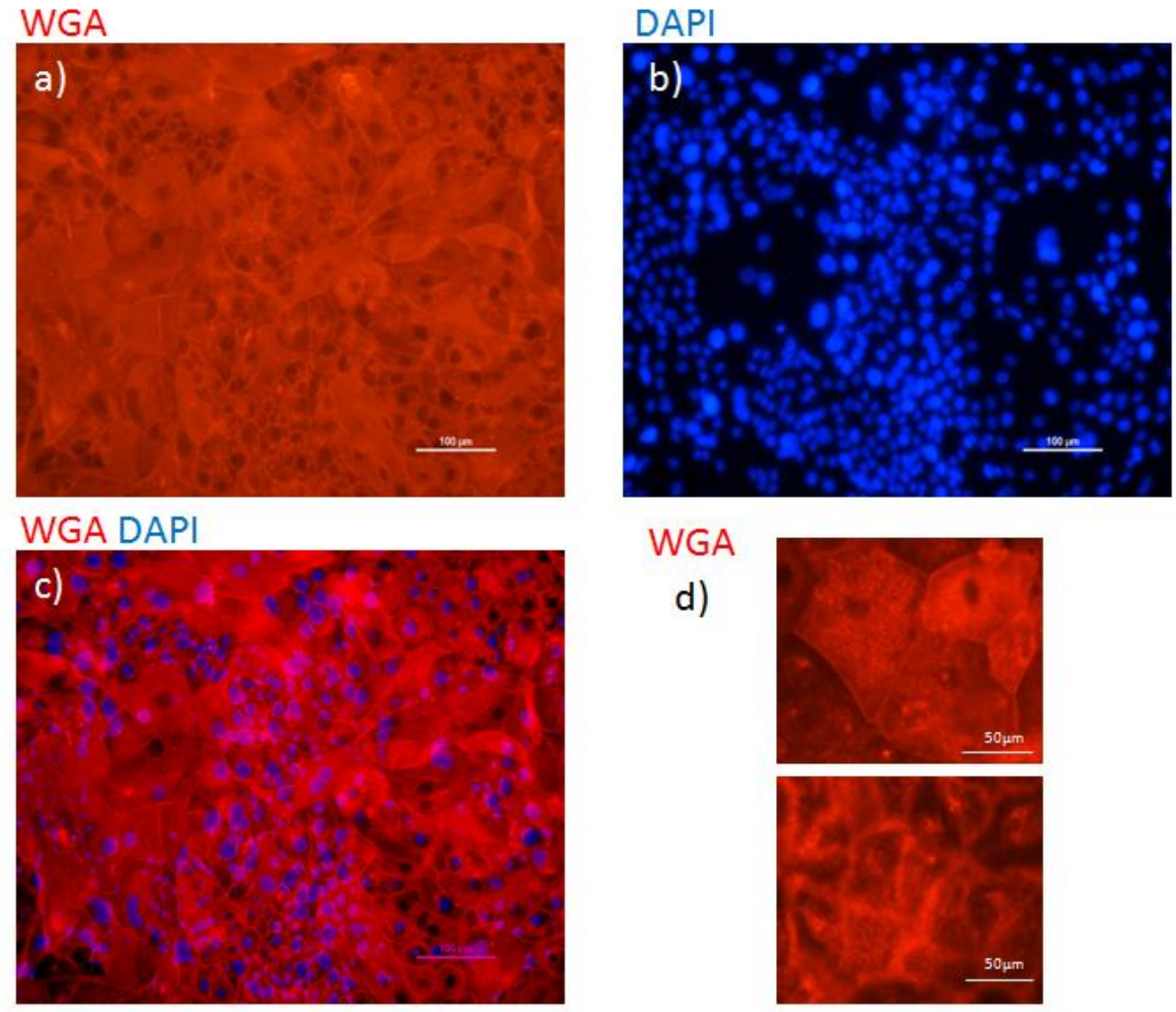

Figure 3.2 – The representative single-channel (A, B, C) and merged (C) 2D pictures of NHU cells. Where indicated, the cell membrane was stained with WGA Alexa Fluor® 555 Conjugate (red); nucleus with DAPI (blue). Additionally, panel (D) shows a difference in morphology between fully differentiated umbrella cells (upper panel), and lower layers of cells that haven't reached terminal differentiation (bottom panel). The fluorophores were excited using filter cubes with Texas Red and DAPI wavelengths excitation ranges 540-580nm, and 340-380nm respectively. The emitted fluorescence was recorded at 400nm (DAPI) and 595nm (Texas Red). Horizontal line in a-c) is 100µm, and in (D) 50µm.Magnification 20x.

3.3.2 Optimisation of NHU cells density prior to differentiation step

In order to develop a gentamicin protection assay for invasion, a uniform surface coverage of a tissue culture dish is important. While a too low cell number could result in empty areas in the tissue culture dish, densely seeded cells would undergo stress, and trigger apoptosis. Both would affect the accuracy of the MOI used. For this purpose the seeding density of NHU cells

just prior to the differentiation stage was optimised. Primary NHU cells were isolated from patients with no history or evidence of urothelial pathology, propagated and preconditioned as described in section 2.8, and seeding densities in the range of 10,000-40,000cells/cm^2 were evaluated. Optimal 3D constructs were obtained on a variety of plastics (12-well plates, Lab-Teks™), glass-bottomed dishes (Corning, USA) at 20,000cells/cm^2.

3.3.3 Correlating CFU concentration and optical density

To confirm the ability of UPEC to invade NHU cells, as previously reported using other *in vitro* and mouse models, the gentamicin protection assay method was chosen to quantify bacterial cell-association and internalisation. Additionally, to test whether in the NHU model FimH is driving the invasion process, two bacterial strains were used in these studies: a wild-type UTI89 strain and a binding pocket mutant UTI89-FimH-Q133K, which is known to abolish FimH binding abilities [83].

In order to achieve an accurate bacteria-to-cell ratio during the gentamicin protection assays, the correlation between CFU titre and optical density was determined. For this purpose cultures of the two bacterial strains at OD_{600nm}=0.5 were plated using a serial dilution and the drop plating method (Materials and Methods 2.9). It was found that the UTI89 strains at OD_{600nm}=0.5 corresponded to 1-1.5*10^8 CFU/ml (Figure 3.3).

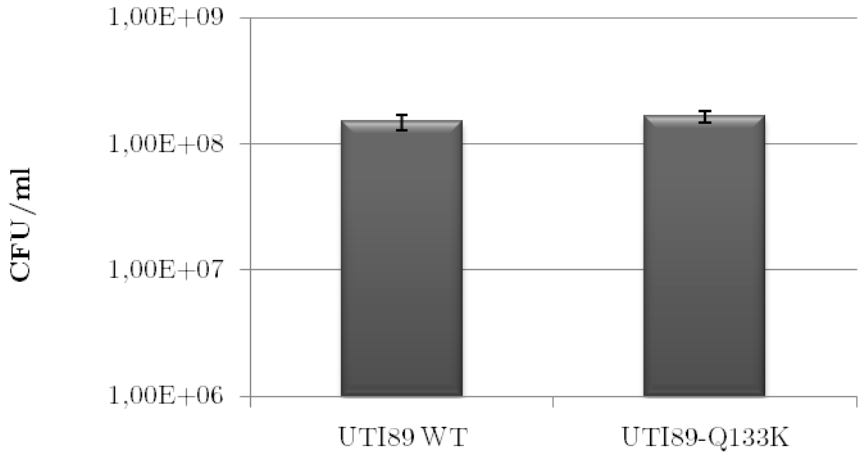

Figure 3.3 – CFU titre for UTI89 UPEC at OD_{600}nm=0.5. N=3, each with three technical replicates. Error bars are standard error of the mean.

3.3.4 Quantification of binding and invasion of UTI89 to NHU cells

Based on most current literature, two methodologies to perform gentamicin protection assay were chosen, so that data generated in the framework of this thesis could be compared with the previous findings. The key differences between the two are the time allowed for bacteria to infect: 1h (method #1) vs 2h (method #2), and examined timepoints: 2hpi (method #1) vs a choice of 3, 6, 12 and 24hpi (method #2).

Differentiated NHU cells were infected with UTI89-FimH-Q133K, or UTI89 strain transformed with GFP-tagged plasmid pANT4 (UTI89-pANT4), which carries GFP, in the presence or absence of 2% (w/v) MαDM, as described in section 2.9. Method #1 showed that UTI89 can remain bound to NHU cells following PBS washes (Figure 3.4a). "Total" CFUs are representative of both adherent and planktonic bacteria in the well at 2hpi. Due to differences in "Total" numbers of the three UTI89 strains (Figure 3.4a), comparison between these strains to assess bacterial association and invasion would be problematic. For this reason the cell-association rates ((Cell-associated CFUs/ Total CFUs)*100%) and invasion rates ((Intracellular CFUs/ Cell-associated CFUs)*100%) were calculated, as described by Martinez *et al.,* [83]. These revealed that after 2h, approximately 8% of bacteria were found to be associated with cells by either being internalised or bound to the epithelial cell surface. Invasion (assessed 2h later with gentamicin-containing media to kill extracellular bacteria) was limited, with its rate being <1% (Figure 3.4b).

(A)

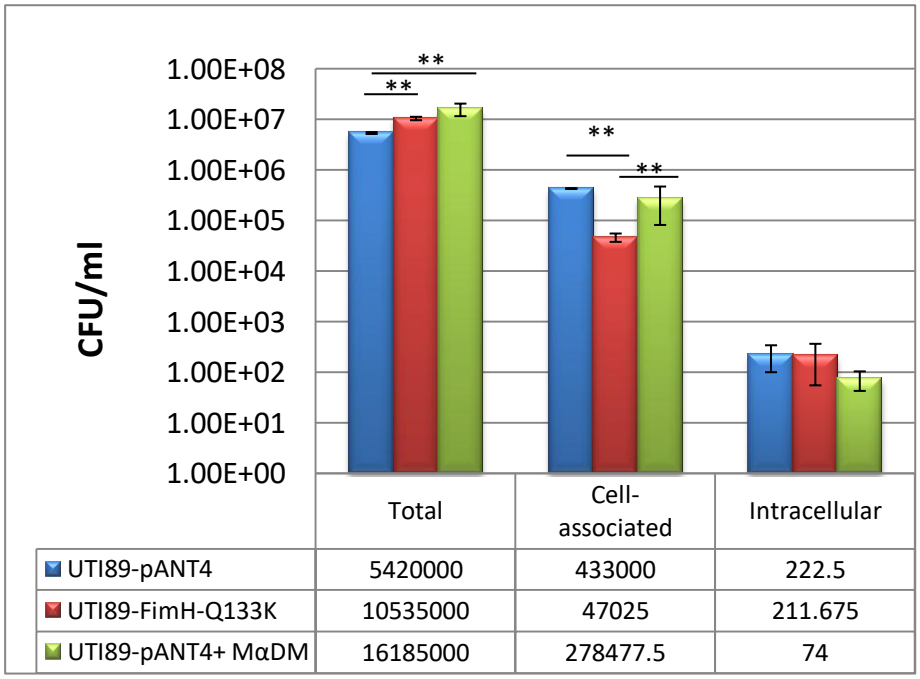

(B)

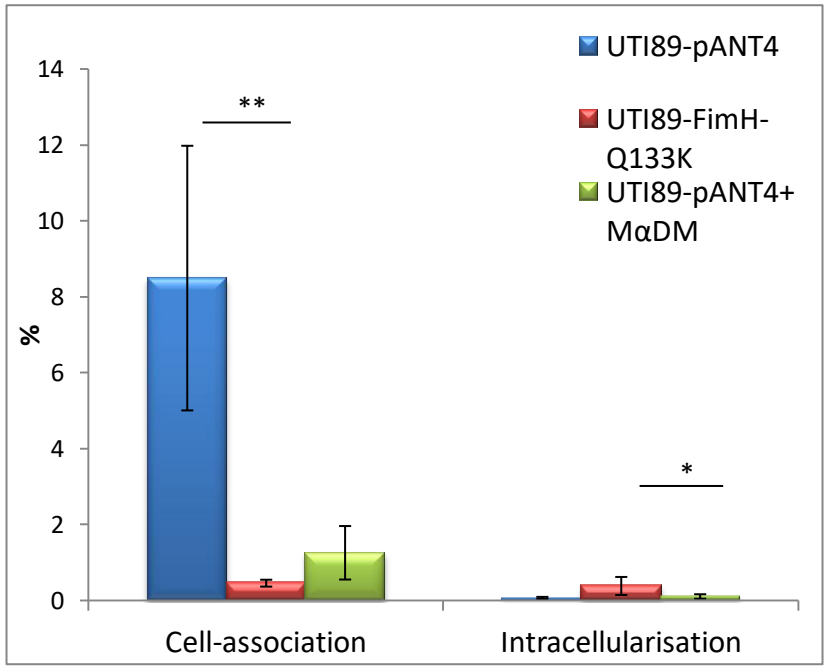

Figure 3.4 – Gentamicin protection assays of NHU cells infected with UTI89-pANT4, UTI89-FimH-Q133K or UTI89-pANT4 strain with FimH chemically blocked by MαDM. (A) Absolute values for total, and cell-associated colony counts (retrieved after PBS washes) 2hpi, and intracellular counts 4hpi (retrieved after 2h of gentamicin treatment). (B) Shows efficiency of cell-association and invasion in the form of Cell-association rate (Cell-associated CFUs/ Total CFUs) and invasion rates (Intracellular CFUs/Cell-associated CFUs). MOI=10. Data are mean. Error bars are S.E.M.. Each graph is representative of three independent experiments, each performed in triplicate or more. The statistical significance was assayed using Kruskal-Wallis One Way Analysis of Variance on Rank, followed by Dunn's method of pairwise multiple comparison procedure (*, $P< 0.05$; **, $P<0.001$).

3.3.5 Assessment of FimH-dependent bacterial internalisation

Since UPEC internalisation is believed to be driven by type-1 pili binding to uroplakins on the surface of host cells, genetic (using UTI89-FimH-Q133K bacterial mutant strain) and chemical (performing the experiment in the presence of 2%(w/v) MαDM) controls were used to verify this process in the NHU model. A statistically significant ($p<0.01\%$) decrease, corresponding to 7-8%, in bacterial cell-association rate was observed in the FimH mutant (Figure 3.4b). A similar decrease, though statistically insignificant, was observed in a chemical control as compared to the wild-type strain. Nevertheless, the level of intracellular bacteria between the three strains remained unchanged, regardless of the number of cell-associated bacteria 2h earlier, suggesting the observed invasion was type-1 pili independent (Figure 3.4b).

In order to investigate this apparent discrepancy with published literature further, binding and invasion of NHU cells by pyelonephritis-causing strains was explored using gentamicin protection method #1 (Figure 3.5). The J96 strain is both *fim*$^+$ and *pap*$^+$, and the importance of the Type 1 fimbriae was tested by blocking its function with MαDM. The absolute values of cell-association showed that MαDM had little effect on the ability of J96 to bind to host cells (Figure 3.5a), though absolute invasion counts of J96 decreased by a magnitude of about half a logarithm. However, cell-association and invasion rates, that give a more accurate reflection of trends (Figure 3.5b) demonstrated little impact of FimH on UPEC's binding and invasion. Further experiments would be required in order to test the statistical significance of these observations.

(A)

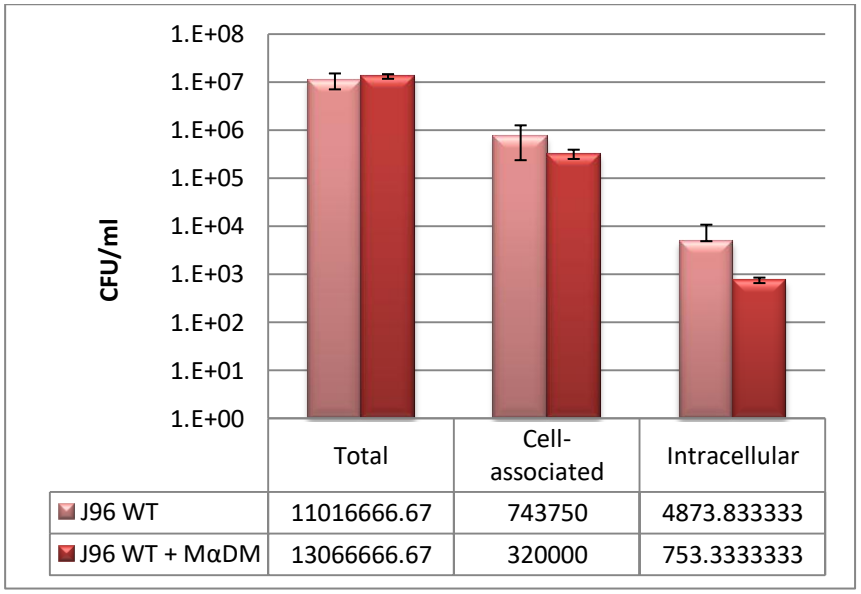

(B)

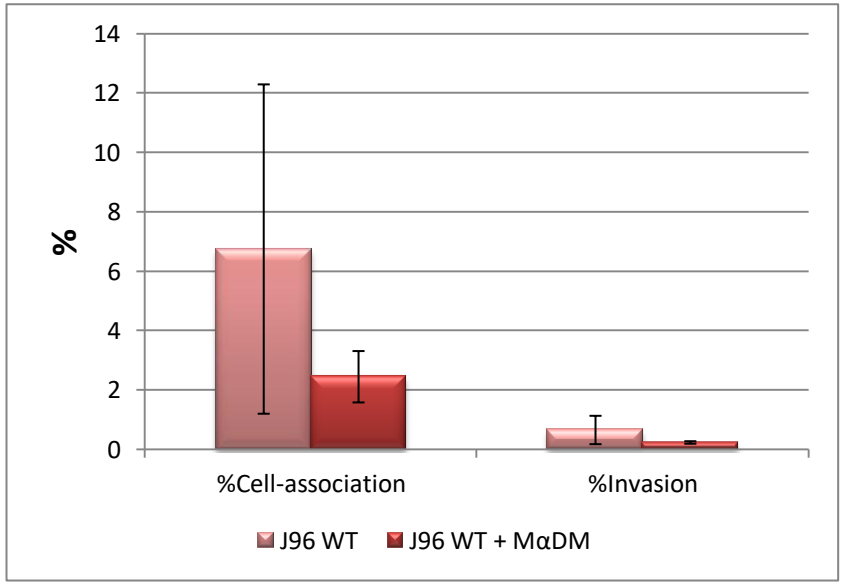

Figure 3.5 – Gentamicin protection assays results of NHU cells infected with J96 wild-type in presence or absence of MαDM. (A) Absolute values for total, and cell-associated bacterial counts (retrieved after PBS washes) 2hpi, and intracellular counts 4hpi (retrieved after 2h of gentamicin treatment). (B) Shows efficiency of cell-association and invasion in the form of Cell-association rate (Cell-associated CFUs/ Total CFUs) and invasion rates (Intracellular CFUs/Cell-associated CFUs). MOI=10. Data are mean. Error bars are S.D. J96 WT data is representative of six independent experiments, each performed in triplicate or more. J96 WT + MαDM data is representative of one independent experiment done in triplicate.

3.3.6 Assessing the fate of intracellular bacteria

In order to gain more insight into what happens to internalised bacteria over the course of time, method #2 of the gentamicin protection assay was used. It was found that both intracellular wild-type and UTI89-FimH-Q133K strains were able to multiply in between 3h and 6hpi timepoints. However, by 24hpi no intracellular bacteria were retrieved from the intracellular niche (Figure 3.6). This may have been due to removal of exfoliated infected cells along with media during PBS washes or escape of intracellular bacteria through the process of fluxing as described in section 1.4.2 of the introduction.

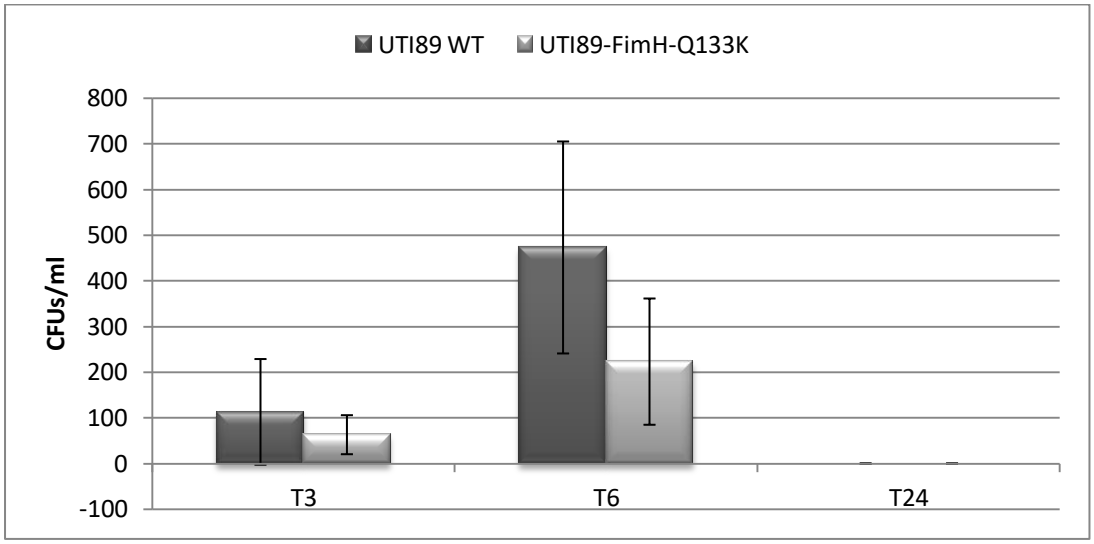

Figure 3.6 – Absolute average numbers of intracellular CFUs recovered 3, 6 and 24hpi with WT UTI89 and UTI89-FimH-Q133K mutant. MOI=10; Data are mean with error bars being SD. Each graph is a representative of an independent experiment, performed in sextuplicate.

The ability of UTI89 to invade NHU cells was further examined using immunofluorescence. NHU and bladder cells contain large numbers of autofluorescent vesicles, which make accurate discrimination of small pockets of intracellular bacteria problematic. Therefore, a series of protocols were used to find optimal conditions of WGA Alexa Fluor 555 Conjugate staining (Table 2.4), permeabilisation (Table 2.5), and primary antibodies (Table 2.6) towards IF imaging (2.13.1). Differentiated NHU cells were infected with UTI89-pANT4 bacteria

that were statically cultured to induce Type-1 piliation, and fixed with NBF at 3, 6 and 24hpi (Figure 3.7).

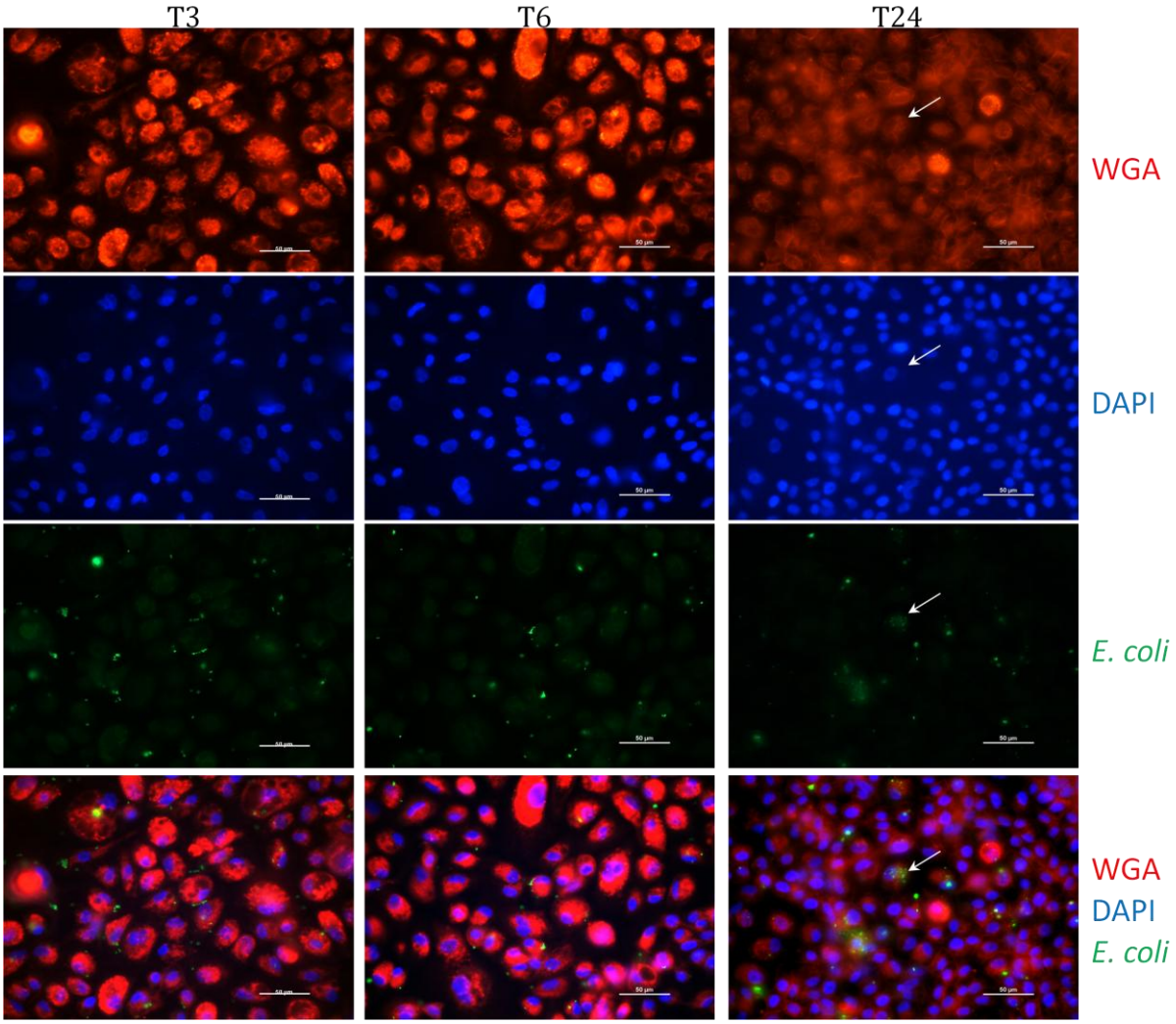

Figure 3.7 – NHU cells at 3, 6 and 24h post infection with UTI89. Only the representative single-channel and merged images are shown. Nucleus (blue) was stained with DAPI; membrane (red) with wheat germ agglutinin Alexa Fluor® 555 Conjugate; *E. coli* UTI89 was immunostained with anti-*E. coli* primary antibodies and Alexa Fluor® 488 Conjugate (green) secondary antibodies. White arrow indicates a location of some internalised bacteria. Horizontal line 50µm. The fluorophores were excited using filter cubes with Texas Red, DAPI and FITC wavelengths excitation ranges 540-580nm, 340-380nm and 465-495nm respectively. The emitted fluorescence was recorded at 595nm (Texas Red), 400nm (DAPI), and 505nm (FITC). Magnification 20x.

Immunostaining was performed to identify *E. coli* localisation in relation to the cell membrane and nuclei. Bacteria were commonly found associated with NHU 3hpi, especially in

the junctions between the facet cells. This is not uncommon as urothelial cells are not typically very flat, and commonly form ruffles [94]. This was also the reason behind why there were only rosettes of images that could have been seen in focus (Figure 3.8). At this timepoint some NHU were found with more than one internalised bacterium per cell, sometimes loosely scattered across the cytoplasm (Figure 3.7). At 6hpi, bacteria were less diffusely distributed across the cells and were more likely to be found in small clumps (Figure 3.8).

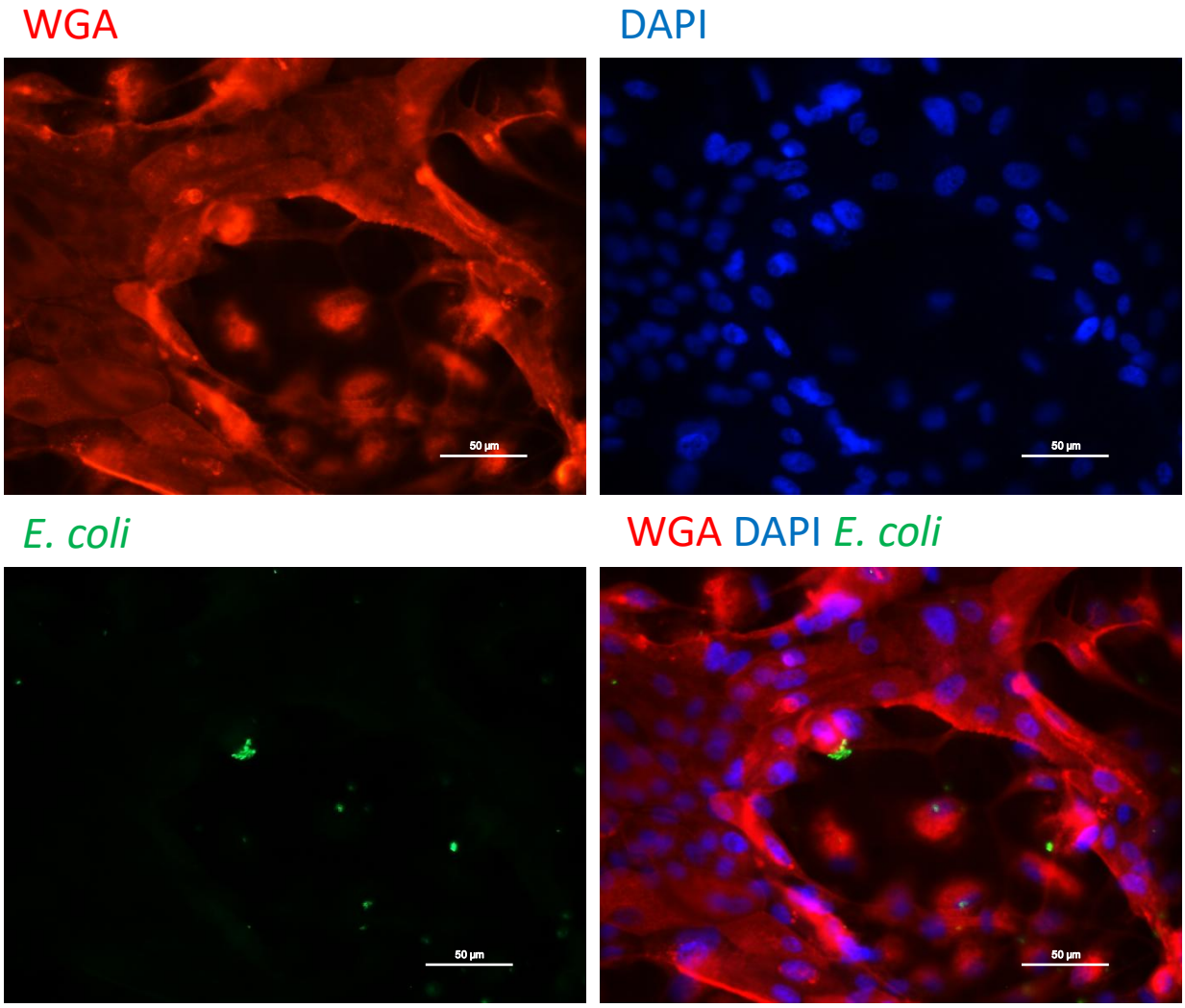

Figure 3.8 – NHU cells at 6h post infection with UTI89. Single-channel and merged images are shown. Nucleus (blue) was stained with DAPI; membrane (red) with wheat germ agglutinin Alexa Fluor® 555 Conjugate; *E. coli* UTI89 was immunostained with anti-*E. coli* primary antibodies and Alexa Fluor® 488 Conjugate (green) secondary antibodies. Horizontal line 50µm. The fluorophores were excited using filter cubes with Texas Red, DAPI and FITC wavelengths excitation ranges 540-580nm, 340-380nm and 465-495nm respectively. The emitted fluorescence was recorded at 595nm (Texas Red), 400nm (DAPI), and 505nm (FITC). Magnification 20x

Larger clusters of intracellular bacteria similar to what might be seen when observing mid-IBCs also were observed suggesting bacterial multiplication had occurred in intracellular niches, and where IBCs persisted, the multiplication has continued until 24hpi, where only sporadic IBC-like pods were found (Figure 3.9). However, the rarity of the observed pods implied that many of them might have been exfoliated. While Figure 3.6 does show no CFUs detected at 24hpi, a combination of low incidence of the infected cells and low counts of intracellular bacteria, could be a likely reason for the plating method not identifying small CFU numbers. Intracellular localisation of UTI89 was confirmed by z-stack imaging (Figure 3.10). NHU cells infected with UTI89-FimH-Q133K were not imaged due to time constraints.

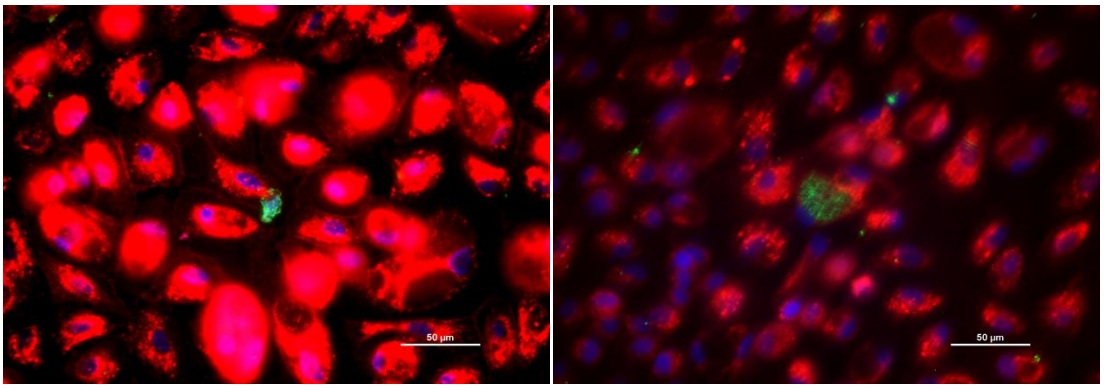

Figure 3.9 – NHU cells at 24h post infection with UTI89. Both images represent merged channels. Nucleus (blue) was stained with DAPI; membrane (red) with wheat germ agglutinin Alexa Fluor® 555 Conjugate; *E. coli* UTI89 was immunostained with anti-*E.coli* primary antibodies and Alexa Fluor® 488 Conjugate (green) secondary antibodies. Horizontal line 50µm. The fluorophores were excited using filter cubes with Texas Red, DAPI and FITC wavelengths excitation ranges 540-580nm, 340-380nm and 465-495nm respectively. The emitted fluorescence was recorded at 595nm (Texas Red), 400nm (DAPI), and 505nm (FITC). Magnification 20x.

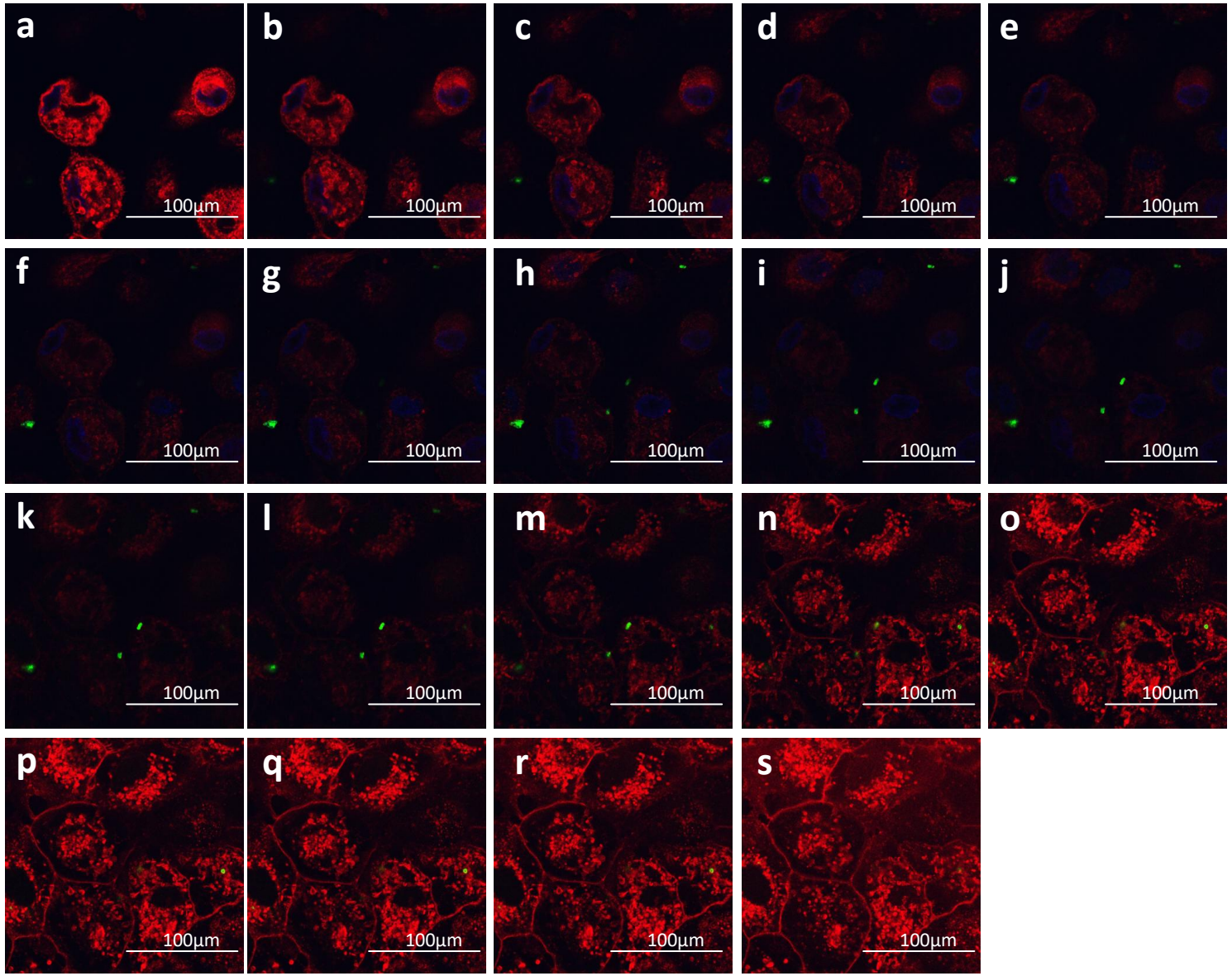

Figure 3.10 – Confocal z-stacks of NHU cells 24hpi showing abundant peri-space bacteria in superficial cell layer. Serial stacks are presented from left to right. Nucleus (blue) was stained with DAPI, excited with 405nm laser; membrane (red) was stained with wheat germ agglutinin- Alexa Fluor® 555 Conjugate excited with 543nm wavelength; *E. coli* stained with anti-*E. coli* primary antibodies followed by Alexa Fluor® 488 Conjugate secondary antibodies, excited at 488nm. Horizontal bar 100µm. Magnification 65x.

3.3.7 Investigation of exfoliation of urothelial cells upon bacterial infection

In vivo in both mice and humans, urothelial cells are known to be tightly attached to each other. Apoptosis can be activated in response to cell stress, i.e due to nutrient deprivation, membrane damage, cell density-dependent or infection. Infected urothelial cells undergo a process of exfoliation in order to remove colonised cells from the host. Therefore, we aimed to determine whether this also occurs in the NHU model and whether it could explain the decrease in IBCs observed in the course of time. Cell culture media was harvested at each timepoint during the course of the gentamicin protection assay (Method #2) for examination of epithelial cells presence. At each timepoint (1, 2, 4 and 8hpi), media was collected, cytospun and immunostained to identify intracellular UPEC in exfoliated cells.

Media collected at 1hpi contained mostly planktonic bacteria, and large clumps that had self-aggregated and failed to bind to or invade NHU cells. Some urothelial cells were also found, with their membrane richly covered in adherent UPEC (Figure 3.11). The sample from the 2hpi timepoint contained clear umbrella cells, and no planktonic bacteria, as these would have been washed away at 1hpi prior to applying gentamicin-containing media. UPEC were found here only in association with cells. Both, bacterial and epithelial cell numbers were decreased at 4hpi, as compared to 2hpi, despite the fact that the media collected at 4hpi was in contact with cells twice as long as that at 2hpi. This suggested that a stronger initial exfoliation response could have been triggered by a high numbers of bacteria residing intracellularly. The greatest level of exfoliation was detected in media from 8hpi. It could be due to the fact that media from this sample was in contact with cells for the longest time (6h). Individual cells were rather uncommon in these samples. Instead sheets of cells infected with a large number of bacteria scattered across the cytoplasm, as well as uninfected ones, were mainly found. The uninfected cells could have been exfoliated due to a number of reasons, i.e. due to the presence of bacterial toxins, invasion-related signalling, or lack of detection of bacteria in some cells.

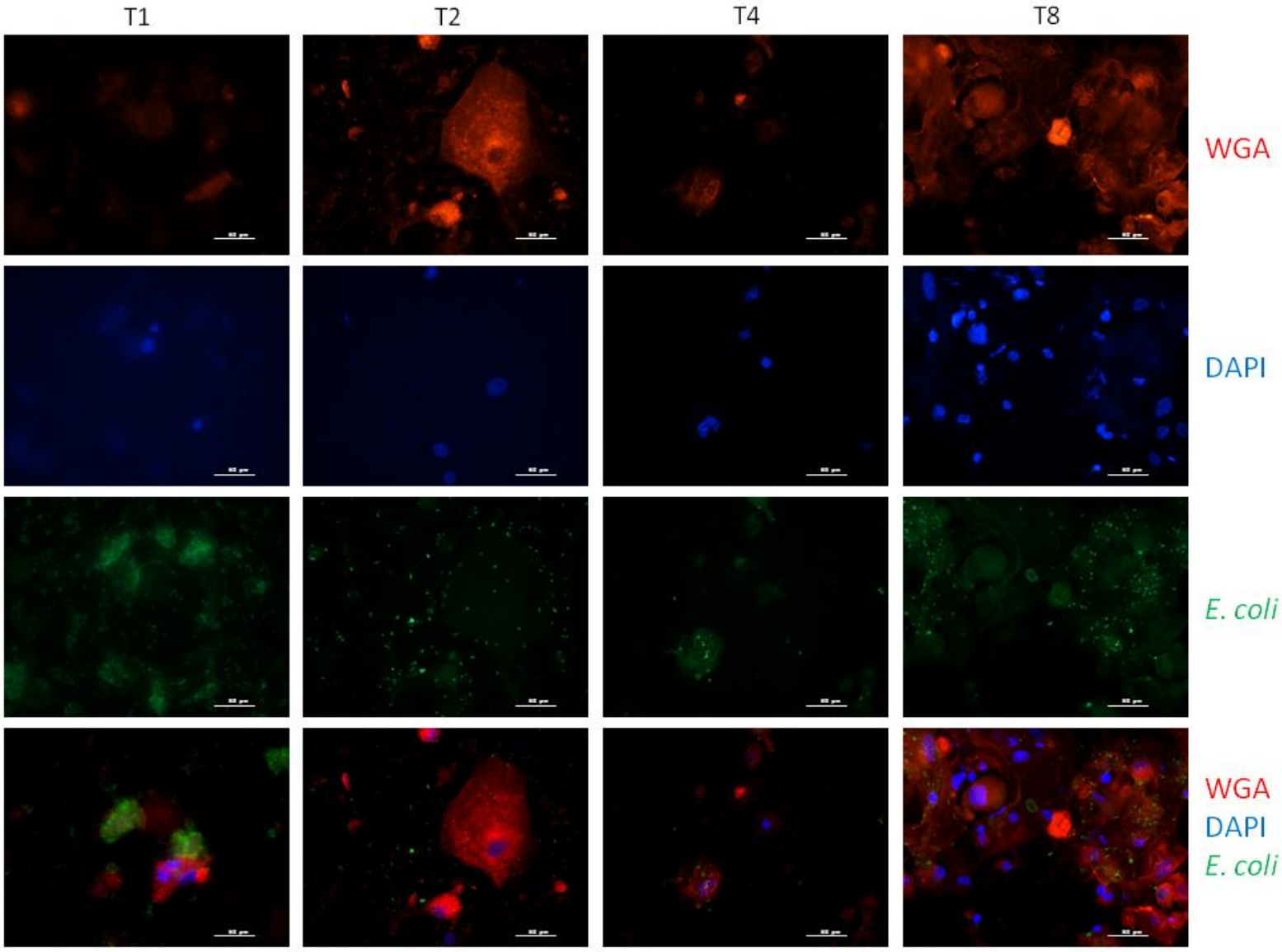

Figure 3.11 – Cytospun NHU cells coming from cell culture media at 1, 2, 4 and 8h post infection with UTI89. Only the representative single-channel and merged images are shown. Nucleus (blue) was stained with DAPI; membrane (red) with wheat germ agglutinin Alexa Fluor® 555 Conjugate; *E. coli* UTI89 was immunostained with anti-*E. coli* primary antibodies and Alexa Fluor® 488 Conjugate (green) secondary antibodies. White arrow indicates a location of some internalised bacteria. Horizontal line 50µm. The fluorophores were excited using filter cubes with Texas Red, DAPI and FITC wavelengths excitation ranges 540-580nm, 340-380nm and 465-495nm respectively. The emitted fluorescence was recorded at 595nm (Texas Red), 400nm (DAPI), and 505nm (FITC). Magnification 20x.

3.4 Discussion

In vitro urothelial cell models are invaluable for studying the genetic and phenotypic host-pathogen adaptations that occur during UTIs. Furthermore, these models are essential to enable us to evaluate novel therapeutic targets. In the past, there has been a limited success in utilising primary cultures of human cells for this purpose. Here, we explored the suitability of an *in vitro* primary urothelial cell model to study UTIs. Once cell propagation and differentiation were optimised and correct cell morphology confirmed, the main focus was placed on determining whether UPEC can bind to and invade superficial cells in an NHU cell model. This was investigated by means of a gentamicin protection assay and immunofluorescence imaging of cytoplasmic bacteria. These studies optimised methods for cell fixation, permeabilisation and immunostaining to produce the best results to image intracellular UPEC.

The gentamicin protection assay results showed that UPEC bind to the surface of NHU cells (~8%). However, only a small proportion of cell associated-bacteria were found to invade the epithelial cells (<1%). Both outcomes were in agreement with follow-up immunocytochemical studies. Furthermore, invasion was found to be FimH-independent, as the absolute numbers of intracellular bacteria of a pocket binding mutant were comparable, despite a statistically significant decrease in absolute "Cell-associated" CFU counts. What's more, the "Cell-association" counts of the chemically inactivated wild-type strain were not significantly altered. Similar trends, supporting little importance of FimH in UPEC binding and invasion of NHU cells was observed with a pyelonephritis strain- J96. Chemical inhibition of its type 1 fimbriae binding pocket didn't result in any major changes in its internalisation and cell-association capabilities.

CFU counts of intracellular bacteria recovered at different timepoints showed that despite an increase in UPEC numbers between 3 and 6hpi, the intracellular population was not sustained as no CFUs were recovered at 24hpi. In spite of showing strong exfoliation of upper cell sheets containing infected cells at later timepoints, as compared to the earlier ones, cell imaging contradicted this finding showing sporadic IBC-like pods at the same timepoint. The size of these pods also suggested successful replication of bacteria within gentamicin-protected cells, rather than a series of transient invasions by individual bacteria. The discrepancies between gentamicin

protection assay and imaging results could possibly be due to the fact that during the former, upon cell lysis, only 1/20th of the mix was plated. Considering the infrequency of these pods, there may not have been enough bacteria within each well to be detected using this plating method. More importantly, intracellular bacteria are exposed to a number of hostile host responses, which may result in bacteria being non-viable upon plating on agar plates but they are still visible with immunocytochemistry.

In comparison, in the published reports, UPEC rate of cell-association with 5637 bladder cell lines was typically found to be ~45%, while that of invasion would vary from 0.5-10% depending on the cell passage number [83, 152]. It has also been well documented that binding and invasion of UPEC are driven by interaction of FimH lectin tip with uroplakins found on the urothelial cell surface, and FimH inhibition significantly abrogates both processes [82, 83, 94, 251, 252]. There appears to be an overestimation in cell association rates, as our model, which is more representative of *in vivo* conditions, suggests that binding rates may be around 9 fold lower. Consequently, cell line models could lead to overestimates of usefulness of anti-adhesives [253].

There are several other plausible explanations for the disparities between these results. Firstly, it could be due to the differences in displayed surface proteins by host cells in the two *in vitro* models. UPEC expressing type-1 pili bind preferentially UP1a and UP1b [254, 255], but it can also induce cell signalling via FimH-UPIIIa interaction, which has been shown to institute further bacterial invasion and apoptotic sensitisation [123, 256]. 5637 monolayers represent more of a basal molecular subtype than the luminal one and therefore display a distorted representation of uroplakins. They were found to constitutively express UPIIIa and its obligatory heterodimer UPIb, but UPIa expression was shown to be much lower than that *in vivo* [123, 229, 231, 254]. NHU cells express more UPII/UPIa than the underlying layers. While UPII can't be used by type-1 piliated bacteria for attachment, UPIa is a key receptor for FimH [47, 254].

Secondly, it needs to be noted that despite a long lasting notion of the urothelium being homogeneous across different regions of the urinary tract, it has been questioned in the literature that this may not be the case [122, 257]. And the size of error bars makes it seem credible that the natural variation between biological replicates inherent to the assay could also play a role in

the differences between the two *in vitro* models. In BALB/c mice, the lower urinary tract is richer in glycoproteins incorporating D-mannose, than the kidney epithelium [258]. Given that the NHU cells used in this study originate from the middle third of the ureter distal to the kidney, it is likely that they may display similar characteristics to cells of the upper urinary tract. Finally, mice studies showed that UPEC strains containing *pap* genes were more successful at persistence than their isogenic *pap* mutants or faecal strains lacking *pap* genes [147, 258]. Observations from a small group of women, showed that only pap^{+} bacterial strains established pyelonephritis in patients with UTIs [259]. While UTI89 does contain a single copy of a *pap* gene, it is a *papG*III version, which binds the globopentaosylceramides that are not found in human urinary tracts [260]. J96 encodes *papG*III and *papG*I adhesins. The latter binds preferentially globotriaosylceramide, which are also abundant on uroepithelial cells [261]. In contrast a more virulent cystitis strain, CFT073 encodes two *papG*II genes, products of which bind glycolipids opulent on the surface of human urothelium- globotetraosylceramide [47]. Therefore it can't be ruled out that UTI89 would show a poor binding and invasion in human ureter-derived cells due to the differences in the type of foremost expressed pili. However, it should be noted that the presence of alternative receptors for PapGIII proteins in humans has been reported [47], and significant differences were found in isoreceptors expressed by mice and human urothelial cells [261, 262].

Furthermore, 5637 cells were previously shown to accommodate other pathways of UPEC invasion, via α3 and β1 integrins [156], a caveolae-mediated, lipid-raft-dependent [233], or through secretory lysosomes [145]. While those other pathways could possibly contribute to the basal level of infection observed in NHU cells, it also appears that the lower infection level can be a more representative of the "normal" *in vivo* state. After all, not every UTI patient suffers from recurrent or persistent infections, whether this is due to differential expression of uroplakins or the virulence of particular bacterial strain.

The exact reason behind the negligible effect of FimH found in this study model is unclear, contradicting published data found in both humans and mice [82], and whether it has any association with low specificity of its function in causing cystitis. Further comparison of NHU cells binding and invasion by other cystitis- and pyelonephritis-causing strains would be

necessary, involving analysis of their pili-expressing types. An in-depth analysis of uroplakin expression pattern among ureter-derived NHU cells, as well as the effect of a potential involvement of bacterial expulsion on persistence, are also necessary. Experiments should be also done with bacteria grown to induce P pili [263, 264].

Despite its finite lifespan, limited availability, and sample-specific variation, the NHU model is one of the most physiologically relevant *in vitro* systems of human urothelium [265]. While there is still room for improvement towards its application in clinical and drug evaluation studies, the use of NHU-based systems in UTI studies represents a valuable alternative. This is especially the case with the phenotypic divergence of urothelial cell lines becoming more evident, and could potentially reduce the gap in translation of results between *in vitro* and *in vivo* systems.

4 Single mouse urothelial cell proteomics

4.1 Author contributions

Dr Xuezhi Bi[1] performed all the LC-Ms/Ms experiments.

Dr Jaran Jainhuknan[2] performed MALDI-TOF testing.

Dr Debarka Sengupta[3] and Dr Shyam Prabhakar[4] helped with performing t-SNE and k-means clustering and analysis.

M.Sc. Milena Lewanczyk performed all the remaining experiments and analysis.

[1] Bioprocessing Technology Institute, A*STAR
[2] Bruker Daltonics
[3] Indraprastha Institute of Information Technology, Delhi
[4] Genome Institute of Singapore, A*STAR

4.2 Introduction

4.2.1 Single cell approaches

The single cell revolution has changed the way researchers approach the analysis of bulk data [266, 267]. Single cell analysis permits lineage tracing and study of cell subpopulations, however it has also revealed the likelihood of misrepresentation of data when relying on population averages [268, 269]. Due to the increase in throughput and the scope and accuracy of single-cell capture techniques and analysis, single cell transcriptomics has become almost a routine process. Consequently, this has led to the application of this technology to the fields of genomics, proteomics, metabolomics and epigenetic states [268, 270].

When it comes to studying UTIs, all previous analyses have been performed at the population level [104, 271, 272]. Trying to dissect host-pathogen interactions during an intracellular UPEC infection using population approaches is likely to provide heavily biased data given that IBC formation does not occur in every cell. In a mouse model, only about 0.01 to 0.001% of bacterial inocula were found to give rise to IBCs, with 50 of them being found on average per bladder at 6hpi [93, 152]. While isolation of single infected bladder cells is crucial for studying rUTIs, most of the available tools for single cell capture, such as fluorescence-activated cell sorting (FACS) or microfluidic systems (e.g. those of Fluidigm®) are not suitable due to their upper cell size limit restriction (mouse bladder epithelial cells are ~150µm in diameter, and can be distended further by the presence of IBCs) [94, 273]. Laser-capture microdissection, on the other hand, doesn't require a prior cell dissociation [274]. However, it is more time consuming, requires expensive equipment, and just like with the use of micromanipulator, a skilled experimentalist is needed [275, 276]. A traditional manual technique involving micropipetting with the use of a glass capillary tube, despite having a lower throughput, evades these issues. With an additional use of a fluorescent marker in the form of GFP-producing bacteria, it allows for an accurate cell selection.

4.3 Aims of this chapter

The aims of this chapter were to validate the suitability of single cell mass spectrometry as a technique for studying both, infected and uninfected, single mouse bladder urothelial cells. More specifically, the aims were:

- To confirm the cell type of analysed cells.
- To assess the overall similarity between samples.
- To analyse the data from the standpoint of differential protein expression.
- To validate targets resulting from the differential expression analysis.
- To study the 3D ultrastructure within IBCs

4.4 Results

4.4.1 Proof of concept

Mass spectrometric analysis of native, untagged (not fused with a bait protein) proteins/peptides found in single infected epithelial cells (siEC) allows us to gain an insight into not only host, but also possibly bacterial, proteomes. To assess the bacterial cell number required to reach the lower threshold limits for prokaryotic protein detection within a siEC, suspensions of either UTI89-vsGFP (SLC-719) strain or 5637 human bladder epithelial cells were subjected to the analysis by two mass spectrometric methods: LC-Ms/Ms, and MALDI-TOF. The latter allowed detection of bacterial proteins starting from $1x10^5$ CFUs, while LC-Ms/Ms allowed detection of around 58-76 protein groups with $1x10^4$ CFUs, and 28 protein groups with $1x10^3$ CFUs. As for the epithelial cells, both techniques indicated detection of *ca.* 200 human protein groups with a single 5637 epithelial cell.

4.4.2 Sample collection

In order to obtain siEC, C57BL/6 mice were transurethrally inoculated with GFP producing UPEC (SLC-719). 6hpi mice were sacrificed, and bladders were removed aseptically

and inverted. Using a fluorescence dissecting microscope, IBCs were gently scraped into PBS. A hand-pulled glass capillary pipette was used to isolate single infected or uninfected cells from a mixed pool of epithelial cells. Cells were then individually washed in a clean droplet of PBS, just prior to being flash frozen in a minimal amount of liquid using liquid nitrogen (Figure 4.1). To certify the sample data were representative of a single cell, the presence of just a single cell was ensured at each stage of isolation with the use of a dissecting microscope. Uninfected cells from uninfected mice (hereafter referred to as the control cells), were isolated in the same way. 16 infected (referred to as the infected cells) and 16 uninfected cells from infected mice (henceforth the uninfected cells) and 16 control cells from uninfected mice were collected (Section 2.10.5). Cells in each group came from more than one mouse (27 infected mice to collect infected and uninfected cells and 3 uninfected mice to collect control uninfected cells) and were analysed via LC-Ms/Ms (Section 2.16).

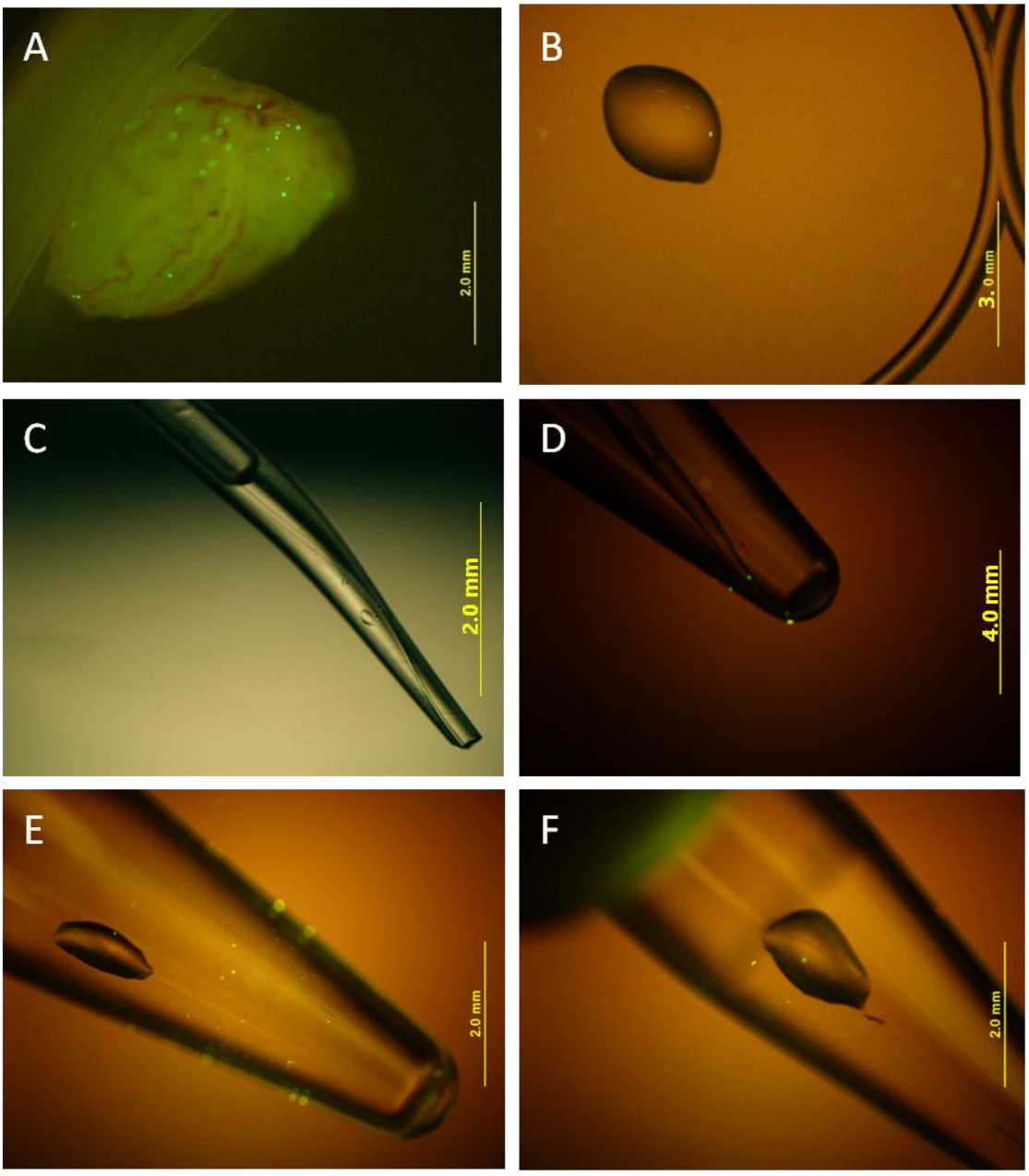

Figure 4.1 – Images of infected mouse bladder and different stages of single bladder epithelial cell isolation. (A) an inverted mouse bladder visualized using fluorescence. Individual IBCs can be seen as bright green focal points on the inner surface of the mouse bladder; (B) individual IBC isolated using a hand-pulled glass capillary pipette, as seen during a wash step; (C) Single uninfected cell as seen in a glass capillary pipette; (D) single infected epithelial cell at a tip of a capillary pipette, just before being released into a PCR tube; (E-F) single infected epithelial cells as found in small volumes of PBS inside PCR tubes. The GFP fluorophore expressed by bacteria was excited using FITC wavelengths excitation range 465-495nm. The emitted fluorescence was collected at 505nm. Magnification 6.7x.

4.4.3 Data exploration

Data from the LC-Ms/Ms analysis (Section 2.16) were analysed using R in combination with NODES- a specialised R package providing methods for normalisation and DE analysis of single cells (Section 2.17). In total 2478 eukaryotic proteins were detected. The range of mouse protein numbers detected per cell was between 176 and 1363, with a median of 642.5. There were significantly fewer detected mouse proteins in control cells coming from uninfected mice than in the other two cell types (n=16, Kruskal-Wallis, $p<0.001$) (Figure 4.2).

The maximum peptide count for a single protein, found in a single cell, was 149 prior to normalisation, and 90 after it. The normalisation involved homogenisation of all of the expression values below a fixed rank in each cell [175]. Because of the unification of the expression values performed during the normalisation process, the data distributions was explored only prior to that procedure. The distributions (the frequency of data spread throughout the range of values) of mean protein expression per cell were comparable between cells coming from infected mice, though the distribution of mean protein expression per cell in control cells was significantly lower (n=2478, Kruskal-Wallis $p<0.001$) (Figure 4.3). The total peptide numbers detected from each cell were also distributed across lower values among control cells than cells isolated from infected mice. Significantly lower numbers of total peptides were detected among control uninfected cells (n=16, Kruskal-Wallis $p<0.001$) (Figure 4.4).

The maximum number of bacterial proteins detected in any of the single cells was 83 Figure 4.5. The number of detected bacterial proteins in infected cells was significantly higher than in the control cells (n=16, Kruskal-Wallis, $p<0.001$). The list of all detected bacterial proteins can be found in Appendix in Table 8.1. Mean raw bacterial protein peptide counts in infected cells were significantly higher than in the other cell types (n=148, Kruskal-Wallis, $p<0.001$) (Figure 4.6). Higher numbers were also observed for total number of bacterial peptide counts detected in infected cells versus the rest (n=16, Kruskal-Wallis, $p<0.001$) (Figure 4.7).

A)

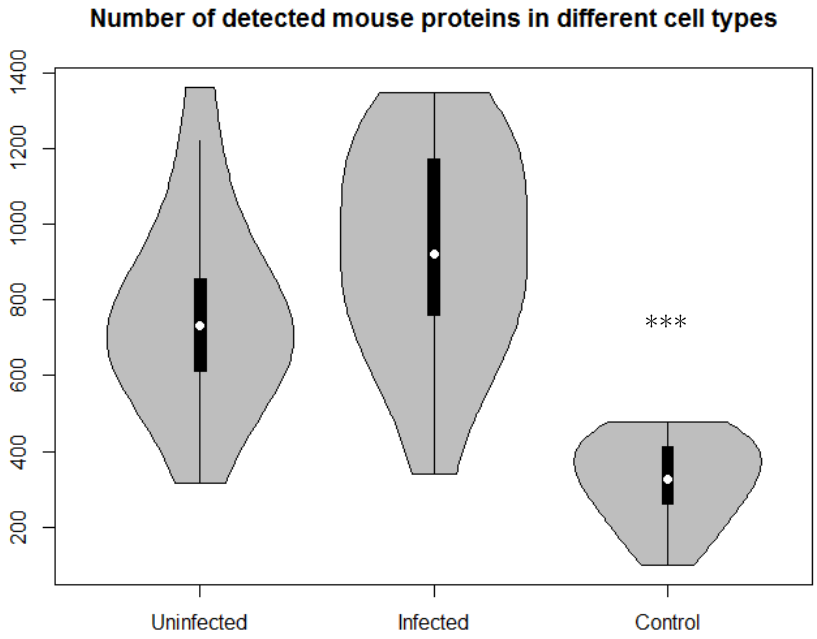

B)

	UTI89-GFP Infected Mice		Uninfected mice
Numbers of Detected Proteins	**Uninfected cells n=16**	**Infected cells n=16**	**Control cells n=16**
Minimum	316.0	340.0	99.0
Lower Quartile (Q1)	611.5	760.8	262.2
Median	734.0	923.0	324.5
Mean	760.1	926.4	322.9
Upper Quartile (Q3)	856.0	1173.8	413.8
Maximum	1363.0	1350.0	478.0

Figure 4.2 –Violin plots of total numbers of mouse proteins per single cell as detected by mass spectrometry in uninfected, infected and control cells. Kruskal-Wallis, n=16, *** $p<0.001$ (A). Statistical summary of numbers of detected mouse proteins within the three different cell types (B). "Uninfected", "Infected" and "Control" refer to uninfected and infected cells coming from infected mice, and control cells isolated from uninfected mice respectively. Mice were culled at 6hpi.

(A)

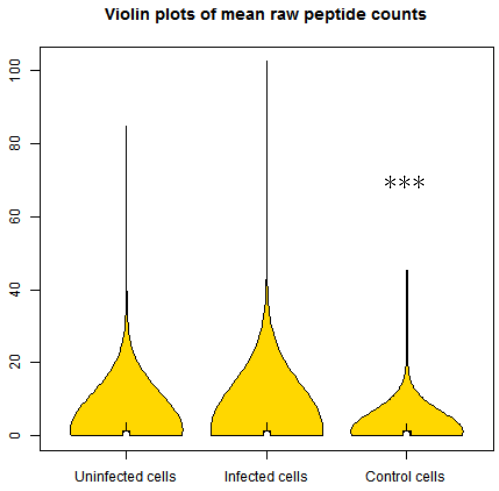

(B)

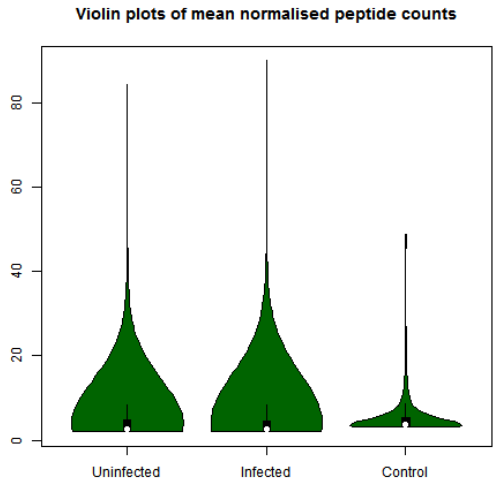

(C)

		UTI89-GFP Infected mice		Uninfected mice
		Uninfected cells n=16	**Infected cells n=16**	**Control cells n=16**
Raw detected peptide counts	**Minimum**	0.0000	0.0000	0.0000
	Lower Quartile (Q1)	0.0625	0.0625	0.1250
	Median	0.3125	**0.2500**	0.3125
	Mean	1.5820	0.6930	1.3040
	Upper Quartile (Q3)	1.4380	1.4380	1.3750
	Maximum	84.6200	102.4000	45.1900
Normalised peptide counts	**Minimum**	2.000	2.000	3.071
	Lower Quartile (Q1)	2.143	2.143	3.179
	Median	2.571	2.643	3.643
	Mean	4.457	4.491	4.987
	Upper Quartile (Q3)	4.661	4.571	5.393
	Maximum	84.430	90.000	48.750

Figure 4.3 – Violin plots of the number of peptides (y axis) mapped to a single mouse protein in a single cell. Data is grouped by cell type (uninfected and infected cells coming from infected mice, and uninfected (control) cells, from uninfected mice) before normalisation, n=2478, Kruskal-Wallis *** $p<0.001$ (A), and after normalization (B). Summary statistics of the distributions of peptide counts per (eukaryotic) protein in a single cell. Data is grouped by the three cell types prior and upon normalization with NODES (C). "Uninfected", "Infected" and "Control" refer to uninfected and infected cells coming from infected mice, and control cells isolated from uninfected mice respectively. Mice were culled at 6hpi.

(A)

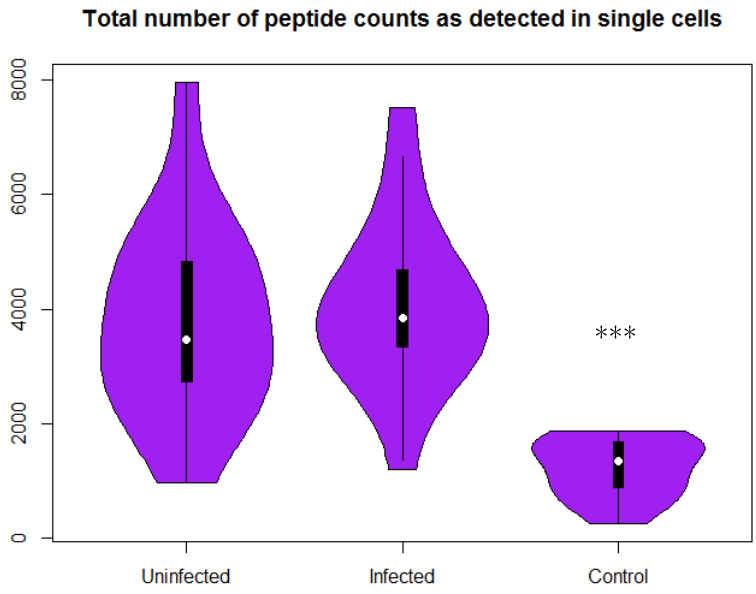

(B)

	UTI89-GFP infected mice		Uninfected mice
Total Detected Peptide Numbers	**Uninfected cells n=16**	**Infected cells n=16**	**Control cells n=16**
Minimum	972	1212	263.0
Lower Quartile (Q1)	2740	3353	880.8
Median	3473	3855	1344.5
Mean	3794	4060	1230.6
Upper Quartile (Q3)	4841	4677	1680.5
Maximum	7959	7513	1869.0

Figure 4.4 – Violin plots of total numbers of mouse peptides detected in single cell samples (y axis) in uninfected and infected cells coming from infected mice, and uninfected (control) cells from uninfected mice. n=16, Kruskal-Wallis *** $p<0.001$ (A). Summary statistics of detected eukaryotic peptides within the three different cell (B). "Uninfected", "Infected" and "Control" refer to uninfected and infected cells coming from infected mice, and control cells isolated from uninfected mice respectively. Mice were culled at 6hpi.

(A)

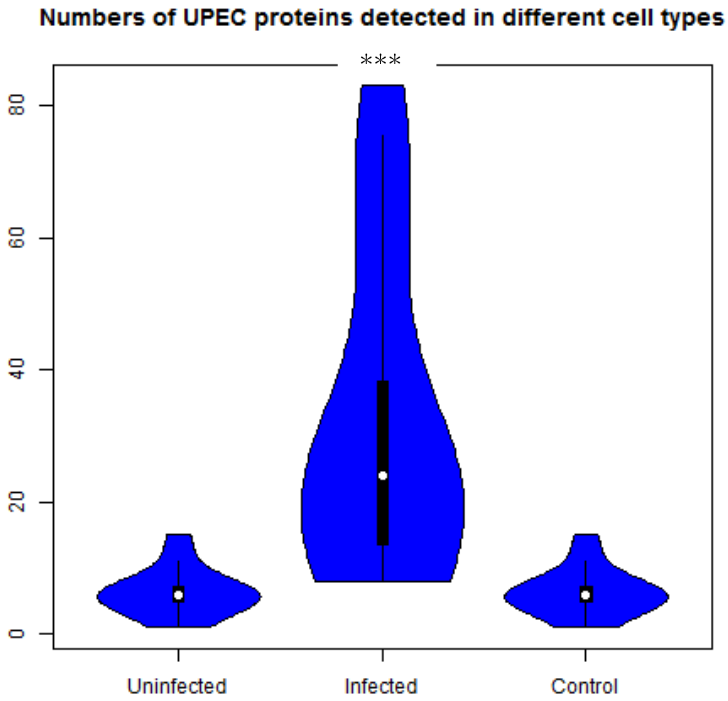

(B)

	UTI89-GFP infected mice		Uninfected mice
Detected Protein Number	**Uninfected cells n=16**	**Infected cells n=16**	**Control cells n=16**
Min	1.000	8.00	0.0000
Q1	4.750	13.50	0.0000
Median	6.000	24.00	0.0000
Mean	6.312	31.75	0.6875
Q3.	7.250	38.25	1.0000
Max.	15.000	83.00	4.0000

Figure 4.5 – Violin plots of total bacterial proteins detected per single cell (y axis) in uninfected and infected cells coming from infected mice, and uninfected (control) cells from uninfected mice; n=16, Kruskal-Wallis, *** $p<0.001$ (A). Summary statistics of detected bacterial proteins within the three different cell types (B). Mice were culled at 6hpi.

(A)

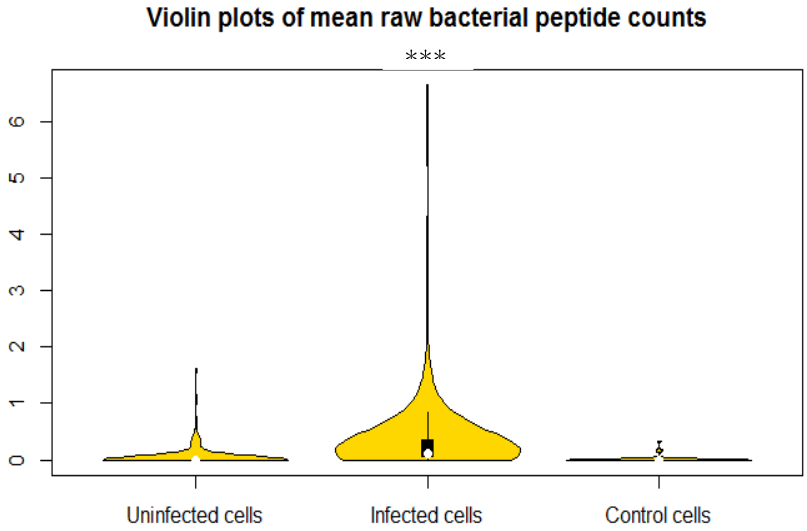

		UTI89-GFP infected mice		Uninfected mice
(B)		Uninfected cells n=16	Infected cells n=16	Control cells n=16
Mean raw bacterial peptide counts as detected per protein per cell	Min	0.00000	0.00000	0.00000
	Q1	0.00000	0.058820.00000	0.00000
	Median	0.00000	**0.11765**0.00000	0.00000
	Mean	0.05279	0.39110	0.01239
	Q3.	0.00000	0.367650.00000	0.00000
	Max.	1.62500		0.33333

Figure 4.6 – Violin plots of raw peptide counts (y axis) of bacterial proteins for single proteins as detected in single uninfected and infected cells coming from infected mice, and uninfected (control) cells, from uninfected mice; n=148, Kruskal-Wallis, *** p<0.001 (A). Summary statistics of mean raw peptide counts for every detected bacterial proteins, per protein, per cell as detected within the three different cell types (B). Mice were culled at 6hpi.

(A)

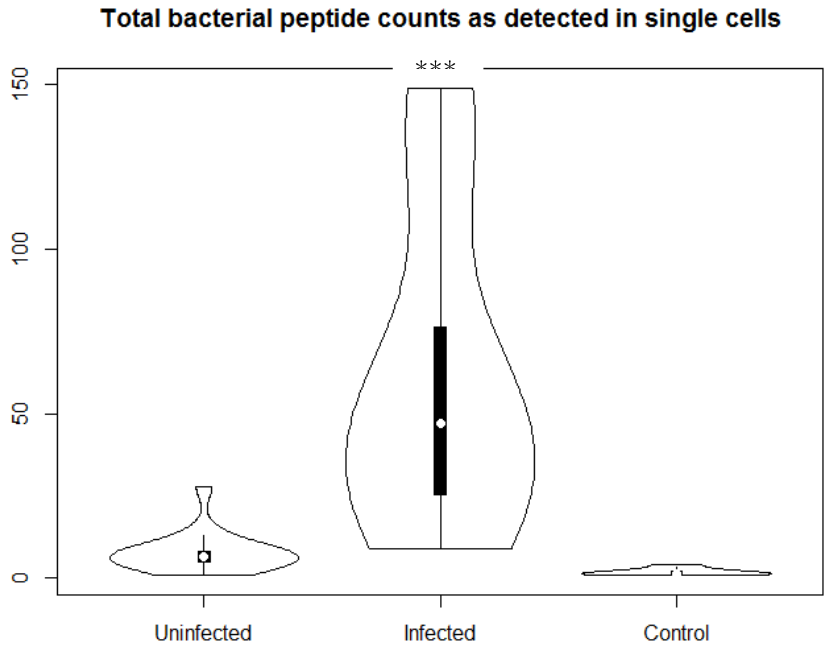

(B)

	UTI89-GFP infected mice		Uninfected mice
Total Detected Peptide Numbers	**Uninfected cells n=16**	**Infected cells n=16**	**Control cells n=16**
Min	1.000	9.00	1.000
Q1	5.000	25.25	1.000
Median	6.500	47.00	1.500
Mean	7.812	61.19	1.833
Q3.	8.250	76.25	2.000
Max.	28.000	149.00	4.000

Figure 4.7 – Violin plots of total numbers of bacterial peptides detected in single cell samples (y axis) in uninfected and infected cells coming from infected mice, and uninfected (control) cells from uninfected mice; n=16, Kruskal-Wallis, *** $p<0.001$ (A). Summary statistics for the three different cell types showing total numbers of bacterial peptide counts, as detected per individual cells(B). Mice were culled at 6hpi.

4.4.4 Cell type confirmation

The single mouse bladder cell proteomics data examined in this work was assumed to come from superficial urothelial cells. While it can be considered true for siECs due to the use of GFP-tag and well characterised infection model, the origin of the uninfected cells could be questioned not only in terms of urothelial cell layer, but also cell type per se. Therefore, the assumption was examined to evaluate a potential misidentification of the studied cells. Detected proteins were inspected for the presence of characteristic urothelial cell markers, as established by [210]. Findings were summarised in Table 4.1.

Uroplakin proteins (UP1a, UP1b, UP2, and UP3a) are the building blocks of AUM plaques found on specialised umbrella cells. Given their abundance in superficial cells, uroplakins are the most well characterised markers of urothelial cells. Having found uroplakins in almost all test samples gives us a high level of certainty that the correct cell type was isolated during our studies.

Cytokeratins are another useful marker for identifying epithelial cells. Each cell layer expresses a different set of cytokeratin proteins, providing insight into cell origin. During the isolation procedure from uninfected mice, it was common for cells from the underlying epithelial cell layers to be mixed in with the superficial cells, due to the absence of a specific marker to decipher the different layers. CK7, CK8, and CK19 are expressed across all urothelial cell layers and were found in all cells. CK18, usually also found throughout all urothelial layers, was found in all but one cell. Cytokeratin 20, which is typically only expressed in superficial cells, was absent in 2 cells, suggesting they may have been from the underlying epithelial layers. 28 out of 42 cells were found to contain CK13, which is typically found in all but superficial cell layers. Normally found to be associated with the basal cell layer, CK5 was detected in all infected and uninfected cells, and 12 of the control cells. Furthermore, the basally expressed CK17 was found in 28 of all cells (seven infected, nine uninfected, and 12 control cells). Having a slow turnover rate, urothelial cells are not expected to express cell cycle-associated antigens, unless found in a "wound response" mode. Accordingly, the proliferation marker Ki67 wasn't detected in any of the cells. Normal urothelium expresses a number of molecules implicated in cell to cell and cell to matrix adhesion, such as E-cadherins, CD44, and β1 and β4 integrins. E-cadherins, and β1

integrins were the only adhesins found, in 11 (seven infected, and four uninfected cells) and eight (three infected, two uninfected and three control cells) samples respectively.

Table 4.1 – A list of human urothelial cell markers, according to their class and expression site, and the number of cells in which they were detected in infected and uninfected cells coming from infected mice and control cells coming from uninfected mice. Total number of cell in each group is 16.

CLASS	MARKER	DETECTED IN x/16		
		UTI89-GFP infected mice		Uninfected mice
		INFECTED	UNINFECTED	CONTROL
UROPLAKINS	UP1a	16	16	16
	UP1b	16	16	14
	UP2	16	16	15
	UP3a	16	16	14
CYTOKERATINS				
• All layers	CK7	16	16	16
	CK8	16	16	16
	CK18	16	16	15
	CK19	16	16	16
• Superficial cells only	CK20	15	16	15
• Present in all but the superficial	CK13	8	9	11
• Basally expressed	CK5	16	16	12
• Basally expressed	CK17	7	9	12
PROLIFERATION MARKER	Ki67	0	0	0
ADHESION MOLECULES	E-cadherin	7	4	0
	CD44	0	0	0
	β1 integrins	3	2	3
	β4 integrins	0	0	0

4.4.5 Technique validation

In order to confirm the validity and reproducibility of the data generated using our technique, Pearson's correlation coefficients (R) were calculated between each pair of single cells. Results in the form of Pearson's distance were presented as a heat map (Figure 4.8). The dominance of lighter colours illustrates a good strength of linear relationship between each and every cell, with mean R= 0.76. Similar results for mean R ranging between 0.79-0.88 were observed when examining each batch of cells separately, all demonstrating a good level of reproducibility. The only cells that may seemingly stand out are U18, I11, C3, C9, and C13, though the red and orange colours describing their correlation relationship with other cells are not tremendously different considering the scale.

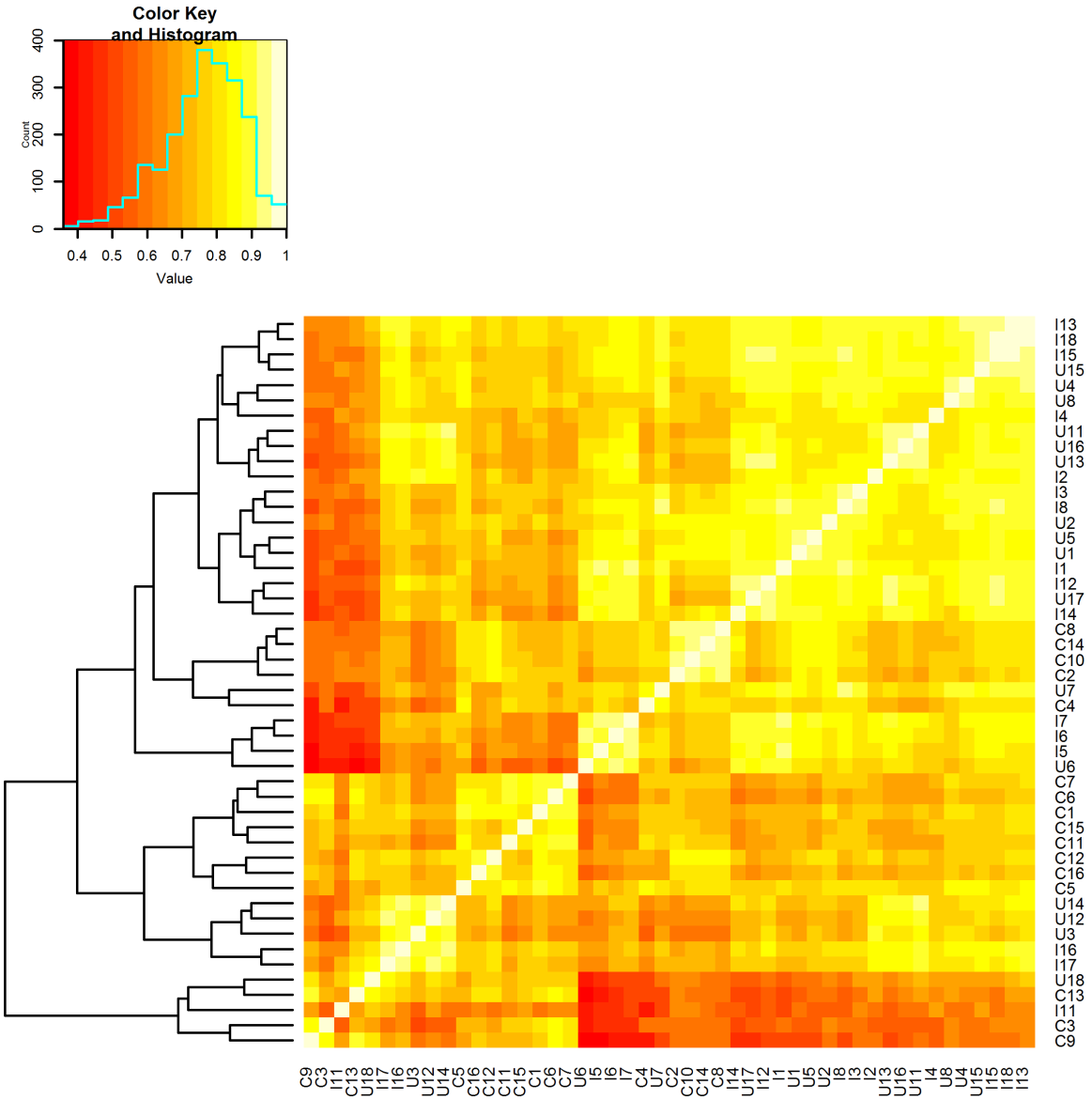

Figure 4.8 – Heat map of cell to cell correlation with dendrogram. Pearson correlation coefficient-based heat map matrix and hierarchical clustering represent the similarity of protein expression profiles based on raw mouse peptide counts detected in single cells. Infected (I) and uninfected (U) cells come from infected mice, and uninfected, control (C) cells come from uninfected mice. The colour scale reflects the distance score (1- Pearson's correlation coefficient) between each pair of cells. Whites and yellows indicate a strong positive correlation, while reds are associated with correlations close to zero.

4.4.6 Proteome depth and coverage analysis

To determine if the peptide detection efforts are sufficient and if all proteins from within each sample have been captured, rarefaction analysis was performed. The rarefaction curves in Figure 4.9 show sampling efficiency in terms of the number of detected proteins for individual single cells, as the function of total number of detected peptides. None of the curves for each single cell reached a saturation plateau, suggesting cells in our data set were undersampled and not all proteins were detected at the current threshold for technique sensitivity.

4.4.7 Determination of the minimum number of single cells required for sampling the whole proteome of urothelial cells

The study design was also examined with respect to the threshold for the minimum number of single cells necessary to sample in order to detect data that is representative of the entire mouse urothelial cell proteome. Figure 4.10 shows how the feature space increases with each additional sample added in our data, and therefore how many more cells we would need to isolate and process in order to cover the entire mouse proteome. The visual investigation of this cumulative plot of total number of detected proteins suggests that we have already reached a saturation, and therefore increasing the number of samples would not notably extend the identified protein pool.

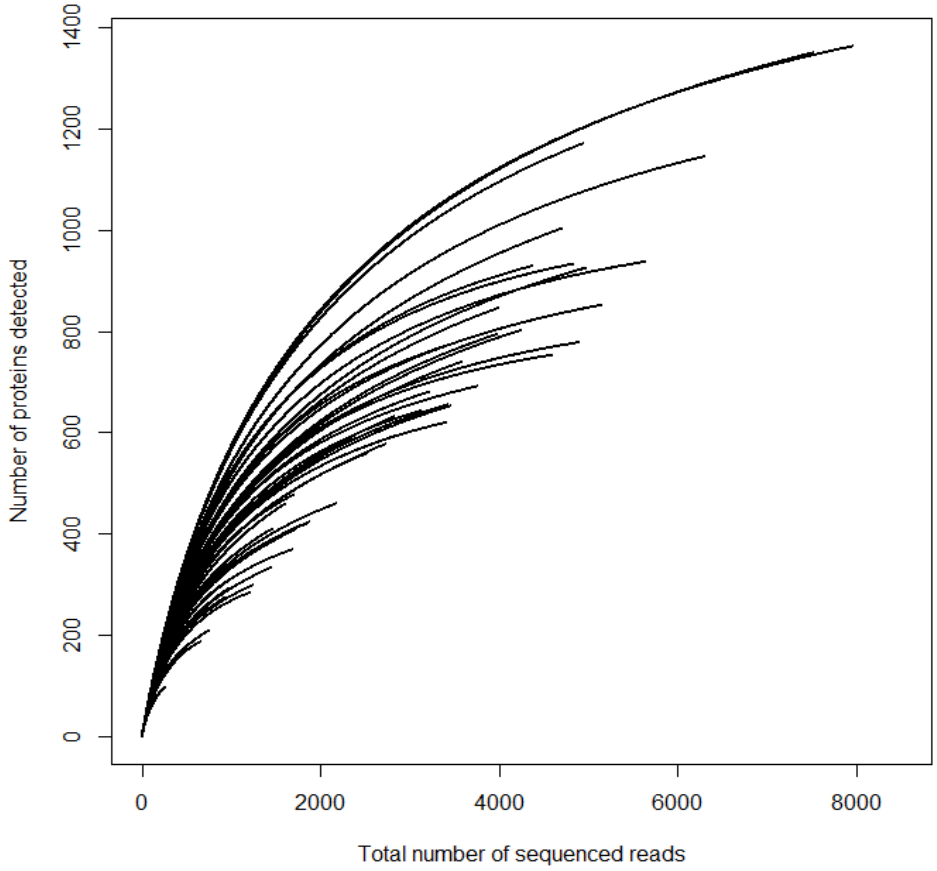

Figure 4.9 – Rarefaction curves of protein richness. Each curve represents one single urothelial cell scaled by the number of proteins detected within it. N=48.

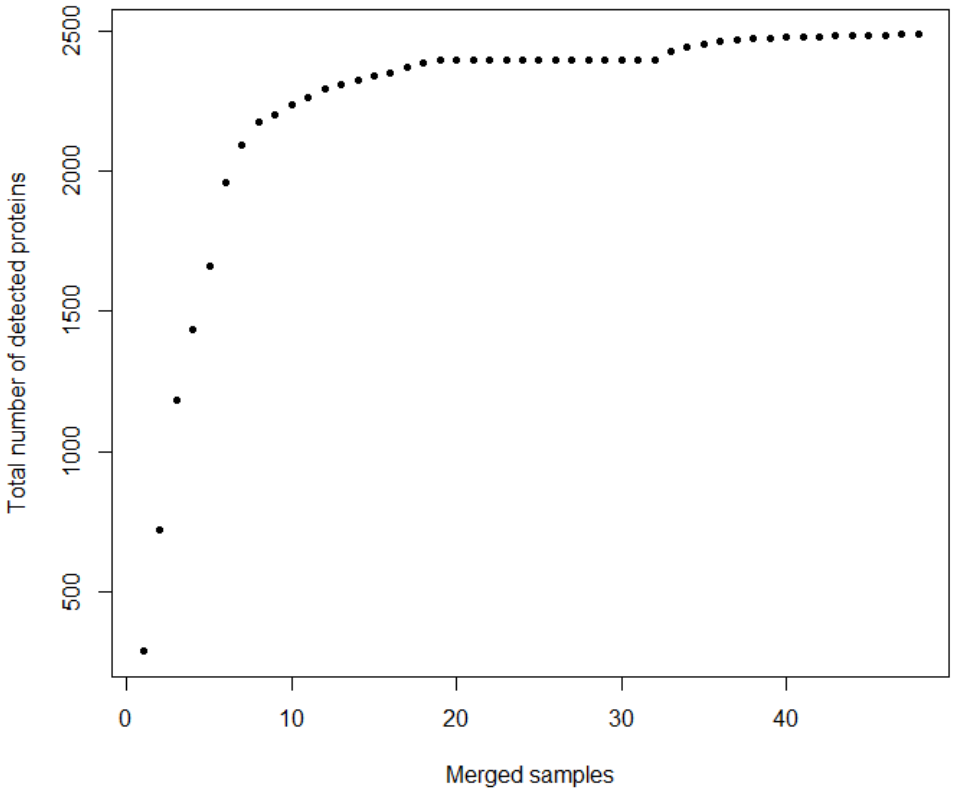

Figure 4.10 – The cumulative plot of total detected proteins. Cumulative number of detected proteins as a function of total number of single urothelial cells used in the data set.

4.4.8 Differential expression analysis

We hypothesised that in response to the presence of IBC(s) within epithelial cells, expression of some eukaryotic proteins would be changed. With the aim of identifying these proteins, differential expression analysis between single infected and uninfected cells was performed. To focus the effort on identifying proteins strictly associated with intracellular UPEC infection and not those induced by lipopolysaccharides, control cells coming from uninfected mice were excluded from this analysis. In view of the fact that data from single cells are very sensitive to non-biologically-interesting features like technical artefacts or batch effect, two within-batch differential expression analyses were performed. Each batch consisted of eight infected and eight uninfected cells, collected several months apart. Due to technical issues a few (about 5) of the uninfected cells in batch 1 were collected from uninfected mice.

4.4.8.1 Quality control

The assumption that distribution of P-values generated by differential expression analysis between infected and uninfected cells comes from a uniform distribution was visually inspected using a quantile-quantile (Q-Q) plot (Figure 4.11A). The diagonal line represents the plot of theoretical quantiles from a uniform distribution. The observed distribution of P-values coming from the differential expression analysis of proteins coming from all infected and all uninfected (32 cells in total) mouse urothelial cells from both batches (n = 1015) seemingly does not match the expectation over most of its range (roughly $0.3 > P > 0.005$) (Figure 4.11A). To study this behaviour and identify whether it could be associated with an accumulation of points in any particular part of the graph, a density plot was generated (Figure 4.11C). The density plot shows the overall distribution of P-values, with the majority of them found in the proximity of the intersection point (0,0) of the QQ-plot where they do fit with the diagonal. This suggested that, in agreement with the initial assumption regarding the distribution of these P-values, the majority of the P-values are uniformly distributed. To evaluate the validity of this observation, control Q-Q (Figure 4.11B) and density plots (Figure 4.11D) were generated using P-values coming from DE analysis of permuted groups of the same data matrix. The permutation test was performed by randomising the cells with respect to infected/uninfected status (i.e. each cell was randomly assigned to be infected or uninfected) and then repeating the analysis for differential gene expression. For log transformed P-values between 0.0 and 0.3 the density plot is found to be flatter, as compared to Figure 4.11C, and in Figure 4.11B. The plot fits better with the diagonal for P-values between 1 and 0.1. These observations supported a statistical model in which the null hypothesis is true on the interval [0.1, 1], where a substantial number of P-values following uniform distribution can be found, while the alternative hypothesis can be true on the interval [0.0000, 0.1] for only some proteins with large effect.

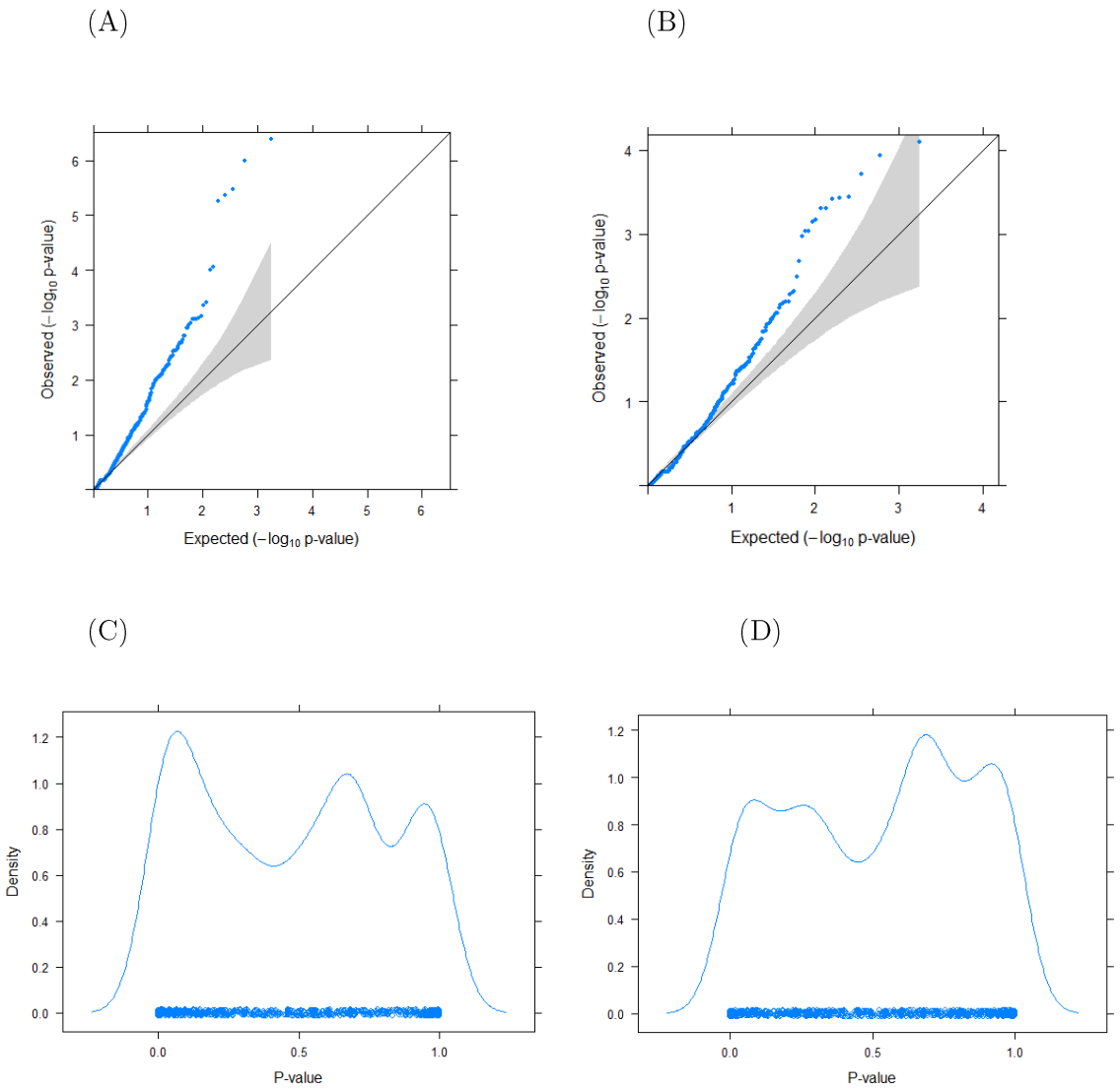

Figure 4.11 – Quantile-quantile and density plots resulting from differential expression analysis. (A) Q-Q plot of observed versus expected P-values coming from differential expression analysis of proteins coming from infected and uninfected mouse urothelial cells (n = 1015). Observed P-values are plotted as –log10 values, as a function of the expected (uniform) distribution. The 95% confidence intervals are shaped by grey. The observed distribution does not match the expected distribution and shows an excess in the tail at ca. $P < 0.2$. (B) Q-Q plot of P-values coming from differential expression analysis of the data set with randomly assigning groups. (C) Density plot shows distribution of observed P-values as seen in Figure 4.11A. (D) Density plot showing distribution of P-values generated by randomly assigning groups to the data matrix. (C-D) X-axis represents coordinates of the points where the density is estimated. Kernel= Gaussian, bandwidth= 0.07128.

4.4.8.2 Identification of differentially expressed genes

The single-cell analysis of differential expression was performed using NODES. Selection criteria for differentially expressed genes (DEGs) included the log fold change threshold greater than one, and false discovery rate filter of less than 0.05. Only four proteins coming from the analysis of batch 2 data (Figure 4.13), and six from batch 1 (Figure 4.12) met these criteria. The ten proteins were equally split into being up- or down-regulated in infected cells. None of them has been previously associated with UPEC infection. They are known to be involved in protein and chemical breakdown, or protease inhibition, glycolysis, or acting as molecular chaperones [281-286].

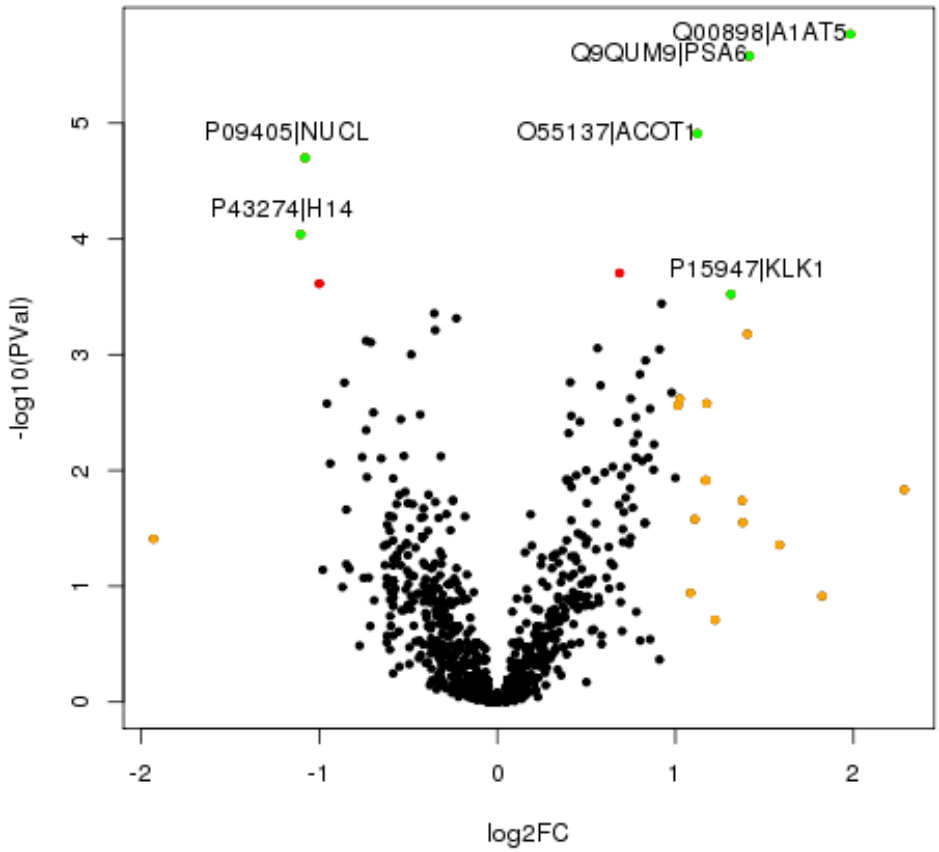

Figure 4.12 – Volcano plot analysis of differentially expressed proteins in batch 1 cells. Log_2 expression fold change in single infected over uninfected mouse urothelial cells is plotted on the x-axis. P-value significance is plotted on the y-axis ($-log_{10}$ scale). Upregulated and downregulated proteins are indicated in red if false discovery rate (FDR)-adjusted significance is <0.05; orange is used to mark protein set with log2FC>1 and green if both requirements are met.

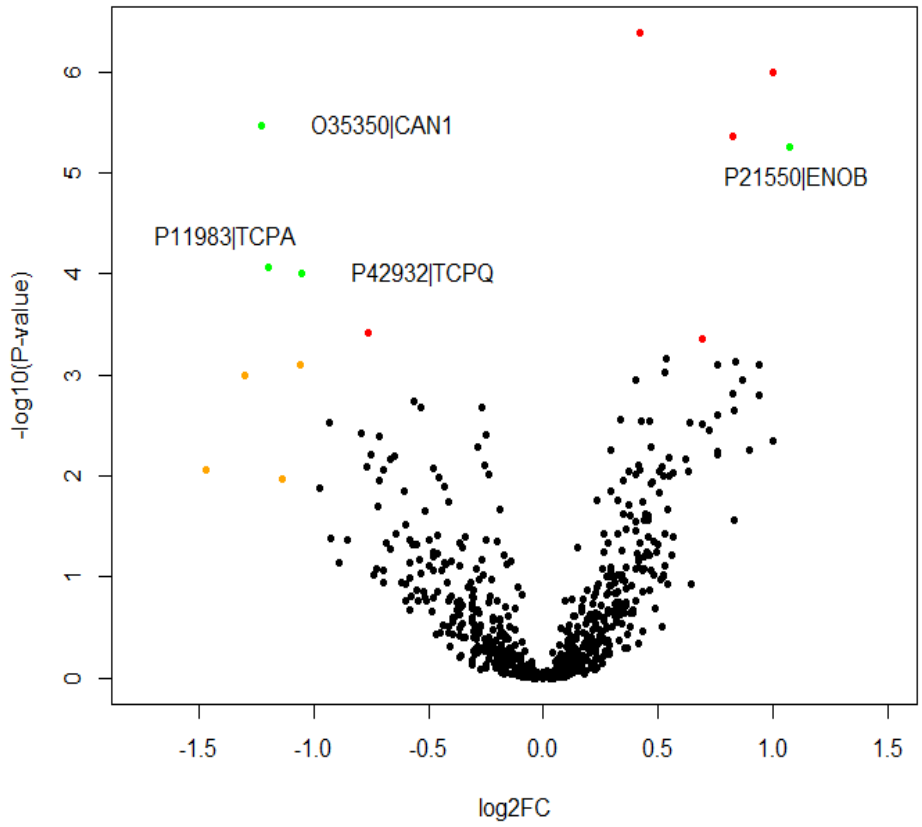

Figure 4.13 – Volcano plot analysis of differentially expressed proteins in batch 2 cells. Log_2 expression fold change in single infected over uninfected mouse urothelial cells is plotted on the x-axis. P-value significance is plotted on the y-axis ($-log_{10}$ scale). Upregulated and downregulated proteins are indicated in red if false discovery rate (FDR)-adjusted significance is <0.05; orange is used to mark protein set with log2FC>1 and green if both requirements are met.

4.4.9 Pathway and biological process enrichment analysis of DEGs

To identify potential classes of proteins that may have an association with infection or other phenotypes, disturbances in molecular interactions and processes were investigated using the set of ten DEGs identified earlier (Acot1, Psa6, Klk1, Nucl, H14, Tcpθ, EnoB A1At5. Tcpα, Can1) (Figure 4.12 and Figure 4.13). To determine the impact of UPEC infection on cellular pathways, KEGG pathway analysis was executed. The enrichment of biological processes among the DEGs was done using the DAVID Functional Annotation Tool. Neither of the analyses revealed any statistically significant results, with the most enriched pathway being a metabolic pathway with two overlapping proteins (Acot1 and EnoB).

4.4.10 Validation of DEGs

4.4.10.1 Spatial distribution of differentially expressed proteins by whole mount mouse bladder immunofluorescence

Initial analysis of single-cell proteomics data identified a number of differentially expressed proteins between intracellularly UPEC-infected and uninfected mouse urothelial cells. To investigate whether these differences are indeed associated with the infection state of urothelial cells, changes in expression were explored by immunofluorescence labelling and microscopy in whole mounted murine bladders infected with a GFP-producing UTI89 (SLC-719) bacterial strain. 6hpi bladders were excised, cut in half along the urethral opening, splayed, fixed and stained as described in sections 2.10.6 and 2.13.2. Bladders were probed with varied concentrations of primary antibodies against Acot1, Psa6 and Klk1. All attempts at optimising this process were unsuccessful, mainly due to low antibody affinity, resulting in no detectable staining, and because of the thickness of bladder tissue preventing an optimal penetration of the reagents .

4.4.10.2 Quantitative Western blot analysis

An attempt to validate the differential expression of genes identified in section 4.4.8 was made using the 5637 cell line model (Methods section 2.7). Briefly, 5637 human urothelial cancer cells were infected with GFP-producing SLC-719 UTI89 bacterial strain (the same one used for mice infection). 4hpi cells were detached and underwent FACS analysis according to the presence of GFP signal (Figure 2.4). The control consisted of cells grown in parallel that have not been subjected to bacterial infection. Whole cell lysates of sorted cells were analysed using SDS-PAGE, and Western blotting using specific antibodies against DEGs (Acot1, Psa6, Klk1, Tcpθ, EnoB, Tcpα, Can1), β-actin and GFP. Due to unavailability of suitable antibodies against Alpha-1-antitrypsin 5, Nucleolin and Histone H1.4, these targets have not been tested by these means (Table 4.2).

Table 4.2– List of differentially expressed proteins, and availability of suitable antibodies to target them by Western blotting. Batch number indicates the batch the analysis of which resulted in revealing a given protein as differentially expressed. ID gives a specific Uniprot ID.

BATCH No.	ID	GENE NAME	ANTIBODY AVAILABLE
2	O35350|CAN1	Calpain-1 catalytic subunit	✓
2	P11983|TCPA	T-complex protein 1 subunit alpha	✓
2	P42932|TCPQ	T-complex protein 1 subunit theta	✓
2	P21550|ENOB	Beta-enolase	✓
1	Q00898|A1AT5	Alpha-1-antitrypsin 5	X
1	Q9QUM9|PSA6	Proteasome subunit alpha type-6	✓
1	O55137|ACOT1	Acyl-coenzyme A thioesterase 1	✓
1	P15947|KLK1	Kallikrein-1	✓
1	P09405|NUCL	Nucleolin	X
1	P43274|H14	Histone H1.4	X

4.4.10.2.1Cell sorting optimization

In order to optimise the FACS process, an MOI that would lead to infection of approximately 50% of 5637 cells per population was sought. MOIs in the range of 1-100 were tested. 5637 cells were infected with respective MOIs, detached and analysed by flow cytometry to investigate the spread of relevant cell populations, as defined based on a GFP signal. Proportions of these were measured using FlowJo (v10). Figure 4.15 shows how the populations of GFP+ve and GFP-ve cells change depending on the MOI used in a preceding infection. Based on this outcome, MOI=10 was used in all the following experiments requiring sorting infected cells based on their infection (GFP) status.

(A)

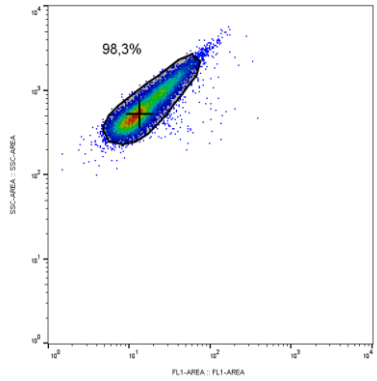

(B)

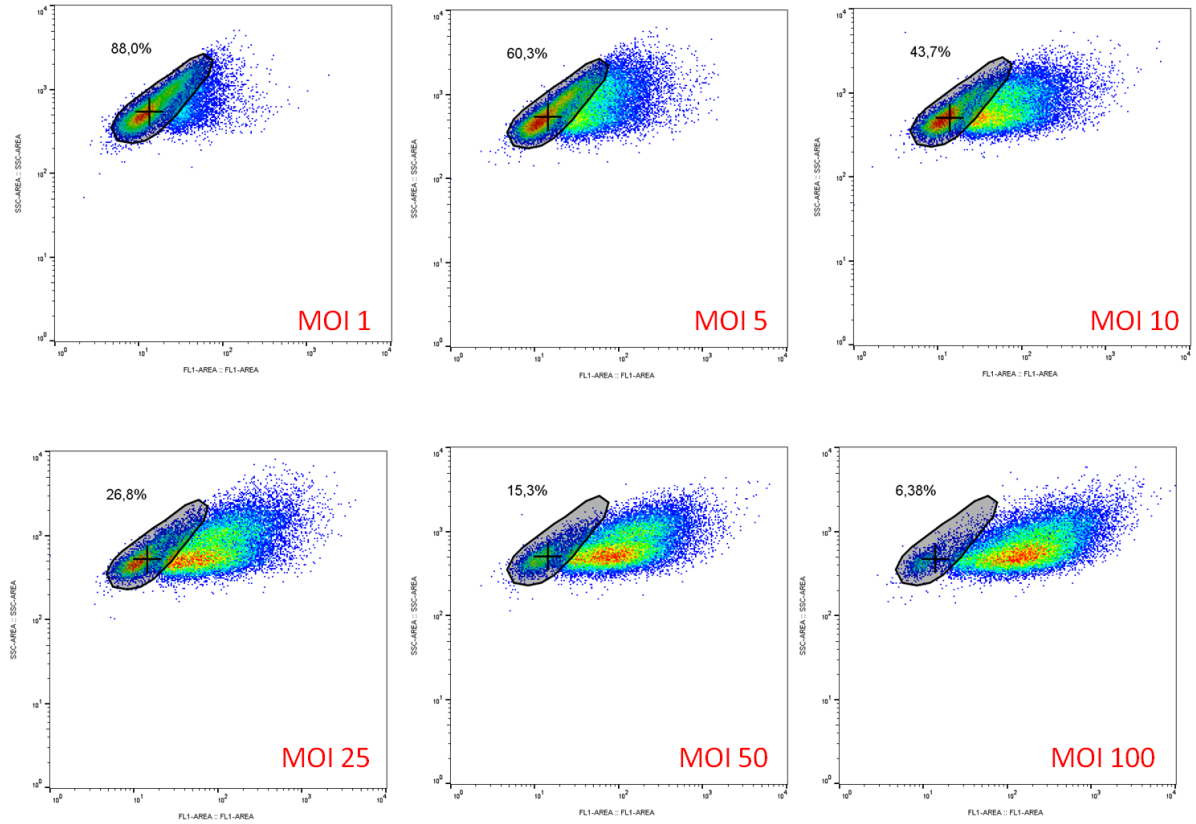

Figure 4.14 – SSC-Area vs FL1-Area density plots of FACS sorted 5637 cells. (A) Control- uninfected cells (B) SLC-719 (UTI89- vsGFP) infected cells at different MOIs, as indicated in bottom right corner of each density plot. Percent values indicate ratio of cells found in the shaded region. SSC- side scatter; FL- fluorescence.

4.4.10.2.2Quality control

Sorting cells in this manner can be a lengthy process (up to 2h if the sample was collected towards testing less abundant proteins), therefore cell viability was tested using trypan blue staining at a time equivalent to that of cell-lysis. Figure 4.15 shows that both populations of cells showed equal viability (~85% live cells) at the time of protein denaturation.

(A) (B)

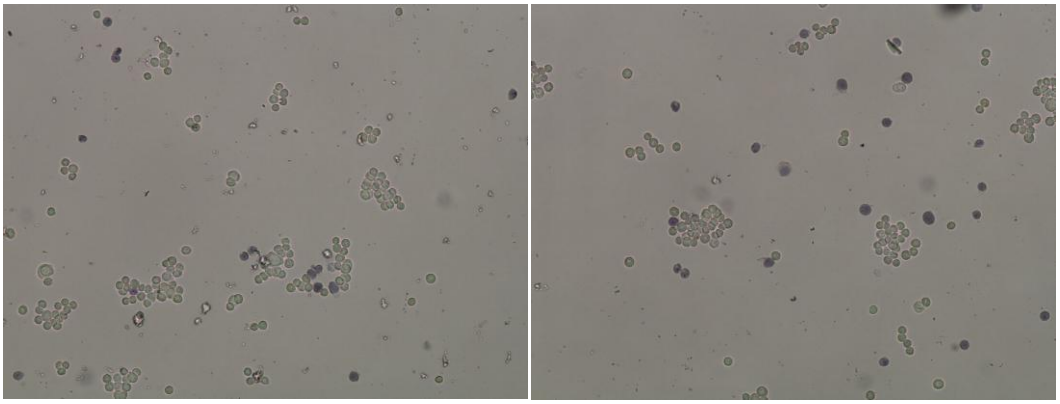

Figure 4.15 – Trypan blue staining of FACS-sorted 5637 cells. The images represent cultured 5637 cells, subjected to infection with SLC-719 bacterial strain. The images were taken upon completion of FACS sorting into (A) GFP+ve cells (B) GFP-ve cells, followed by staining with trypan blue. The dark cells represent dead trypan blue positive cells. Cells with bright centers are considered live.

To test the detection limit of FACS, the presence of GFP+ve cells 'contaminating' GFP-ve fractions, and vice versa, were tested for by culture. Approximately $1.7x10^6$ of intact control uninfected cells were plated on agar and compared to ~$1x10^4$ GFP-ve cells processed and plated in the same way. The former yielded no bacterial growth. But on average 0.097% of the GFP-ve population (cells uninfected, as defined based on GFP signal by FACS, coming from the cell population subjected to UPEC infection) turned out to be infected (n=3). Recovered CFUs were investigated under fluorescent microscope, confirming their fluorescence, and therefore likely source of the contamination being SLC-719 coming from GFP+ve cells.

The assumption of one GFP+ve cell yielding one CFU was also tested. On average only seven CFUs were recovered per 100 whole GFP+ve cells. And eight CFUs per 1000 of Triton X-100-treated cells plated on LB agar (0.81%) (n=7). One explanation of these findings is that GFP

was still present within the urothelial cells, even if the intracellular bacteria were killed by the host. Other possibilities could include the contamination of the GFP+ve fractions of cells by the GFP-ve ones; or the detection of false positive signal by FACS.

4.4.10.3 Quantitative analysis

In order to confirm the changes in relative abundance of Tcpθ, Tcpα, Can1, EnoB, Acot1, Psa6, Klk1 identified by DE analysis of single cell proteomics, we performed quantification of protein expression during intracellular infection with UPEC by Western blotting. Primary antibody concentrations were optimised against all of the aforementioned targets, but due to their low expression in cells of interest and low antibody affinity Acot1, Psa6, and Klk1 gave inconsistent results being upregulated in one replicate, and downregulated in another. Therefore, we only sought to investigate whether there was downregulation of Tcpθ, Tcpα, and Can1, and upregulation of EnoB in GFP+ve cells as compared to GFP-ve cells. Uninfected 5637 cells that were not exposed to bacteria, were used as a reference to control for a basal expression of each of the proteins of interest. Protein expression was presented as a percentage of the 43kDa βactin control in units of relative intensity (Figure 4.16). As an additional control, whenever possible, expression of GFP was explored also by Western blotting.

No statistically significant differences in expression of tested proteins between the urothelial cell types were observed. However, a large degree of variability between the replicates of data obtained using quantitative Western blotting (Figure 4.16) reduced the power of detecting any differences, and therefore made it difficult to confirm whether the proteins of interest were indeed differentially expressed.

(A)

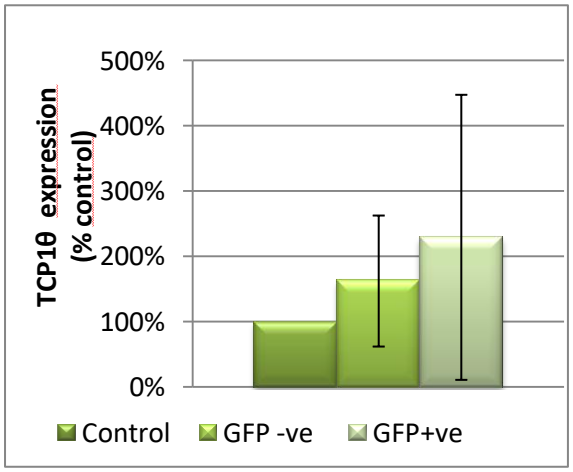
TCP1θ expression (% control)
500%
400%
300%
200%
100%
0%
Control
GFP -ve
GFP+ve

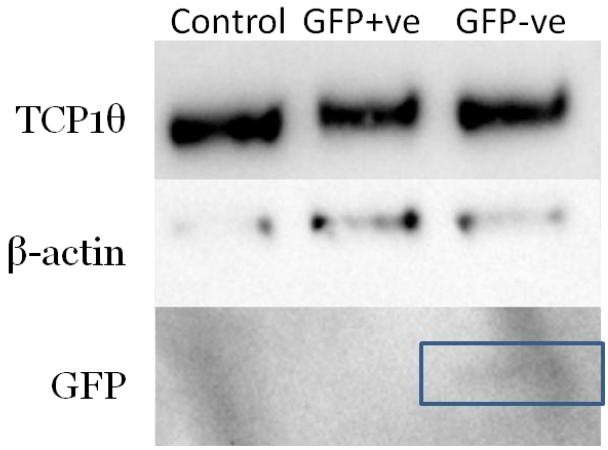
Control
GFP+ve
GFP-ve
TCP1θ
β-actin
GFP

(B)

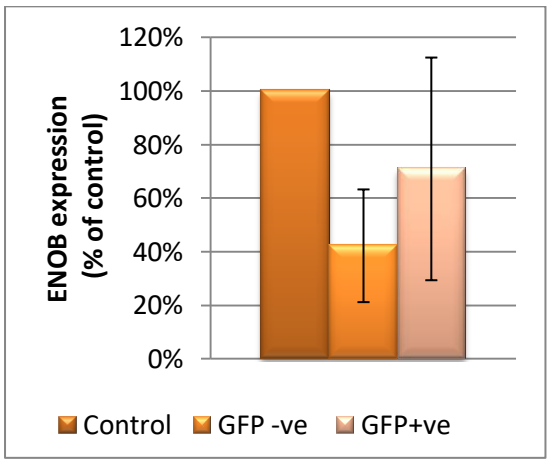
ENOB expression (% of control)
120%
100%
80%
60%
40%
20%
0%
Control
GFP -ve
GFP+ve

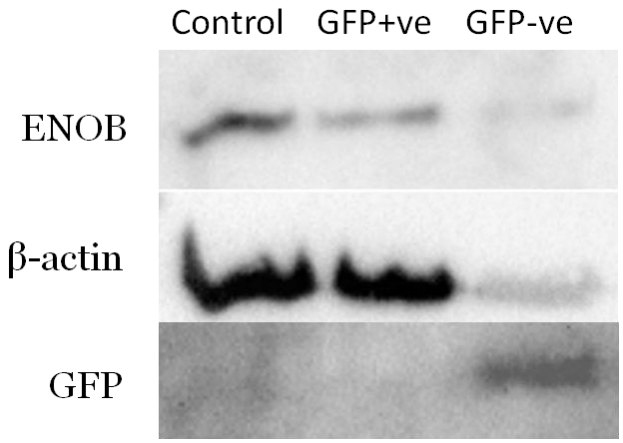
Control
GFP+ve
GFP-ve
ENOB
β-actin
GFP

(C)

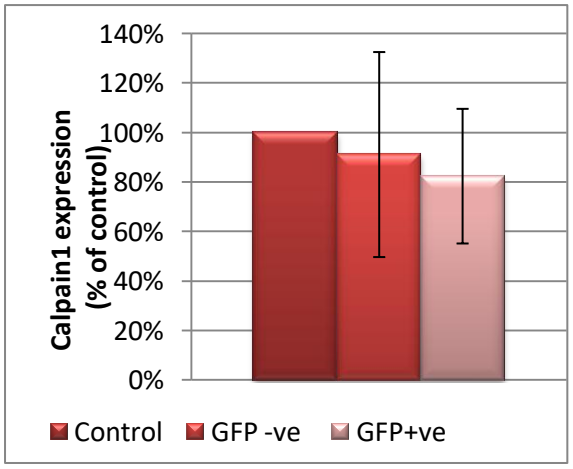
Calpain1 expression (% of control)
140%
120%
100%
80%
60%
40%
20%
0%
Control
GFP -ve
GFP+ve

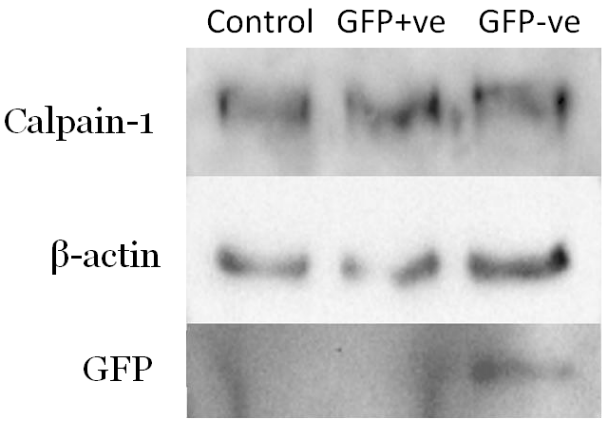
Control
GFP+ve
GFP-ve
Calpain-1
β-actin
GFP

(D)

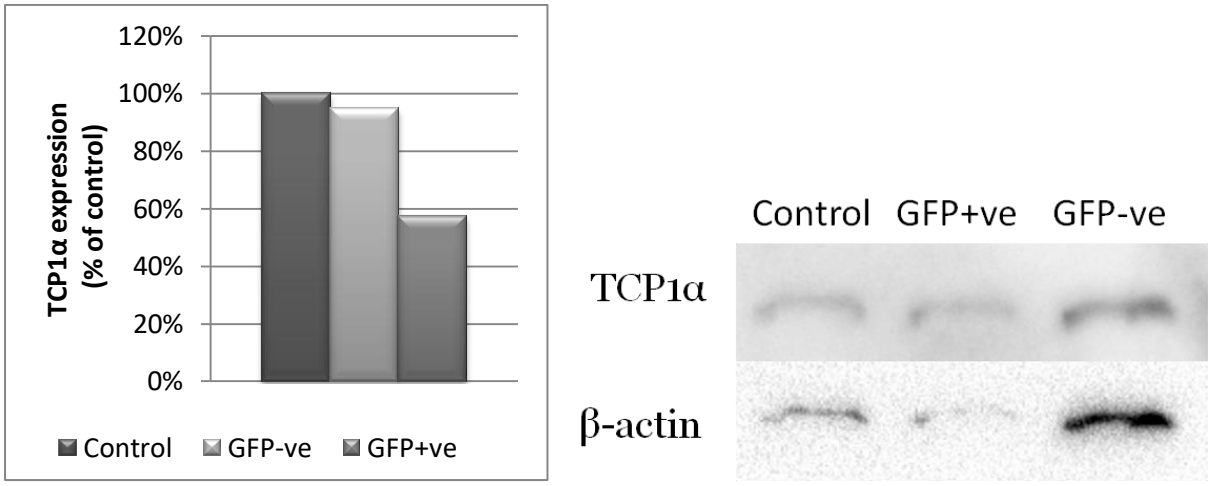

Figure 4.16 – Quantitative Western blotting analysis of expression of (A) Tcpθ (n=4); (B) EnoB (n=2); (C) Calpain-1 (n=3) and (D) Tcpα (n=1) proteins in control 5637 human urothelium cancer cells. GFP+ve and GFP-ve 5637 cells were collected 4hpi with SLC-719. Graphs are presented as mean values in units of relative intensity compared to beta actin control blots. Representative blots probed with specific antibodies are shown to the right of each histogram. Bands correspond to expression (from the left) in control cells, GFP+ve and GFP-ve cells. The statistical significance was assayed using Kruskal-Wallis One Way Analysis of Variance on Rank, followed by Dunn's method of pairwise multiple comparison procedure. No significant difference in the expression of protein is seen in any of the samples; Error bars= SD.

4.4.10.4 Immunohistochemical analysis of A1AT protein distribution

Since validation of DEGs using quantitative Western blotting analysis did not result in any definitive answers, we sought further confirmation of our data using immunohistochemical analysis in the mouse urinary bladder. A1AT was found to show the greatest level of differential regulation, therefore we chose it as our target protein to investigate whether we could detect differential expression patterns using this technique. As staining intensity depends on the antibody concentration, the optimal dilution of the anti-A1AT5 antibody was determined using mouse bladder tissue. Because A1AT5 is typically secreted by liver cells [287], rat and human liver tissues were used as positive controls (Figure 4.17). A 1 in 200 dilution was found optimal.

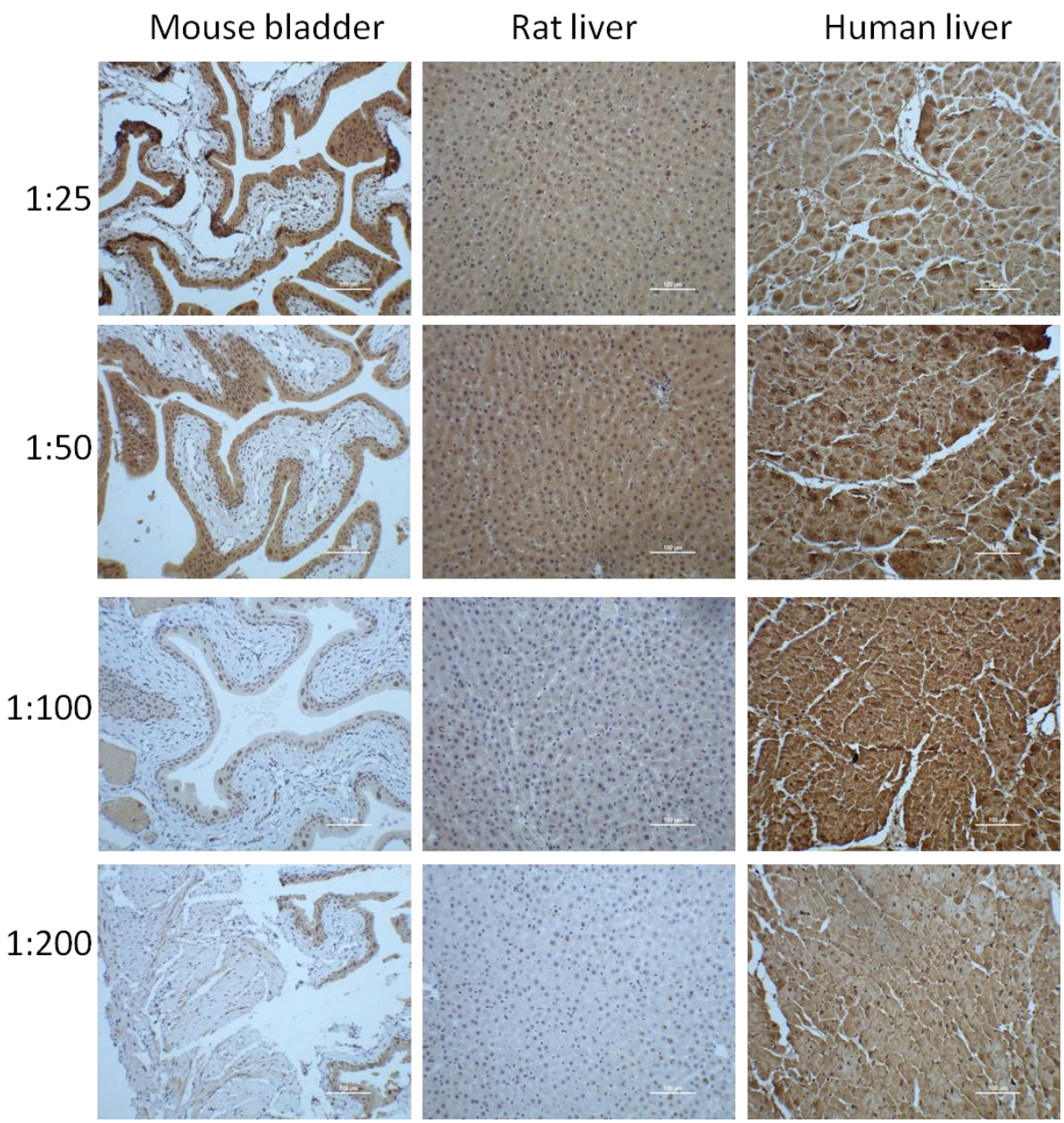

Figure 4.17 – Optimisation of anti-A1AT5 antibody dilution. A1AT5 protein staining was tested in uninfected mice bladders, rat and human livers using four dilutions in the range of 1:25- 1:200. Representative light micrographs of immunohistochemical staining of tissue sections are shown. Cell nuclei were counterstained with Gills haematoxylin Scale bars = 100μm. Magnification 20x.

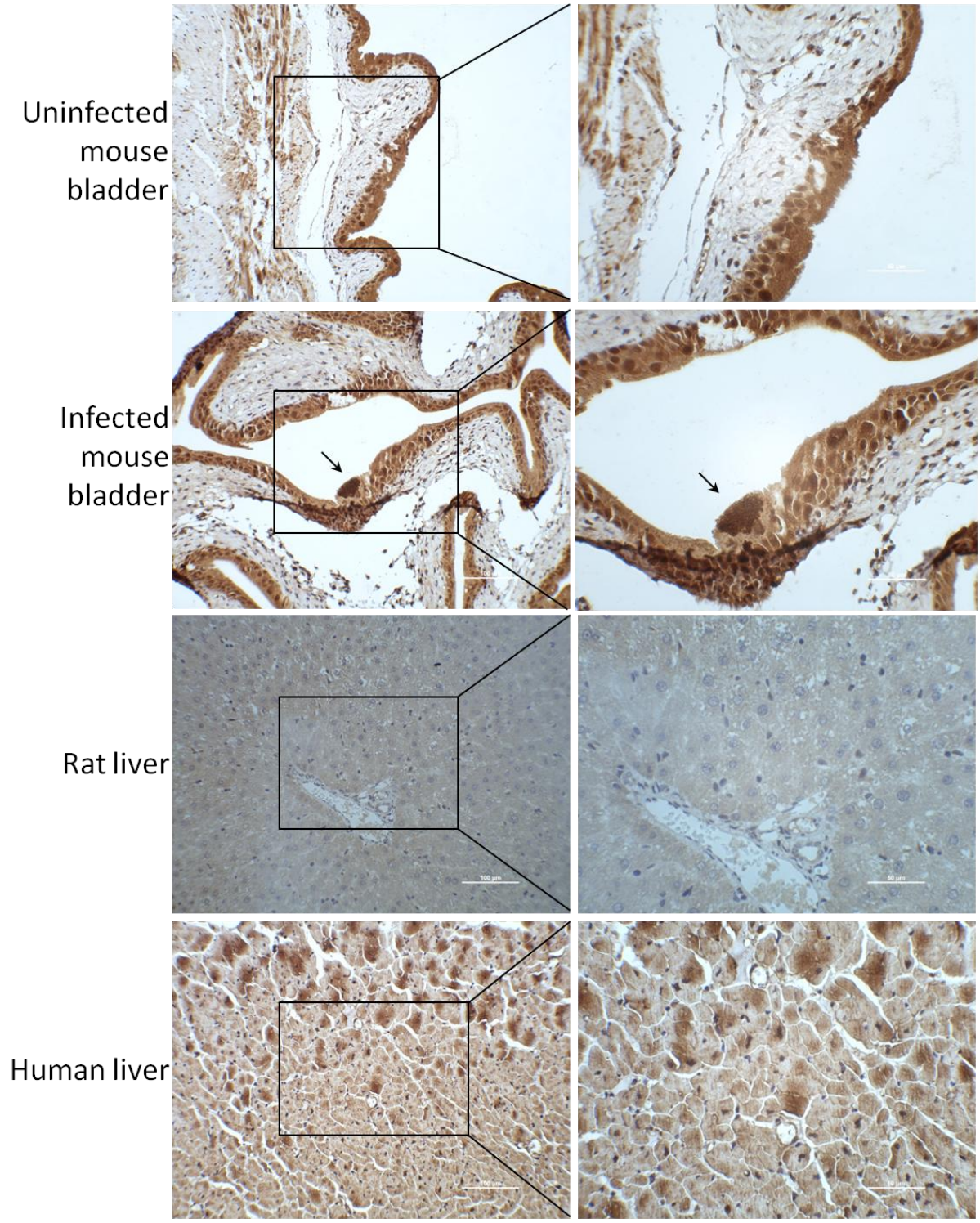

Figure 4.18 – A1AT5 protein distribution in infected and uninfected mice bladders, and rat and human livers. Representative light micrographs of immunohistochemical staining of serial sections (20x magnification; Scale bars = 100µm) and zoomed in areas marked with a black rectangle (40x magnification; Scale bars = 50µm). Distribution of A1AT5 protein was determined by immunohistochemistry using anti-A1AT5 antibody. Cell nuclei were stained with Gills haematoxylin. Black arrow indicates a location of an IBC.

Immunohistochemical staining of urinary bladder sections with antibodies against A1AT5 revealed that it was densely expressed by urothelial cells, with moderate expression by smooth muscle cells in some bladders (Figure 4.18). Urothelial cells in the infected bladders did not show any differences in expression of the protein, as shown by densitometric analysis using ImageJ 1.48v. (NIH, USA). However the staining intensity varied depending on which bladder the section was taken from, and the staining of sections was often found to be patchy. Therefore, further analysis is required to determine whether this variation is representative of the mouse population or artefact.

4.4.11 Clustering of single-cell mass spectrometric data

Due to the inability to validate the differentially expressed proteins identified by single cell mass spectrometry analysis, a further insight into data was made. One of the potential reasons could be associated with batch effect, a common complication among high-throughput technologies [288]. The raw peptide count data (Figure 4.19A) showed different levels of distribution between samples from between batches. After normalisation, these variations were reduced (Figure 4.19B). To test whether the resultant normalised data set is still confounded by non-biological batch effects a principle component analysis (PCA) was plotted (Figure 4.20). Principle component (PC)1, which is typically represented by technical batch effect, appears to be still notable, suggesting it was not entirely eliminated and could potentially result in artefacts related to this batch effect.

4.4.11.1 K-means clustering

Other than technical issues, the possibility that the superficial cell layer may contain a heterogenous population of epithelial cells, unrelated to the infection state was also considered. To examine whether the data, that are confounded by the two batches of cells, clusters due to the infection status and/or the presence of multiple cell types, rather than due to the batch effect, we used an unbiased k-means clustering [289]. This technique is very sensitive to batch effect, and would therefore reveal any of its residual effects. The data were normalised, and data for every protein were batch mean-centered, followed by the addition of the overall average protein expression prior to k-means clustering [290].

(A)

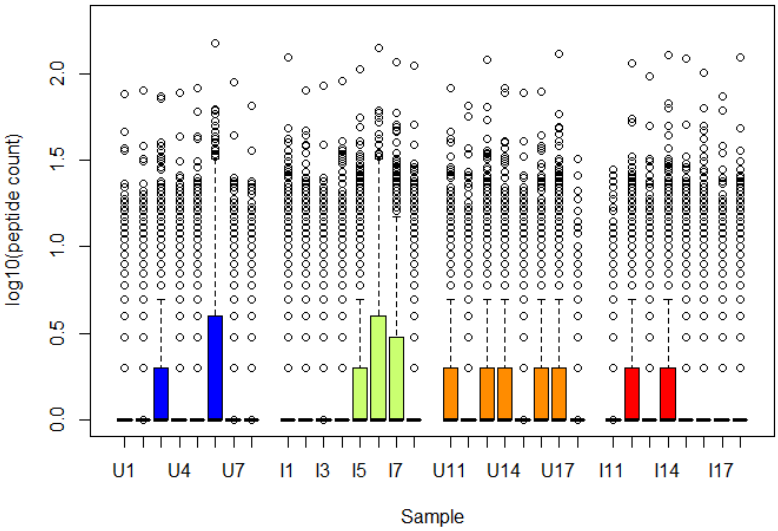

(B)

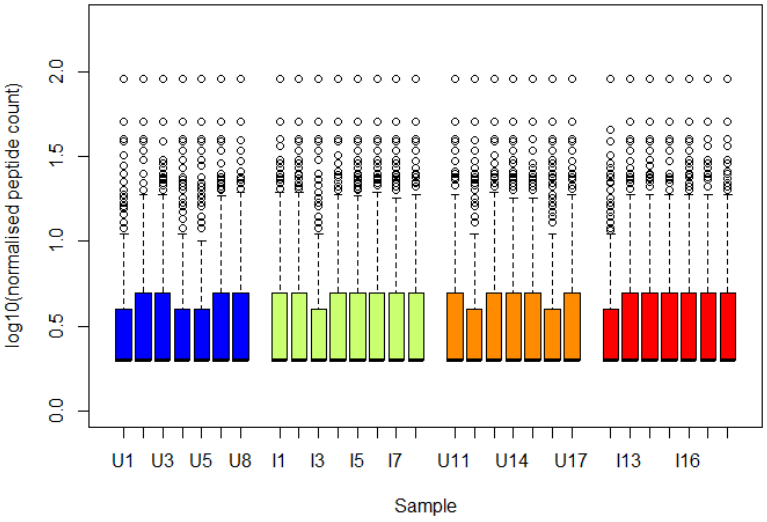

Figure 4.19 – Box plots of (A) raw protein expression data obtained on different processing dates and expressed in peptide counts and log10 transformed ; (B) Box plots of the same data normalised with NODES, which uses a pseudo quantile normalization to force the distribution of the raw signal intensities from the high throughput data to be the same in all samples [175]. In blue- Batch 1 uninfected cells; Olive- Batch 1 infected cells; Orange- Batch 2 uninfected cells; Red- Batch 2 infected cells.

(A) (B)

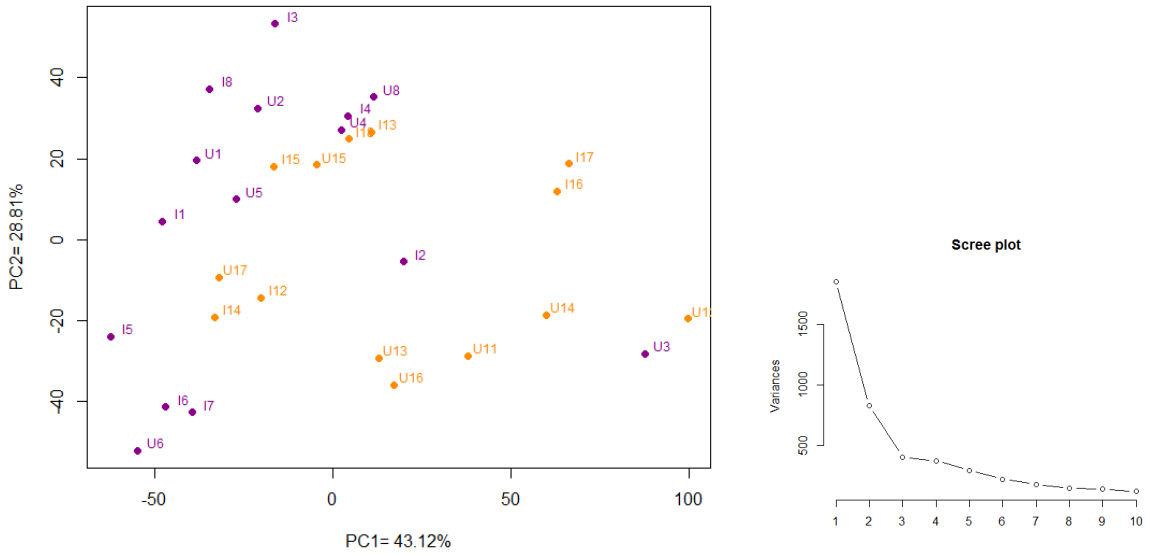

Figure 4.20 – Principal component analysis of normalised peptide expression data coming from single infected and uninfected mouse urothelial cells. PC1 versus PC2 of the normalised peptide counts (A). Colours discriminate the two batches (purple- batch 1, orange –batch 2). I- Infected, and U- Uninfected cells come from infected mice. The percent of the total variance explained by each component is indicated on corresponding axis. (B) Scree plot corresponding to panel A, showing proportion of the total variation in a dataset that is explained by each of the components in a PCA analysis of normalised data.

The output of *k*-means clustering depends on the number of centroids (clusters) defined prior to the analysis, though this number is not known in advance [291]. To determine it, 1000 clustering simulations of the same run with different values specified for k (k=2; k=3; k=4 and k=5) were performed. Each pair of cells was assigned a correlation score which was calculated as the number of times they co-clustered in the *k*-means analysis (out of the 1000 simulations). The results were presented in the form of correlation heat maps. Visual investigation of the four of them showed that each time we ended up with three well separated clusters that converge on the same clustering solution regardless of the number of centroids specified (Figure 4.21).

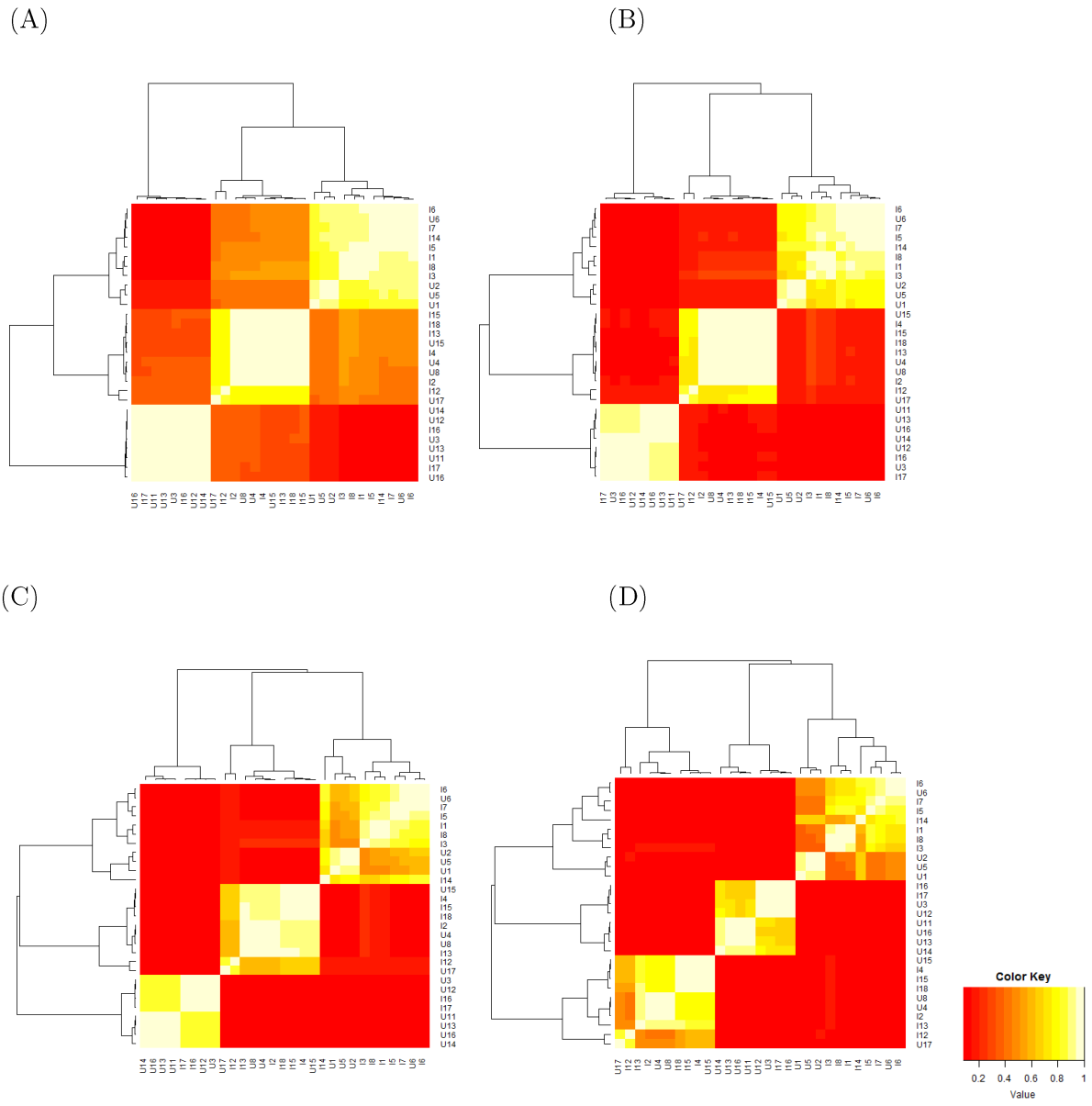

Figure 4.21 – Simulation results of 1000 simulations of *k*-means clustering with different numbers of centroids specified *k*=2 (A); *k*=3 (B); *k*=4 (C) and *k*=5 (D). The data for 29 cells was normalised and batch mean-centered prior to bootstrapping and is presented in the form of a correlation heat map matrices with dendrograms. The colour scale reflects the frequency of the two cells being clustered together. Whites and yellows indicate a high frequency, while reds are associated with low incidence of the two samples being clustered together. I- Infected, and U- Uninfected cells come from infected mice. Single digit numbers in cell labels indicate cells coming from batch 1, cells with two digit numbers come from batch 2.

Based on the above results, *k*-means clustering of normalised and batch mean-centered single-cell data was performed. The number of seeds was specified to k=3, and information regarding the most frequent clustering outcome was incorporated (Figure 4.22). *K*-means clustering led to identification of three groups not related to cell infection state or batch. These data give an additional visualisation insight into the nature of our cell population, uncovering its confoundedness by not only a technical batch effect, but also infection state and inherent intercellular heterogeneity of likely biological significance.

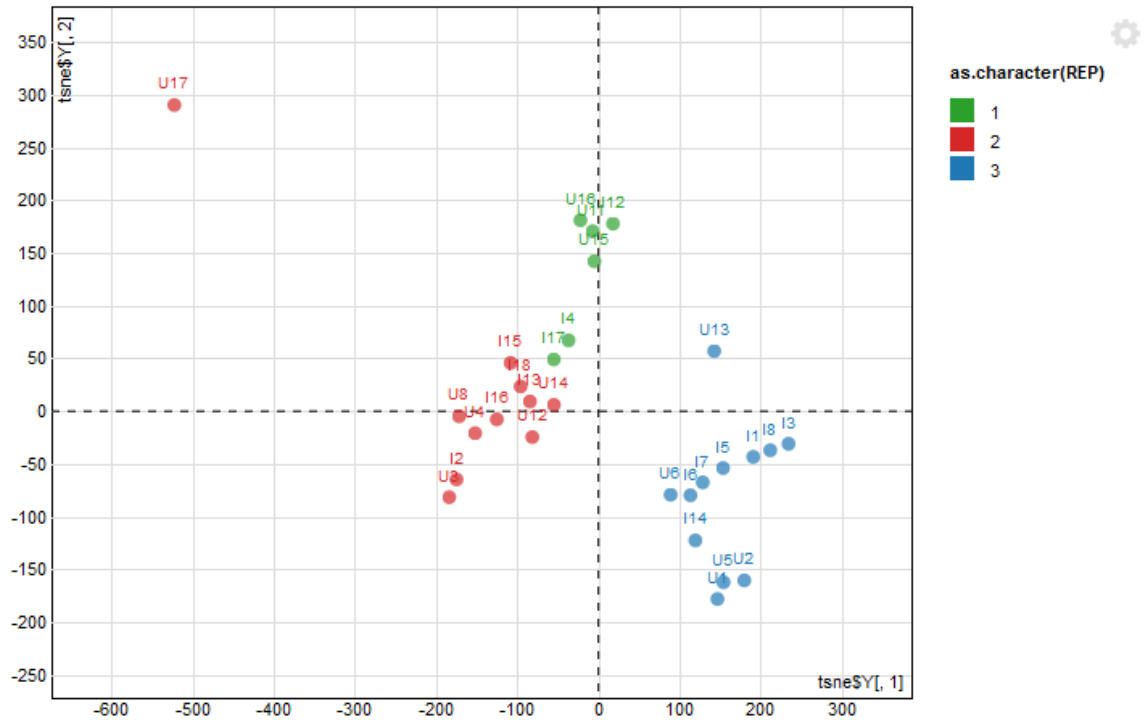

Figure 4.22 – Dimensionality reduction using t-Distributed Stochastic Neighbour Embedding algorithm on normalised and batch mean-centered data coming from infected and uninfected cells. Colours label clusters based on the *k*-means bootstrapping results. I- Infected, U- Uninfected cell. One digit numbers indicate cells coming from batch 1, cells with two digit numbers come from batch 2.

4.4.12 Differential expression analysis of intercellular heterogeneity

To further examine the hypothesis of intercellular heterogeneity identified in the collection of mouse urothelial cells, the same proteomics data were used to perform differential expression analysis and identify any prospective biomarkers of these cell groups. To identify proteins differentiating the three groups of cells, NODES was used to identify DEGs in pseudocounted quantile normalised data between the three clusters identified by the bootstrapping k-means clustering. Cut-off points of log fold change >1 and FDR <0.5 were used. 67 proteins were identified this way (Figure 4.23). The visual examination of the dendrogram in Figure 4.23 distinguishes formation of at least five hierarchical clusters of DEGs with varied expression profiles between cell groups.

4.4.13 Validation of intercellular heterogeneity

4.4.13.1 Validation with control cells dataset

The intercellular heterogeneity reported in section 4.4.11.1 was identified in a mixture of infected and uninfected cells (test samples) extracted from infected mice. To validate the presence of three heterogenous groups of cells, and also to confirm that the differences are not associated with exposure to bacteria, proteomics data from control cells from uninfected mice were used as a validation set. The expression profiles of the 67 proteins differentially expressed between three clusters in the collection of infected and uninfected cells were examined in the raw, as well as pseudocounted quantile normalised peptide expression data coming from control cells (Figure 4.24). Out of 67 DEGs, 58 was detected in raw data coming from control cells. But upon data normalisation, only 35 genes remained, as the process removes genes below certain expression level. The comparative analysis of protein expression patterns between the three groups of cells in test and control sample populations has showed that there isn't much of an overlap.

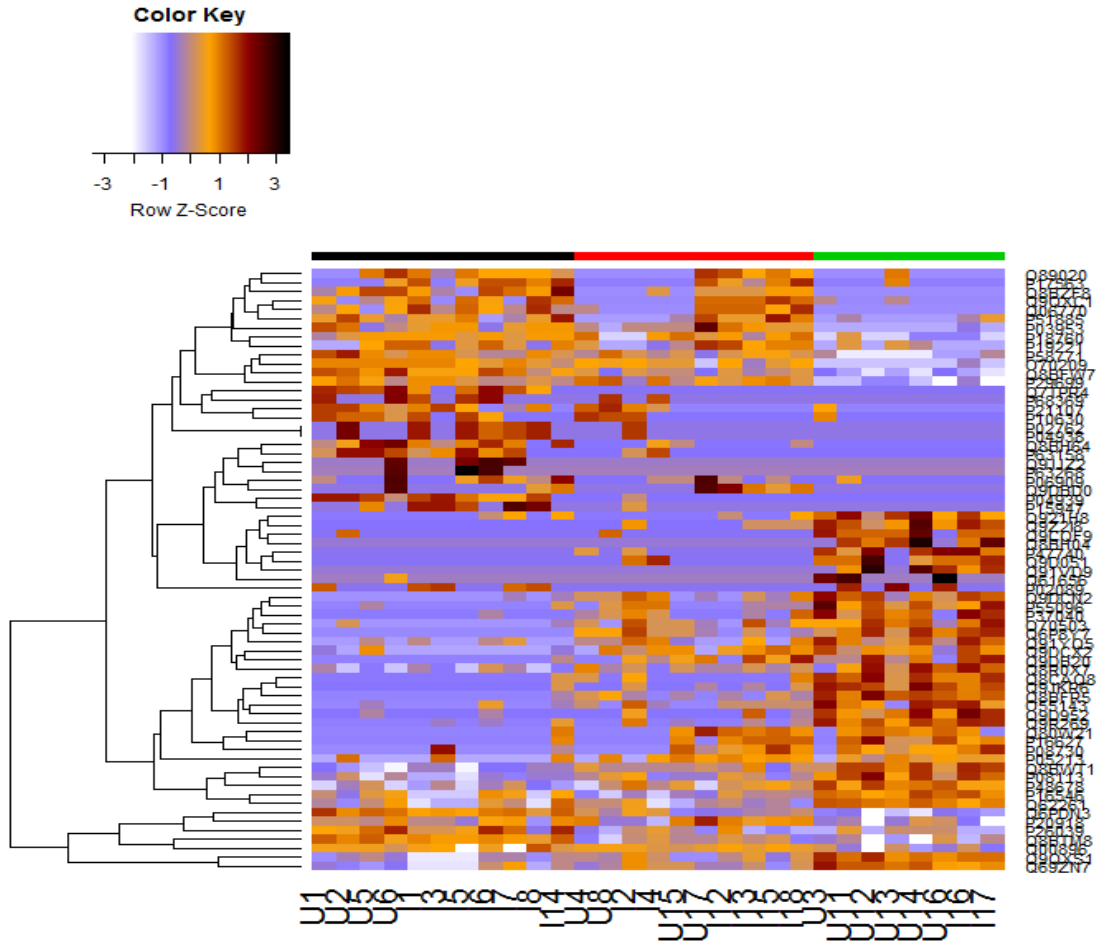

Figure 4.23 – The heat map of standardized signal values (Z-score) for 67 differentially expressed proteins. Patterns of changes in peptide abundance in 29 cells are shown as a heatmap for a set of 67 proteins. Proteins presented were selected based on cut-off thresholds of log fold change >1 and FDR < 0.5. Hierarchical clustering presented by the dendrogram represents the similarity of protein expression profiles based on normalised and cell groups-centered mouse peptide counts detected in single cells. I- Infected, and U- Uninfected cells come from infected mice. The colour scale reflects the Z-score distance score centered and scaled in the row direction. Browns and oranges indicate an enrichment of the protein expression relative to other samples, while blues and whites represent a relative decrease in the protein abundance. Reds are associated with correlations close to zero. The black, red, and green coloured panels on top of the heatmap distinguish the three groups of cells, as identified by *k*-means bootstrapping.

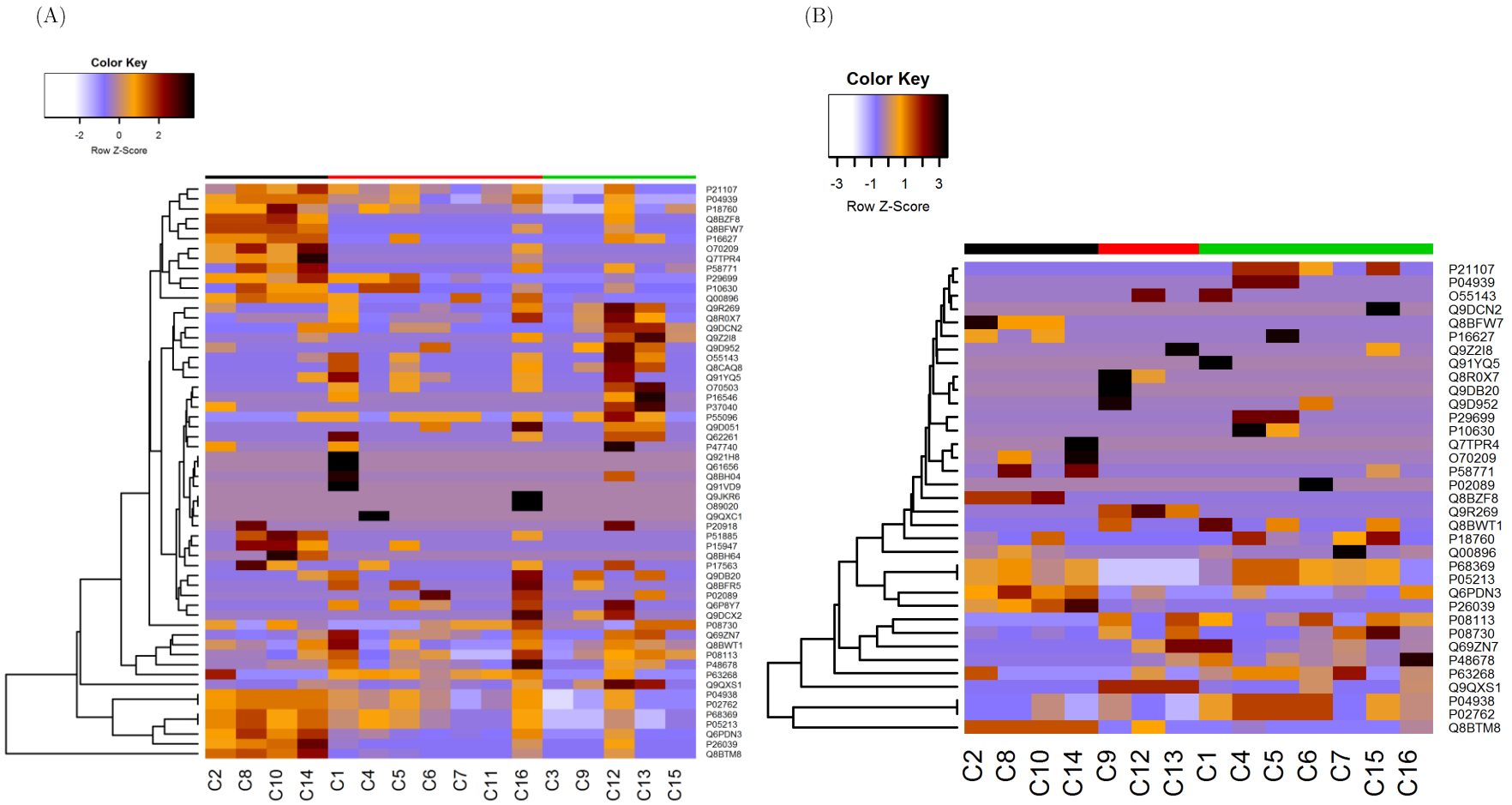

Figure 4.24 – The heat map of standardised signal values (Z-score) of differentially expressed proteins in control mouse urothelial cells. (A) Patterns of changes in raw peptide abundance in 16 control cells are shown as a heatmap for a set of 58 proteins. (B) Patterns of changes in normalised peptide abundance in 16 control cells are shown for a set of 35 proteins. Proteins presented were selected based on the analysis of infected and uninfected cells described in section 4.4.12. Hierarchical clustering presented by the dendrogram represents the similarity of protein expression profiles based on normalised and cell groups-centered mouse peptide counts detected in single cells. C- Control cells come from unfected mice. The colour scale reflects the Z-score distance score centered and scaled in the row direction. Browns and oranges indicate an enrichment of the proteins expression relative to other samples, while blues and whites represent a relative decrease in the protein abundance. Reds are associated with correlations close to zero. The black, red, and green coloured panels on top of the heatmap distinguish the three groups of cells, as identified by k-means bootstrapping.

4.5 Discussion

Recurrent urinary tract infections are very common, with ~30% of UTI patients developing the recurrent infection within six months since the primary one [20]. Prophylactic antibiotic treatment is the only practiced approach to treating rUTIs. Where small doses of antibiotic are then administered daily for prolonged (months) periods of time, with a standard *ad hoc* empirical antibiotic therapy being instilled once the infection is already elicited. However, facing the era of increased spread of antibiotic resistance, novel treatment and preventive approaches, limiting the unnecessary use of antibiotics, are required. A diagnostic, prognostic and/or predictive biological marker for rUTIs could play a role in improved therapeutics, whilst allowing for personalised clinical decision-making, and diminishing the chances of developing UTI symptoms. It is known that rUTIs are linked with intracellular bacterial infections in urothelial cells. In order to understand the intricacies of rUTIs, real-time study of the interplay between the host and pathogen is necessary. Therefore comprehension of the events following bacterial colonisation of the urothelial cell's cytoplasm, either via exploring its proteome or transcriptome, are crucial.

A novel approach for extracting single infected and uninfected murine urothelial cells using hand-pulled glass capillary pipette has been previously developed within the Chen Laboratory (Chen S.L., unpublished). Further processing of the extracted cells by LC-Ms/Ms confirmed the samples to be of urothelial origin, and in the majority of cases to be superficial cells. Using a combination of single cell isolation techniques and mass spectrometric analysis gave reproducible outcomes allowing for analysis of mouse urothelial proteomes. Only a single study was previously reported to specifically study siEC, which used laser capture microdissection and Affymetrix GeneChips [292]. The study however, failed to precisely separate the infected cells from the uninfected ones, leading to the transcriptional analysis being performed on pooled populations of cells. Such an approach masks any potential intercellular differences. The only study that investigated the urothelial proteome, was population-based and used whole mouse bladder urothelium and nanoflow LC-Ms/Ms, leading to the identification of 3998 proteins [104]. The work presented in this chapter, on the other hand, reports identification of 2398 proteins in superficial cells only. This outcome represents (potentially more than) 60% of the previously reported proteome. It needs to be noted that the 2398 proteins were not detected within each of

the cells, and the mean reproducibility level of the detected proteins was found to be at 76%. This is a very satisfactory result, considering the data comes from single cells, and yet falls within the general reproducibility range for LC-Ms/Ms of 70-80% [293].

To identify differentially regulated proteins that could potentially act as biomarkers for rUTIs, siECs were separated from the uninfected cells and their protein expression profiles were compared at a single cell resolution. Adapting NODES, a specialised single cell differential expression analysis package in R, to our proteomics data (both single-cell RNA-seq and proteomics produce count data for each gene/protein, and thus similar analytical techniques can be used), ten differentially expressed host proteins were identified: Acot1, Psa6, Klk1, Nucl, H14, Tcpθ, EnoB, A1At5, Tcpα, and Can1.

Alpha-1 antitrypsin is a circulating serine protease inhibitor expressed by liver in response to inflammation or infection. While A1At5 is mainly produced by hepatocytes, other monocytes, macrophages, pulmonary alveolar, intestinal and corneal epithelial cell were also found to express it, though to a smaller extent. It can be also found in body fluids such as saliva, tears, semen and urine [294]. And interestingly, A1At5 was found to be apically expressed in Madin-Darby Canine Kidney Epithelial cells [295]. The anti-inflammatory effect of alpha-1 antitrypsin occurs as a consequence of inhibition of cytokine-induced activation of inflammatory cells [286, 296]. Impairment of secretion of this protein can lead to liver cirrhosis or pulmonary emphysema [297]. Further studies have shown that alpha-1 antitrypsin reduces the severity of *Pseudomonas aeruginosa* pneumonia lung infection in mice by preventing disruption of the lung's epithelial lining and cell apoptosis [285]. Hence it would not be unreasonable for A1At5 to play a similar role in UTIs.

Kallikrein-1 is a serine protease regulating kinin production. The kallikrein-kinin system mediates a broad range of physiological processes, including tubular pro-inflammation pathways, dilation of blood vessels, and many cancer-related processes [284]. This system has also been investigated for potential use as cancer-biomarkers [298]. The presence of kallikrein in urine was demonstrated in several previous reports [299], and several parasitic infections were also found to elicit inflammatory response activating the kallikrein-kinin system [300, 301]. It is possible that due it its hypotensive properties, kallikrein-kinin system is activated by bacteria-driven contact to

reduce the influx of neutrophils and macrophages that would lead to killing of the bacteria [301]. Calpain-1 is also a protease and has been found to be involved in the breakdown of substrates associated with remodelling of the cytoskeleton such as microtubules subunits [302]. But it was also found previously to be activated due to infection in order to resolve inflammation, simultaneously making bacterial entry more likely [303]. Collectively it suggests that calpains-1 are likely to play a role during the UTI, especially that it is known that FimH-mediated UPEC intracellularisation involves cytoskeletal rearrangements [304].

Acyl-coenzyme A thioesterase 1 is a hydrolase expressed in kidney, heart, and fat tissue which catalyses breakdown of acyl-CoAs to free fatty acids and coenzyme A. Due to its ability to modulate fatty acid metabolism and cell signaling, cytosolic ACOT1 was found to play a potential function in ameliorating cardiac dysfunction due to sepsis-associated fatty acids oxidation [305]. It was speculated that ACOT1 could also be localised to peroxisomes, which in turn were found to be involved in erradication bacterial infections [306, 307]. Presuming the true existence of this link, its involvement in response to UTIs could also be a possibility.

Proteasome subunit alpha type-6 is one of the essential subunits of the 20S proteosome complex, implicated in protein degradation [308]. The proteasome subunit alpha type-6 was found to have an antiviral effect in hepatitis by modulating proteosome-ubiquitin pathway, which is found to be manipulated by viruses to promote their intracellular replication, persistence and immune evasion [309]. Since ubiquitination is involved in aspects associated with bacterial infection and host defense mechanism [310], it seems plausible that a similar process could exist in case of UPEC and proteasome subunit alpha type-6.

T-complex protein 1 subunits alpha and theta act as molecular chaperones, assisting protein folding. Being a part of the chaperonin complex, subunit alpha was found associated with viral infections [311]. The subunit theta was also identified as a candidate biomarker of tissue damage for bovine parainfluenza virus type 3 [312], also a likely prospect in IBCs.

Beta-enolase can be found expressed in most tissues. It takes part in a glycolysis subpathway associated with carbohydrate degradation [313]. Whether this indicates a need of

high energy level to fight the infection or a general inhibition of the carbohydrate metabolism as a result of UPEC infection remains unclear [314].

Attempts to validate these findings by means of whole mount immunofluorescence, quantitative Western blot analysis, and immunohistochemical staining of fixed tissue sections were made; none of the outcomes was, however, found affirmative. Also no association between any of these proteins and UTI infections was found to be reported previously.

A further in-depth examination of the data using more sensitive tools for spatial dimension reduction and clustering revealed the presence of previously unreported, inherent intercellular heterogeneity among the umbrella cells. Cells clustered into three distinct groups, discriminated by 67 proteins showing a significant differential expression patterns . Potentially the divergence between the three groups could be reflected by gradual or continuous changes unassociated with batch effect, or infection state of the cells, though further research is needed to explore this possibility. The only variation among urothelial cells talked about in the existing literature is associated with location of the cells across the urinary tracts. At least three lineages can be distinguished: renal pelvis/ureter, bladder/trigone, and proximal urethra. Urothelial cells in each of these niches show a distinct physiology, as reflected in cell growth potential and expression of uroplakins and keratin. While the location associated variation in cell functionality arises due to differences in embryonic origin, it is unclear what drives the intercellular heterogeneity defined by the clustering in the proteomics data, especially that all the analysed cells come from the same organ [257].

Detection limit is the major problem associated with single cell omics experiments, and is largely dependent on the sensitivity of current technology. While proteomics on single bacterial cells is still beyond our capacity, IBCs that are clonal structures could potentially represent a large enough collection of bacteria with presumably identical protein expression profiles that could give insights into what the environment within the urothelial cells is like and what changes these pathogens undergo while growing within the cytoplasm. The use of LC-Ms/Ms to study single urothelial cell proteomics did not prove useful for studying the proteome of IBCs. Despite numerous bacteria forming a single IBC, the total number is still less than that required for current LC-Ms/Ms detection. An IBC within a mouse urothelial cell 6hpi was previously reported

to contain about $1x10^4$ CFUs [93]. The most recent data obtained by culture of siECs suggest this number may be overestimated, as a CFU median was found around $1x10^{2.5}$, with values oscillating between 10 and $1x10^4$ CFU. Concurrently, qPCR analysis of siECs suggests roughly half a logarithm higher numbers than those obtained by culture method (Chen S.L., unpublished data). These values indicate the experiment should be feasible, despite being close to the edge of the detection limit of the state of the art mass spectrometric equipment. Unfortunately, the detection limit is not a simple cut-off point, and depends on other factors, such as the level of background noise. The numbers of bacterial proteins detected in this experiment were outnumbered multiple times by the mammalian proteins. This disproportion of mouse to bacterial proteins certainly played a significant role in the inability to detect larger numbers of bacterial peptides. Circumventing the issue to gain insight into the IBC proteome would be very difficult at the moment, and if the approach would not rely on the improvement of protein detection sensitivity by the available technology, it would need to require isolation of the IBC from the epithelial cell. While such procedure could be attempted by means of, for example, epithelial cell lysis, this procedure could result in induction of changes of the proteome of interest. Nonetheless, the number of the detected proteins could possibly serve as an indirect, rough indicator of the size/maturation level of IBCs, though further studies would need to follow.

Other limitations associated with the proposed approach to single cell proteomics are related to the cell extraction stage. The uninfected urothelial cells are not marked with any reporter gene, therefore assessment of whether the given cell originates from the urothelium, or specifying from which urothelial layer it comes from, is done purely by eye assessment based on its size. Such judgment, despite its crudeness, did prove quite successful, as confirmed by the analysis of characteristic urothelial cell markers. In a few cases, though, assessment of the cell differentiation was confounded, as markers typical of more than one urothelial layer were detected. Despite the thorough washing off each cell individually in a clean droplet of PBS just prior to flash freezing it, the most likely explanation is that the extra proteins were coming from the PBS the cells were suspended in. While transferring the individual cells, a small volume of PBS is still included. It could be contaminated with proteins coming from other cells, and while washing would dilute the contamination, it may not guarantee a complete removal of them. Another concern in terms of choosing uninfected cells for the analysis is that one wouldn't be

able to tell apart cells that have been previously infected, and gone through the stage of bacterial fluxing, or whether they contained a low number of bacteria, as could be the case with QIRs. While, both are highly unlikely due to the timepoint at which the cells were collected, it could confuse the data.

What's more, as many single cell studies using technologies such as FACS or microfluidics often use hundreds of cells [273], the sample size generated in the framework of this project could be considered small. While it would seem that increasing the number of analysed cells could help with improving the coverage of the proteome, rarefaction analysis showed that this wouldn't solve all of the issues, as undersampling of the proteome within individual cells is one limiting factor. While collecting more cells could be bothersome due to the low-throughput of manual extraction, and performing further LC-Ms/Ms is costly, it wouldn't significantly increase the number of detected proteins, though it would make the statistical analysis stronger, and dilute the concerns associated with PBS contamination and misidentification of uninfected cells.

In terms of validation of DEGs, the attempts to adapt whole mount immunofluorescence to gain insights into their spatial distribution and paracrine signalling didn't bring the desirable outcomes. Immunofluorescence on cytospun mouse urothelial cells (upon scraping them off the bladder surface), and immunoflow cytometry, were considered as other techniques to serve this purpose. But while cytospinning cells can result in their significant damage, as well as loss of cell spatial information, in terms of their distribution and urothelial layer origin, the immunoflow cytometry, besides being difficult to optimise, due to the size limit allowed by all currently available automated sorting techniques, could be only done on immortalised human cells (~30µm) [5, 14]. Mouse bladder epithelial cells typically ~150µm in diameter [94] can be further augmented by the presence of IBCs, and therefore would be unsuitable for this purpose. While quantitative Western blot analysis done on a collection of single cells coming from mice would be an ideal validation method, performing it was unfeasible due to a high ($1x10^4$-$1x10^5$) number of single cells that would need to be collected manually. For this purpose urothelial cells coming from 5637 cell line were used instead. This choice could be difficult when it comes to data interpretation due to switching from a murine to a human model, and from normal to immortalised cells. Nevertheless, past research proved 5637 cell line to show a lot of correspondence with the mouse model.

The extraction of thousands of urothelial cells required the assistance of FACS, the use of which introduced a few issues. While the lengthiness of the process was shown to affect the viability of only a small portion of cells, these could serve as a potential source of error in the measurements of protein expression at later stages of the validation. Fixing cells just prior to sorting, to preserve their proteomic state, could be a potential solution, though it is unknown how it would affect antibody affinity and the overall results. Furthermore, a significant inconsistency was observed in association with the cell count performed by the machine. It was found to impede with loading equal amounts of protein on SDS-PAGE gels. In spite of the meticulous standardisation of cell numbers per sample, noteworthy differences were found in the amount of proteins recovered from samples prepared during different runs. Errors in cell counts by cell sorters typically result from aggregates found in cell suspension subjected to sorting. These were, however, eliminated by gravity filtration preceding cell sorting. Finally, FACS sorting appeared to have an impact on the non-viability of bacteria found within siEC. Upon cell sorting, and regardless of whether siECs were lysed, only a minute portion of UPEC found in those cells were recovered by agar plating. Attempts to recover the bacteria by growing them for a couple of hours in Terrific broth upon sorting also didn't improve the yield of recovered bacteria. It was verified that neither the sheath fluid used by the sorter, nor any other substance in contact with the cells could result in bacterial cell death. Also, the probability of cells bursting during the sorting process is also very low. While a small error (of about 10%) could be expected in terms of cell sorting, it is far from explaining the observed outcome. No credible explanation of this observation was found so far, and thus any potential experiment that would require recovering intracellular UPEC in such a way could be problematic in the future. Nevertheless, since it's the host proteins that are the focus of this work, bacterial viability shouldn't have an effect on the outcome of the experiment.

Both the quantitative Western blot analysis and IHC showed that difference between host proteomes of infected and uninfected mouse urothelial cells were too subtle to detect due to the inherent differences between the cells. As the experiments validating this discovery are still pending, it is still unknown whether these potential differences could have an impact on the virulence of UPEC. Thanks to the single cell resolution that has been possible only for a relatively short period of time, our knowledge regarding the extent of cellular heterogeneity

among many tissues and cell types expands. Since the discovery of the superficial cell heterogeneity in urinary bladder, questions about the heterogeneity in other parts of the urinary tract, such as urethra or ureters, also arise, just like whether this finding translates to humans. Human samples, especially from healthy donors, are difficult to acquire, but ureter samples obtained from healthy kidney donors, like those used in section 3.3 could serve the purpose. Furthermore, it would be interesting to look into the marginal distribution of the heterogeneity by performing a pseudo-temporal ordering [315]. This could give an insight into the relationship between the cells, the heterogeneity dynamics in the cell population and whether they undergo a continuous transition of their proteomes, or whether the divergence is due to the differences of their origin. Even though protein and RNA levels are generally difficult to correlate [316], combining the two approaches to enhance the analysis could potentially strengthen the investigation.

This work unveiled the feasibility of the untagged single cell proteomics on mouse urothelial cells for the purpose of studying mammalian proteome. The approach initially aimed at deepening our understanding of the interplay between the host and UPEC during rUTI. Instead, it led to being inferred the existence of intercellular heterogeneity among umbrella cells in mice bladders, potentially adding to our knowledge of bladder physiology. The association between variation in protein levels and displayed difference in cell function, supported by the "variation is function" hypothesis [317], could, however, influence the bladder's ability to prevent UTIs, and/or UPECs ability to bind, invade or sustain within the cells. Further research will be necessary to support or refute such eventualities.

5 Experimental system for genome siRNA screening for novel urothelial host factors during UTIs

5.1 Introduction

5.1.1 Mechanism of siRNA

The discovery of RNA mediated interference has revolutionised modern genomics since its first discovery in *Caenorhabditis elegans* two decades ago [318]. The process relies on longer (>300 base pairs) double stranded RNA molecules introduced into the cell by viral infection or transfection, or they may also be produced endogenously by the host cell. The long RNAs are cut by a Dicer, an RNaseIII endonuclease which yields double stranded RNA fragments that are approximately 22 nucleotides in length. These short double stranded RNA molecules are referred to as small interfering RNA (siRNA). The siRNA fragments are then incorporated into the RNA-induced silencing complex (RISC) which separates the double stranded complex liberating siRNAs. One complementary strand of the siRNA is then guided by RISC to an mRNA containing a homologous antisense sequence. The siRNA undergoes complementary binding, and as a result of the nuclease activity of the assisting RISC, the targeted mRNA is degraded (Figure 5.1) [319]. In consequence, levels of the corresponding target protein are reduced (knocked-down) rather than entirely eliminated. This is particularly helpful with studying essential genes, knock-out of which would otherwise result in cell death. The knock-down isn't permanent, and as cell growth and the protein turnover continue, protein levels eventually revert back to its normal levels, especially in fast dividing cells [320].

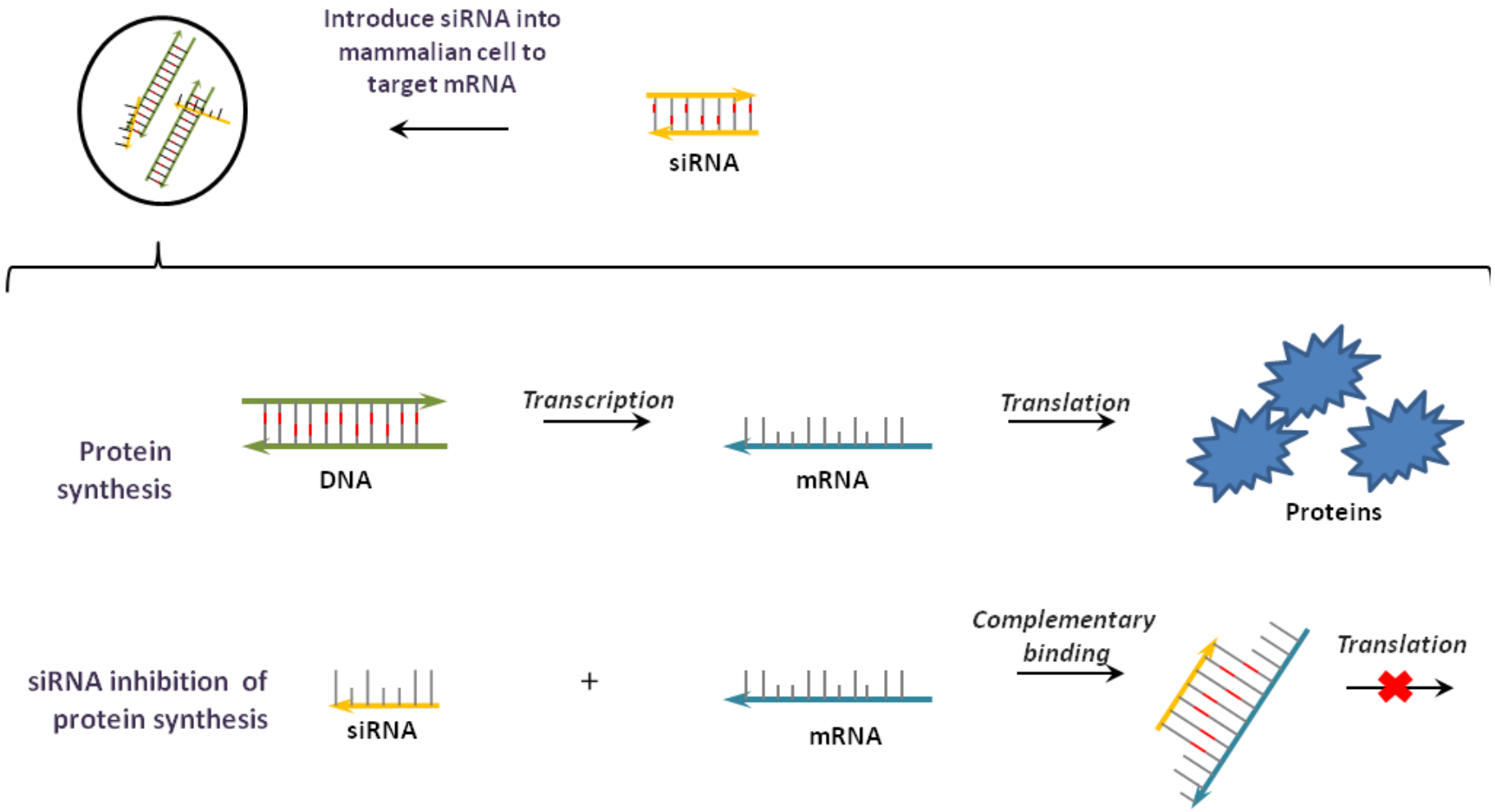

Figure 5.1 – Mechanism of siRNA knock-down of protein synthesis. Single-gene knock-downs are achieved by introducing small double-stranded siRNAs into the cytoplasm. These are processed by exogeneous RISC (not shown) separating the strands. It then uses one of them to recognise a complementary mRNA to be silenced. Once the complex localises the targeted mRNA, the latter is cleaved by a ribonuclease (not shown) [321].

5.1.2 siRNA as a gene silencing strategy

Individual genes can be silenced independently due to the high specificity of siRNA for its target gene and the low non-specific effects [321]. But the use of long dsRNA in mammalian cells for this purpose, apart from gene silencing induces also an unwanted nonspecific mRNA degradation (interferon response). This isn't the case with the use of siRNA, which therefore provides a robust tool for examination of transient effects on cells or organisms generated by perturbed genes [320, 322, 323]. Such approach proved useful for the controlled study of cascades of events in insulin signal transduction pathway in a number of *Drosophila* cell lines [324]. Since, significant advances have been made in both academic and commercial research settings. These have led to the development of efficient strategies to introduce siRNAs into mammalian cells and whole organisms. In turn, the development of genome-wide siRNA libraries allows for independent knock-down of every protein found within a genome covered by a given library [322, 323]. The initial screens studied orthodox phenotypes, such as cell division, lethality, or sterility [325, 326]. Such classical phenotypes were often assessed by eye, but as the quantitative and qualitative phenotypic screens have become more elaborate, so did the challenge of detecting a given phenotype. To address this issue, the read-out methodologies often involve the use of reporter genes, which commonly involve the use of luminescent or fluorescent proteins [320, 323, 326, 327].

5.1.3 The utility of siRNA silencing in high-throughput screens in translational biology

Many questions in both basic and translational biology in uni- and multi-cellular organism can be best addressed using siRNA screens performed in a high-throughput manner [328]. High-throughput siRNA screens have already facilitated identification of genes associated with a vast array of biological processes, including stress-response, cell trafficking, self-renewal or pluripotency [329-332]. It has also proven useful in identification of host factors that modulate viral and bacterial infections. And an siRNA screen performed in a human mammary epithelial cell line, identified genes that regulate invasion of *Salmonella enterica* serovar Typhimurium into host cells and key mediators of intracellular growth [333, 334].

There are a number of well characterised host factors that regulate UPEC colonisation of host urothelial cells and intracellular replication. Many of these factors such as uroplakin proteins, which act as receptors on the apical surface of superficial cells, have been well studied in a number of mammalian models, however, there are many unanswered questions regarding the cascade of events that occur during the interactions between urothelial cells and UPEC. Therefore, utilisation of a high-throughput siRNA screen could prove to be a powerful tool to determine which genes regulate key stages in the pathogenic cycle.

5.2 Aims of this chapter

In order to facilitate the identification of as yet uncharacterised interactions that occur between urothelial cells and UPEC during infection, the aim of the work presented in this chapter was to develop an experimental system for whole genome siRNA screening, including optimisation of a gentamicin protection assay using urothelial cell lines and UTI89.

5.3 Results

5.3.1 Components of the experimental system

The 5637 cell line is one of the most frequently cited urothelial cell line models used in the study of UTIs. This cell line has been previously used to determine binding and invasion rates of a panel of UPEC (CI5, ORN103(pSH2), NU14, K12 MG1655, K12 AAEC185/pSH2, UTI89, J96 and CFT073 [118, 141, 156, 233, 335]), and other bacterial strains (*Listeria monocytogenes, Staphylococcus saprophyticus, Staphylococcus aureus, Staphylococcus carnosus, Staphylococcus epidermidis* [233, 336]) by means of gentamicin protection assay, allowing an assessment of bacterial virulence in terms of their role in invasiveness and the ability to associate with host cells. The gentamicin-protection assay provides a simple model to assess the effect of siRNA gene knockdowns on virulence traits and bacterial pathogenicity. The primary aim was therefore to use the 5637 cell line and GFP-tagged wild-type UTI89, to optimise a gentamicin protection assay that would be suitable to be taken forward for an *in vitro* whole-genome siRNA screen [83, 118, 152]. The widespread use of this cell line and GFP-tagged UTI89 strain in previous studies from other groups provided extensive baseline data that was used as a benchmark to determine the efficacy and reproducibility of the studies presented in this chapter.

In addition to the wild-type GFP-tagged UTI89, *fim* operon deletion (UTI89Δ*fim*), and binding pocket (UTI89-FimH-Q133K) mutants of Type 1 fimbriae were also used in these studies. Inclusion of the operon deletion mutant and the binding pocket mutant allowed us to verify the widely reported findings by other groups concerning the dependence of UPEC binding and invasion on Type 1 fimbriae [83, 84, 94, 337-339]. To further test these assumptions, chemical controls with MαDM were included due to the binding specificity of Type 1 fimbriae for mannosylated glycoproteins. Disruption of FimH in UPEC is known to almost entirely abolish binding and invasion. Incorporating strains with defective or absent FimH protein would enable determining the minimum adherence and binding during an siRNA screen, enabling developing a system that incorporates the optimal range for detection of up- and down-regulation of genes in conditions with maximum and minimum cell-association and intracellularisation rates. Lastly, the reproducibility of imaging-based assays which quantify intensity of fluorescence is known to be poor in automated high-throughput assays due to experimental variability and issues with photo-

bleaching. Quantification relies largely upon ratiometric comparison of siRNA knockdown-treated infected cells to control cells which have also been infected with UPEC but not subjected to siRNA knockdown procedures. Consequently, the margin for introducing experimental bias in these studies is large, and as such requires careful optimisation [322]. Therefore, the studies in this chapter aimed to optimise all parameters that might introduce experimental variability in imaging-based analyses of a high-throughput siRNA screen. High MOIs are known to induce cell exfoliation, therefore studies were performed to characterise the range of bacterial titres that gave reproducible rates of intracellularisation into host cells. Furthermore these studies aimed to determine whether the introduction of different GFP-encoding genes affects pathogenicity in UTI89. Previous studies have also identified that the use of cells from higher passage lineages can cause significant variation in intracellular bacterial titres [83], therefore we aimed to characterise this effect in our 5637 model and also sought to understand whether there was biological variability in infection rates between different bladder cell lines.

5.3.2 Determination of MOI levels for use in the experimental system

Intensity of a fluorescent signal originating from GFP-tagged bacteria serves as a marker of cellular bacterial load during the siRNA screen. To enable an optimal signal reading, during its quantification, an MOI which would give equal chance for potential up- and down-regulation of cell infection rates was pursued. Elevated MOI can induce cell exfoliation and/or saturate the fluorescent signal coming from bacteria, making it impossible to detect any changes in the experimental system. Too low MOI on the other hand would result in a problematic signal-to-noise ratio. Most scientific reports using a gentamicin protection assay to study UPEC invasion and replication used MOI of ~10 [83, 152]. Therefore, in order to determine whether this MOI would also produce suitable intracellularisation rates in our laboratory setting, a range of MOI values from 1 to a 100 were tested in a 5637 cell line model (Figure 5.2). Gentamicin protection assays are normally quantified by drop plating where 10µl drops of cell lysate are plated in replicates of five to quantify intracellular bacteria. However, this method of quantification does not discriminate between host cell and bacterial cell number. A single host cell infected with 100 bacteria in a population of 100 cells would give the same CFU count as 100 host cells each

infected with a single bacterium. For this reason quantification of infected urothelial cells was performed using FACS analysis.

Infected cells produce a fluorescent signal generated by intracellular GFP-tagged bacteria. This signal can then be detected by a FACS machine enabling the number of infected cells to be determined and correlated with MOI. Four UPEC strains were used in this study, and three of them were not GFP-tagged. These strains (UTI89-FimH-Q133K; UTI89Δ*fim*, and the complemented *fim* mutant UTI89Δfim/pfim) were transformed with a plasmid pSC101 expressing GFP to generate a fluorescent signal measurable by FACS (Materials and Methods 2.10). The four bacterial strains were used to infect 5637 cells at six MOIs between 1 and 100 (Materials and Methods 2.10). Infection was followed by gentamicin treatment as performed to determine intracellular bacterial numbers (Materials and Methods 2.9.2, section for samples denoted as "Intracellular"). Though, instead of lysing the epithelial cells, they were detached, as described in Materials and Methods 2.7.2. 3000 urothelial cells from each condition were analysed for their GFP signal. The calculated proportions of GFP-positive cells are shown in Figure 5.2. An MOI=10 was found to be the most suitable bacteria-to-cell ratio, as it resulted in infection of approximately 50% of urothelial cells when GFP-tagged wild-type strains were used. The experiment also confirmed a previously reported abolishment of epithelial cell invasion upon deletion of type 1 fimbriae in *E. coli* [82, 83].

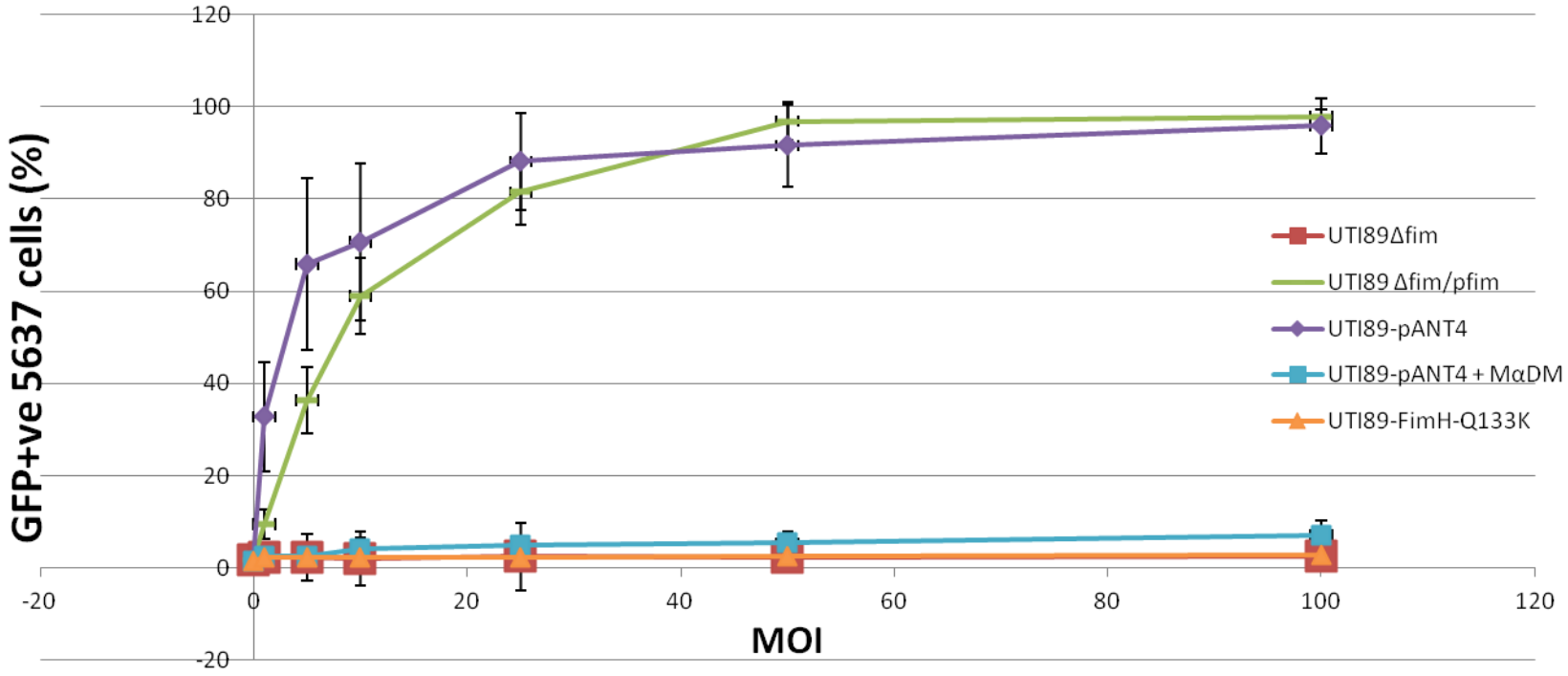

Figure 5.2 – Infection efficacy of UTI89-FimH-Q133K/pSC101-P2-GFP, UTI89Δfim/pSC101-P2-GFP, UTI89Δfim/pfim, UTI89-pANT4, and UTI89-pANT4 in the presence of MαDM depending on bacteria-to-cell ratios from 0-100. 5637 cells were infected with respective *E.coli* strains for 2h, followed by 2h of gentamicin treatment prior to host cell detachment and processing by FACS. At each data point 3000 cells were collected. Error bars are S.D. from n = 3 independent experiments.

5.3.3 Effect of GFP on bacterial virulence

Since the siRNA screen uses fluorescence as a marker of UPEC number and hence pathogenicity, the impact of GFP production on bacterial pathogenicity per se had to be determined. For this purpose, the virulence in terms of bacterial cell-association and invasion was assessed using a gentamicin protection assay as described in Materials and Methods 2.9.2. Figure 5.3a shows absolute numbers for "Total", "Cell-associated" and "Intracellular" bacterial CFU counts. Due to the variability between the "Total" numbers, and to simplify contrasting the different bacterial strains, the results were also presented in the form of percentage rates of "Cell-association" and "Invasion" (Figure 5.3b). The comparison of these confirmed no effect of chromosomal expression of GFP (UTI89-vsGFP) on bacterial virulence (cell association rate: 9.58±0.69%, intracellularisation rate: 6.56±1.78%), as compared to the wild-type UTI89 strain (cell association rate: 9.13±1.09% and intracellularisation rate: 7.64±2.45%) [164]. The UTI89-pANT4 with plasmid-encoded GFP, showed no difference in its invasive capabilities (2.86±1.17%), though it had a significantly higher ($p<0.01$) cell-association rate than the wild-type strain (23.4±4.67%). While the observed intracellularisation rates were consistent with previously published data that reported them to be at 1-10% (depending on the cell passage number), the binding rates in this work were found to be lower (published binding rates are ~45% as of input) [83, 152, 156].

(A)

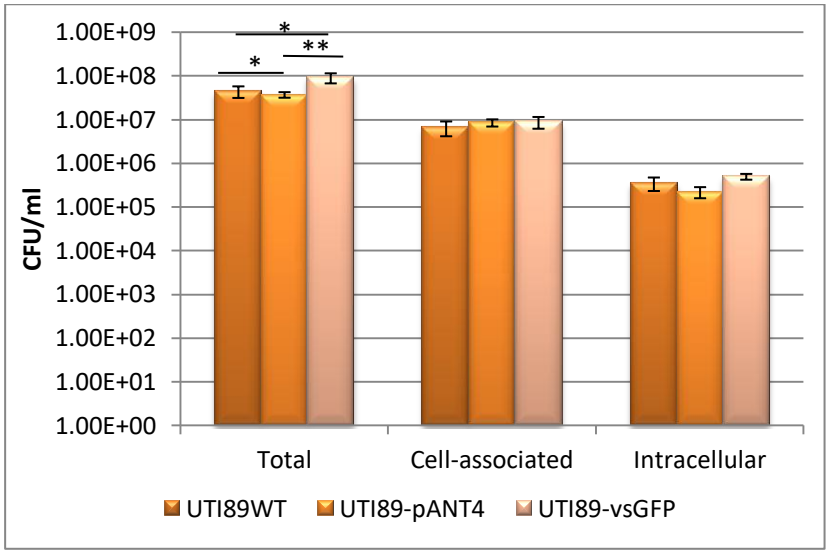

(B)

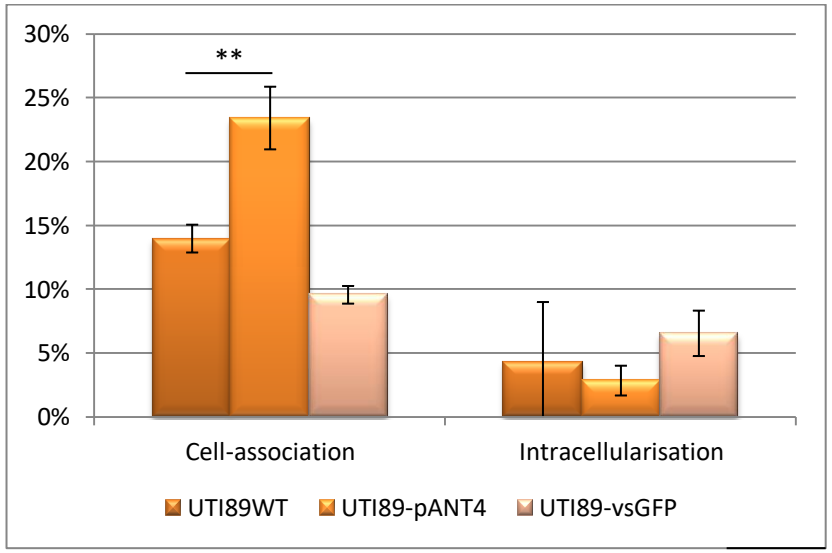

Figure 5.3 – Binding and intracellularisation rates of different UTI89 strains. 5637 cells were infected with UTI89WT, UTI89-pANT4 and UTI89-vsGFP. (A) Absolute values for total, and cell-associated colony counts (retrieved after PBS washes) 2hpi, and intracellular counts 4hpi (retrieved after 2h of gentamicin treatment). (B) Shows efficiency of cell-association and invasion in the form of Cell-association rate (Cell-associated CFUs/ Total CFUs) and Intracellularisation rates (Intracellular CFUs/Cell-associated CFUs). MOI=10. Data are means of at least three independent experiments, each with at least three technical replicates. Error bars are standard error of the mean. The statistical significance was assayed by using Kruskal-Wallis One Way Analysis of Variance on Rank, followed by Dunn's method of pairwise multiple comparison procedure (*, $P< 0.05$; **, $P<0.001$).

5.3.4 Confirmation of FimH expression and its importance in UPEC's binding and invasion

For the purpose of the siRNA screen, dynamic ranges for cell-association and intracellularisation rates had to be defined. FimH inhibition was previously shown to be important for bacterial cell-association and intracellularisation rates [83, 155] and would therefore be a suitable reference to establish detection range and lower limit of detection.

Using guinea pig RBCs, agglutination assays were conducted during every experiment in this study for each of the wild-type and mutant strains. That was to ensure the correct phenotype, confirm and quantify FimH expression and its binding specificity, and detect early a potential contamination [340]. The average results for RBCs agglutination are shown in Table 5.1. UPEC strains were serially subcultured under static conditions to induce FimH expression. UTI89 wild-type strains and GFP-tagged mutants had a HA titre of 7 with no detectable HA in the presence of mannose. Deletion of the *fim* operon (UTI89 Δ*fim*) or induction of a critical mutation in the mannose binding pocket (FimH-Q133K) abolished the ability of these strains to agglutinate RBCs. The wild-type HA phenotype was restored in the *fim* operon-deletion mutant (UTI89 Δ*fim)* in the presence of a plasmid complementing the deleted genes (UTI89 Δ*fim*/pfim). The HA titres were in agreement with published data, and confirmed the importance of the type 1 pili in this phenotype. In conclusion, these outcomes showed expected results validating the strains tested in these studies and the importance of mannose-sensitive type 1-piliation.

Using gentamicin protection assays, the cell-association and intracellularisation rates of wild-type UTI89 and its UTI89-FimH-Q133K isogenic mutant were compared and contrasted (Figure 5.4). The dependence of these processes on FimH binding was further confirmed using a non-metabolisable mannose analogue (M**α**DM) as a control. This control relies on saturation and simultaneous inhibition of mannose-binding pocket of FimH (Figure 5.5). Due to significant ($p<0.01$) differences in the "Total" numbers of CFUs between wild-type and FimH mutant strains (Figure 5.4a), comparison of the two strains could appear problematic. In its place, relative rates were considered for assessment (Figure 5.4b). In previous published reports, a binding pocket mutant, UTI89-FimH-Q133K, was shown to have impaired binding and

consequently invading capabilities [155, 341]. Our studies also showed a WT UTI89 performing better in terms of cell-association rates (significant drop at $p<0.01$), but not in relative intracellularisation rate, where the mutant significantly outperformed its wild-type counterpart ($p<0.01$) (Figure 5.4b) [83, 152]. The same patterns were observed when both UTI89-pANT4 and UTI89-vsGFP were tested in the presence of MαDM (Figure 5.5b and d). In both chemical and genetic controls, FimH-driven epithelial cell binding was decreased by ~1.5 log (Figure 5.4a, Figure 5.5a and c). As much as it showed that FimH is important for bacterial attachment, this process was not fully FimH-dependent, supporting the hypothesis that there may be other adhesins involved that mediate cell association in this model [82, 83, 342].

Table 5.1 UTI89 strain-specific ability to agglutinate guinea pig red blood cells (RBCs)

Strain	**HA titer (1:2^x) in guinea pig RBCs*:**	
	Without mannose	**With mannose**
UTI89 WT	7	0
UTI89/pANT4	7	0
UTI89-vsGFP	7	0
UTI89-*fimH*-Q133K	0	0
UTI89 Δfim	0	0
UTI89 Δfim/pfim	7	0
UTI89-*fimH*-Q133K /pSC101-P2-GFP	0	0
UTI89 Δfim/pSC101-P2-GFP	0	0

*HA titer data are representative of one independent experiment for strains containing pSC101-P2-GFP, two for UTI89 Δfim/pfim and at least three biological replicates for the rest of the strains.

(A)

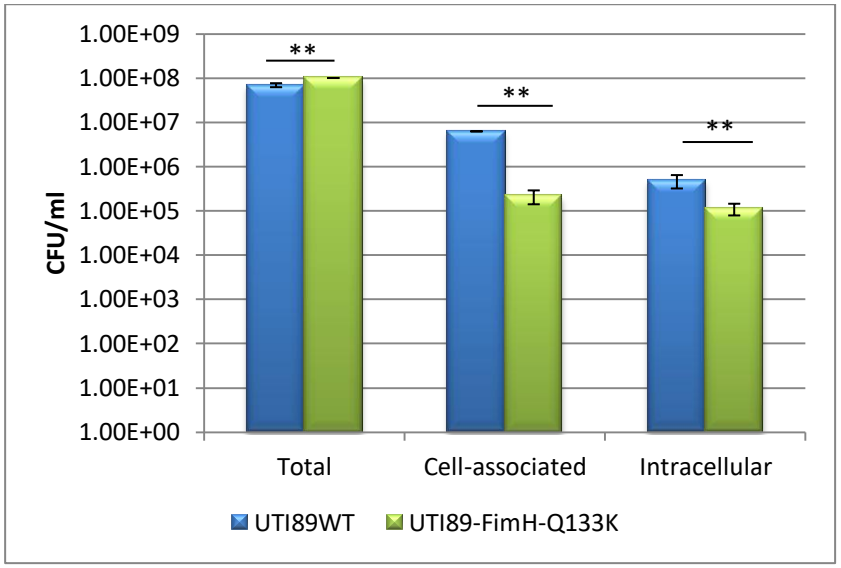

(B)

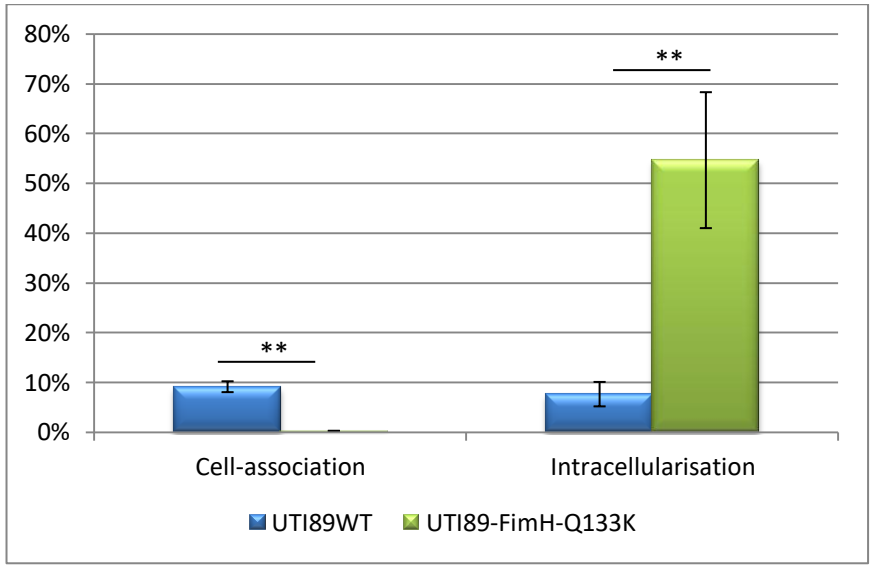

Figure 5.4 – Binding and intracellularisation rates of UTI89 WT and UTI89-FimH-Q133K upon infection of 5637 cells at MOI=10. In (A) absolute values of total, and cell-associated colony counts (retrieved after PBS washes) 2hpi, and intracellular counts 4hpi (retrieved after 2h of gentamicin treatment). (B) Shows efficiency of cell-association and invasion in the form of Cell-association rate (Cell-associated CFUs/ Total CFUs) and Intracellularisation rates (Intracellular CFUs/Cell-associated CFUs). The former is calculated by dividing the number of bacteria retrieved after PBS washes 2hpi, by the total number of bacteria present at a time. Intracellularisationrate was calculated by dividing bacteria retrieved after gentamicin treatment (4hpi) by the bacteria retrieved after PBS washes 2hpi. MOI=10. Data are means of at least three independent experiments, each with three technical replicates. Error bars are standard error of the mean. The statistical significance was assayed by using Mann-Whitney U Statistic (*, $P< 0.05$; **, $P<0.001$).

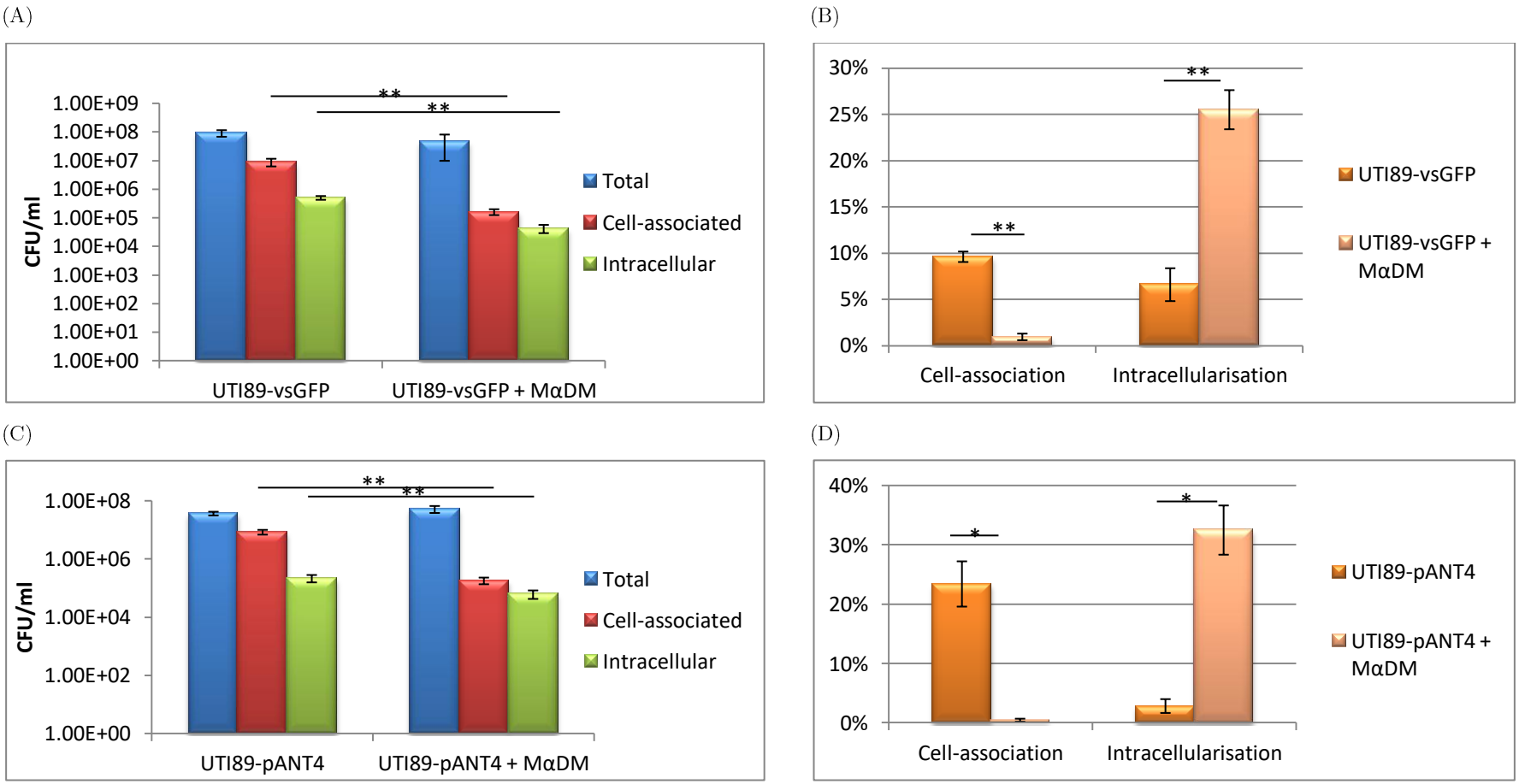

Figure 5.5 – Gentamicin protection assays results of 5637 cells infected with UTI89-vsGFP, UTI89-pANT4 alone or in the presence of MαDM. (A) and (C) show absolute numbers of total, and cell-associated colony counts 2hpi, and intracellular counts 4hpi (after 2h of gentamicin treatment). (B) and (D) show efficiency of cell-association and invasion in the form of Cell-association rate (Cell-associated CFUs/ Total CFUs) and Intracellularisation rates (Intracellular CFUs/Cell-associated CFUs). MOI=10. Data are means of at least three independent experiments, each with at least three technical replicates. Error bars are standard error of the mean. The statistical significance was assayed by using Kruskal-Wallis One Way Analysis of Variance on Rank, followed by Dunn's method of pairwise multiple comparison procedure (*, $P< 0.05$; **, $P<0.001$).

5.3.5 Troubleshooting the conflicts with published data

The above presented findings resulted in a much smaller dynamic range than it was anticipated based on the published data. The smaller difference between the maximum and minimum bacterial levels would reduce the sensitivity of the experimental system, making it ineffective. Because of the discrepancy between outcomes of this work and published reports, we aimed to investigate potential reasons why these differences were observed.

Testing potential bacterial contamination and gentamicin efficiency

Contamination of bacterial cell culture was considered as one possibility. Infecting cell lines with other bacterial strain(s) could lead to higher binding and intracellularisation rates, whether it is due to them being more potent pathogens, compromising host cells' health, or making the innate responses less effective. There is also the possibility that non-UPEC bacteria could be insensitive to gentamicin and not susceptible to the effects of saturation with MαDM if they do not express type-1 fimbriae. After contamination was eliminated as a potential cause, the efficacy of gentamicin was evaluated. If the antibiotic wasn't fully active, it wouldn't be fully effective in killing extracellular bacteria leading to higher than expected cell-associated rates. Gentamicin effectiveness was tested in a modified gentamicin-protection assay, where 2hpi different combinations of the antibiotic and Triton X-100 were used (Figure 5.6). Triton X-100 permeabilises epithelial cell membranes, thus exposing intracellular bacteria to the bactericidal action of gentamicin. The antibiotic was shown to be fully potent at killing more than $1x10^7$ CFU/ml, and therefore lack of gentamicin efficacy was excluded as a potential problem. It has to be noted that the bacterial strain used in this experiment was a UTI89Δ*fim* mutant, which should show the same phenotype as the UTI89-FimH-Q133K mutant. Still, the cell-association level observed with the UTI89Δ*fim* mutant was found at the same level as in previous experiments with wild-type, FimH-Q133K and GFP-tagged wild-type UPECs in the presence or absence of mannose.

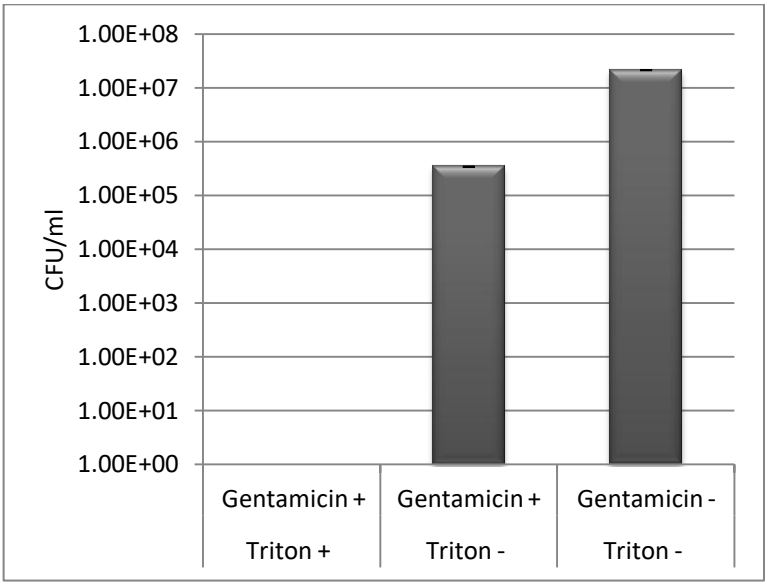

Figure 5.6 – Efficiency of gentamicin was assayed 4hpi of 5637 cells infection with UTI89 Δ*fim* mutant (SLC-154) in combination with Triton X-100 treatment. MOI=10. Data are mean of 6 technical replicates per condition coming from 1 biological replicate. Error bars are standard deviation.

Testing the impact of 5637 cell passage number

Extended propagation of cell lines can affect their viability and physiological characteristics, therefore further troubleshooting included testing the influence of the passage number on cell association and intracellular bacterial load. In addition, to eliminate any issues associated with phenotypic drift that might have occurred in the laboratory stocks of 5637 cells, a new cell line was ordered from ATCC®. All previously described experiments were performed on cells at passage number 56 (High Passage No.). Experiments using new stocks of 5637 cells were performed at passage number 46 (Low Passage No. #1). The initial comparison between p56 and p46 batches of cells didn't show any differences in terms of their binding and invasion (Figure 5.7). Therefore, a second new batch of 5637 cells (Low Passage No. #2) was tested to determine binding and intracellularisation rates at passage number 43. The results presented in Figure 5.7 show that the passage numbers available to us did not affect the rates of UPEC's binding and invasion in a way that would make it more representative of the published data, or more helpful in establishing a useful dynamic range.

(A)

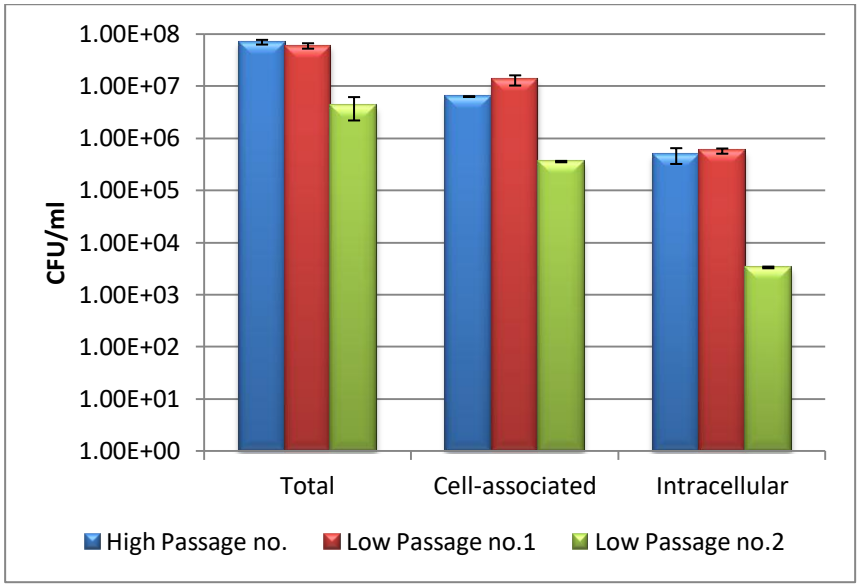

(B)

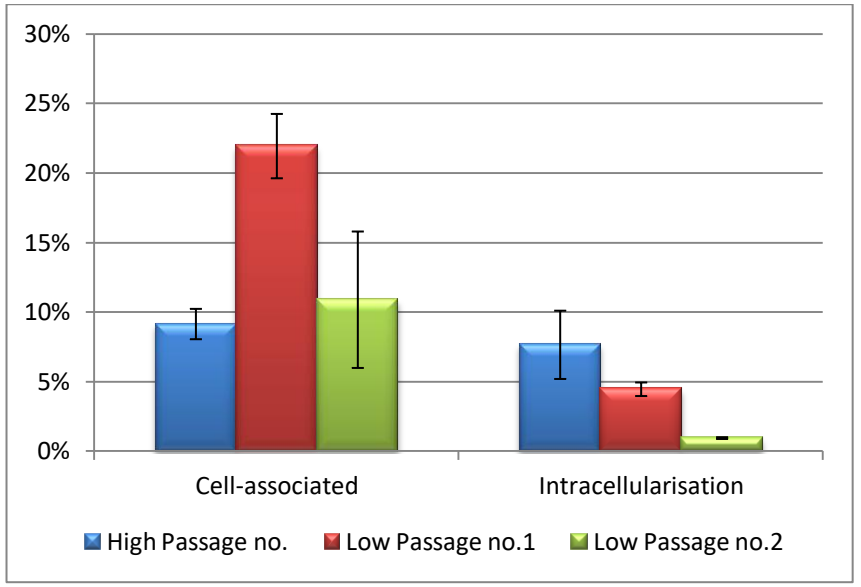

Figure 5.7 – Effect of passage number of 5637 cells on results of gentamicin protection assay using UTI89WT. (A) Shows absolute numbers of total, and cell-associated colony counts 2hpi, and intracellular counts 4hpi (after 2h of gentamicin treatment). (B) Efficiency rates of cell-association (Cell-associated CFUs/ Total CFUs) and intracellularisation (Intracellular CFUs/Cell-associated CFUs). Low Passage no.1 and 2 correspond to cell lines readily acquired from ATCC on two separate occasions at passage numbers 46 and 43 respectively. High Passage no. Corresponds to cells at passage number 56. Data of absolute numbers are means of two biological replicates, each with at least three technical replicates. MOI=10. Error bars are standard error of the mean.

Testing the impact of cell confluency and defining basal bacterial uptake by 5637 cells

Our studies showed that using the seeding densities and propagation times cited in published literature did not yield confluent cultures within 24h as reported [118, 156, 343, 344]. For this reason, the impact of 5637 cells confluency on binding and intracellularisation rates was tested. In addition, despite being non-phagocytic, 5637 cells display a limited basal level of bacterial uptake in other studies [336, 345]. For assessment of background invasion/phagocytosis of 5637 cells, a non-invasive K12 MG1655 laboratory strain was used as a non-pathogenic control.

Despite cells with greater levels of confluency showing higher levels of bacterial intake in most of the tested conditions (Figure 5.8), it did not have any major impact on the overall results, as the FimH mutant showed a higher intracellularisation rate than that of the wild-type UTI89 regardless of the cell confluency (Figure 5.9). Simultaneously, the basal invasion was established to be in the region of $1x10^4$ CFU/ml. This result was comparable with those found earlier for UTI89-FimH-Q133K and UTI89-FimH$^+$ in MαDM (Figure 5.4 and Figure 5.5). However, similar studies from other groups suggest that basal levels of binding and invasion in their experiments may have been comparably lower (~$1*10^3$CFU/ml) to those found in our studies [83, 336, 346].

Assessment of other potential factors

Further validation steps were undertaken to determine the potential existence of factors leading to our data contradicting previously published studies. Given that the environmental factors can have significant effects on cell growth, replication, as well as membrane trafficking, steps were taken to ensure that external factors were not influencing our results. No direct effects could be attributed to systems used to maintain temperature, pH and oxygenation of the culture environment. Furthermore, no significant difference was found when comparing cell culture media and PBS (commercial or prepared in-house). No significant differences could be attributed to the type and size of vessels used to grow bacteria, bacterial suspension volume, or systems used to generate the UTI89-FimH-Q133K mutants. Given that none of these modifications led to any significant changes in the experimental outcomes bringing these data in line with other published studies, they can be excluded from being potential issues. Though there may be other variables

leading to the discrepancies, but at this point they remain unknown. Nevertheless, the data presented here appear to be reproducible.

5.3.6 The utility of other urothelial cell lines towards the development of a system for siRNA screening

Given the inability to achieve the useful dynamic range, as found in previously published data, other commonly used bladder urothelial cell lines, T24 and RT4, were tested to determine whether they could provide a larger difference between minimum and maximum bacterial load in terms of the cell association and intracellularisation (Figure 5.10 and Figure 5.11) [343]. Cell-association and intracellularisation rates in these two cell lines showed analogous patterns to those found in previous sections (5.3.3, 5.3.4 and 5.3.5). Despite the good concordance among the experimental outcomes of this work, the findings in T24 and RT4 cell lines were not in line with the aforementioned reports of loss of invasion in UPECΔ*fimH* mutants (UTI89 Δ*fimH* and UTI89-FimH-Q133K). As a result the difference between the minimum and baseline intracellularisation was much smaller than previously anticipated. This made the use of these cell lines unsuitable for further experiments towards developing a system for a genome-wide siRNA screen, as the optimal detection range of up- and down-regulation of genes would make it difficult to interpret [347]. That seemed to be especially the case with RT4, which did not form homogenous monolayers like those seen in 5637 or T24 cells, but tended to form domed clusters. This phenomenon has been observed previously and thus makes this cell line unsuitable for studies that aim to recapitulate an infections of an intact urothelial layer [182].

(A)

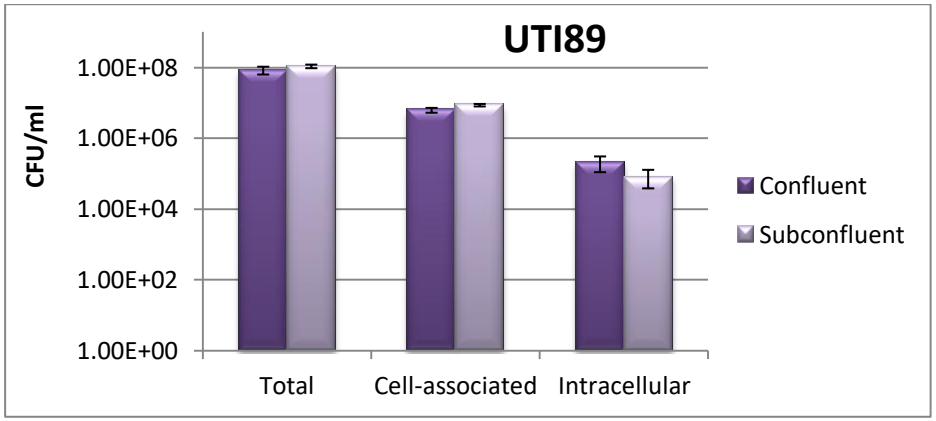

(B)

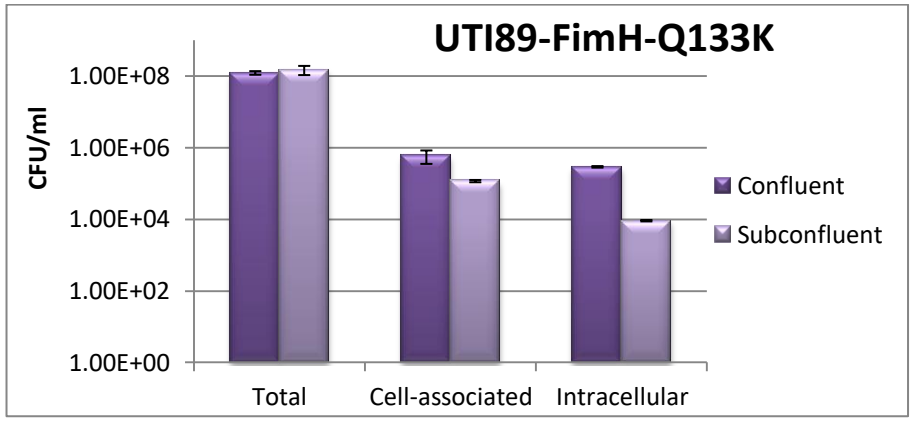

(C)

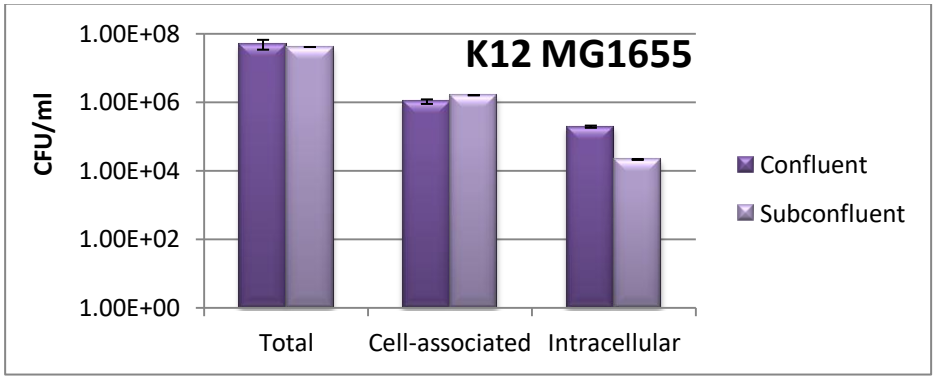

Figure 5.8 – Differences in gentamicin protection assays results depending on confluency level of urothelial cells. Confluent (100% confluency) or subconfluent (70% confluency) 5637 cells were infected with UTI89 WT (A), UTI89-FimH-Q133K (B) or K12 MG1655 (C) *E. coli* strains at MOI=10. Mean absolute numbers of total, and cell-associated colony counts 2hpi, and intracellular counts 4hpi (after 2h of gentamicin treatment) are showed. N = 1 with two technical replicates each. Error bars are standard deviation.

(A)

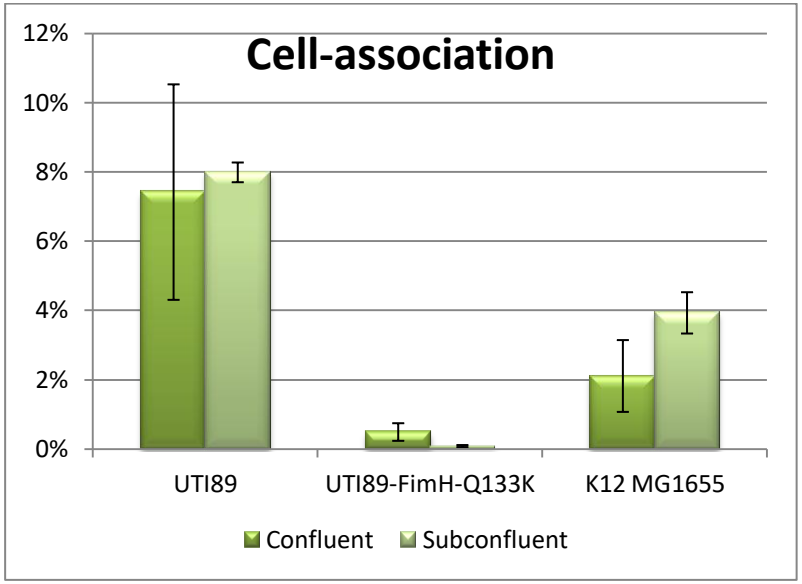

(B)

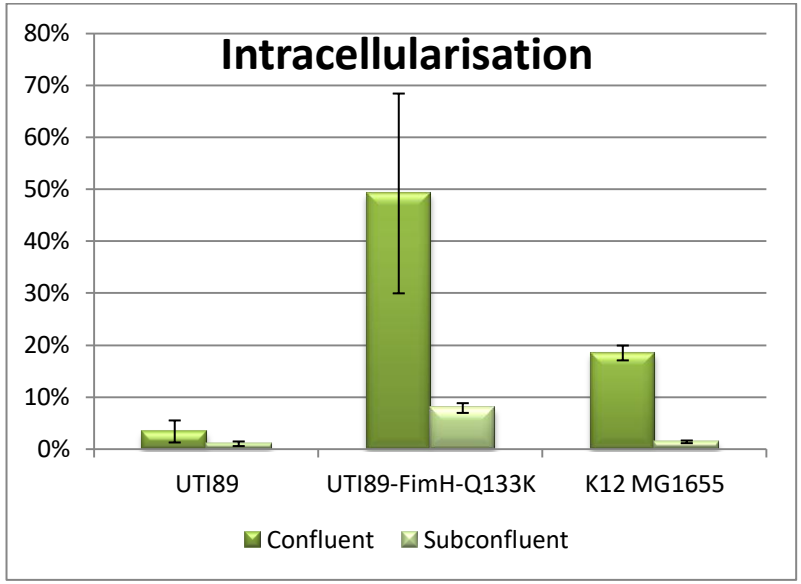

Figure 5.9 – Differences in gentamicin protection assays results depending on confluency level of urothelial cells. Confluent (100% confluency) or subconfluent (70% confluency) 5637 bladder cells were infected with UTI89 WT, UTI89-FimH-Q133K or K12 MG1655 *E. coli* strains at MOI=10. Mean cell-association and intracellularisation rates were calculated using absolute data presented in Figure 5.8 coming from one biological replicate, with two technical replicates per condition. Cell-association and intracellularisation rates were calculated using the following formulae respectively: (Cell-associated CFUs/ Total CFUs); (Intracellular CFUs/Cell-associated CFUs). Error bars are standard deviation.

(A)

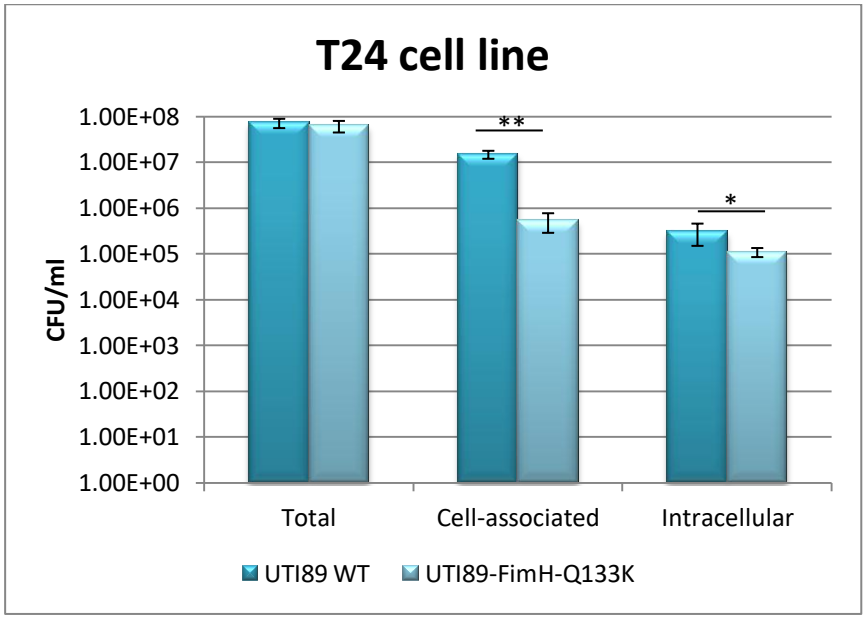

(B)

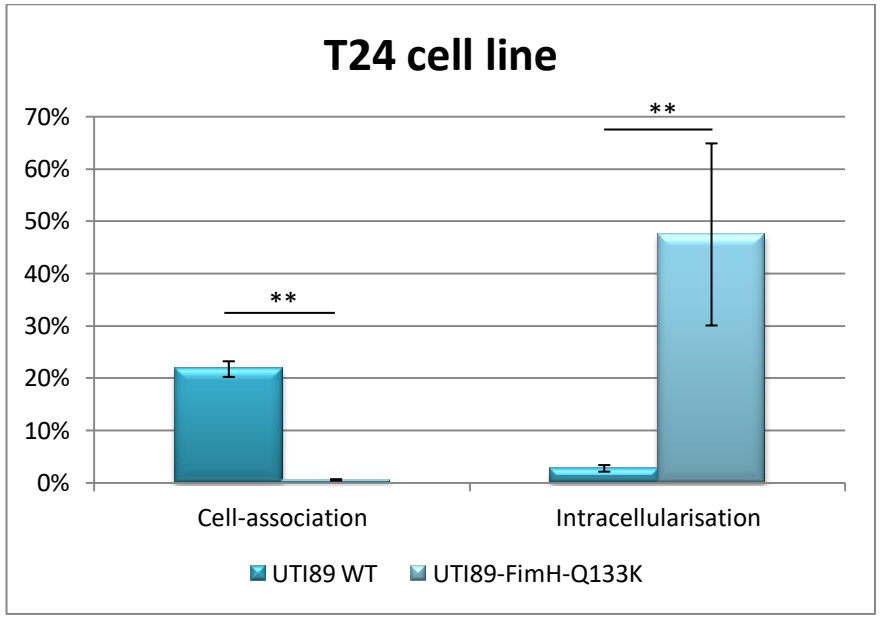

Figure 5.10 – Gentamicin protection assay in T24 cell line using UTI89WT and UTI89-FimH-Q133K UPEC strains. (A) Absolute values for total, and cell-associated colony counts (retrieved after PBS washes) 2hpi, and intracellular counts 4hpi (retrieved after 2h of gentamicin treatment). (B) Shows efficiency of cell-association and invasion in the form of Cell-association rate (Cell-associated CFUs/ Total CFUs) and Invasion rates (Intracellular CFUs/Cell-associated CFUs). MOI=10. Data show means of 5 independent experiments, each with three technical replicates. Error bars are standard error of the mean. The statistical significance was assayed by using Mann-Whitney rank sum test (*, $P< 0.05$; **, $P<0.001$).

(A)

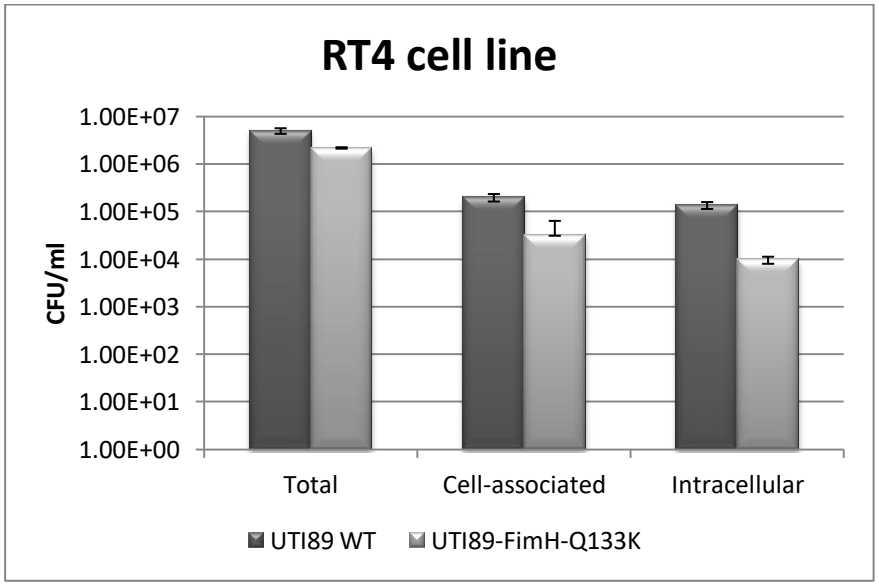

(B)

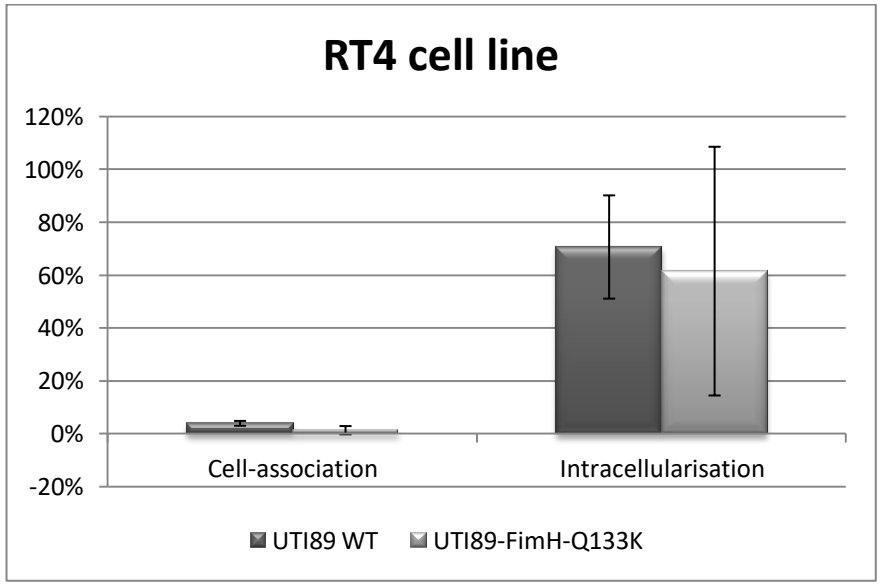

Figure 5.11 – Gentamicin protection assay results in RT4 cell line using UTI89WT and UTI89-FimH-Q133K UPEC strains. (A) Absolute values for total, and cell-associated colony counts (retrieved after PBS washes) 2hpi, and intracellular counts 4hpi (retrieved after 2h of gentamicin treatment). (B) Shows efficiency of cell-association and invasion in the form of Cell-association rate (Cell-associated CFUs/ Total CFUs) and Intracellularisation rates (Intracellular CFUs/Cell-associated CFUs). MOI=10. Data show means of one biological replicate, with four technical replicates per condition. Error bars- standard deviation.

5.4 Discussion

UTIs caused by UPEC are highly prevalent and have a tendency to recur in a significant proportion of patients. Due to a highly predictable etiology of UTIs and the spectrum of their antibiotic resistance, current approaches to their treatment focus on empirical antibiotic therapy. However, the growing problem of antibiotic resistance suggests that new modes of treatment will be needed [42, 43]. A thorough understanding of the factors and mechanisms that regulate how the host responds to infection is fundamental to improving our ability to detect and treat these infections. Deciphering novel urothelial cell responses during bacterial contact or invasion may help to identify new molecular candidates that can be exploited therapeutically and is therefore of a paramount importance.

In this study, we used an invasion assay as a phenotypic tool to assess infection status. Optimisation of binding and invasion, both of which are well studied processes in this system, was undertaken to later correlate the CFU counts with fluorescent signal measurements. FimH is one of the most studied adhesins, responsible for binding of UPEC to bladder cells and mutating it was found to have a highly potent effect on the bacterial binding and invasion. It was used therefore to define a dynamic range of changes in cell-association and/or intracellularisation that could be expected upon a knock-down of genes significant in the face of UPEC infection. The differential change between wild-type and FimH mutants was found to be of the order of 30 times lower in terms of cell-association rate and ~9 times increased for invasion. The trend was analogous in all chemical and genetic controls. The results, however, using either chemical or genetically induced conditions, did not reflect the values reported in previous scientific studies that showed an almost complete abolishment of bacterial association and invasion of human cells. For example, values of ~45 times decrease for cell-association and ~40 times decrease for intracellularisation have been reported [83, 152]. The major difference in the intracellularisation rate was due to a high baseline invasion observed in 5637 cells, which was mostly unaffected by the functionality of FimH, a dependency discordant with the general observations by other studies [83]. This high baseline invasion lowers the dynamic range to such an extent that it would make an siRNA screen impractical due to low dynamic range between minimum and maximum invasion rates. This way subtle changes in phenotype would not be detected.

An extensive literature search of other reports has resulted in the collection of a range of data for the 5637 cells, bacterial strains and protocols from other publishing labs also using this assay. These have been compared, and contrasted. Unfortunately, the majority of reports do not deliver absolute numbers, and show normalised data, with reference strains represented as 100%. Due to this transformation of data, comparing binding and invasion data found in our study with these previous studies was not possible [118, 141, 156, 233, 335, 343, 344, 348]. Only a sub-set of reports could be used for such evaluation [83, 118, 339]. Aside from confirmation that bacterial GFP expression has no effect on its wild-type phenotype, the data show inconsistencies with published data, despite extensive validation and controls. This still could be due to the passage number available at a time of the studies. Martinez *et al.,* reported all the experiments being done using cell lines at passage numbers between 10 and 24 [83]. At the time of this study, the cell lines originating from the distributor were only available at passages 41, 38 and 175 for 5637, T24 and RT4 respectively, and lower passages were not available to us.

Interestingly, analysis of infected populations of host cells using FACS analysis (Figure 5.2) demonstrated the expected intracellularisation trends in strains with both genetic or chemical disruption of FimH function. In the traditional gentamicin protection assay, total CFUs from all infected epithelial cells in a single well are measured. FACS analysis, on the other hand, provides a quantification of CFU per epithelial cell. This suggests a poor ability to assess CFU counts, as translated from fluorescent signal by FACS. It also implies that optimising the model based purely on the intensity of GFP signal produced by bacteria could potentially yield a more accurate reflection of host cell bacterial load. This would, however, require access to the high-throughput microscopy that would have been used for the purpose of the siRNA screen. Unfortunately due to time constrains associated with the project, such approaches were not possible. Future studies would be required to corroborate the validity of this experimental approach.

While the importance of FimH in mediating bacterial association with urothelial cells was demonstrated in these experiments, contrary to previous studies, loss of FimH appeared to have a negligible effect on the potential of bacteria to access the intracellular environment of host cells. In spite of detailed analysis of published protocols in an attempt to optimise this assay,

reproduction of the reported results using gentamicin protection assay was not possible. The data presented here do not show explicitly that disabling the functionality of FimH has no effect on the abilities of UPEC to invade. It also cannot be excluded that once these bacteria enter the host cell, they might be more successful at persisting and/or replicating. But our observations suggest that the effect is not universal when using binding/invasion assays, and that there may be other factors that can compensate for its effect. For instance, UPEC can encode up to 16 of these adhesive factors. UTI89 contains 10 intact chaperone-usher pilus operons (*pap, fim, sfa, auf, F17, yad, yfc, yqi, yeh,* and *fml*), half of which are not well characterised. Little is also known about their role in pathogenesis during UTIs [85, 349, 350], or cross-talk with other pili [351, 352]. It was shown in other strains, like CFT073, that disabling one type of fimbriae resulted in overexpression of another type [261, 352]. Optimisation of this model, based on fluorescent ratios to discriminate between infected and uninfected cells and establish the thresholds for what constitutes a significant change in fluorescence can be considered the gold standard for future studies in this area.

6 Final discussion

6.1 Motivation

The most recent report released by the World Health Organisation (WHO) on "A global priority for research and development" [353] stressed the great importance of developing new antimicrobial agents. Facing a growing problem of antibiotic resistance, a list of priority pathogens was generated to highlight the key bacteria against which new drugs are urgently needed. *Enterobacteriaceae*, a family to which *E. coli* belongs, was identified as requiring a critical focus for antimicrobial research. *E. coli*, such as the globally disseminated and multi-drug resistant ST131, not only cause UTIs and bloodstream infections, but also play a role in the further spread of antibiotic resistance. Taking into consideration that UTIs are one of the most common bacterial infections among humans, developing appropriate techniques for control over UPEC is of a paramount importance. This is especially the case for rUTIs, the management of which typically involves long-term usage of antibiotics, a strategy that provides little long-term benefit, while encouraging development and spread of antibiotic resistance [354].

Experimental study models are a critical component of not only drug discovery, but also basic science and clinical development. Whilst *in vitro* and animal model systems are inherently critical in translational studies, there is a generally poor overlap between these. The existence of the gap in translation between *in vitro* and *in vivo* systems, as well as between these and the actual human environment, is a significant hindrance to antimicrobial studies [355]. For these reasons it is important to study UTIs in models demonstrating the best reflection of the true interactions that exist in natural settings.

6.2 Aim

To address these issues, in the framework of this thesis, several different approaches were undertaken, with the main aims being: characterisation of an NHU system, as a novel *in vitro* model for studying UPEC; characterisation of host responses of urothelial cells to UPEC invasion by means of single mouse bladder cell proteomics; revising an experimental system for the

purpose of genome-wide siRNA screen also to study host responses of urothelial cells to infections with UPEC.

6.3 Contributions of the thesis

6.3.1 NHU model system

As it would arguably be the most physiologically relevant *in vitro* system [265], an NHU model was optimised towards its use in a gentamicin protection assay to study UPEC binding and invasion. Both binding and invasion are known to be dependent on a specific interaction of the FimH adhesin with urothelial cells. The degree of FimH-dependence was not confirmed in the current study. And while binding of the UTI89 strain was confirmed, it showed a limited invasion in NHU cells. While the result is in agreement with another study utilising human bladder epithelial progenitor cells that form morphologically correct urothelial organoids [356], it did not agree with the previously published studies utilising classic urothelial cell line models [83]. This exposes a potential issue with the relevance of the phenotype observed in either the NHU or the classical cell lines that will need to be resolved prior to further studies of host-pathogen interactions, drug evaluation, or basic science studies.

6.3.2 Model for genome-wide siRNA screen

The relationship between the host and UPEC during rUTIs is poorly understood. Investigating it at a protein and transcriptional level could lead to expanding our understanding of which pathways and genes are central during the process. Therefore, I attempted to establish a phenotypic, fluorescence-based system to study host responses in association with bacterial binding and invasion. I initially attempted to replicate previously published results demonstrating a large difference in invasion between WT and FimH-mutant strains. Unfortunately, I was unable to reproduce all of the published data [83]. The major issue was a baseline invasion rate higher than that reported in the literature, which reduced the useful dynamic range of the assay. The experimental results coming from this study further hint at potential difficulties with cell line models, as quantitative invasion efficiencies seem to be significantly affected by passage number of the immortalized cell lines. Another discrepancy requiring further study was the poor

correlation between CFU counts, as defined by a gentamicin protection assay, and fluorescence as measured by FACS.

6.3.3 Single cell proteomics

I also explored the use of single cell proteomics to understand the changes in bladder epithelial cells upon infection by UPEC. I proved that manual isolation of mouse urothelial cells could be used for downstream untagged mass spectrometric analysis to study the mammalian proteome. The project aimed at identification of biomarkers of intracellular UPEC infection that could be used to improve treatment strategies among patients suffering from rUTIs. While few protein changes were identified between infected and uninfected cells, I discovered that isolated superficial bladder epithelial cells appeared to have three separate proteome profiles, potentially indicating an unknown heterogeneity among this morphologically uniform cell type. Of note, other recent single cell studies have identified additional cell types among cell types previously thought to be uniform [269, 357]. In this assay, technical sensitivity was also a main limiting factor. It led to undersampling of the cells at the point of protein identification. In consequence, we were not able to achieve a full coverage of the mouse proteome. However, we are the first to perform an unbiased single cell proteomics on urothelial cells.

6.4 Future directions

With the continuous extension of research done in the field of UTIs, the complexity of the disease and its intricacies become more apparent. The difficulty arises not only as a result of a vast array of phenotypes expressed by UPEC and other uropathogens, but also intra and inter-individual variations among host urothelial cells. In addition, the former also varies with anatomical location in the urinary tract. Identification of these differences has been enabled by technological advancements. Nevertheless, the current state of the art is still not sufficiently sensitive to reach the single cell level. Therefore, further advances in technical sensitivity should enable more extensive insights that can build on the optimisation work and new hypotheses I have described in this thesis.

One of the most important developments of this work would involve inclusion of a larger sample of single cell data, not only to improve the statistical analysis, but most importantly to

aid choosing protein candidates for further research. The proteomic analysis of single mouse urothelial cells presented in this work represents a starting point for the selection of candidate proteins to be assessed for their potential as future biomarkers of differentiation between the potential subgroups of urothelial cells. Further validation of those differentially expressed proteins by quantitative IHC and if possible whole mount immunofluorescence in murine bladders and human ureter samples would be needed. In the event that their value as markers should be confirmed, functional characterisation studies using knockout animals with normal or infected bladders could be used in future experiments. Furthermore, the NHU model could potentially be used in combination with gene silencing techniques. Both could be applied to improve our understanding of the urothelial physiology, as well as potential implications of the intercellular heterogeneity as a mean to resist bacterial infections. Should it be discovered that a particular protein epitope is essential for bacterial infection, trialling of antibody mediated therapy blocking the binding sites in the urinary tract could be a potentially fruitful area for further research.

The scope of the single cell proteomics study was limited to trying to understand host responses to the infection. While at a time of the research it wasn't fully possible, eventually, given the technological advancement, it would be interesting to explore the proteome of an IBC, whether that would be by eliminating the noise associated with host proteins, or by a task more difficult to execute technically- having the IBC extracted from a host cell, and analysed separately. But once possible, an important inclusion would be to study the changes in the bacterial proteome at different stages of if the intracellular infection.One of the acknowledged limitations of this study is that it focussed on the use of specific bacterial strains. UTIs can be caused by a number of bacterial strains and species. For a more comprehensive understanding of how host responses function, the scope of studied microorganisms would need to be broadened to include other bacterial strains. Therefore, further work is needed to explore in detail host-pathogen interactions to achieve more representative picture of what could be happening in the human body during the infection.

Furthermore, since the morphological and phenotypic divergence of cell lines is becoming more apparent, new *in vitro* studies should be performed using human-based cells to complement results obtained from mouse models and traditional immortalised cell line studies. This could

provide real and exciting opportunity for transforming the traditional approach to study human tissues. While the NHU model appears to be the most representative *in vitro* system to study processes occurring in the urothelium, it is important however, that we have some understanding of the implications of interindividual variation, or the use of serum in the media. These still need to be addressed so that their use and data analysis could be effectively tailored to specific experiments. Fortunately such efforts are not specific to the bladder epithelium, and knowledge gained throughout these avenues will hopefully be applicable to research on other epithelial tissues or infectious diseases. It would be especially valuable to address the impact of the sex of patients, from whom the NHU cells were extracted, on bacterial invasion and progression capabilities. The preliminary data indicates noteworthy differences between bacterial invasion capabilities found in male and female test samples. It could be possible that incorporation of this information could sufficiently reduce the issues associated with the interindividual variation. It also opens up an avenue of research into personalised medicine approaches to treating UTI.

Future work should also aim at addressing the shortcomings of the current gentamicin protection assay looking at the progression of intracellular infections. Integrating more frequent timepoints and a longer time scales would help to gather a more detailed picture of the changes happening within the cell upon bacterial invasion. Plating larger volumes of the bacteria-containing media during the assay, could help in obtaining more precise bacterial counts, making the data more reliable.

Additionally, re-evaluating the use of cell line model and binding/invasion assay towards siRNA screen by basing it purely on fluorescent signal without trying to correlate it with CFU counts, would be interesting to explore. If functional, it could be used to investigate host-pathogen interactions further.

In conclusion, this work has contributed significantly towards the advancement of the field, and has pushed forward the technological advancement of what we thought was possible in studying the proteome of infected cells. While many problems both bigger and smaller remain to be researched, it only shows that the field remains an exciting one for a number of years to come.

7 References

1. Lewis, S.A. (2000) Everything you wanted to know about the bladder epithelium but were afraid to ask. American Journal of Physiology-Renal Physiology 278 (6), F867-F874.

2. Hicks, R.M. (1975) The mammalian urinary bladder: an accommodating organ. Biol Rev Camb Philos Soc 50 (2), 215-46.

3. Birder, L.A. and de Groat, W.C. (2007) Mechanisms of disease: involvement of the urothelium in bladder dysfunction. Nat Clin Pract Urol 4 (1), 46-54.

4. Khandelwal, P. et al. (2009) Cell biology and physiology of the uroepithelium. Am J Physiol Renal Physiol 297 (6), F1477-501.

5. Keshtkar, A. and Lawford, P. (2007) Cellular morphological parameters of the human urinary bladder (malignant and normal). Int J Exp Pathol 88 (3), 185-90.

6. Jost, S.P. et al. (1989) The morphology of normal human bladder urothelium. J Anat 167, 103-15.

7. Dotsikas, G. et al. (1987) Cellular heterogeneity in normal and neoplastic human urothelium: a study using murine monoclonal antibodies. Br J Cancer 56 (4), 439-44.

8. Jost, S.P. (1989) Cell cycle of normal bladder urothelium in developing and adult mice. Virchows Arch B Cell Pathol Incl Mol Pathol 57 (1), 27-36.

9. Liu, Y. et al. (2015) Dual ligand/receptor interactions activate urothelial defenses against uropathogenic E. coli. Sci Rep 5, 16234.

10. Apodaca, G. (2004) The uroepithelium: not just a passive barrier. Traffic 5 (3), 117-28.

11. Kreft, M.E. et al. (2005) Urothelial injuries and the early wound healing response: tight junctions and urothelial cytodifferentiation. Histochem Cell Biol 123 (4-5), 529-39.

12. Lobban, E.D. et al. (1998) Uroplakin gene expression by normal and neoplastic human urothelium. Am J Pathol 153 (6), 1957-67.

13. Olsburgh, J. et al. (2003) Uroplakin gene expression in normal human tissues and locally advanced bladder cancer. J Pathol 199 (1), 41-9.

14. Cross, W.R. et al. (2005) A biomimetic tissue from cultured normal human urothelial cells: analysis of physiological function. Am J Physiol Renal Physiol 289 (2), F459-68.

15. Hu, P. et al. (2002) Role of membrane proteins in permeability barrier function: uroplakin ablation elevates urothelial permeability. Am J Physiol Renal Physiol 283 (6), F1200-7.

16. Perrone, R. et al. (1996) Immortalized human bladder cell line exhibits amiloride-sensitive sodium absorption. American Journal of Physiology-Renal Physiology 270 (1), F148-F153.

17. Bouhout, S. et al. (2013) Potential of Different Tissue Engineering Strategies in the Bladder Reconstruction. In Regenerative Medicine and Tissue Engineering (Andrades, J.A. ed), p. Ch. 23, InTech.

18. Brod, J. (1956) Chronic pyelonephritis. The Lancet 267 (6930), 973-981.

19. Najar, M.S. et al. (2009) Approach to urinary tract infections. Indian J Nephrol 19 (4), 129-39.

20. Foxman, B. (2002) Epidemiology of urinary tract infections: incidence, morbidity, and economic costs. Am J Med 113 Suppl 1A, 5S-13S.

21. Roberts, J.A. (1991) Etiology and pathophysiology of pyelonephritis. Am J Kidney Dis 17 (1), 1-9.

22. Johansen, T.E. et al. (2011) Critical review of current definitions of urinary tract infections and proposal of an EAU/ESIU classification system. Int J Antimicrob Agents 38 Suppl, 64-70.

23. Foxman, B. (2014) Urinary tract infection syndromes: occurrence, recurrence, bacteriology, risk factors, and disease burden. Infect Dis Clin North Am 28 (1), 1-13.

24. Hooton, T.M. et al. (2010) Diagnosis, prevention, and treatment of catheter-associated urinary tract infection in adults: 2009 International Clinical Practice Guidelines from the Infectious Diseases Society of America. Clin Infect Dis 50 (5), 625-63.

25. Flores-Mireles, A.L. et al. (2015) Urinary tract infections: epidemiology, mechanisms of infection and treatment options. Nat Rev Microbiol 13 (5), 269-84.

26. Berry, R.E. et al. (2009) Urothelial cultures support intracellular bacterial community formation by uropathogenic Escherichia coli. Infect Immun 77 (7), 2762-72.

27. Hannan, T.J. et al. (2012) Host-pathogen checkpoints and population bottlenecks in persistent and intracellular uropathogenic Escherichia coli bladder infection. FEMS Microbiol Rev 36 (3), 616-48.

28. Mantle, S., Reducing HCAI- What the Commissioner needs to know, NHS England, 2015.

29. Fenwick, E.A. et al. (2000) Management of urinary tract infection in general practice: a cost-effectiveness analysis. Br J Gen Pract 50 (457), 635-9.

30. MeReC, Urinary tract infection, in: NHS (Ed.) MeReC Bulletin, UK, 1995, pp. 1-7.

31. Foxman, B. (2010) The epidemiology of urinary tract infection. Nat Rev Urol 7 (12), 653-60.

32. Hilbert, D.W. (2011) Uropathogenic Escherichia coli: the pre-eminent urinary tract infection pathogen. In E.coli infections: causes, treatment and prevention (Rogers, M.C. and Peterson, N.D. eds), Study of Uropathogenic Escherichia coli Host-Pathogen Interactions Using Novel Infection Models.

33. Hagan, E.C. et al. (2010) Escherichia coli global gene expression in urine from women with urinary tract infection. PLoS Pathog 6 (11), e1001187.

34. Foxman, B. et al. (2000) Urinary tract infection: self-reported incidence and associated costs. Ann Epidemiol 10 (8), 509-15.

35. Totsika, M. et al. (2012) Uropathogenic Escherichia coli mediated urinary tract infection. Curr Drug Targets 13 (11), 1386-99.

36. Cove-Smith A., M.A. (2007) Management of urinary tract infections in the elderly. Trends in Urology Gynaecology & Sexual Health 12 (4), 31-34.

37. Harper, M.a.F.G. (2007) 3. Management of urinary tract infections in men. Trends in Urology, Gynaecology & Sexual Health 12 (1), 30--35.

38. Lotan, Y. et al. (2013) Impact of fluid intake in the prevention of urinary system diseases: a brief review. Curr Opin Nephrol Hypertens 22 Suppl 1, S1-10.

39. Beetz, R. (2003) Mild dehydration: a risk factor of urinary tract infection? Eur J Clin Nutr 57 Suppl 2, S52-8.

40. Tannen, R.L. et al. (1969) Vasopressin-resistant hyposthenuria in advanced chronic renal disease. N Engl J Med 280 (21), 1135-41.

41. Durojaiye, C.O.a.H.B. (2015) Urinary tract infections: diagnosis and management. Prescriber 26 (11), 21--29.

42. Newell, A. et al. (2005) Multicentre audit of the treatment of uncomplicated urinary tract infection in South Thames. Int J STD AIDS 16 (1), 74-7.

43. Gupta, K. et al. (2001) Increasing antimicrobial resistance and the management of uncomplicated community-acquired urinary tract infections. Ann Intern Med 135 (1), 41-50.

44. Kahlmeter, G. et al. (2015) Antimicrobial Resistance of Escherichia coli Causing Uncomplicated Urinary Tract Infections: A European Update for 2014 and Comparison with 2000 and 2008. Infect Dis Ther 4 (4), 417-23.

45. Vahlensieck, W. et al. (2016) Management of Uncomplicated Recurrent Urinary Tract Infections. European Urology Supplements 15 (4), 95-101.

46. Naber, K.G. et al. (2008) Surveillance study in Europe and Brazil on clinical aspects and Antimicrobial Resistance Epidemiology in Females with Cystitis (ARESC): implications for empiric therapy. Eur Urol 54 (5), 1164-75.

47. Wiles, T.J. et al. (2008) Origins and virulence mechanisms of uropathogenic Escherichia coli. Exp Mol Pathol 85 (1), 11-9.

48. Foxman, B. et al. (2005) Choosing an appropriate bacterial typing technique for epidemiologic studies. Epidemiol Perspect Innov 2, 10.

49. Totsika, M. et al. (2011) Insights into a multidrug resistant Escherichia coli pathogen of the globally disseminated ST131 lineage: genome analysis and virulence mechanisms. PLoS One 6 (10), e26578.

50. Gibreel, T.M. et al. (2012) Population structure, virulence potential and antibiotic susceptibility of uropathogenic Escherichia coli from Northwest England. J Antimicrob Chemother 67 (2), 346-56.

51. Bien, J. et al. (2012) Role of Uropathogenic Escherichia coli Virulence Factors in Development of Urinary Tract Infection and Kidney Damage. Int J Nephrol 2012, 681473.

52. Brzuszkiewicz, E. et al. (2006) How to become a uropathogen: Comparative genomic analysis of extraintestinal pathogenic Escherichia coli strains. PNAS 103 (34), 12879-12884.

53. Oelschlaeger, T.A. et al. (2002) Pathogenicity islands of uropathogenic E. coli and the evolution of virulence. Int J Antimicrob Agents 19 (6), 517-21.

54. Schmidt, H. and Hensel, M. (2004) Pathogenicity islands in bacterial pathogenesis. Clin Microbiol Rev 17 (1), 14-56.

55. Karimian, A. et al. (2012) Detection of uropathogenic Escherichia coli virulence factors in patients with urinary tract infections in Iran. Afr J Microbiol Res 6 (39), 6811-6816.

56. Johnson, J.R. (1991) Virulence factors in Escherichia coli urinary tract infection. Clin Microbiol Rev 4 (1), 80-128.

57. Marrs, C.F. et al. (2005) Escherichia coli mediated urinary tract infections: are there distinct uropathogenic E. coli (UPEC) pathotypes? FEMS Microbiol Lett 252 (2), 183-90.

58. Wiles, T.J. et al. (2008) Inactivation of host Akt/protein kinase B signaling by bacterial pore-forming toxins. Mol Biol Cell 19 (4), 1427-38.

59. Mann, R. et al. (2017) Metabolic Adaptations of Uropathogenic E. coli in the Urinary Tract. Front Cell Infect Microbiol 7, 241.

60. Christensen, M.G. et al. (2015) [Ca2+]i Oscillations and IL-6 Release Induced by α-Hemolysin from Escherichia coli Require P2 Receptor Activation in Renal Epithelia. J Biol Chem 290 (23), 14776-84.

61. Uhlén, P. et al. (2000) Alpha-haemolysin of uropathogenic E. coli induces Ca2+ oscillations in renal epithelial cells. Nature 405 (6787), 694-7.

62. Anderson, G.G. et al. (2003) Intracellular bacterial biofilm-like pods in urinary tract infections. Science 301 (5629), 105-7.

63. Justice, S.S. et al. (2004) Differentiation and developmental pathways of uropathogenic Escherichia coli in urinary tract pathogenesis. Proc Natl Acad Sci U S A 101 (5), 1333-8.

64. Justice, S.S. et al. (2006) Filamentation by Escherichia coli subverts innate defenses during urinary tract infection. Proc Natl Acad Sci U S A 103 (52), 19884-9.

65. Horvath, D.J. et al. (2011) Morphological plasticity promotes resistance to phagocyte killing of uropathogenic Escherichia coli. Microbes Infect 13 (5), 426-37.

66. Olson, P.D. and Hunstad, D.A. (2016) Subversion of Host Innate Immunity by Uropathogenic Escherichia coli. Pathogens 5 (1).

67. Cavalieri, S.J. and Snyder, I.S. (1982) Effect of Escherichia coli alpha-hemolysin on human peripheral leukocyte viability in vitro. Infect Immun 36 (2), 455-61.

68. Russo, T.A. et al. (2005) E. coli virulence factor hemolysin induces neutrophil apoptosis and necrosis/lysis in vitro and necrosis/lysis and lung injury in a rat pneumonia model. Am J Physiol Lung Cell Mol Physiol 289 (2), L207-16.

69. Davis, J.M. et al. (2005) Cytotoxic necrotizing factor type 1 production by uropathogenic Escherichia coli modulates polymorphonuclear leukocyte function. Infect Immun 73 (9), 5301-10.

70. Davis, J.M. et al. (2006) Cytotoxic necrotizing factor type 1 delivered by outer membrane vesicles of uropathogenic Escherichia coli attenuates polymorphonuclear leukocyte antimicrobial activity and chemotaxis. Infect Immun 74 (8), 4401-8.

71. Loughman, J.A. and Hunstad, D.A. (2011) Attenuation of human neutrophil migration and function by uropathogenic bacteria. Microbes Infect 13 (6), 555-65.

72. Loughman, J.A. and Hunstad, D.A. (2012) Induction of indoleamine 2,3-dioxygenase by uropathogenic bacteria attenuates innate responses to epithelial infection. J Infect Dis 205 (12), 1830-9.

73. Klumpp, D.J. et al. (2001) Uropathogenic Escherichia coli potentiates type 1 pilus-induced apoptosis by suppressing NF-kappaB. Infect Immun 69 (11), 6689-95.

74. Hunstad, D.A. et al. (2005) Suppression of bladder epithelial cytokine responses by uropathogenic Escherichia coli. Infect Immun 73 (7), 3999-4006.

75. Billips, B.K. et al. (2007) Modulation of host innate immune response in the bladder by uropathogenic Escherichia coli. Infect Immun 75 (11), 5353-60.

76. Busch, A. and Waksman, G. (2012) Chaperone-usher pathways: diversity and pilus assembly mechanism. Philos Trans R Soc Lond B Biol Sci 367 (1592), 1112-22.

77. Geibel, S. and Waksman, G. (2014) The molecular dissection of the chaperone-usher pathway. Biochim Biophys Acta 1843 (8), 1559-67.

78. Davis, N.F. and Flood, H.D. (2011) The Pathogenesis of Urinary Tract Infections. In Clinical Management of Complicated Urinary Tract Infection (Nikibakhsh, A. ed), p. Ch. 07, InTech.

79. Le Bouguenec, C. et al. (1992) Rapid and specific detection of the pap, afa, and sfa adhesin-encoding operons in uropathogenic Escherichia coli strains by polymerase chain reaction. Journal of clinical microbiology 30 (5), 1189-1193.

80. Holden, N. et al. (2007) Regulation of P-fimbrial phase variation frequencies in Escherichia coli CFT073. Infection and immunity 75 (7), 3325-3334.

81. Qin, X. et al. (2013) Comparison of adhesin genes and antimicrobial susceptibilities between uropathogenic and intestinal commensal Escherichia coli strains. PLoS One 8 (4), e61169.

82. Langermann, S. et al. (1997) Prevention of mucosal Escherichia coli infection by FimH-adhesin-based systemic vaccination. Science 276 (5312), 607-11.

83. Martinez, J.J. et al. (2000) Type 1 pilus-mediated bacterial invasion of bladder epithelial cells. The EMBO journal 19 (12), 2803-2812.

84. Wright, K.J. et al. (2007) Development of intracellular bacterial communities of uropathogenic Escherichia coli depends on type 1 pili. Cell Microbiol 9 (9), 2230-41.

85. Chen, S.L. et al. (2006) Identification of genes subject to positive selection in uropathogenic strains of Escherichia coli: a comparative genomics approach. Proc Natl Acad Sci U S A 103 (15), 5977-82.

86. Korea, C.G. et al. (2010) Escherichia coli K-12 possesses multiple cryptic but functional chaperone-usher fimbriae with distinct surface specificities. Environ Microbiol 12 (7), 1957-77.

87. Flo, T.H. et al. (2004) Lipocalin 2 mediates an innate immune response to bacterial infection by sequestrating iron. Nature 432 (7019), 917-21.

88. Steigedal, M. et al. (2014) Lipocalin 2 imparts selective pressure on bacterial growth in the bladder and is elevated in women with urinary tract infection. J Immunol 193 (12), 6081-9.

89. Welch, R.A. et al. (2002) Extensive mosaic structure revealed by the complete genome sequence of uropathogenic Escherichia coli. Proc Natl Acad Sci U S A 99 (26), 17020-4.

90. Klein, E.A. and Gitai, Z. (2013) Draft Genome Sequence of Uropathogenic Escherichia coli Strain J96. Genome Announc 1 (1).

91. Miller, F.G. and Grady, C. (2001) The ethical challenge of infection-inducing challenge experiments. Clin Infect Dis 33 (7), 1028-33.

92. Hung, C.S. et al. (2009) A murine model of urinary tract infection. Nat Protoc 4 (8), 1230-43.

93. Schwartz, D.J. et al. (2011) Population dynamics and niche distribution of uropathogenic Escherichia coli during acute and chronic urinary tract infection. Infect Immun 79 (10), 4250-9.

94. Mulvey, M.A. et al. (1998) Induction and evasion of host defenses by type 1-piliated uropathogenic Escherichia coli. Science 282 (5393), 1494-1497.

95. Rosen, D.A. et al. (2007) Detection of intracellular bacterial communities in human urinary tract infection. PLoS Med 4 (12), e329.

96. Mulvey, M.A. et al. (2000) Bad bugs and beleaguered bladders: interplay between uropathogenic Escherichia coli and innate host defenses. Proc Natl Acad Sci U S A 97 (16), 8829-35.

97. Rubenwolf, P.C. et al. (2012) Aquaporin expression contributes to human transurothelial permeability in vitro and is modulated by NaCl. PLoS One 7 (9), e45339.

98. Ratner, J.J. et al. (1981) Bacteria-specific antibody in the urine of patients with acute pyelonephritis and cystitis. J Infect Dis 143 (3), 404-12.

99. Chan, C.Y. et al. (2013) Mast cell interleukin-10 drives localized tolerance in chronic bladder infection. Immunity 38 (2), 349-59.

100. Abraham, S.N. and Miao, Y. (2015) The nature of immune responses to urinary tract infections. Nat Rev Immunol 15 (10), 655-63.

101. Sivick, K.E. and Mobley, H.L. (2010) Waging war against uropathogenic Escherichia coli: winning back the urinary tract. Infect Immun 78 (2), 568-85.

102. Gur, C. et al. (2013) Natural killer cell-mediated host defense against uropathogenic E. coli is counteracted by bacterial hemolysinA-dependent killing of NK cells. Cell Host Microbe 14 (6), 664-74.

103. Engel, D. et al. (2006) Tumor necrosis factor alpha- and inducible nitric oxide synthase-producing dendritic cells are rapidly recruited to the bladder in urinary tract infection but are dispensable for bacterial clearance. Infect Immun 74 (11), 6100-7.

104. Hannan, T.J. et al. (2014) Inhibition of Cyclooxygenase-2 Prevents Chronic and Recurrent Cystitis. EBioMedicine 1 (1), 46-57.

105. Zhang, D. et al. (2004) A toll-like receptor that prevents infection by uropathogenic bacteria. Science 303 (5663), 1522-6.

106. Wu, J. et al. (2017) The multiple antibacterial activities of the bladder epithelium. Ann Transl Med 5 (2), 35.

107. Benson, M. et al. (1996) Interleukin (IL)-6 and IL-8 in children with febrile urinary tract infection and asymptomatic bacteriuria. J Infect Dis 174 (5), 1080-4.

108. Hedlund, M. et al. (2001) Type 1 fimbriae deliver an LPS- and TLR4-dependent activation signal to CD14-negative cells. Mol Microbiol 39 (3), 542-52.

109. Hang, L. et al. (1999) Macrophage inflammatory protein-2 is required for neutrophil passage across the epithelial barrier of the infected urinary tract. J Immunol 162 (5), 3037-44.

110. Czaja, C.A. et al. (2009) Prospective cohort study of microbial and inflammatory events immediately preceding Escherichia coli recurrent urinary tract infection in women. J Infect Dis 200 (4), 528-36.

111. Shahin, R.D. et al. (1987) Neutrophil recruitment and bacterial clearance correlated with LPS responsiveness in local gram-negative infection. J Immunol 138 (10), 3475-80.

112. Schiwon, M. et al. (2014) Crosstalk between sentinel and helper macrophages permits neutrophil migration into infected uroepithelium. Cell 156 (3), 456-68.

113. Stone, M.J. et al. (2017) Mechanisms of Regulation of the Chemokine-Receptor Network. Int J Mol Sci 18 (2).

114. Song, J. et al. (2007) A novel TLR4-mediated signaling pathway leading to IL-6 responses in human bladder epithelial cells. PLoS Pathog 3 (4), e60.

115. Akira, S. and Takeda, K. (2004) Toll-like receptor signalling. Nat Rev Immunol 4 (7), 499-511.

116. Schilling, J.D. et al. (2003) CD14- and Toll-like receptor-dependent activation of bladder epithelial cells by lipopolysaccharide and type 1 piliated Escherichia coli. Infect Immun 71 (3), 1470-80.

117. Hunstad, D.A. and Justice, S.S. (2010) Intracellular lifestyles and immune evasion strategies of uropathogenic Escherichia coli. Annu Rev Microbiol 64, 203-21.

118. Song, J. et al. (2009) TLR4-mediated expulsion of bacteria from infected bladder epithelial cells. Proc Natl Acad Sci U S A 106 (35), 14966-71.

119. Hayes, B.W. and Abraham, S.N. (2016) Innate Immune Responses to Bladder Infection. Microbiol Spectr 4 (6).

120. Miao, Y. et al. (2016) Ubiquitination of Innate Immune Regulator TRAF3 Orchestrates Expulsion of Intracellular Bacteria by Exocyst Complex. Immunity 45 (1), 94-105.

121. Miao, Y. et al. (2015) A TRP Channel Senses Lysosome Neutralization by Pathogens to Trigger Their Expulsion. Cell 161 (6), 1306-19.

122. Klumpp, D.J. et al. (2006) Uropathogenic Escherichia coli induces extrinsic and intrinsic cascades to initiate urothelial apoptosis. Infect Immun 74 (9), 5106-13.

123. Thumbikat, P. et al. (2009) Bacteria-induced uroplakin signaling mediates bladder response to infection. PLoS Pathog 5 (5), e1000415.

124. Barber, A.E. et al. (2016) Strengths and Limitations of Model Systems for the Study of Urinary Tract Infections and Related Pathologies. Microbiol Mol Biol Rev 80 (2), 351-67.

125. Coulthard, M.G. et al. (2002) Renal scarring caused by vesicoureteric reflux and urinary infection: a study in pigs. Pediatr Nephrol 17 (7), 481-4.

126. Wiles, T.J. et al. (2009) Use of zebrafish to probe the divergent virulence potentials and toxin requirements of extraintestinal pathogenic Escherichia coli. PLoS Pathog 5 (12), e1000697.

127. Zhao, L. et al. (2009) Comparison of virulence factors and expression of specific genes between uropathogenic Escherichia coli and avian pathogenic E. coli in a murine urinary tract infection model and a chicken challenge model. Microbiology 155 (Pt 5), 1634-44.

128. Guiton, P.S. et al. (2013) Enterococcus faecalis overcomes foreign body-mediated inflammation to establish urinary tract infections. Infect Immun 81 (1), 329-39.

129. Rosen, D.A. et al. (2008) Utilization of an intracellular bacterial community pathway in Klebsiella pneumoniae urinary tract infection and the effects of FimK on type 1 pilus expression. Infect Immun 76 (7), 3337-45.

130. Murphy, C.N. et al. (2013) Role of Klebsiella pneumoniae type 1 and type 3 fimbriae in colonizing silicone tubes implanted into the bladders of mice as a model of catheter-associated urinary tract infections. Infect Immun 81 (8), 3009-17.

131. Bialek, S. et al. (2010) Membrane efflux and influx modulate both multidrug resistance and virulence of Klebsiella pneumoniae in a Caenorhabditis elegans model. Antimicrob Agents Chemother 54 (10), 4373-8.

132. Prajsnar, T.K. et al. (2013) Zebrafish as a novel vertebrate model to dissect enterococcal pathogenesis. Infect Immun 81 (11), 4271-9.

133. Bode, N.J. et al. (2015) Transcriptional analysis of the MrpJ network: modulation of diverse virulence-associated genes and direct regulation of mrp fimbrial and flhDC flagellar operons in Proteus mirabilis. Infect Immun 83 (6), 2542-56.

134. Lebreton, F. et al. (2009) ace, Which encodes an adhesin in Enterococcus faecalis, is regulated by Ers and is involved in virulence. Infect Immun 77 (7), 2832-9.

135. Glover, M. et al. (2014) Recurrent urinary tract infections in healthy and nonpregnant women. Urol Sci 25 (1), 1-8.

136. Howlett, A.R. et al. (1986) Epithelial-stromal interactions in the adult bladder: urothelial growth, differentiation, and maturation on culture facsimiles of bladder stroma. Dev Biol 118 (2), 403-15.

137. Berger, H. et al. (1982) Cloning of the chromosomal determinants encoding hemolysin production and mannose-resistant hemagglutination in Escherichia coli. J Bacteriol 152 (3), 1241-7.

138. Hultgren, S.J. et al. (1986) Regulation of production of type 1 pili among urinary tract isolates of Escherichia coli. Infect Immun 54 (3), 613-20.

139. Fukushi, Y. et al. (1979) An electron microscopic study of the interaction between vesical epitherlium and E. Coli. Invest Urol 17 (1), 61-8.

140. McTaggart, L.A. et al. (1990) The pathogenesis of urinary tract infections associated with Escherichia coli, Staphylococcus saprophyticus and S. epidermidis. J Med Microbiol 32 (2), 135-41.

141. Mulvey, M.A. et al. (2001) Establishment of a persistent Escherichia coli reservoir during the acute phase of a bladder infection. Infect Immun 69 (7), 4572-9.

142. Garofalo, C.K. et al. (2007) Escherichia coli from urine of female patients with urinary tract infections is competent for intracellular bacterial community formation. Infection and immunity 75 (1), 52-60.

143. Hopkins, W.J. et al. (1998) Time course and host responses to Escherichia coli urinary tract infection in genetically distinct mouse strains. Infect Immun 66 (6), 2798-802.

144. Schaeffer, A.J. et al. (1987) Relationship of type 1 pilus expression in Escherichia coli to ascending urinary tract infections in mice. Infection and immunity 55 (2), 373-380.

145. Bishop, B.L. et al. (2007) Cyclic AMP-regulated exocytosis of Escherichia coli from infected bladder epithelial cells. Nat Med 13 (5), 625-30.

146. Gunther, N.W. et al. (2001) In vivo dynamics of type 1 fimbria regulation in uropathogenic Escherichia coli during experimental urinary tract infection. Infect Immun 69 (5), 2838-46.

147. Hagberg, L. et al. (1983) Ascending, unobstructed urinary tract infection in mice caused by pyelonephritogenic Escherichia coli of human origin. Infect Immun 40 (1), 273-83.

148. Hvidberg, H. et al. (2000) Development of a long-term ascending urinary tract infection mouse model for antibiotic treatment studies. Antimicrob Agents Chemother 44 (1), 156-63.

149. Lane, M.C. et al. (2007) Expression of flagella is coincident with uropathogenic Escherichia coli ascension to the upper urinary tract. Proc Natl Acad Sci U S A 104 (42), 16669-74.

150. Malaviya, R. et al. (2004) Contribution of mast cells to bacterial clearance and their proliferation during experimental cystitis induced by type 1 fimbriated E. coli. Immunol Lett 91 (2-3), 103-11.

151. Hopkins, W.J. et al. (1995) Induction of urinary tract infection by intraurethral inoculation with Escherichia coli: refining the murine model. J Infect Dis 171 (2), 462-5.

152. Justice, S.S. et al. (2006) Maturation of intracellular Escherichia coli communities requires SurA. Infect Immun 74 (8), 4793-800.

153. Haraoka, M. et al. (1999) Neutrophil recruitment and resistance to urinary tract infection. J Infect Dis 180 (4), 1220-9.

154. Hung, C.S. et al. (2002) Structural basis of tropism of Escherichia coli to the bladder during urinary tract infection. Mol Microbiol 44 (4), 903-15.

155. Chen, S.L. et al. (2009) Positive selection identifies an in vivo role for FimH during urinary tract infection in addition to mannose binding. Proceedings of the National Academy of Sciences 106 (52), 22439-22444.

156. Eto, D.S. et al. (2007) Integrin-mediated host cell invasion by type 1-piliated uropathogenic Escherichia coli. PLoS Pathog 3 (7), e100.

157. Struve, C. and Krogfelt, K.A. (1999) In vivo detection of Escherichia coli type 1 fimbrial expression and phase variation during experimental urinary tract infection. Microbiology 145 (Pt 10), 2683-90.

158. Hull, R.A. et al. (1981) Construction and expression of recombinant plasmids encoding type 1 or D-mannose-resistant pili from a urinary tract infection Escherichia coli isolate. Infect Immun 33 (3), 933-8.

159. Riley, M. et al. (2006) Escherichia coli K-12: a cooperatively developed annotation snapshot--2005. Nucleic Acids Res 34 (1), 1-9.

160. Blattner, F.R. et al. (1997) The complete genome sequence of Escherichia coli K-12. Science 277 (5331), 1453-62.

161. Metcalf, W.W. et al. (1990) Identification of phosphate starvation-inducible genes in Escherichia coli K-12 by DNA sequence analysis of psi::lacZ(Mu d1) transcriptional fusions. J Bacteriol 172 (6), 3191-200.

162. Khetrapal, V. et al. (2015) A set of powerful negative selection systems for unmodified Enterobacteriaceae. Nucleic Acids Res 43 (13), e83.

163. Lee, A.K. and Falkow, S. (1998) Constitutive and inducible green fluorescent protein expression in Bartonella henselae. Infect Immun 66 (8), 3964-7.

164. Eshaghi, M. et al. (2016) Brighter Fluorescent Derivatives of UTI89 Utilizing a Monomeric vGFP. Pathogens 5 (1).

165. Krogfelt, K.A. et al. (1990) Direct evidence that the FimH protein is the mannose-specific adhesin of Escherichia coli type 1 fimbriae. Infect Immun 58 (6), 1995-1998.

166. Klemm, P. (1985) Fimbrial adhesions of Escherichia coli. Rev Infect Dis 7 (3), 321-40.

167. Duguid, J.P. et al. (1955) Non-flagellar filamentous appendages ("fimbriæ") and hæmagglutinating activity in Bacterium coli. The Journal of Pathology and Bacteriology 70 (2), 335-348.

168. Rubenwolf, P.C. et al. (2009) Expression and localisation of aquaporin water channels in human urothelium in situ and in vitro. Eur Urol 56 (6), 1013-23.

169. Dulbecco, R. and Vogt, M. (1954) Plaque formation and isolation of pure lines with poliomyelitis viruses. J Exp Med 99 (2), 167-82.

170. Laemmli, U.K. (1970) Cleavage of structural proteins during the assembly of the head of bacteriophage T4. Nature 227 (5259), 680-5.

171. Weber, K. and Osborn, M. (1969) The reliability of molecular weight determinations by dodecyl sulfate-polyacrylamide gel electrophoresis. J Biol Chem 244 (16), 4406-12.

172. O'Farrell, P.H. (1975) High resolution two-dimensional electrophoresis of proteins. J Biol Chem 250 (10), 4007-21.

173. Towbin, H. et al. (1979) Electrophoretic transfer of proteins from polyacrylamide gels to nitrocellulose sheets: procedure and some applications. Proc Natl Acad Sci U S A 76 (9), 4350-4.

174. Maddox, P.H. and Jenkins, D. (1987) 3-Aminopropyltriethoxysilane (APES): a new advance in section adhesion. J Clin Pathol 40 (10), 1256-7.

175. Sengupta, D. et al. (2016) Fast, scalable and accurate differential expression analysis for single cells. bioRxiv.

176. Burrows, M.T. et al. (2017) Studies on the Growth of Cells: The Cultivation of Bladder and Prostatic Tumors Outside the Body. J Urol 197 (2S), S2-S14.

177. Bregman, R.U. and Bregman, E.T. (1961) Tissue culture of benign and malignant human genitourinary tumors. J Urol 86, 642-9.

178. Walker, D.G. et al. (1965) Observations on primary short-term cultures of human tumors. A second 5-year study. Eur J Cancer 1 (3), 265-73.

179. Jones, G.W. (1967) Primary and metastatic epithelial tumors of the human kidney and bladder in tissue culture. Cancer 20 (11), 1893-8.

180. Moore, G.E. and Koike, A. (1964) Growth of human tumor cells in vitro and in vivo. Cancer 17, 11-20.

181. Atala, A. (2017) Urological Tissue Cultures. J Urol 197 (2S), S15-S16.

182. Rigby, C.C. and Franks, L.M. (1970) A human tissue culture cell line from a transitional cell tumour of the urinary bladder: growth, chromosone pattern and ultrastructure. Br J Cancer 24 (4), 746-54.

183. O'Toole, C. et al. (1974) Lymphoid cells mediating tumor-specific cytotoxicity to carcinoma of the urinary bladder. Separation of the effector population using a surface marker. J Exp Med 139 (3), 457-66.

184. O'Toole, C. et al. (1976) A cell line (SCABER) derived from squamous cell carcinoma of the human urinary bladder. Int J Cancer 17 (6), 707-14.

185. Kato, T. et al. (1977) Cell cycles in two cell lines of human bladder carcinoma. Tohoku J Exp Med 121 (2), 157-64.

186. Kato, T. et al. (1978) Morphological characterization of two established cell lines, T24 and MGH-U1, derived from human urinary bladder carcinoma. Tohoku J Exp Med 124 (4), 339-49.

187. Bubeník, J. et al. (1973) Established cell line of urinary bladder carcinoma (T24) containing tumour-specific antigen. Int J Cancer 11 (3), 765-73.

188. Povey, S. et al. (1976) Characterisation of human cell lines and differentiation from HeLa by enzyme typing. Nature 264 (5581), 60-3.

189. Rasheed, S. et al. (1977) Human bladder carcinoma: characterization of two new tumor cell lines and search for tumor viruses. J Natl Cancer Inst 58 (4), 881-90.

190. Yajima, T. (1970) [Monolayer culture of human urinary bladder tumors. II]. Nihon Hinyokika Gakkai Zasshi 61 (8), 805-21.

191. Elliott, A.Y. et al. (1974) Characterization of a cell line from human transitional cell cancer of the urinary tract. J Natl Cancer Inst 53 (5), 1341-9.

192. Nayak, S.K. et al. (1977) A cell line from an anaplastic transitional cell carcinoma of human urinary bladder. Br J Cancer 35 (2), 142-51.

193. Kato, T. et al. (1977) Estimation of cell damage in monolayer culture using 14C-leucine incorporation. Tohoku J Exp Med 121 (4), 403-4.

194. Fogh, J. et al. (1977) Absence of HeLa cell contamination in 169 cell lines derived from human tumors. J Natl Cancer Inst 58 (2), 209-14.

195. Masters, J.R. et al. (1986) Tissue culture model of transitional cell carcinoma: characterization of twenty-two human urothelial cell lines. Cancer Res 46 (7), 3630-6.

196. Earl, J. et al. (2015) Erratum to: The UBC-40 Urothelial Bladder Cancer Cell Line Index: a genomic resource for functional studies. BMC Genomics 16 (1), 1019.

197. Crallan, R.A. et al. (2006) Experimental models of human bladder carcinogenesis. Carcinogenesis 27 (3), 374-81.

198. Truschel, S.T. et al. (1999) Primary uroepithelial cultures A model system to analyze umbrella cell barrier function. Journal of Biological Chemistry 274 (21), 15020-15029.

199. Barrila, J. et al. (2010) Organotypic 3D cell culture models: using the rotating wall vessel to study host-pathogen interactions. Nat Rev Microbiol 8 (11), 791-801.

200. Christian, B.J. et al. (1987) Characterization of human uroepithelial cells immortalized in vitro by simian virus 40. Cancer Res 47 (22), 6066-73.

201. Petzoldt, J.L. et al. (1995) Immortalisation of human urothelial cells. Urol Res 23 (6), 377-80.

202. Reznikoff, C.A. et al. (1996) Elevated p16 at senescence and loss of p16 at immortalization in human papillomavirus 16 E6, but not E7, transformed human uroepithelial cells. Cancer Res 56 (13), 2886-90.

203. Chapman, E.J. et al. (2009) Integrated genomic and transcriptional analysis of the in vitro evolution of telomerase-immortalized urothelial cells (TERT-NHUC). Genes Chromosomes Cancer 48 (8), 694-710.

204. Georgopoulos, N.T. et al. (2011) Immortalisation of normal human urothelial cells compromises differentiation capacity. Eur Urol 60 (1), 141-9.

205. Herz, F. et al. (1979) Short-term culture of epithelial cells from urine of adults. Proc Soc Exp Biol Med 161 (2), 153-7.

206. Sutherland, G.R. and Bain, A.D. (1972) Culture of cells from the urine of newborn children. Nature 239 (5369), 231.

207. Hoehn, H. et al. (1975) Cultivated cells from diagnostic amniocentesis in second trimester pregnancies. III. The fetal urine as a potential source of clonable cells. Humangenetik 29 (4), 285-90.

208. Zhang, D. et al. (2014) Urine-derived stem cells: A novel and versatile progenitor source for cell-based therapy and regenerative medicine. Genes Dis 1 (1), 8-17.

209. Felix, J.S. et al. (1980) Human epithelial cells cultured from urine: growth properties and keratin staining. In Vitro 16 (10), 866-74.

210. Southgate, J. et al. (2002) Culture of Human Urothelium. In Culture of Epithelial Cells, pp. 381-399, John Wiley & Sons, Inc.

211. Rheinwald, J.G. and O'Connell, T.M. (1985) Intermediate filament proteins as distinguishing markers of cell type and differentiated state in cultured human urinary tract epithelia. Ann N Y Acad Sci 455, 259-67.

212. Detrisac, C.J. et al. (1983) In vitro culture of cells exfoliated in the urine by patients with diabetes mellitus. J Clin Invest 71 (1), 170-3.

213. Elliott, A.Y. et al. (1975) Technique for cultivation of transitional epithelium from mammalian urinary bladder. In Vitro 11 (5), 251-4.

214. Trifillis, A.L. et al. (1993) Culture and characterization of normal epithelium from cystoscopic biopsies of human bladder. In Vitro Cell Dev Biol Anim 29A (12), 908-11.

215. Reznikoff, C.A. et al. (1983) Growth and characterization of normal human urothelium in vitro. In Vitro 19 (4), 326-43.

216. Scriven, S.D. et al. (1997) Reconstitution of human urothelium from monolayer cultures. J Urol 158 (3 Pt 2), 1147-52.

217. Chlapowski, F.J. and Haynes, L. (1979) The growth and differentiation of transitional epithelium in vitro. J Cell Biol 83 (3), 605-14.

218. Kirk, D. et al. (1985) Selective growth of normal adult human urothelial cells in serum-free medium. In Vitro Cell Dev Biol 21 (3 Pt 1), 165-71.

219. Loretz, L.J. and Reznikoff, C.A. (1988) Clonal growth of normal human uroepithelial cells. In Vitro Cell Dev Biol 24 (4), 333-42.

220. Schmidt, W.W. et al. (1984) Cultures of normal human urothelial cells from ureters of perfused cadaver transplant kidneys. J Urol 132 (6), 1262-4.

221. Varley, C.L. and Southgate, J. (2011) Organotypic and 3D reconstructed cultures of the human bladder and urinary tract. Methods Mol Biol 695, 197-211.

222. Pariente, J.L. et al. (2000) Cultured differentiated human urothelial cells in the biomaterials field. Biomaterials 21 (8), 835-9.

223. Southgate, J. et al. (1994) Normal human urothelial cells in vitro: proliferation and induction of stratification. Lab Invest 71 (4), 583-94.

224. Lebeaux, D. et al. (2013) From in vitro to in vivo Models of Bacterial Biofilm-Related Infections. Pathogens 2 (2), 288-356.

225. Grunow, B. et al. (2011) Isolation of cells from Atlantic sturgeon Acipenser oxyrinchus oxyrinchus and optimization of culture conditions. Aquatic Biology 14 (1), 67-75.

226. Janssen, R. et al. (2008) Host-pathogen interactions in Campylobacter infections: the host perspective. Clinical microbiology reviews 21 (3), 505-518.

227. Kim, J. et al. (2011) An hTERT-immortalized human urothelial cell line that responds to anti-proliferative factor. In Vitro Cell Dev Biol Anim 47 (1), 2-9.

228. Southgate, J. et al. (1995) Loss of cyclin-dependent kinase inhibitor genes and chromosome 9 karyotypic abnormalities in human bladder cancer cell lines. Br J Cancer 72 (5), 1214-8.

229. Warrick, J.I. et al. (2016) FOXA1, GATA3 and PPARγ Cooperate to Drive Luminal Subtype in Bladder Cancer: A Molecular Analysis of Established Human Cell Lines. Sci Rep 6, 38531.

230. Schilling, J.D. et al. (2001) Bacterial invasion augments epithelial cytokine responses to Escherichia coli through a lipopolysaccharide-dependent mechanism. J Immunol 166 (2), 1148-55.

231. Smith, Y.C. et al. (2006) Novel three-dimensional organoid model for evaluation of the interaction of uropathogenic Escherichia coli with terminally differentiated human urothelial cells. Infection and Immunity 74 (1), 750-757.

232. Martinez, J.J. and Hultgren, S.J. (2002) Requirement of Rho-family GTPases in the invasion of Type 1-piliated uropathogenic Escherichia coli. Cell Microbiol 4 (1), 19-28.

233. Duncan, M.J. et al. (2004) Bacterial penetration of bladder epithelium through lipid rafts. J Biol Chem 279 (18), 18944-51.

234. Quentmeier, H. et al. (1997) The human bladder carcinoma cell line 5637 constitutively secretes functional cytokines. Leuk Res 21 (4), 343-50.

235. Ghoniem, G. et al. (2011) Differential profile analysis of urinary cytokines in patients with overactive bladder. Int Urogynecol J 22 (8), 953-61.

236. Kaashoek, J.G. et al. (1991) Cytokine production by the bladder carcinoma cell line 5637: rapid analysis of mRNA expression levels using a cDNA-PCR procedure. Lymphokine Cytokine Res 10 (3), 231-5.

237. Svanborg, C. et al. (1993) Bacterial adherence and epithelial cell cytokine production. Zentralbl Bakteriol 278 (2-3), 359-64.

238. Svanborg, C. et al. (1994) Bacterial adherence and mucosal cytokine production. Ann N Y Acad Sci 730, 162-81.

239. Hedges, S. et al. (1992) Interleukin-6 response of epithelial cell lines to bacterial stimulation in vitro. Infect Immun 60 (4), 1295-301.

240. Lau, M.E. and Hunstad, D.A. (2013) Quantitative assessment of human neutrophil migration across a cultured bladder epithelium. J Vis Exp (81), e50919.

241. Garthwaite, M. et al. (2014) Use of donor bladder tissues for in vitro research. BJU Int 113 (1), 160-6.

242. Southgate, J. et al. (1999) Urothelial tissue regulation. Unraveling the role of the stroma. Adv Exp Med Biol 462, 19-30.

243. Smith, B.A. et al. (2001) Identification of genes involved in human urothelial cell-matrix interactions: implications for the progression pathways of malignant urothelium. Cancer Res 61 (4), 1678-85.

244. Varley, C.L. et al. (2004) Activation of peroxisome proliferator-activated receptor-gamma reverses squamous metaplasia and induces transitional differentiation in normal human urothelial cells. Am J Pathol 164 (5), 1789-98.

245. Southgate, J. et al. (1995) Patterns of splice variant CD44 expression by normal human urothelium in situ and in vitro and by bladder-carcinoma cell lines. Int J Cancer 62 (4), 449-56.

246. Southgate, J. et al. (1995) Expression and in vitro regulation of integrins by normal human urothelial cells. Cell Adhes Commun 3 (3), 231-42.

247. Smith, N.J. et al. (2015) The human urothelial tight junction: claudin 3 and the ZO-1 α (+) switch. Bladder (San Franc) 2 (1), e9.

248. Fleming, J.M. et al. (2012) Differentiation-associated reprogramming of the transforming growth factor β receptor pathway establishes the circuitry for epithelial autocrine/paracrine repair. PLoS One 7 (12), e51404.

249. Böck, M. et al. (2014) Identification of ELF3 as an early transcriptional regulator of human urothelium. Dev Biol 386 (2), 321-30.

250. Rubenwolf, P. and Southgate, J. (2011) Permeability of differentiated human urothelium in vitro. Methods Mol Biol 763, 207-22.

251. Connell, I. et al. (1996) Type 1 fimbrial expression enhances Escherichia coli virulence for the urinary tract. Proc Natl Acad Sci U S A 93 (18), 9827-32.

252. Thankavel, K. et al. (1997) Localization of a domain in the FimH adhesin of Escherichia coli type 1 fimbriae capable of receptor recognition and use of a domain-specific antibody to confer protection against experimental urinary tract infection. J Clin Invest 100 (5), 1123-36.

253. Greene, S.E. et al. (2014) Pilicide ec240 disrupts virulence circuits in uropathogenic Escherichia coli. MBio 5 (6), e02038.

254. Wu, X.R. et al. (1996) In vitro binding of type 1-fimbriated Escherichia coli to uroplakins Ia and Ib: relation to urinary tract infections. Proc Natl Acad Sci U S A 93 (18), 9630-5.

255. Xie, B. et al. (2006) Distinct glycan structures of uroplakins Ia and Ib: structural basis for the selective binding of FimH adhesin to uroplakin Ia. J Biol Chem 281 (21), 14644-53.

256. Thumbikat, P. et al. (2009) Differentiation-induced uroplakin III expression promotes urothelial cell death in response to uropathogenic< i> E. coli</i>. Microbes and Infection 11 (1), 57-65.

257. Liang, F.X. et al. (2005) Cellular basis of urothelial squamous metaplasia: roles of lineage heterogeneity and cell replacement. J Cell Biol 171 (5), 835-44.

258. Tseng, C.C. et al. (2007) PapG II adhesin in the establishment and persistence of Escherichia coli infection in mouse kidneys. Kidney Int 71 (8), 764-70.

259. Rodriguez-Pastrana, A.F. et al. (2007) Patient's UPEC isolates fim+/pap- only correlated with low UTI whereas pyelonephritis isolates were fim+/pap+. Kidney International 72 (10), 1289.

260. Strömberg, N. et al. (1990) Host-specificity of uropathogenic Escherichia coli depends on differences in binding specificity to Gal alpha 1-4Gal-containing isoreceptors. EMBO J 9 (6), 2001-10.

261. Lane, M.C. and Mobley, H.L. (2007) Role of P-fimbrial-mediated adherence in pyelonephritis and persistence of uropathogenic Escherichia coli (UPEC) in the mammalian kidney. Kidney Int 72 (1), 19-25.

262. Lanne, B. et al. (1995) Glycoconjugate receptors for P-fimbriated Escherichia coli in the mouse. An animal model of urinary tract infection. J Biol Chem 270 (15), 9017-25.

263. Evans, D.J. et al. (1980) Hemagglutination typing of Escherichia coli: definition of seven hemagglutination types. J Clin Microbiol 12 (2), 235-42.

264. Holden, N.J. et al. (2006) Demonstration of regulatory cross-talk between P fimbriae and type 1 fimbriae in uropathogenic Escherichia coli. Microbiology 152 (Pt 4), 1143-53.

265. Baker, S.C. et al. (2014) Biomimetic urothelial tissue models for the in vitro evaluation of barrier physiology and bladder drug efficacy. Mol Pharm 11 (7), 1964-70.

266. Shalek, A.K. et al. (2013) Single-cell transcriptomics reveals bimodality in expression and splicing in immune cells. Nature 498 (7453), 236-40.

267. Dominguez, M.H. et al. (2013) Highly multiplexed quantitation of gene expression on single cells. J Immunol Methods 391 (1-2), 133-45.

268. Heath, J.R. et al. (2016) Single-cell analysis tools for drug discovery and development. Nat Rev Drug Discov 15 (3), 204-16.

269. Paul, F. et al. (2015) Transcriptional Heterogeneity and Lineage Commitment in Myeloid Progenitors. Cell 163 (7), 1663-77.

270. Linnarsson, S. and Teichmann, S.A. (2016) Single-cell genomics: coming of age. Genome Biol 17, 97.

271. Suh, M.J. et al. (2014) Proteomes of pathogenic Escherichia coli/Shigella group surveyed in their host environments. Expert Rev Proteomics 11 (5), 593-609.

272. Kim, M.S. et al. (2014) A draft map of the human proteome. Nature 509 (7502), 575-81.

273. Poulin, J.F. et al. (2016) Disentangling neural cell diversity using single-cell transcriptomics. Nat Neurosci 19 (9), 1131-41.

274. Saliba, A.E. et al. (2014) Single-cell RNA-seq: advances and future challenges. Nucleic Acids Res 42 (14), 8845-60.

275. Curran, S. et al. (2000) Laser capture microscopy. Mol Pathol 53 (2), 64-8.

276. Bheda, P. and Schneider, R. (2014) Epigenetics reloaded: the single-cell revolution. Trends Cell Biol 24 (11), 712-23.

277. Lučič, V. et al. (2013) Cryo-electron tomography: the challenge of doing structural biology in situ. J Cell Biol 202 (3), 407-19.

278. Harris, K.M. et al. (2006) Uniform serial sectioning for transmission electron microscopy. J Neurosci 26 (47), 12101-3.

279. Dolph, M.C. and Santeufemio, C. (2014) Exploring cryogenic focused ion beam milling as a Group III–V device fabrication tool. Nuclear Instruments and Methods in Physics Research Section B: Beam Interactions with Materials and Atoms 328, 33-41.

280. Hsieh, C. et al. (2014) Practical workflow for cryo focused-ion-beam milling of tissues and cells for cryo-TEM tomography. J Struct Biol 185 (1), 32-41.

281. Ohtomo, T. et al. (2013) Expression and distribution of acyl-CoA thioesterases in the white adipose tissue of rats. Histochem Cell Biol 140 (2), 223-32.

282. Strand, D.W. et al. (2012) PPARγ isoforms differentially regulate metabolic networks to mediate mouse prostatic epithelial differentiation. Cell Death Dis 3, e361.

283. Sexton, D.J. et al. (2009) Specific inhibition of tissue kallikrein 1 with a human monoclonal antibody reveals a potential role in airway diseases. Biochem J 422 (2), 383-92.

284. Yiu, W.H. et al. (2014) Tissue kallikrein mediates pro-inflammatory pathways and activation of protease-activated receptor-4 in proximal tubular epithelial cells. PLoS One 9 (2), e88894.

285. Pott, G.B. et al. (2013) Alpha-1 antitrypsin reduces severity of pseudomonas pneumonia in mice and inhibits epithelial barrier disruption and pseudomonas invasion of respiratory epithelial cells. Front Public Health 1, 19.

286. Lockett, A.D. et al. (2013) α_1-Antitrypsin modulates lung endothelial cell inflammatory responses to TNF-α. Am J Respir Cell Mol Biol 49 (1), 143-50.

287. Perlmutter, D.H. (2002) Liver injury in alpha1-antitrypsin deficiency: an aggregated protein induces mitochondrial injury. J Clin Invest 110 (11), 1579-83.

288. Leek, J.T. et al. (2010) Tackling the widespread and critical impact of batch effects in high-throughput data. Nat Rev Genet 11 (10), 733-9.

289. Maaten, L.v.d. and Hinton, G. (2008) Visualizing data using t-SNE. Journal of Machine Learning Research 9 (Nov), 2579-2605.

290. Lazar, C. et al. (2013) Batch effect removal methods for microarray gene expression data integration: a survey. Brief Bioinform 14 (4), 469-90.

291. Altman, N. and Krzywinski, M. (2017) Points of Significance: Clustering. Nature Methods 14, 545–546.

292. Reigstad, C.S. et al. (2007) Functional genomic studies of uropathogenic Escherichia coli and host urothelial cells when intracellular bacterial communities are assembled. J Biol Chem 282 (29), 21259-67.

293. Tabb, D.L. et al. (2010) Repeatability and reproducibility in proteomic identifications by liquid chromatography-tandem mass spectrometry. J Proteome Res 9 (2), 761-76.

294. Janciauskiene, S.M. et al. (2011) The discovery of α 1-antitrypsin and its role in health and disease. Respir Med 105 (8), 1129-39.

295. Vogel, L.K. and Larsen, J.E. (2000) Apical and non-polarized secretion of serpins from MDCK cells. FEBS Lett 473 (3), 297-302.

296. Lockett, A.D. et al. (2014) Active trafficking of alpha 1 antitrypsin across the lung endothelium. PLoS One 9 (4), e93979.

297. Guo, S. et al. (2014) Antisense oligonucleotide treatment ameliorates alpha-1 antitrypsin-related liver disease in mice. J Clin Invest 124 (1), 251-61.

298. Kontos, C.K. and Scorilas, A. (2012) Kallikrein-related peptidases (KLKs): a gene family of novel cancer biomarkers. Clin Chem Lab Med 50 (11), 1877-91.

299. Bhoola, K.D. et al. (1992) Bioregulation of kinins: kallikreins, kininogens, and kininases. Pharmacol Rev 44 (1), 1-80.

300. Scharfstein, J. et al. (2012) The kallikrein-kinin system in experimental Chagas disease: a paradigm to investigate the impact of inflammatory edema on GPCR-mediated pathways of host cell invasion by Trypanosoma cruzi. Front Immunol 3, 396.

301. Wu, Y. (2015) Contact pathway of coagulation and inflammation. Thromb J 13, 17.

302. Sorimachi, H. et al. (1990) A novel member of the calcium-dependent cysteine protease family. Biol Chem Hoppe Seyler 371 Suppl, 171-6.

303. Ji, J. et al. (2016) Critical role of calpain in inflammation. Biomed Rep 5 (6), 647-652.

304. Lewis, A.J. et al. (2016) Invasion of Host Cells and Tissues by Uropathogenic Bacteria. Microbiol Spectr 4 (6).

305. Xia, C. et al. (2015) Cardiomyocyte specific expression of Acyl-coA thioesterase 1 attenuates sepsis induced cardiac dysfunction and mortality. Biochem Biophys Res Commun 468 (4), 533-40.

306. Hunt, M.C. et al. (2012) The emerging role of acyl-CoA thioesterases and acyltransferases in regulating peroxisomal lipid metabolism. Biochim Biophys Acta 1822 (9), 1397-410.

307. Di Cara, F. et al. (2017) Peroxisome-Mediated Metabolism Is Required for Immune Response to Microbial Infection. Immunity 47 (1), 93-106.e7.

308. Zhang, W. and Wei, Q. (2011) Calcineurin stimulates the expression of inflammatory factors in RAW 264.7 cells by interacting with proteasome subunit alpha type 6. Biochem Biophys Res Commun 407 (4), 668-73.

309. Broering, R. et al. (2016) Hepatic expression of proteasome subunit alpha type-6 is upregulated during viral hepatitis and putatively regulates the expression of ISG15 ubiquitin-like modifier, a proviral host gene in hepatitis C virus infection. J Viral Hepat 23 (5), 375-86.

310. Ashida, H. and Sasakawa, C. (2017) Bacterial E3 ligase effectors exploit host ubiquitin systems. Curr Opin Microbiol 35, 16-22.

311. Zhang, J. et al. (2014) The chaperonin CCT α is required for efficient transcription and replication of rabies virus. Microbiol Immunol 58 (10), 590-9.

312. Gray, D.W. et al. (2017) Identification of candidate protein markers of Bovine Parainfluenza Virus Type 3 infection using an in vitro model. Vet Microbiol 203, 257-266.

313. Kim, A.Y. et al. (2016) The TFG-TEC oncoprotein induces transcriptional activation of the human β-enolase gene via chromatin modification of the promoter region. Mol Carcinog 55 (10), 1411-23.

314. Eisenreich, W. et al. (2013) Metabolic host responses to infection by intracellular bacterial pathogens. Front Cell Infect Microbiol 3, 24.

315. Ji, Z. and Ji, H. (2016) TSCAN: Pseudo-time reconstruction and evaluation in single-cell RNA-seq analysis. Nucleic Acids Res 44 (13), e117.

316. Genshaft, A.S. et al. (2016) Multiplexed, targeted profiling of single-cell proteomes and transcriptomes in a single reaction. Genome Biol 17 (1), 188.

317. Dueck, H.a.E.J.a.K.J. (2016) Variation is function: Are single cell differences functionally important? BioEssays 38 (2), 172--180.

318. Fire, A. et al. (1998) Potent and specific genetic interference by double-stranded RNA in Caenorhabditis elegans. Nature 391 (6669), 806-11.

319. Zeng, Y. et al. (2003) MicroRNAs and small interfering RNAs can inhibit mRNA expression by similar mechanisms. Proc Natl Acad Sci U S A 100 (17), 9779-84.

320. Carpenter, A.E. and Sabatini, D.M. (2004) Systematic genome-wide screens of gene function. Nat Rev Genet 5 (1), 11-22.

321. Mocellin, S. and Provenzano, M. (2004) RNA interference: learning gene knock-down from cell physiology. J Transl Med 2 (1), 39.

322. Conrad, C. and Gerlich, D.W. (2010) Automated microscopy for high-content RNAi screening. J Cell Biol 188 (4), 453-61.

323. Echeverri, C.J. and Perrimon, N. (2006) High-throughput RNAi screening in cultured cells: a user's guide. Nat Rev Genet 7 (5), 373-84.

324. Clemens, J.C. et al. (2000) Use of double-stranded RNA interference in Drosophila cell lines to dissect signal transduction pathways. Proc Natl Acad Sci U S A 97 (12), 6499-503.

325. Kamath, R.S. et al. (2003) Systematic functional analysis of the Caenorhabditis elegans genome using RNAi. Nature 421 (6920), 231-7.

326. Gönczy, P. et al. (2000) Functional genomic analysis of cell division in C. elegans using RNAi of genes on chromosome III. Nature 408 (6810), 331-6.

327. Heo, W.D. and Meyer, T. (2003) Switch-of-function mutants based on morphology classification of Ras superfamily small GTPases. Cell 113 (3), 315-28.

328. Mohr, S.E. et al. (2014) RNAi screening comes of age: improved techniques and complementary approaches. Nat Rev Mol Cell Biol 15 (9), 591-600.

329. Chia, N.Y. et al. (2010) A genome-wide RNAi screen reveals determinants of human embryonic stem cell identity. Nature 468 (7321), 316-20.

330. Kavanaugh, G. et al. (2015) A whole genome RNAi screen identifies replication stress response genes. DNA Repair (Amst) 35, 55-62.

331. Anitei, M. et al. (2014) A high-throughput siRNA screen identifies genes that regulate mannose 6-phosphate receptor trafficking. J Cell Sci 127 (Pt 23), 5079-92.

332. Sharma, S. and Rao, A. (2009) RNAi screening: tips and techniques. Nat Immunol 10 (8), 799-804.

333. Thornbrough, J.M. et al. (2012) Human genome-wide RNAi screen for host factors that modulate intracellular Salmonella growth. PLoS One 7 (6), e38097.

334. Thornbrough, J.M. et al. (2016) Human Genome-Wide RNAi Screen for Host Factors That Facilitate Salmonella Invasion Reveals a Role for Potassium Secretion in Promoting Internalization. PLoS One 11 (11), e0166916.

335. Debnath, I. et al. (2013) The Cpx stress response system potentiates the fitness and virulence of uropathogenic Escherichia coli. Infect Immun 81 (5), 1450-9.

336. Szabados, F. et al. (2008) Staphylococcus saprophyticus ATCC 15305 is internalized into human urinary bladder carcinoma cell line 5637. FEMS Microbiology Letters 285 (2), 163--169.

337. Subramanian, P. et al. (2014) Graphene-coated surface plasmon resonance interfaces for studying the interactions between bacteria and surfaces. ACS Appl Mater Interfaces 6 (8), 5422-31.

338. Schwartz, D.J. et al. (2013) Positively selected FimH residues enhance virulence during urinary tract infection by altering FimH conformation. Proc Natl Acad Sci U S A 110 (39), 15530-7.

339. Lo, A.W. et al. (2014) Suppression of type 1 pilus assembly in uropathogenic Escherichia coli by chemical inhibition of subunit polymerization. J Antimicrob Chemother 69 (4), 1017-26.

340. Rosen, D.A. et al. (2008) Molecular variations in Klebsiella pneumoniae and Escherichia coli FimH affect function and pathogenesis in the urinary tract. Infect Immun 76 (7), 3346-56.

341. Greene, S.E. et al. (2015) Human Urine Decreases Function and Expression of Type 1 Pili in Uropathogenic Escherichia coli. MBio 6 (4), e00820.

342. Crépin, S. et al. (2012) Decreased expression of type 1 fimbriae by a pst mutant of uropathogenic Escherichia coli reduces urinary tract infection. Infect Immun 80 (8), 2802-15.

343. Dhakal, B.K. and Mulvey, M.A. (2009) Uropathogenic Escherichia coli invades host cells via an HDAC6-modulated microtubule-dependent pathway. J Biol Chem 284 (1), 446-54.

344. Eto, D.S. et al. (2006) Actin-gated intracellular growth and resurgence of uropathogenic Escherichia coli. Cell Microbiol 8 (4), 704-17.

345. Szabados, F. et al. (2011) Fbl is not involved in the invasion of eukaryotic epithelial and endothelial cells by Staphylococcus lugdunensis. FEMS Microbiology Letters 324 (1), 48--55.

346. Dikshit, N. et al. (2015) Intracellular Uropathogenic E. coli Exploits Host Rab35 for Iron Acquisition and Survival within Urinary Bladder Cells. PLoS Pathog 11 (8), e1005083.

347. Bokil, N.J. et al. (2011) Intramacrophage survival of uropathogenic Escherichia coli: differences between diverse clinical isolates and between mouse and human macrophages. Immunobiology 216 (11), 1164-71.

348. Blango, M.G. et al. (2014) Forced Resurgence and Targeting of Intracellular Uropathogenic Escherichia coli Reservoirs. PLoS One 9 (3), e93327.

349. Wurpel, D.J. et al. (2013) Chaperone-usher fimbriae of Escherichia coli. PLoS One 8 (1), e52835.

350. Spaulding, C.N. et al. (2017) Selective depletion of uropathogenic E. coli from the gut by a FimH antagonist. Nature 546 (7659), 528-532.

351. Holden, N.J. and Gally, D.L. (2004) Switches, cross-talk and memory in Escherichia coli adherence. J Med Microbiol 53 (Pt 7), 585-93.

352. Snyder, J.A. et al. (2005) Coordinate expression of fimbriae in uropathogenic Escherichia coli. Infect Immun 73 (11), 7588-96.

353. Antibacterial agents in clinical development: An analysis of the antibacterial clinical development pipeline, including tuberculosis, World Health Organisation, Geneva, 2017.

354. Ali, A.S.M. et al. (2017) Targeting Deficiencies in the TLR5 Mediated Vaginal Response to Treat Female Recurrent Urinary Tract Infection. Sci Rep 7 (1), 11039.

355. Jonsson, M.K. et al. (2016) Towards Creating the Perfect In Vitro Cell Model. Stem Cells Int 2016, 3459730.

356. Horsley, H. et al. (2017) A urine-dependent human urothelial organoid offers a viable alternative to rodent models of infection. bioRxiv.

357. Li, H. et al. (2017) Reference component analysis of single-cell transcriptomes elucidates cellular heterogeneity in human colorectal tumors. Nat Genet 49 (5), 708-718.

8 Appendix

Table 8.1 – List of all bacterial proteins detected by LC-Ms/Ms. The table lists all bacterial proteins as detected in all cells within each of the three cell groups: uninfected, infected and control. The uninfected and infected cells come from infected ice, and uninfected (control) cells come from uninfected mice. N=16.

UTI89-GFP infected mice				Uninfected mice	
Uninfected cells n=16		Infected cells n=16		Control cells n=16	
GenInfo Identifier	Protein	GenInfo Identifier	Protein	GenInfo Identifier	Protein
91072570	glyceraldehyde-3-phosphate dehydrogenase A	91072570	glyceraldehyde-3-phosphate dehydrogenase A	91071398	hypothetical protein UTI89_C0793
91070645	chaperone Hsp70; DNA biosynthesis; autoregulated heat shock proteins	91074351	protein chain elongation factor EF-Tu (duplicate of tufB)	91075468	putative member of ShlA/HecA/FhaA exoprotein family
91075120	glucose-6-phosphate isomerase	91074389	translation elongation factor EF-Tu	91072653	pyruvate kinase II
91075468	putative member of ShlA/HecA/FhaA exoprotein family	91071626	outer membrane protein A precursor	91072999	putative channel/filament proteins
91071357	phosphoglycerate mutase 1	91070645	chaperone Hsp70; DNA biosynthesis; autoregulated heat shock proteins	91074901	adenylate cyclase
91073367	transaldolase A	91075120	glucose-6-phosphate isomerase	91074337	probable general secretion pathway protein E
91075273	putative toxin of osmotically regulated toxin-antitoxin system associated with programmed cell death	91074382	50S ribosomal subunit protein L7/L12	91070645	chaperone Hsp70; DNA biosynthesis; autoregulated heat shock proteins
91074567	glutathione reductase	91071357	phosphoglycerate mutase 1	91072773	putative peptide synthetase-like protein
91073958	malate synthase G	91073367	transaldolase A		
91071000	putative transferase	91073196	hypothetical protein YfcL		
91072828	putative transferase	91071586	30S ribosomal subunit protein S1		
91072156	exoribonuclease II	91074391	30S ribosomal subunit protein S7		
91074833	membrane-bound ATP synthase F1 sector alpha-subunit	91074321	30S ribosomal subunit protein S3		
91072716	flagellin	91073958	malate synthase G		
91074351	protein chain elongation factor EF-Tu (duplicate of tufB)	91074049	4-dihydroxy-2-butanone 4-phosphate synthase		
91074389	translation elongation factor EF-Tu	91072616	cold shock protein CspC		
91071626	outer membrane protein A precursor	91075387	valyl-tRNA synthetase		
91072033	Hns transcriptional dual regulator	91071227	Alkyl hydroperoxide reductase, C22 subunit detoxification of hydroperoxides		
91075387	valyl-tRNA synthetase	91075267	GroEL (chaperone Hsp60)		
91074382	50S ribosomal subunit	91070654	30S ribosomal subunit protein		

	protein L7/L12		S20
91072464	murein lipoprotein	91074576	outer membrane hemin receptor ChuA
		91072033	Hns transcriptional dual regulator
		91075557	invasion protein IbeA
		91074367	DNA-binding protein HU-alpha (HU-2)
		91074390	translation elongation factor EF-G GTP-binding protein chain
		91074332	30S ribosomal subunit protein S10
		91071083	trigger factor
		91074644	cold shock protein 7.4 transcriptional activator of hns
		91075326	50S ribosomal subunit protein L9
		91071604	aspartate transaminase
		91073719	enolase
		91071821	acyl carrier protein
		91074383	50S ribosomal subunit protein L10
		91072768	putative salicylate synthetase
		91074386	50S ribosomal subunit protein L11
		91074575	putative heme/hemoglobin transport protein
		91075273	putative toxin of osmotically regulated toxin-antitoxin system associated with programmed cell death
		91074329	50S ribosomal subunit protein L4
		91074384	50S ribosomal subunit protein L1
		91073326	O-acetylserine sulfhydrolase A
		91074230	malate dehydrogenase
		91071940	putative iron transport protein, periplasmic-binding protein SitA
		91073611	ribonucleoside-diphosphate reductase 2 beta chain
		91071000	putative transferase
		91072828	putative transferase
		91074223	30S ribosomal subunit protein S9
		91072183	hypothetical oxidoreductase YcjS
		91074127	N-acetylgalactosamine-specific PTS system enzyme IIB component
		91072463	pyruvate kinase I
		91074567	glutathione reductase
		91075468	putative member of

	ShlA/HecA/FhaA exoprotein family
91074833	membrane-bound ATP synthase F1 sector alpha-subunit
91075133	maltoporin precursor
91074295	50S ribosomal subunit protein L17
91072171	phage shock protein A
91072999	putative channel/filament proteins
91072268	hypothetical protein YncE precursor
91070756	pyruvate dehydrogenase E1 component
91073875	fructose-bisphosphate aldolase class II
91072192	thiol peroxidase
91074297	30S ribosomal subunit protein S4
91074306	30S ribosomal subunit protein S5
91073876	phosphoglycerate kinase
91070758	dihydrolipoamide dehydrogenase
91075041	glycerol kinase
91070812	30S ribosomal protein S2
91074831	membrane-bound ATP synthase F1 sector beta-subunit
91074309	50S ribosomal subunit protein L6
91074296	RNA polymerase alpha subunit
91072464	murein lipoprotein
91074298	30S ribosomal subunit protein S11
91071867	NADP Isocitrate dehydrogenase
91071578	formate acetyltransferase 1
91074300	30S ribosomal subunit protein S13
91073167	phosphate acetyltransferase
91074363	Phosphoribosylamine--glycine ligase
91074837	membrane-bound ATP synthase F0 sector subunit b
91072037	CoA-linked acetaldehyde dehydrogenase
91070638	transaldolase B
91071468	arginine-binding periplasmic protein 2 precursor
91074326	50S ribosomal subunit protein L2
91070757	pyruvate dehydrogenase
91074323	50S ribosomal subunit protein L22
91074827	L-glutamine:D-fructose-6-phosphate aminotransferase

91074314	50S ribosomal protein L24
91072126	tryptophan synthase alpha subunit
91073382	phosphoribosylaminoimidazole-succinocarboxamide synthetase
91073500	heat shock protein
91073016	colicin I receptor precursor
91074303	50S ribosomal subunit protein L15
91071246	cold shock-like protein CspE
91071819	3-oxoacyl-[acyl-carrier-protein] reductase
91073867	ribose-5-phosphate isomerase A
91074728	50S ribosomal subunit protein L28
91074224	50S ribosomal subunit protein L13
91074320	50S ribosomal subunit protein L16
91074380	RNA polymerase beta subunit
91075339	FKBP-type 22KD peptidyl-prolyl cis-trans isomerase (a rotamase)
91072504	50S ribosomal subunit protein L20
91073094	hypothetical protein YfaQ precursor
91073890	transketolase 1
91072778	putative pesticin receptor precursor
91075325	30S ribosomal subunit protein S18
91073449	serine hydroxymethyltransferase
91071335	succinyl-CoA synthetase beta subunit
91074316	50S ribosomal subunit protein L14
91074588	hypothetical protein UTI89_C4040
91072777	yersiniabactin siderophore biosynthetic protein
91071121	chaperone Hsp90 heat shock protein C 62.5
91074597	glutamate decarboxylase alpha
91072304	glutamate decarboxylase beta
91073412	hypothetical protein YfgL
91074183	50S ribosomal subunit protein L21
91072774	HMWP1 nonribosomal peptide/polyketide synthase
91071715	S fimbriae outer membrane usher
91075535	periplasmic chaperone protein FimC precursor

	91074331	50S ribosomal subunit protein L3	
	91071331	succinate dehydrogenase flavoprotein subunit	
	91074101	hypothetical protein UTI89_C3536	
	91070809	2,3,4,5-tetrahydropyridine-2,6-dicarboxylate N-succinyltransferase	
	91071731	outer membrane heme/hemoglobin receptor	
	91074392	30S ribosomal subunit protein S12	
	91074741	RNA polymerase omega subunit	
	91070822	histone-like protein located in outer membrane or nucleoid	
	91071423	outer membrane protein X	
	91075371	conserved hypothetical protein	
	91072981	hypothetical protein YehQ	
	91074990	glutamine synthetase	
	91071280	glutamine-hydrolyzing asparagine synthetase B	
	91074630	periplasmic dipeptide transport protein precursor	
	91070842	D-methionine-binding transport system MetQ precursor	
	91071654	cold shock-like protein G	
	91075022	Mn superoxide dismutase	
	91071334	dihydrolipoamide succinyltransferase component of 2-oxoglutarate dehydrogenase complex	
	91071327	citrate synthase	
	91075354	inorganic pyrophosphatase	
	91071398	hypothetical protein UTI89_C0793	
	91071209	ferric enterobactin transport ATP-binding protein fepC	
	91071600	cell division protein MukB	
	91071317	hypothetical protein YbgA	